Characterising the evolution of Himalayan debris covered glaciers.

Owen King

Submitted in accordance with the requirements for the degree of Doctor of Philosophy

The University of Leeds, School of Geography

2018

The candidate confirms that the work submitted is his/her own, except where work which has formed part of jointly-authored publications has been included. The contribution of the candidate and the other authors to this work has been explicitly indicated below. The candidate confirms that appropriate credit has been given within the thesis where reference has been made to the work of others.

The work presented in Chapter three of this thesis has appeared in the following publication:

King, O. Quincey, D.J. Carrivick, J.L. and Rowan, A.V. 2017. Spatial variability in mass change of glaciers in the Everest region, central Himalaya, between 2000 and 2015. *The Cryosphere.* **2017**, 1-35. doi..org/10.5194/tc-11-407-2017.

OK was responsible for the study design, all data production and analyses, preparation of the figures and manuscript. All authors commented on early drafts of the manuscript, and Ann Rowan contributed to the writing of the discussion section.

The work presented in Chapter three of this thesis has appeared in the following publication:

King, O. Dehecq, A. Quincey, D.J. and Carrivick, J.L. 2018. Contrasting geometric and dynamic evolution of lake and land-terminating glaciers in the central Himalaya. *Global and Planetary Change*. **2018,** 46-60. doi.org/10.1016/j.gloplacha.2018.05.006

OK was responsible for the study design, data analyses, preparation of the figures and manuscript. Amaury Dehecq generated the glacier velocity data used in this study. All authors commented on early drafts of the manuscript.

The work presented in Chapter five of this thesis has been prepared for submission to Geomorphology.

OK was responsible for the study design, the production of analysed datasets, metric data analysis, preparation of the figures and manuscript. Andy Turner produced the metric data. All authors commented on early drafts of the manuscript.

Acknowledgements

I owe huge thanks to Duncan Quincey, Jonathan Carrivick and Ann Rowan for their fantastic support, advice and encouragement over the past three and a half years. The relaxed and friendly manner with which my supervisors have coaxed me through my PhD has made the whole experience an incredibly enjoyable and rewarding one. I must also thank David Rounce and Amaury Dehecq for their hard work and creative input into collaborative projects that we've undertaken alongside my own PhD work.

I am incredibly lucky to have had the unwavering support of my partner Ashleigh, who has provided encouragement, listened to my worries patiently and put up with my crankiness on numerous occasions, all whilst completing her own PhD. Being completely bamboozled by the standard of her work has also made me strive to improve my own research. I must also thank the many other PhD students in the School of Geography for providing plentiful distractions from work, whether in the form of tea breaks, evenings in the climbing wall, or nights in the pub.

Dhananjay Regmi and his team at Himalayan Research Expeditions in Kathmandu are thanked for their invaluable support in our field seasons, particularly Mahesh Magar and Surya Kulung for their guidance in the Khumbu valley.

Lastly, I am grateful to my family (Jean, Graeme and Amy), for their continued support in my pursuit of a career in academia, and for letting me empty the fridge completely on each visit home to Grimsby.

Abstract

The majority of the 20,000 glaciers found in the Himalaya are in a state of negative mass balance, and have been for decades. Broad spatial trends in ice mass loss have been identified by large scale geodetic mass balance studies, but regional averaging of mass loss data has masked catchment or glacier scale variability. This thesis has the broad aim of examining the catchment scale variability of ice mass loss, in order to identify factors that might promote, or inhibit, more substantial ice mass loss from the region in the future.

Ice mass loss rates from Everest region glaciers were calculated using the geodetic approach, over the period 2000-2015, and compared depending on glacier terminus type. Lake-terminating glaciers were found to have lost 32% more ice mass than land-terminating glaciers, and maximum surface lowering rates of lake-terminating glaciers peaked at more than twice the rate of land-terminating counterparts. Glacier hypsometry was found to be contrasting at the catchment scale, and predicted accumulation area ratio (AARs) change in response to different RCP warming scenarios emphasises the importance of considering glacier area-altitude distribution in future ice loss estimates.

A more detailed assessment of the evolving geometry, dynamics and ice loss rates of nine lake-terminating glaciers suggested two phases of glacier-lake interaction may exist. A phase of dynamic lake-terminating glacier retreat was evident where terminus proximal surface lowering rates were high (up to 3 m a^{-1}), ice front retreat rates were steady or accelerating, and surface velocities increased (by up to 10 m a^{-1}, between 1999 and 2015). Alternatively, a phase of retreat typified by surface lowering rates akin to land-terminating glaciers (~1 m a^{-1}), where ice front retreat rates were steady or diminishing, and where surface velocity reduction occurred. The dynamic phase of ice loss observed on lake-terminating glaciers in the Everest region is not of the same magnitude as larger water-terminating glaciers found in other glacierised regions, probably because of the topographic confinement of host glaciers and the dominance of resistive stresses, but the now populous nature of glacial lakes in the region means the potential for amplified future ice loss exists.

The impact of long-term ice loss on the topographic characteristics of debris covered glacier surfaces was also examined. Ice cliff and supraglacial pond expansion was identified as the main driver of topographic change on slow flowing, land-terminating glaciers. A more pitted surface topography of greater relief developed on most glaciers, which has implications for the energy balance at the glacier surface, and for supraglacial hydrology. Overall, the results of this thesis emphasise the need to incorporate a range of glacier dynamics scenarios and melt processes into simulations of future ice loss in the Himalaya.

Table of Contents

List of tables

Supplementary Table 3. Hypsometric Index (HI) scores and classification, accumulation area ratio (AAR) and total area loss for each glacier included in the study. EQ = Equidimensional; BH = Bottom Heavy; VBH = Very Bottom Heavy; TH = Top Heavy. The ELA of the Lhotse and Melung glaciers are now above their altitudinal ranges, thus AARs cannot be calculated. Catchments: TK- Tama Koshi; DK- Dudh Koshi; TP- Tibetan Plateau. Lake- terminating glaciers are in bold; mean values are italicised.

Supplementary Table 4. Glaciers highlighted in the study (chapter 4). Data on glacier area and altitudinal range are taken from the GLIMS database. Glacier length is measured along centrelines from the bergschrund.

Supplementary Table 5. Landsat archive scenes used in lake-terminating glacier ice front positions delineation and glacial lake area mapping.

List of figures

Figure 3.6. Surface lowering and glacier hypsometry curves for clean ice and lake-terminating glaciers in the study area.

Figure 3.7. Projected AARs (averaged across each catchment) based on different scenarios of temperature increase relative to the present day and accompanying ELA rise. Temperature rise scenarios have been used from the IPCC AR5 Working Group report. TP- Tibetan Plateau; DK- Dudh Koshi; TK- Tama Koshi; Clean- Clean ice glaciers. Each point represents a projected AAR given minimum, mean or maximum temperature rise under each RCP scenario.

Figure 4.1. The Everest region of the central Himalaya. Black glacier outlines show the extent of the RGI version 5.0, whereas white glacier outlines mark the glaciers we focus on in this study. Pro- and supraglacial lakes are also marked, along with mountain peaks above 8000 m in the area. Background imagery is a Landsat OLI image from 2014 available from http://earthexplorer.usgs.gov/

Figure 4.2. Surface elevation (A), surface elevation change (dH/dT) (B), surface slope (C), surface slope change (D), surface velocity (E) and surface velocity change (F) of five land-terminating glaciers in the study area. The coverage of high-resolution satellite imagery shown in Figure 7 is marked on velocity difference panels. Thresholds of surface slope (2˚) and surface velocity (4 m a^{1}) required for surface meltwater ponding are also marked.

Figure 4.3. Surface elevation (A), surface elevation change (dH/dT) (B), surface slope (C), surface slope change (D), surface velocity (E) and surface velocity change (F) of four land-terminating glaciers in the study area. The coverage of high-resolution satellite imagery shown in Figure 7 is marked on velocity difference panels. Thresholds of surface slope (2˚) and surface velocity (4 m a^{1}) required for surface meltwater ponding are also marked.

Figure 4.4. Surface elevation (A), surface elevation change (dH/dT) (B), surface slope (C), surface slope change (D), surface velocity (E) and surface velocity change (F) of five lake-terminating glaciers in the study area. The coverage of high-resolution satellite imagery shown in Figure 7 is marked on velocity difference panels. Thresholds of surface slope (2˚) and surface velocity (4 m a^{1}) required for surface meltwater ponding are also marked.

Figure 4.5. Surface elevation (A), surface elevation change (dH/dT) (B), surface slope (C), surface slope change (D), surface velocity (E) and surface velocity change (F) of four lake-terminating glaciers in the study area. The coverage of high-resolution satellite imagery shown in Figure 7 is marked on velocity difference panels. Thresholds of surface slope (2˚) and surface velocity (4 m a^{1}) required for surface meltwater ponding are also marked.

Figure 4.6. A) Cumulative ice front; B) Ice front retreat rate; C) Lake area increase; and D) Lake area expansion rates for the 9 glaciers hosting lakes over the period 1989-2015.

Figure 4.7. Satellite imagery (Geoeye, Worldview) of the terminal areas of land-terminating glaciers we focus on in this study. Panels A-E are of glaciers that meet the criteria required for glacial lake formation, whereas panels F-I show glaciers that do not meet these criteria.

Figure 5.1. The six glaciers we focus on in this study, and the extent of the DEM datasets. WV-DEM coverage is complete for the entire study area and is therefore not shown on the figure. Background image is a RapidEye scene captured in April 2015.

Figure 5.2. An example of the SMR metric classes over the terminal regions of Lhotse, Lhotse Nup and Ama Dablam glaciers, and a RapidEye (left) scene of the same area (17th Nov. 2017).

Figure 5.3. The difference in surface elevation calculated by differencing the AP-DEM (1984) and WV-DEMs (2015/16). Inset shows the subset area covered by SfM-MVS DEMs in Figures 4 & 9.

Figure 5.4. Glacier surface elevation profiles taken from AP- and WV-DEMs. Semi-transparent lines are flow-parallel surface elevation profiles spaced 100 m apart across each glaciers surface, and the opaque elevation profiles represent a mean of flowline-parallel profiles. Locations of debris covered- clean ice transition are also shown.

Figure 5.5. The difference in surface elevation between the WV-DEM (Jan 2015) and SfM-DEMs acquired in October 2015, May 2016 and May 2017.

Figure 5.6. The percentage of glacier surface area made up of different classes of topography distinguished by the sum of negative elevation differences in a local (8 pixel) area for Khumbu and Lhotse Nup glaciers. Also shown is the change in the area covered by different topographic classes over the period 1984-2015/16. SMR_{75} (A) represents gently undulating, debris covered glacier surfaces, $SMR_{75\text{-}125}$ (B) represents debris covered areas of sufficient slope to allow debris slumping, $SMR_{125\text{-}175}$ (c) represents ice cliff flanks & SMR_{175} (D) represents ice cliff faces.

Figure 5.7. The percentage of glacier surface area made up of different classes of topography distinguished by the sum of negative elevation differences in a local (8 pixel) area for Lhotse and Ama Dablam glaciers. Also shown is the change in the area covered by different topographic classes over the period 1984-2015/16. SMR_{75} (A) represents gently undulating, debris covered glacier surfaces, $SMR_{75\text{-}125}$ (B) represents debris covered areas of

sufficient slope to allow debris slumping, $SMR_{125-175}$ (c) represents ice cliff flanks & SMR_{175} (D) represents ice cliff faces.

Figure 5.8. The percentage of glacier surface area made up of different classes of topography distinguished by the sum of negative elevation differences in a local (8 pixel) area for Lhotse Shar and Imja glaciers. Also shown is the change in the area covered by different topographic classes over the period 1984-2015/16. SMR_{75} (A) represents gently undulating, debris covered glacier surfaces, SMR_{75-125} (B) represents debris covered areas of sufficient slope to allow debris slumping, $SMR_{125-175}$ (c) represents ice cliff flanks & SMR_{175} (D) represents ice cliff faces.

Figure 5.9. Supraglacial pond area mapped using the AP-DEM and data from Watson et al. (2016, 2018 in review)

Figure 5.10. SMR metric scores generated using the WV-DEM over the lower reaches of Khumbu glacier in Janurary 2015 (A) and May 2017 (B). Panel C shows the difference in metric scores between these two time periods.

Figure 5.11. The terminal areas of Lhotse (foreground), Lhotse Nup (middle) and Nuptse (farthest) glaciers. Nuptse glacier (not included in morphometric analyses) and Lhotse Nup glaciers have prominent terminal moraines and decoupled supraglacial-proglacial hydrological systems. Lhotse glacier is lacking a distinct terminal moraine and therefore has a linked supraglacial-proglacial hydrological system.

Supplementary Figure 1. Elevation differences for stable ground (off-glacier) between SETSM and SRTM DEMs, plotted against elevation. There is no clear relationship between DEM differences and increasing/ decreasing elevation (often labelled an elevation dependent bias).

Supplementary Figure 2. Elevation differences between the SRTM and SETSM DEMs over stable ground away from glacier surfaces.

Supplementary Figure 3. An example of flowline data extracted from DEM (A) and glacier velocity difference (B) datasets. Semi-transparent elevation and velocity profiles in panels C and D represent different flow parallel profiles taken across the glacier surface (spaced apart by 100 m), with the bold profile representing the mean surface elevation or surface velocity profile from each time period.

Supplementary Figure 4. The variability of estimates of glacier surface slope depending on

different bin lengths for Lhotse glacier. Semi-transparent elevation profiles represent different flow parallel profiles taken across the glacier surface, with the bold red profile representing the mean surface elevation profile.

Supplementary Figure 5. DEM hillshades generated from SETSM (2014/2015) data and ice front positions of the nine lake-terminating glaciers between 1989 and 2015.

Supplementary Figure 6. Comparison of SumNeg metrics generated using different window sizes over an area of the Khumbu glacier hosting numerous ice cliffs (A). B) 4 cell diameter window, C) an 8 cell diameter and, D) a 16 cell diameter moving window. The surface topography and SMR profiles shown in Supplementary Figure 7 were taken from X to X'.

Supplementary Figure 7. A) Surface elevation profile taken along the X – X' profile shown in Figure S1. B) The variability in SumNeg values taken along the X – X' profile depending on window diameter.

Supplementary Figure 8. Comparison of metric class prevalence off-glacier. Analyses has been limited to areas of surface slope of less than 15° to limit the impact of spurious data caused by topographic shading or poor image quality.

List of abbreviations

AAR- Accumulation Area Ratio

ALOS- Advanced Land Observing Satellite

ASTER- Advanced Spaceborne Thermal Emission and Reflection Radiometer

DEM- Digital Elevation Model

ENVI- Environment for Visualising Images

ELA- Equilibrium Line Altitude

EGM- Earth Gravitational Model

ETM+- Enhanced Thematic Mapper plus

GCP- Ground Control Point

GLIMS- Global Land Ice Measurements from Space

GLOF- Glacial Lake Outburst Flood

GNSS- Global Navigation Satellite System

GRMSE- Geometric Root Mean Square Error

HI- Hypsometric Index

HKKH- Hindu Kush Karakoram Himalaya

ICIMOD- International Centre for Integrated Mountain Development

IPCC- Intergovernmental Panel on Climate Change

LGM- Last Glacial Maximum

LIA- Little Ice Age

NDWI- Normalised Difference Water Index

OLI- Operational Land Imager

OBIA- Object Based Image Analyses

RCP- Rational Coefficient Pathways

RGI- Randolph Glacier Inventory

RMS- Root Mean Squared

SETSM- Surface Extraction with TIN-based Search-space Minimization

SfM-MVS- Structure from Motion Multi View Stereo

SRTM- Shuttle Radar Topographic Mission

TopCAT- Topographic Point Cloud Analysis Toolkit

TM- Thematic Mapper

TIN- Triangular Irregular Network

USGS- United States Geological Service

WGMS- World Glacier Monitoring Service

Chapter 1

1. Introduction

The Himalaya contains more than 20,000 glaciers (Frey et al., 2014) which store between 2955 and 4737 km^3 of glacial ice. As with other glaciers around the world, the mass balance of Himalayan glaciers is predominantly negative, and has been for several decades (Bolch et al., 2011; Maurer et al., 2016; Robson et al., 2018). A plethora of research has been conducted to assess the current state, and potential fate of glaciers in the region. Cryospheric research in the Himalaya is motivated by a requirement to understand the potential meltwater yield of the region's ice bodies into the future (Immzerzeel et al., 2010); because of the threat posed by GLOFs (Rounce et al., 2017); and because mountain glaciers are currently a majority contributor to sea level rise (Radic and Hock., 2011).

An abundance of recent research has a identified a broad longitudinal gradient in the levels of mass loss from Himalayan glaciers (Gardelle et al., 2013; Gardner et al., 2014; Brun et al., 2017). Glaciers of the Karakoram have remained in balance since the 1970s (Bolch et al., 2017; Zhou et al., 2018), most probably because of a contrast in the dominant climatic regime (westerly flow) in this region compared to the rest of the Himalaya. Further east, towards Nepal, the Bhutan and Hengduan Shan, glacier mass balance is more negative, and glaciers here have been losing ice since at least the 1970s (Pellicciotti et al., 2015; Maurer et al., 2016; Robson et al., 2018). The prolonged mass loss from glaciers served by the Indian monsoon in the central and eastern Himalaya has been attributed to long-term air temperature increases (Shrestha et al., 1999), reductions in the intensity of the monsoon, and therefore reductions in snow and ice accumulation (Bollasina et al., 2011), and changes in precipitation phase (Bhutiyana et al., 2010).

Although large-scale geodetic studies (e.g. Brun et al., 2017) have revealed important trends in mass loss across the Himalaya, their regional averaging of ice loss data has masked any inter-, intra-catchment, or glacier terminus type variability in mass loss rates, thus our knowledge of factors that might serve to amplify glacier mass loss rates in the future in the Himalaya remains somewhat limited. In other glacierised regions of the world, ice mass loss rates from marine- and lake-terminating glaciers have been shown to be elevated above their land-terminating counterparts (Willis et al., 2012; McNabb and Hock, 2014; Melkonian et al., 2016; Truffer and Motyka, 2016; Tsutaki et al., 2016). As there are now nearly 5000 glacial lakes in the Himalaya (Nie et al., 2017), an assessment of the impact of glacial lake development on their host glaciers is needed and currently poorly quantified.

The comparability of Himalayan debris cover mass balance with clean ice glaciers elsewhere (Pellicciotti et al., 2015; Vincent et al., 2016), despite the insulating effect of extensive, thick debris mantles that should inhibit substantial surface melt (Østrem, 1959; Nicholson and Benn, 2006), suggests the presence of processes at the glacier scale that may be amplifying melt. Recent studies have shown that ice cliff and supraglacial pond network development may be responsible for large portions of ice loss in debris mantled areas, despite these features commonly occupying <10% of the glacier surface. The spread of such features, which has been documented in different studies in the central Himalaya (Miles et al., 2016; Watson et al., 2016, 2017), has certainly had an impact on the morphometry of glacier surfaces, but assessments of glacier surface topography change are lacking. A clear understanding of glacier surface morphometry change is important because of its links to supraglacial hydrology (Irvine-Fynn et al., 2017) and glacier surface energy balance, and therefore melt modelling (Rounce et al., 2016).

This thesis focusses on, 1) assessing the impact of glacial lake growth on the mass balance and dynamics of a lakes host glacier, and 2) examining the impact of prolonged ice loss and debris deposition on the morphological characteristics of glacier surfaces. Temporally extensive remotely sensed datasets have been combined with short-term field-based measurements to study glacier evolution, to improve our understanding of glacier evolution in the central Himalaya.

1.1 The evolution of debris covered glaciers

Debris covered glaciers are prevalent in the Himalaya because the heightened weathering rates of mountains within tectonically-active landscapes of extreme altitude and relief provides an amplified flux of debris to valley floors and glacier surfaces. Due to similar conditions, clusters of debris covered glaciers also exist in the Patagonia (Glasser et al., 2016), New Zealand (Quincey et al., 2009), the European Alps (Berthier et al., 2016), the Canadian High Arctic (Mattson, 2000), Iceland (Spedding, 2000) and Alaska (Kienholz et al., 2015). Approximately 23% of the total glacier area in the Himalaya is debris covered (Scherler et al., 2011), although this proportion varies substantially between regions. In the Everest region, approximately 32% of the glacierised area is debris covered, but the concentration of this debris cover in glacier ablation zones increases its importance in glacier mass loss processes. The total debris covered glacier area has increased in recent decades in the Everest region; Thakuri et al. (2014) showed a 13 ± 3.1% increase in debris cover over the period 1962-2011. The presence of a debris mantle at the surface of a glacier impacts on the surface melt regime because of the non-linear relationship between debris thickness and sub-debris melt. A thin (<2-3 cm) layer of debris enhances melt rates in

comparison to clean ice because of its lower albedo, thus it preferentially absorbs and efficiently transfers incident solar radiation to the ice surface below. When debris layers exceed approximately 5 cm in thickness, levels of sub-debris melt begin to decline below those of clean ice (Østrem, 1959; Nicholson and Benn, 2006; Reznichenko et al., 2010) because energy absorbed at the surface of the debris layer dissipates within the debris mantle, rather than being quickly transferred to the ice below. Debris layers of >~40 cm thickness may not transmit enough energy to allow for any surface melt. As debris thicknesses generally increase down-glacier, a gradient of surface lowering is often evident on debris covered glaciers, with maximum surface lowering rates occurring mid-glacier, close to the debris covered to clean ice transition zone, as opposed to at the terminus of clean-ice glaciers.

The reversed gradient of surface lowering present on debris-covered glaciers reduces the longitudinal surface slope over their ablation zones, and, in combination with sustained thinning, lower surface gradients lead to driving stress reductions and therefore slower flow (Quincey et al., 2009; Benn et al., 2012). Stagnant debris covered tongues have been documented in many regions of the central Himalaya (Quincey et al., 2009; Ragettli et al., 2016; Robson et al., 2018) and it is not uncommon for the lowermost several kilometres of large debris covered glaciers to display negligible flow. Meltwater ponds readily form on low slope areas of debris covered glaciers, and the limited ice motion precludes the formation of crevasses to aid supraglacial meltwater drainage or rerouting (Quincey et al., 2007). Supraglacial pond area can increase rapidly over relatively short timescales (Watson et al., 2016), and their absorption of incident solar radiation leads to enhanced supraglacial (Thompson et al., 2016; Watson et al., 2017b) and englacial ice loss (Miles et al., 2016). Where surface lowering has been sufficient to allow supraglacial ponding at the hydrological base level of a glacier (the elevation at which water leaves the glacier), ponds often coalescence behind a glacier's terminal moraine to initiate the growth of a glacial lake that may expand several kilometres up-glacier, should the moraine remain intact (Hambrey et al., 2008). Benn et al. (2012) consider the growth of a glacial lake to be the final scenario of debris covered glacier retreat, should the supraglacial and proglacial hydrological networks remain disconnected by a terminal moraine, thus the number of potentially hazardous glacial lakes may increase given continued glacier recession in the Himalaya.

1.2 Glacier-lake interactions

The number of new, and area of pre-existing glacial lakes have both increased in recent decades in many glacierised regions. Across the Himalaya, the number and total area of glacial lakes increased by 9 and 14%, respectively, over the period 1990-2015 (Nie et al.,

2017). In the Central Andes, Northern Patagonia and Southern Patagonia, the number and area of glacial lakes increased by 43 & 7%, respectively, over the period 1986-2016 (Wilson et al., 2018). Large glacial lakes are also common at the periphery of Alaskan icefields (e.g. Trussel et al., 2013; Boyce et al., 2007), many of which occupy overdeepenings formed during the LIA. Smaller populations of expanding glacial lakes can also be found in New Zealand (e.g. Warren and Kirkbride, 2003; Allen et al., 2008; Chinn et al., 2012), British Columbia (Koch et al., 2009; Chernos et al., 2016), and the European Alps (Paul et al., 2007).

Lake-terminating glacier area losses in response to lake expansion are typically elevated above the area loss of neighbouring land-terminating glaciers. Basnett et al. (2013) and Wang et al. (2017) compared lake- and land-terminating glacier area changes in the Sikkim Himalaya and the Hengduan Shan of the Indian Himalaya and southeastern Tibetan Plateau, and found 5-6 times greater glacier area loss on lake-terminating glaciers compared to neighbouring land-terminating glaciers (both over the period 1990-2014). Davies and Glasser (2012) calculated glacier area loss rates for the Southern Patagonian Icefield over the period 1870-2011 and showed both higher and lower retreat rates for lake-terminating glaciers when compared with land-terminating glaciers, highlighting non-linear responses to external forcing and bedrock topography as controlling factors in their total area loss. Chinn (1996) estimated a 24% reduction in land-terminating glacier area in New Zealand since the Little Ice Age (LIA) (until 1995), although Chinn (1996) estimates a higher (41%) mean area loss for land-terminating glaciers over the same time period. More recent studies (Allen et al., 2008; Quincey and Glasser, 2009) have shown dramatic, contemporary lake-terminating glacier retreat in New Zealand.

Lake-terminating glaciers lose more ice at their terminus than the rest of their ablation zones because of the impact of both calving and subaqueous melt. Depending on the setting, either of these melt components can be the dominant factor in ice front retreat in both space and time (Truffer and Motyka, 2016). The magnitude of subaqueous melt primarily depends on the temperature and salinity of the water body a glacier flows into. Small, proglacial lakes are much cooler than coastal, marine water (Chikita, 2007; Truffer and Motyka, 2016), and there is typically negligible density contrast between glacial meltwater and that of a proglacial lake to drive circulation, although wind may drive some near-surface circulation (Sakai et al., 2009). Although of limited number, studies of Himalayan glacial lake temperature have observed low water temperatures (2-3˚C) and typically only a very limited (top 20 m) surface layer of warmer (3-6˚C) and so subaqueous melt over the entirety of a lake-terminating glaciers ice front may not be a substantial contributing factor to ice front retreat on Himalayan glacial lakes. On the other hand, calving driven ice front retreat has

been shown to be rapid on lake-terminating glaciers in the Himalaya (Sakai et al., 2009), driven mainly by the level of thermal notch cutting that does occur in the warmer surface layer of glacial lakes (Warren and Kirkbride, 2003). Sakai et al. (2009) suggested that ice cliff calving can occur once the fetch of a glacial lake exceeds just 80 m, thus calving retreat can occur from the early stages of glacial lake growth.

Ice mass loss rates can be severe from lake-terminating glaciers. Chinn et al. (2012) calculated that more than two thirds of the total ice mass loss of glaciers located in the Southern Alps of New Zealand had occurred on just 12 glaciers due to calving and terminus-proximal surface lowering, from 1976-2008. Tsutaki et al. (2016) showed mean elevation change rates of the lake-terminating Bowdoin glacier (northwest Greenland) to be 1.5 times higher than the neighbouring, land-terminating, Tugto glacier. Larsen et al. (2015) showed consistently high (>3 m a^{-1}) surface lowering rates in the terminal regions of 32 Alaskan lake-terminating glaciers, especially where large proglacial lakes have developed behind LIA moraines. Larsen et al. (2007, 2015) show that, in Alaska, lake-terminating glaciers contribute a greater portion of the total ice mass loss budget than tidewater-terminating glaciers, despite previous studies (see van der Veen, 2002 and references within) showing calving rates to be higher on marine terminating glaciers rather than lake-terminating glaciers. Willis et al. (2012) showed that the thinning of only a few land-terminating glaciers on the eastern side of the Southern Patagonian icefield accounted for ~40% of the total ice loss budget of the entire icefield. In complete contrast, Willis et al. (2012) showed how Pio-Xi glacier, also located in the Southern Patagonian icefield, but on the western side, advanced and thickened (+2.4 ± 0.4 m a^{-1}) over the same period 2000-2012.

Ice flow fields are also heavily altered by the presence of a glacial lake. Flow velocities peak at the calving front of lake-terminating glaciers, and can reach values of several hundreds of metres per year (Melkonian et al., 2016). Again, ice flow has been found to be amplified above neighbouring, land-terminating glaciers (Burgess et al., 2013; Melkonian et al., 2016), especially when compared to effectively stagnant, debris covered, land-terminating glaciers. The evolution of flow velocities on lake-terminating glaciers seems spatially and temporally complex. Melkonian et al. (2016) showed the substantial acceleration of three lake-terminating glaciers at the periphery of the Stikine icefield, but also identified one lake-terminating glacier in the same study area which slowed down over the same study period. Mouginot and Rignot (2015) detected a doubling of ice flow rates on Glaciar Upsala (Southern Patagonian Icefield) from 1985 to 2001, then a 20% decrease in velocity between 2001 and 2005, and a 50% increase in flow between 2005 and 2010.

Mouginot and Rignot (2015) also showed a steady decrease in ice flow on Glaciar O'Higgins, located approximately 100 km north of Glaciar Uppsala, from 1985 to 2015.

The variable mass loss intensity and the divergent ice velocity changes that have been detected on lake-terminating glaciers suggest that dynamic instabilities may operate on some, but not necessarily all glaciers that develop large glacial lakes. Larsen et al. (2015) suggest that the presence of large proglacial lakes that occupy substantial glacier overdeepenings may lead to a geometry that is more akin to tidewater glaciers, thus similar feedbacks may operate to induce front retreat and ice loss. The duration and magnitude of ice loss from land-terminating glaciers therefore depends on the size of each glaciers overdeepening, with glaciers only reaching equilibrium once the terminus can retreat to an altitude above the lake they host.

Few observations of lake-terminating glacier behaviour exist for Himalayan glaciers. Thakuri et al. (2016) quantified glacier thinning rates and glacier velocities for Imja Tsho glacier in the Everest region of the central Himalaya. They showed increased surface lowering rates over the lower reaches of the glacier between 2001 and 2014, but decreased surface velocities between 1992 and 2014, suggesting that decreased accumulation might be driving the observed changes. Quincey et al. (2009) measured high surface velocities (25 m a^{-1} or more) over Yanong glacier (their Figure 4, panel D), with neighbouring, land-terminating, debris-covered glaciers stagnant over much of their lower reaches. Maurer et al. (2016) compared glacier mass balance estimates for clean ice, land-terminating & debris covered, lake- and land-terminating glaciers in the Bhutan Himalaya over the period 1974-2006. Maurer et al. (2016) calculated that clean ice glaciers lost ice at a rate of –0.13 ± 0.06 m w.e.a^{-1}, debris covered, land-terminating glaciers lost ice at a rate of –0.19 ± 0.11 m w.e.a^{-1} and lake-terminating glaciers at a rate of –0.28 ± 0.11 m w.e.a^{-1}.

1.3 Societal implications of lake growth

Glacial lakes are equally prevalent on both sides of the Himalayan orographic divide (Nie et al., 2017), thus the potential GLOF threat is equally as pertinent to downstream communities in Tibet as it is in Nepal, Bhutan or northern India. The population density on the southern flank of the Himalaya is much higher, however, thus levels of infrastructure investment (primarily hydropower) arguably increases the vulnerability to flood risk here. Carrivick and Tweed (2016) compiled a record of 216 GLOF events from 78 sites in central Asia, and rank the region as the most susceptible in a damage index considering recorded deaths, property and infrastructure destruction and evacuations. GLOF risk assessment is a difficult task, and many different frameworks (e.g. Rounce et al., 2017) have been proposed

that have attempted to assess the importance and likelihood of the various potential GLOF trigger mechanisms (see Westoby et al., 2014), along with the likely path and magnitude of released floods. Ultimately, the distal nature of glacial lakes and the multitude of factors that may cause a GLOF makes the regular monitoring of glacial lakes and their surroundings impractical, and remediation efforts (lake lowering) have recently been preferred to decrease GLOF risk. Imja Tsho (in the Everest region) was lowered by 3 m in 2016, and Tsho Rolpa was lowered by 3 m in 2016 (Watson, 2017c).

The Everest region seems particularly prone to GLOFs. The floods produced by Nare Lake in 1977 (Buchroithner et al. 1982), Sabai Tsho in 1988 (Osti et al., 2011), Chubung Tsho in 1991 (Reynolds et al., 1999) and Dig Tsho in 1985 (Vuichard and Zimmerman, 1987) had far reaching impacts in the Dudh Koshi and Tama Koshi catchments, including the loss of life and damage to households, hydropower and infrastructure. A number of other glacial lakes have been identified as being potentially hazardous in the Everest region (including the Dudh Koshi and Tama Koshi catchments). Rounce et al. (2017) examined 56 lakes in this area and identified 10 as being 'very high hazard'. Rounce et al. (2017) consider this type of lake to be vulnerable to avalanches, bound by an unstable terminal moraine and capable of inundating more than 20 buildings downstream. In a broader assessment, ICIMOD (2011) identified 21 critically hazardous (out of 1466) glacial lakes in Nepal, six of which they classified as high priority, requiring detailed field based examination and monitoring. The ability of glacial lakes to expand rapidly over short time periods (Nie et al., 2017; Song et al., 2017) makes the investigation of the link between lake expansion and glacier behaviour pertinent, particularly in a climate that continues to warm (Shrestha et al., 1999).

1.4 Debris covered glacier surface processes

Ice cliffs and supraglacial ponds are ubiquitous features on debris covered glaciers. A single debris covered glacier may be covered in hundreds of each feature (Watson et al., 2016, 2017), with each cliff varying in size, aspect and slope, and each pond varying in size, temperature, turbidity and hydrological connectivity (Watson et al., 2016; 2018). Watson et al. (2016) suggest an area limit of 20,000 m^2 for supraglacial ponds, thus larger water bodies are considered as glacial lakes. The substantial ablative role of supraglacial pond and ice cliff network expansion has long been recognised on debris covered glaciers. Many studies have identified the amplified backwasting rates of individual ice cliffs (Sakai et al., 2000) or the contribution of ice cliff and supraglacial pond networks to the overall mass loss budget of the ablation zone of different debris covered glaciers (Immerzeel et al., 2014; Thompson et al., 2016).

Estimates of the contribution of ice cliff and pond-related melt to the overall ice loss budget have varied from glacier to glacier and by the method used to estimate ice loss. Through differencing high resolution (2m) DEMs, Thompson et al. (2016) estimated that ice cliffs and supraglacial ponds covered ~5% of the stagnant area of Ngozumpa glacier, but their retreat accounted for 40% of the total volume loss of the subset of the glacier they studied. Buri et al. (2016a) applied a physically based 3-D model of ice cliff evolution to simulate the evolution of four ice cliffs on Lirung glacier, and found that, despite occupying just 0.19% of the glacier surface area, these four cliffs were responsible for 3.25% of the total sub-debris melt. Similarly, Buri et al., (2016b) applied an alternative, grid-based model of cliff evolution to simulate the behaviour of two heavily instrumented cliffs on Lirung glacier, and suggested that, despite occupying just 0.09% of the glacier tongue area, their retreat accounted for 1.23% of total melt from the glacier tongue. In contrast, Sakai et al. (1998) estimated that ice cliffs covering 1.8% of the area of Lirung glacier could account for 69% of the total ice mass loss of the glacier. This variability in melt estimates perhaps reflects the range in size and aspect of studied cliffs, and their ability to retreat at variable rates through a melt season (Watson et al., 2017b); nonetheless they are obviously an important feature in the evolution of debris covered glaciers. The quantification of surface melt processes such as ice cliff retreat and supraglacial pond expansion is a vital step in the improvement of any model that could accurately quantify debris covered glacier evolution (Shea et al., 2015; Rowan et al., 2015).

The multi-temporal documentation of ice cliff extent and density carried out by Watson et al. (2017a, b) for several glaciers in the Everest region showed how ice cliff networks can expand over relatively short time periods on debris covered glaciers. Of the 12 glaciers assessed by Watson et al. (2017a), seven showed up-glacier expanding ice cliff networks between 2003-2015 or 2009-2015. Aside from the substantial ablative role of ice cliff and supraglacial pond networks, their development heavily impacts on glacier surface topography and the setup of the supraglacial hydrological network. Irvine-Fynn et al. (2017) demonstrated the potential for supraglacial ponds to influence meltwater discharge on Khumbu glacier, calculating that the cascade of supraglacial ponds on Khumbu glacier are capable of a minimum daily storage capacity that equates to 23% of the daily discharge from the glacier. Given the trajectory of pond development on Khumbu glacier (Watson et al., 2016), and others in the Everest region (Watson et al., 2016), this estimate may serve as a lower bound of any estimate of discharge buffering in the future, complicating predictions of freshwater availability in the broader regions.

A less well studied aspect of ice cliff and pond expansion is their impact on glacier surface topography and morphometry. Ice cliff backwasting and pond expansion related calving

should develop a more rugged, pitted glacier surface topography, but not all cliffs develop into sheer faces (Watson et al., 2017b); some may backwaste and develop a shallower angle, eventually becoming inundated with slumped debris. Debris slumping from unstable lateral moraines may also serve to infill surface depressions on a debris covered glacier, but only at its periphery. It is important that the topographic evolution of glacier surfaces is well understood because of the link between glacier topography and the turbulent heat fluxes (Rippin et al., 2015; Brock et al., 2006), thus glacier topography change can directly influence the energy available for ice melt. Energy balance models designed to be applied to debris covered glaciers (e.g. Rounce et al., 2015) do generally account for variability in surface topography by using a range of roughness values, but these may be inappropriate should surface topography characteristics vary substantially across or along a debris covered glacier, rather than the entire surface being characterised by one tighter range of roughness values determined locally (Quincey et al., 2017).

1.5 Study region

The Everest region is arguably the best studied glaciated region in the Himalaya. The topographic surveys of Edwin Schneider were undertaken in the region as early as the 1950's, alongside the pioneering expeditions to the Khumbu valley and, ultimately, the summit of Mount Everest. Field based glaciological research was undertaken in the region as early as the 1980s (e.g. Nakawo et al., 1986), and the timeline of studies examining glacier change and glacier processes in operation in the area has remained unbroken to the present day.

The glaciers of the Everest region can be grouped into three main categories:

1) Debris covered glaciers flowing down from mountain massifs such as Everest, Lhotse, Cho Oyu and Makalu (all >8000 m a.s.l.) that terminate on land and account for the greatest portion of glacierised area in the region. These glaciers have debris covered tongues of variable length, ranging from 1-2 km beneath steep headwalls, to more than 10 km long when glaciers are fed by broad, high-altitude accumulation zones. These debris covered glaciers are flanked by large Little Ice Age (LIA) moraines, the crests of which may be greater than 100 m above current glacier surface elevation. The thickness of debris layers varies from a few centimetres to several metres in thickness in terminus proximal areas (Nakawo et al., 1986; 1999).

2) Lake-terminating glaciers of variable size (3-12 km) and surface cover (0-100% debris mantled). The area of the lakes each glacier hosts is equally as broad, varying from less than 1 km^2 (numerous) to nearly 4 km^2 (Tsho Rolpa). The majority of the glacial lakes in the

region are proglacial (n = 56 >0.1 km^2 from Rounce et al., 2017), although large supraglacial lakes have developed in the last 20-30 years on Rongbuk and Drogpa Nagtsang glaciers. Satellite era data (first acquired in the early 1960s) shows how many of the now proglacial lakes were first supraglacial, with up- and down-glacier supraglacial pond coalescence responsible for lake area gain in the past 5 decades (Gardelle et al., 2011).

3) Numerous smaller (< ~4 km^2) glaciers devoid of debris cover located at high elevation (>5000 m a.s.l.), mostly north of the orographic divide. These glaciers have shown limited front retreat or surface lowering in recent decades, and typically do not host glacial lakes.

Previous work on glaciers of the Everest region has been diverse. Glacier area change studies (e.g. Thakuri et al., 2014) have shown little front retreat of debris covered glaciers, due to the insulating effect of thick debris mantles in terminus proximal areas, since the 1960's. Assessments of lake-terminating glacier retreat rates have been more selective. Somos-Valenzuela et al. (2014) measured a front retreat rate of 43.0 m yr^{-1} over the period 1992-2012 for Imja-Lhotse Shar glacier as a result of the expansion of Imja Tsho glacial lake (1.26 km^2 in 2012). Geodetic mass balance studies have shown widespread surface lowering and glacier mass loss since at least the 1970s in the Everest region (Bolch et al., 2011). Regionally averaged estimates of glacier mass loss (Nuimura et al., 2008; Gardelle et al., 2013; Li et al., 2018) covering comparable periods (1999-2011) have yielded mass balance estimates ranging from –0.26 ±0.14 m $w.e.a^{-1}$ (Gardelle et al., 2013) to –0.38 ± 0.04 $m.w.e.a^{-1}$ (Li et al., 2018), which is slightly below the global average of glacier mass balance (WGMS, 2017). Bolch et al. (2011) showed accelerated mass loss rates since the 1970s. Bolch et al. (2011) estimated the mass balance of a subset of glaciers in the Khumbu and Imja valleys to be –0.32 ±0.08 m $w.e.a^{-1}$ over the period 1970-2007, but the mass balance of the same glaciers to be –0.79 ±0.52 m $w.e.a^{-1}$ over the period 2002-2007.

The prolonged mass loss of Everest region glaciers has caused large portions of debris covered areas to become stagnant or to flow very slowly. Quincey et al. (2009) quantified glacier surface velocities in the area and, of the 20 glaciers in their sample, which were all land-terminating, only one (Kangshung) showed detectable flow to its terminus, 12 showed some evidence of flow in their higher reaches, and seven showed no evidence of flow. Over stagnant areas of debris covered glacier tongues, extensive networks of supraglacial ponds and ice cliffs are common (Watson et al., 2016). The predominance of ice cliffs and the total ponded area has expanded since 2000 (Watson et al., 2016, 2017a) on a number of the larger debris covered glaciers in the region, although there is much inter-annual variability in pond area because of the impact of the monsoon on glacier surface hydrology.

Imja Tsho is the best studied of the glacial lakes found in the Everest region. It has expanded at a rate of 0.026 ± 0.001 km^2 a^{-1} since the early 1960's (Thakuri et al., 2016). It is also deepening (Chikita, 2007; Fujita et al., 2009; Somos-Valenzuela et al., 2014) close to the glacier's calving front, although the lake likely still overlies dead ice towards the glacier's terminal moraine. Thakuri et al. (2016) quantified glacier surface velocities over the land-terminating Lhotse Shar glacier, and showed active (>20 m a^{-1}) flow to the terminus of the glacier. Rounce et al. (2017) suggest that, as the lake expands up-valley, it will become more prone to avalanche impacts. Several hazard assessments (ICIMOD, 2011; Rounce et al., 2017) have identified Imja Tsho as glacial lake that may soon produce a GLOF, and this resulted in Imja Tsho being lowered by approximately 3 m in 2016 (Watson, 2017). There are 13 other glacial lakes in the Everest region that rank highly on the risk assessment of Rounce et al. (2017), and Watson et al. (2016) have suggested that Khumbu glacier may be in the early stages of lake development.

1.6 Aims and objectives

Aim: The primary aim of this thesis is to identify glaciological processes in operation in the Everest region of Nepal that may impact on glacier evolution in coming decades.

Objectives:

1. To quantify recent (2000-2015) glacier mass loss rates in the Everest region of the central Himalaya, and assess the variability in mass loss depending on glacier terminus type and glacier hypsometry.

2. To quantify and compare recent (2000-2015) changes in glacier geometry and glacier flow, depending on whether a glacier is lake- or land-terminating.

3. To examine the impact of sustained glacier mass loss on glacier surface morphometry, and to identify the surface processes driving morphometric change.

Each of the objectives listed above require the application of various methods to examine a number of different glacier attributes. The methods used, and the research questions addressed in this thesis are summarised in Table 1, below.

Table 1. The objective approach taken to achieve the main aims of this thesis.

Objective addressed	Research question	Methods used
1	Is the mass balance of lake- Vs land-terminating glaciers markedly different?	Co-register and difference DEMs from two different time periods that cover a large sample of glaciers across the Everest region
1	Is the hypsometry of glaciers contrasting at a catchment scale?	Classify glaciers based on their hypsometry
1	If hypsometry is clearly contrasting, what impact will this variability have on potential future ice loss scenarios?	Calculate current glacier AARs and estimate potential future glaciers AARs in response to future warming scenarios
2	Has the flow of glaciers of different terminus type evolved in a consistent manner in the last 15 years?	Calculate glacier velocity change datasets for lake- and land-terminating glaciers in the Everest region
2	Has the geometry of the surface of glaciers of different terminus type altered in the same way over the last 15 years?	Generate glacier surface slope data for glaciers of contrasting terminus type
2	Can glacier velocity and glacier geometry data be used in combination to predict sites of glacial lake formation?	Compare the location of coalescing glacier ponds with glacier velocity and glacier geometry data to identify conditions required for lake coalescence.

3	Can glacier surfaces be classified based on their topographic characteristics?	Generate DEMs of sufficient resolution to capture the vertical relief of different supraglacial ice facies.
3	Have the topographic characteristics of glacier surfaces changed over the last few decades of sustained ice loss?	Compare and contrast topographic classification data for different time periods and glaciers.
3	Which processes have driven topographic change on glacier surfaces over the period of sustained ice loss?	Generate and difference high spatial and temporal resolution DEMs of the ablation zone of Khumbu glacier.

Chapter 2

Summary of methods

Spatially or temporally extensive glacier change can be efficiently assessed through the examination of archives of satellite imagery, the availability and resolution of which have both increased in recent decades. The majority of the work completed towards this thesis has been based on the analyses of moderate- and high-resolution optical satellite imagery, aerial photographs and terrestrial photographs. Various methods were used to generate the glacier mass balance, glacier geometry, glacier morphometry and glacier retreat rate data used to address the research questions outlined in section 1.6. The methods used to generate such primary datasets are briefly described below, with more detailed descriptions and additional analyses of secondary datasets described in detail in chapters 3, 4 and 5.

2.1 Glacier surface lowering and mass balance (Chapter 3)

Glacier mass balance studies derive and compare net mass loss and gain over an entire glacier surface during a given time period. There are three main methods of deriving glacier mass balance; the field-based glaciological method, the hydrological method, and the geodetic method (Cox and March, 2004). The geodetic approach was followed in this work, which involves glacier wide surface elevation comparisons, typically with multi-epoch digital elevation models (DEMs). The differencing of glacier surface DEMs on a pixel by pixel basis and the subsequent multiplication of elevation differences by pixel area yields estimates of volumetric changes over the study period. This volume change can then be converted to mass change, a more relevant quantity for climate impact assessments of sea level rise contributions and mountain hydrology, through the multiplication with the density of glacier/ firn ice (Huss, 2013).

Two main sources of error can lead to the generation of inaccurate glacier surface elevation change and therefore geodetic mass balance data, 1) poor image quality or contrast that leads to the generation of spurious surface elevation data points, and 2) misalignment of sequential DEMs that leads to the differencing of data of incorrect geolocation. Errors due to DEM misalignment may occur because of horizontal offsets between DEMs, vertical offsets between DEMs, vertical offsets along a gradient in x and y directions, or all three. The abundance of imagery available in satellite archives often circumvents the first issue, with the repeat capture nature of contemporary satellite missions increasing the chances of glaciers being imaged when ground and meteorological conditions are appropriate. To prevent the production of erroneous difference data over glacier surfaces through the

subtraction of DEMs with inconsistent geolocation, the methods of Nuth and Kääb (2011) were followed to co-register DEMs with inadequate horizontal coregistration. These methods are based on the relationship between elevation differences and the derivatives of slope and aspect of two misaligned DEMs, where the magnitude of the elevation differences are directly related to the shift vectors required to eliminate the bias. Only areas of DEMs that can be realistically assumed to have been stable over the time separating the acquisition dates of scenes are used to derive offset vectors. An example of pre- and post-coregistration difference data are shown in Figure 2.1.

Vertical offsets along a gradient in x or y directions, (put more simply- DEM tilts), are common when differencing DEMs produced from different optical sensors, likely because of the different satellite geometry models used in each case. Tilts were removed from DEMs using regression (either linear or higher order polynomial) models fitted through DEM difference data in cross or along track directions, depending on the direction of the tilt. An example of DEM difference data before and after de-tilting is also shown in Figure 2.1.

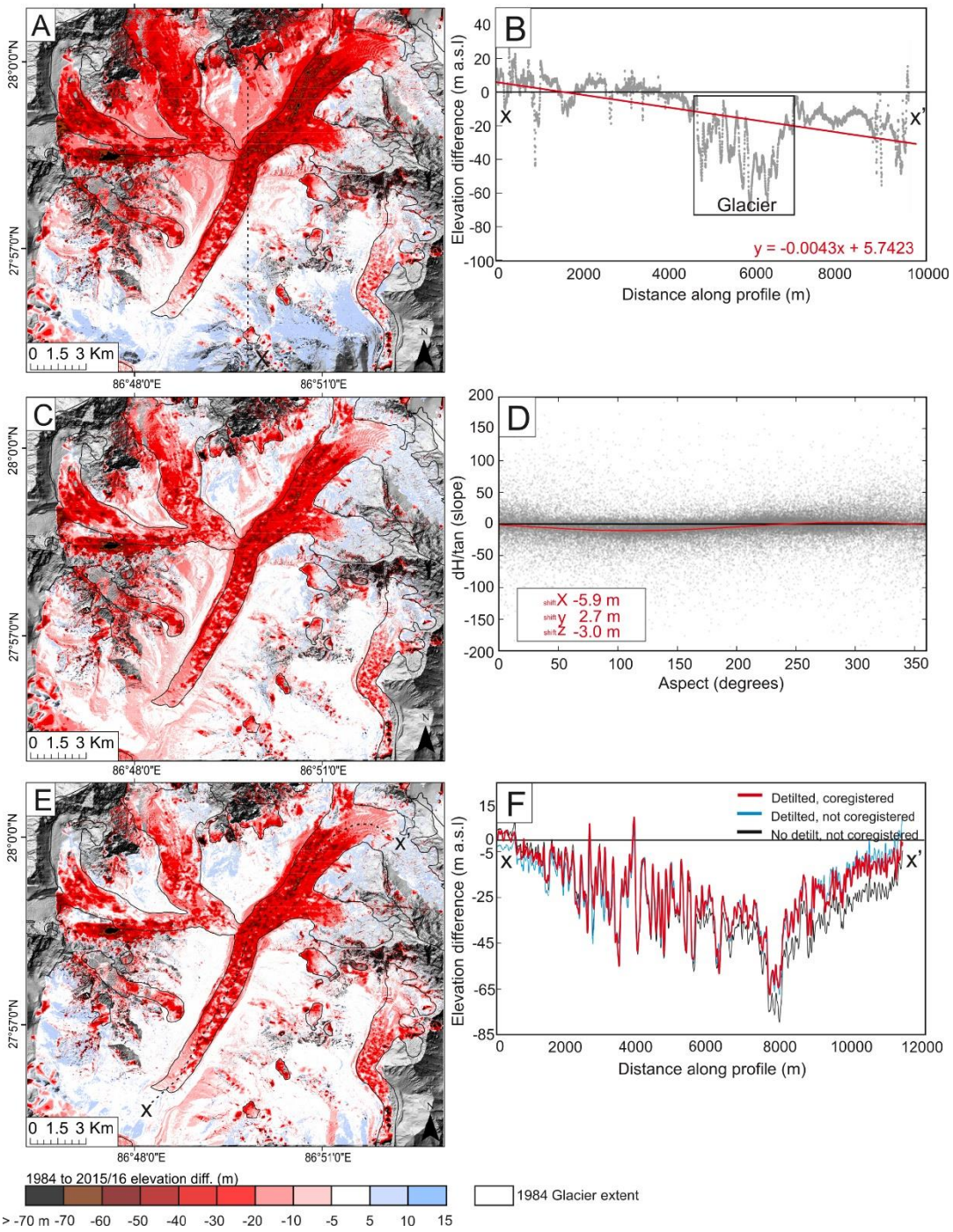

Figure 2.1. An example of the de-tilting and co-registration of a 1984 DEM of the Khumbu valley generated from aerial photographs. A) Initial differences between the 1984 DEM and a 2015 DEM generated from WorldView imagery, B) Linear trend fitted to off-glacier difference data in the along track direction, C) DEM difference data following detilting, but prior to horizontal and vertical DEM coregistration, D) The relationship between the derivatives of slope and aspect along with the shift vectors calculated from the amplitude of the slope-aspect relationship, E) DEM difference data following detilting and coregistration, and F) glacier centreline surface elevation difference profiles following each step of bias removal.

Both the detilting and coregistration processes require an iterative approach to minimise off-glacier terrain differences between DEMs. The detilting process was repeated until no visible trend was apparent in difference data in either along or cross track directions. The coregistration process was repeated until the improvement in the standard deviation of off-glacier terrain differences was less than 2%, as suggested by Nuth and Kääb (2011). The minimum and maximum elevation differences considered in the calculation of shift vectors were reduced by 10 m for each coregistration iteration to ensure a more refined adjustment at each iteration.

Following DEM coregistration, glacier surface elevation change data were filtered using threshold values of <30 & >-100 m, which was assumed to eliminate spurious data not representative of actual glacier surface elevation change. In several cases, data gaps were present over glacier surfaces, particularly in accumulation zones where snow cover resulted in poor contrast in optical satellite imagery (WorldView 1, 2 and 3) used to generate SETSM DEMs. As the geodetic approach requires the calculation of mass loss over the entire glacier surface, data gaps were filled with median values of elevation change derived from the same 100 m elevation band (over the glacier surface) in which the data gap was situated. A conversion factor of 850 kg m^{-3} was used to account for the density of glacier ice for all glaciers (Huss, 2013).

2.2 Glacier geometry and attributes (chapters 3 and 4)

Glacier hypsometry, the distribution of glacier area with altitude, was assessed using Randolph Glacier Inventory (RGI) version 5.0 glacier outlines and co-registered, detilted DEMs. In the case of the work presented in chapter 3, this was the SETSM DEMs, which had been coregistered to the SRTM DEM. Glacier extents were split into segments covering 100 m elevation range bands, and the area of each segment calculated, allowing a hypsometric curve to be generated for each glacier in each of the three catchments studied (Figures 3.5 and 3.6). Glacier hypsometry is governed by valley shape, relief and ice-volume distributions (Jiskoot et al., 2009), so it may be highly variable across and between glacierised catchments. Mean area-altitude distribution curves were calculated for groups of glaciers located in different catchments to allow for an assessment of the inter-catchment contrasts in glacier properties. The hypsometric index (HI) approach of Jiskoot et al. (2009) was also followed to provide a clear classification of glacier hypsometry, where:

$$\boldsymbol{HI} = \frac{(\boldsymbol{H_{max}} - \boldsymbol{H_{med}})}{(\boldsymbol{H_{med}} - \boldsymbol{H_{min}})} \quad (1)$$

and H_{max} and H_{min} are the maximum and minimum elevations of the glacier, and H_{med} the median elevation that divides the glacier area in half (Jiskoot et al., 2009). Glaciers were

grouped into five HI categories: 1- HI < –1.5, very top heavy; 2- HI –1.2 to –1.5, top heavy; 3- HI –1.2 to 1.2, equidimensional; 4- HI 1.2 to 1.5, bottom heavy; and 5- HI > 1.5, very bottom heavy. Top heavy glaciers store more ice at higher elevation, for example in broad accumulation zones, whereas bottom heavy glaciers have small accumulation zones and long tongues. Elevation ranges were normalised to allow the direct comparison of glacier hypsometry regardless of termini elevation. The approach of Arendt et al. (2006) was followed to normalise elevation ranges:

$$\boldsymbol{H_{norm}} = \frac{(\boldsymbol{H} - \boldsymbol{H_{min}})}{(\boldsymbol{H_{max}} - \boldsymbol{H_{min}})} \quad (2)$$

where H_{min} and H_{max} are the elevations of the glacier terminus and the elevation maximum of each glacier.

Glacier surface slope was assessed using an adaptation of the method employed by Quincey et al. (2009) and Miles et al. (2017). These studies calculated glacier surface slope on a pixel by pixel basis from a point fixed at the glacier terminus (Quincey et al., 2009), or at the down-glacier end of a moving window (Miles et al., 2017). In this work, surface slope was calculated by fitting linear regression models through mean glacier surface elevation profiles calculated for 750 m long segments of each glacier (Figure 2.2). Mean surface elevation profiles were calculated as the average of parallel surface elevation profiles spaced 100 m apart across the glacier surface. An initial centreline profile was manually delineated and then buffered by 100 m to generate sets of flowline parallel surface elevation profiles. The number of flowline parallel elevation profiles used to calculate mean elevation profiles depended on glacier width, but was either 3, 5 or 7. This approach was taken using the SRTM and SETSM DEMs, to allow for the comparison of glacier surface slope change over the study period (2000-2015). This approach estimates longitudinal glacier surface slope, rather than including any component of cross-glacier slope (Quincey et al., 2007; Miles et al., 2017), which may be substantial where a glacier has developed a convex cross-glacier surface.

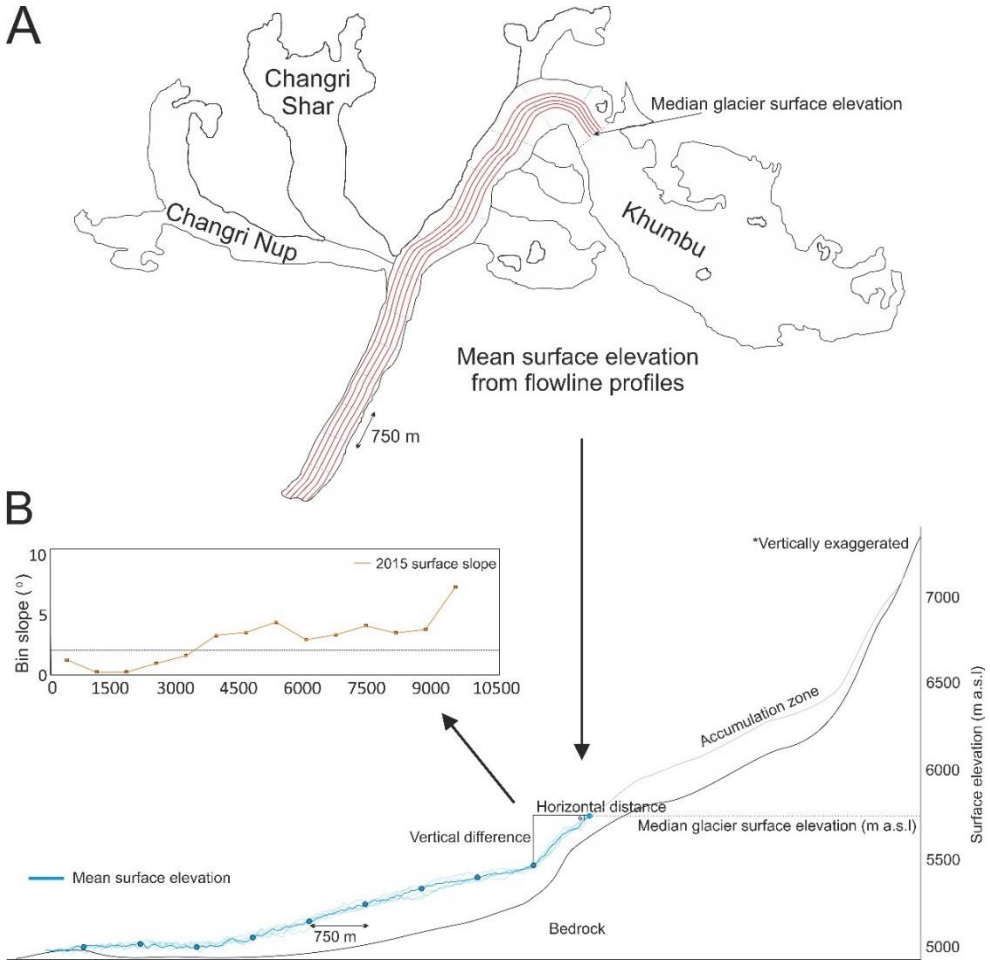

Figure 2.2. An example of the approach taken to generate glacier surface slope estimates on Khumbu glacier. A) The glacier centreline surface elevation profile and surface elevation profiles spaced 100 m apart parallel to the centreline were used to calculate a mean surface elevation profile. B) Slope was calculated along 750 m lengths of the mean elevation profile using basic trigonometry.

Glacier accumulation area ratios (AARs) were calculated as:

$$AAR = \frac{(A_{acc})}{(A)} \quad (3)$$

where A_{acc} is the accumulation area and A is the total glacier area. We used the median altitude of each glacier (taken from the RGI 5.0 glacier attribute tables) as an estimate of the ELA to divide glaciers into accumulation and ablation zones. Such an approach has been taken before in studies of Himalayan glaciers (Sakai et al., 2015), and is more reliable than the use of the end of ablation season snowline altitude (e.g. Thakuri et al., 2014) as this is a transient feature that may be affected by avalanche material.

2.3 Glacial lake area expansion and ice front retreat (chapter 4)

Water bodies present at the surface of glaciers can be distinguished from clean ice or debris cover and mapped in remotely sensed imagery, either manually or in a semi-automated fashion (e.g. Watson et al., 2016). Semi-automatic approaches include the use of the Normalised Difference Water Index (NDWI), typically applied to multi-spectral imagery such as that in the Landsat archives, or through the use of object based image analysis (OBIA) to segment imagery. Both of these techniques were used to map glacial lake area (NDWI) in a time series of Landsat 5, Landsat ETM+ and Landsat OLI imagery, and to map supraglacial pond extent (OBIA) in aerial photographs.

The NDWI can be used to map water bodies because of water's low reflectance in the near or shortwave infrared spectral bandwidths, and its high reflectance in the blue or green bandwidths. The NDWI is calculated through:

$$NDWI = \frac{(Band_{NIR} - Band_{Blue})}{(Band_{Blue} + Band_{NIR})} \quad (4)$$

Threshold NDWI values were determined for different imagery types (e.g. Landsat 5 Vs Landsat OLI) to classify water bodies. It was assumed that the lake perimeter had been classified to an accuracy of +/- 1/2 pixel (Fujita et al., 2009), a reasonable approach since the size of glacial lakes is always above minimum mapping thresholds that have been used to map smaller water bodies (supraglacial ponds) using the NDWI (Gardelle et al., 2011; Nie et al., 2013).

OBIA clusters groups of similar pixels into vector objects. OBIA is a powerful tool for edge detection, feature extraction and classification concepts and has been used to map glacial lakes (e.g. Nie et al., 2013) and supraglacial ponds (e.g. Watson et al., 2016) in the Himalaya. OBIA was used to map supraglacial ponds (rather than the NDWI) because of its ability to delineate water body edges regardless of size and because of its use of homogeneous polygons, which reduces the influence of image noise in classification outputs. The approach of Watson et al. (2016) was followed to digitise pond extents in archived aerial photography (from 1984). Images were over-segmented, to avoid the incorporation of surrounding terrain caused by under-segmenting (Watson et al., 2016), using ENVI (version 5.2) and the results inspected manually. Polygons were merged where several features represented one single pond.

Lake-terminating glacier terminus positions were delineated manually from scenes contained in the Landsat TM, Landsat ETM+ and Landsat OLI archives, yielding a record of ice front positions from 1989 to 2015. Terminus retreat rates were calculated following

the box method proposed by Moon and Joughin (2008), as calving termini are rarely straight, thus retreat rates can vary slightly across a single ice front. The box method involves the division of the total area of a polygon occupying the area between the ice front and a reference transect higher up-glacier by the width of the reference transect.

2.4 Glacier surface velocity (chapter 4)

Estimates of glacier surface lowering (section 2.1), glacier hypsometry and glacier geometry (section 2.2) were paired with glacier surface velocity datasets to examine glacier behaviour in response to lake growth in chapter 4. Glacier surface velocity datasets were generated by Amaury Dehecq (NASA Jet Propulsion Laboratory) using a feature tracking approach on a series of Landsat 7 (ETM+) and 8 (OLI) panchromatic images (both 15 m spatial resolution) (c.f. Dehecq et al., 2015). Feature tracking was undertaken on all image pairs contained in the Landsat 7 (ETM+) and Landsat 8 (OLI) archives whose acquisition dates were separated by approximately 1 year, over the time periods 1999-2003 (ETM+) and 2013-2015 (OLI). Orientation correlation (Fitch et al., 2002) was used to create 120 m resolution velocity field grids from image pairs over these time periods. Velocity fields over these two time windows were then stacked together, with a median value taken for each pixel. This approach yielded spatially extensive velocity data of sufficient time separation to examine glacier velocity changes in response to lake growth in the Everest region.

A similar approach to the generation of average surface elevation profiles was taken to summarise and compare glacier surface velocity datasets generated for different time periods. Previous studies focused on glacier surface velocity and glacier surface velocity change have compared glacier centreline velocities from different time periods (e.g. Sakakibara et al., 2014; Thakuri et al., 2016). However, glacier centreline velocity profiles are most likely a representation of maximum glacier surface velocity due to the influence of drag at the periphery of a glacier, which causes substantial cross-glacier variations in surface velocity. In this work, mean values of glacier surface velocity and glacier surface velocity change were again calculated using the mean of numerous (3, 5 or 7, depending on glacier width) flow parallel velocity profiles, spaced 100 m apart across the glacier. This method produces an estimate of the mean, glacier-wide surface velocity, along the length of each glacier, and therefore a more robust estimate of glacier velocity change when more than one time period is considered (e.g. Figures 4.2-4.5).

2.5 Field based data collection and processing (chapter 5)

The ablation zone of the Khumbu glacier was surveyed through terrestrial photography during three field campaigns to the Khumbu valley in October 2015 by D.Quincey, prior to the start of this PhD, and again in May 2016 and May 2017 by the author. The surface of the glacier and its lateral moranic troughs were photographed using the same routes for each survey and using the same camera (Canon powershot G11), and photographs were taken using the same (30 pace) distribution to ensure similar photographic coverage (~1400 photographs in each set) and data point density at each epoch. A differential global positioning system (dGPS) base station (Leica GS10 unit) was set up and ran for the duration of each photographic survey, with a second dGPS unit being used to geolocate easily visible ground control points (GCPs) across the different photographic surveys. All GCPs were located on large boulders that would have remained stationary across all three terrestrial photographic surveys. Following each field campaign, the GNSS base station data were post-processed (using Leica Geoffice) against the permanent Syangboche station (27.8093 N, 86.7122 E) data located approximately 17 km from the Khumbu field site. GCPs were then adjusted against this GNSS base station data, leading to a mean 3-D positional uncertainty of 5.1 mm for the 70 GCPs collected.

Photographic surveys were processed in Agisoft Photoscan 1.2.3 to create high spatial and temporal resolution point clouds of the surface of Khumbu glacier using the Structure-from-motion Multi-view stero (SfM-MVS) workflow (e.g. Smith et al., 2015). The Topographic Point Cloud Analysis Toolkit (ToPCAT) (Brasington et al., 2012) was used to filter the resulting point clouds, and a minimum point density of $10/m^2$ was used to produce a 2 m resolution DEM from each time period.

2.6 Glacier surface metrics (chapter 5)

To quantify the impact of ice loss on the characteristics of debris covered glacier surfaces, a set of metrics was generated from various fine resolution DEMs that provided a statistical measure of glacier surface topographic variability over different time periods. Metric data were generated by Andy Turner (School of Geography, University of Leeds). The metric used in this thesis characterised the local relief of surface topography, and was generated by calculating an average value of negative elevation differences when compared to a central cell in a moving window. A metric that quantified surface relief was chosen because melt features, such as ice cliffs and supraglacial ponds, are typified by sharp breaks in local topography (ice cliffs), or by flat surfaces (ponds) in fine-resolutions DEMs, thus they could be identified clearly across different glaciers and in DEMs from different time periods. The

clarity with which cliff and pond features were identified, along with the magnitude of estimated relief, varied depending on the size of the circular window. The negative elevation differences averaged over an 8-cell diameter (16m) window were found to most accurately reflect local relief (Supplementary Figures 7 and 8) and to delineate cliff and pond features most clearly, thus all metric grids were generated using this size of moving window.

Metric grids were used to perform topographic classifications for different time periods, whereby specific ranges of metric values associated with surface topography facies were assigned to specific metric classes. Topographic class area was summed for 500 m long bins along the length of each glacier to better understand the spatial variability of glacier surface topography, and repeating the same approach for DEMs from different time periods allowed an assessment of glacier surface topographic change in a decadal timescale.

Chapter 3

Spatial variability in mass loss of glaciers in the Everest region, central Himalaya, between 2000 and 2015

Owen King[1], Duncan J. Quincey[1], Jonathan L. Carrivick[1], Ann V. Rowan[2]

Published in The Cryopshere, doi: doi.org/10.5194/tc-11-407-2017

3.1 Abstract.

Region wide averaging of Himalayan glacier mass change has masked any catchment or glacier scale variability in glacier recession, thus the role of a number of glaciological processes in glacier wastage remains poorly understood. In this study, we quantify mass loss rates over the period 2000–2015 for 32 glaciers across the Everest region and assess how future ice loss is likely to differ depending on glacier hypsometry. The mean mass balance of all 32 glaciers in our sample was –0.52 ± 0.22 m water equivalent (w.e.) a^{-1}. The mean mass balance of 9 lacustrine terminating glaciers (–0.70 ± 0.26 m w.e. a^{-1}) was 32 % more negative than land-terminating, debris covered glaciers (–0.53 ± 0.21 m w.e. a^{-1}). The mass balance of lacustrine-terminating glaciers is highly variable (–0.45 ± 0.13 m w.e. a^{-1} to –0.91 ± 0.22 m w.e. a^{-1}), perhaps reflecting glacial lakes at different stages of development. To assess the importance of hypsometry on glacier response to future temperature increases, we calculated current (Dudh Koshi- 0.41, Tama Koshi- 0.43, Pumqu- 0.37) and prospective future glacier Accumulation Area Ratios (AARs). IPCC AR5 RCP 4.5 warming (0.9-2.3 ^{o}C by 2100) could reduce AARs to 0.29 or 0.08 in the Tama Koshi catchment, 0.27 or 0.17 in the Dudh Koshi catchment, and 0.29 or 0.18 in the Pumqu catchment. Our results suggest that glacial lake expansion across the Himalaya could expedite ice mass loss and the prediction of future contributions of glacial meltwater to river flow will be complicated by spatially-variable glacier responses to climate change.

Keywords: Himalaya, glacier mass, debris-cover, Everest region, glacial lakes

3.2 Introduction

Estimates of Himalayan glacier ice volume range from 2,300 km^3 to 7,200 km^3 (Frey et al., 2014 and references within) distributed amongst more than 54,000 glaciers across the Hindu Kush, Himalaya and the Karakoram (Bajracharya et al., 2015). The current mass balance of Himalayan glaciers is predominantly negative, with accelerating mass loss having been observed over the past few decades (Bolch et al., 2012; Thakuri et al., 2014). This mass loss is occurring because of a combination of processes. Shrestha et al. (1999) show a rise in the mean annual air temperature of 0.057 °C a^{-1} across the Himalaya between 1971 and 1994. Bollasina et al. (2011) show a reduction in total precipitation (–0.95 mm day^{-1}) amounting to 9 to 11% of total monsoon rainfall over a broad area of northern India between 1950 and 1999. Bhutiyana et al. (2010) show both decreasing total precipitation and a changing precipitation phase, with a lower proportion of precipitation falling as snow across the northwest Himalaya between 1996 and 2005. The snow cover season has been shortening as a result (Pepin et al., 2015). Under different climate scenarios, glacier imbalance in the region may contribute 8.7–17.6 mm of sea level rise by 2100 (Huss and Hock, 2015). Prolonged mass loss from Himalayan glaciers may cause diminishing discharge of the largest river systems originating in the region (Immerzeel et al., 2010; Lutz et al., 2013), thereby impacting on Asian water resources in the long-term.

Recent studies have identified spatial heterogeneity in mass loss across the Himalaya in the first decade of the 21st century (Kääb et al., 2012; Gardelle et al., 2013; Kääb et al., 2015). Glaciers in the Spiti Lahaul and Hindu Kush are losing mass most quickly (Kääb et al., 2015). Glaciers in the central Himalaya appear to have less negative mass balances (Gardelle et al., 2013). The anomalous balanced, or even slightly positive, glacier mass budget in the Karakoram is well documented (Bolch et al., 2012; Gardelle et al., 2012). Few previous studies have assessed the variability of glacier mass loss within catchments (Pellicciotti et al., 2015). Nuimura et al. (2012) examined the altitudinal distribution of glacier surface elevation change in the Khumbu region, Nepal, and found similar surface lowering rates over debris-free and debris-covered glacier surfaces. Gardelle et al. (2013) detected enhanced thinning rates on lacustrine terminating glaciers in Bhutan, West Nepal, and the Everest region, but did not make an explicit comparison with land terminating glacier recession rates. Similarly, Basnett et al. (2013) have shown that lacustrine terminating glaciers in Sikkim, Eatern Indian Himalaya experienced greater area loss between ~1990 and 2010 compared to land terminating glaciers. Benn et al. (2012) have considered the role of glacial lakes in the wastage of debris-covered glaciers and proposed a conceptual model of Himalayan glacier recession that included important thresholds between regimes of ice dynamics and mass loss at different stages of lake development.

Benn et al. (2012) suggest that an expansive, moraine dammed and potentially hazardous glacial lake may represent the end product of the wastage of a debris-covered glacier.

We aim to quantify glacier mass loss rates in three major catchments of the central Himalaya and assess the glacier-scale variability of ice loss within and between catchments. We specifically examine the mass balance, hypsometry and total area change of each glacier and compare those terminating in a glacial lake with those terminating on land. We use these data together with climatic data from the region to define the major mechanisms that may have driven mass loss in recent decades, and to assess scenarios of likely future ice loss from our sample of glaciers.

3.3 Study area

We studied glaciers in three catchments of the Everest region (Figure 1), spanning both Nepal and Tibet (China). Two of the catchments, the Dudh Koshi and the Tama Koshi, are located in north-eastern Nepal and drain the southern flank of the Himalaya. The third catchment is located to the north of the main orographic divide, and the glaciers drain north into Tibet (China). Most glaciers in the studied catchments are characterised by long (10–15 km), low-slope angle, debris-covered tongues that are flanked by large (tens of metres high) moraine ridges (Hambrey et al., 2008). Some glaciers have accumulation areas several kilometres wide that reach extreme altitudes (up to 8000 m in the case of the Western Cwm of Khumbu Glacier). Others sit beneath steep hillslopes (e.g. Lhotse and the Lhotse face), are fed almost exclusively by avalanches and are less than 1 km in width for their entire length.

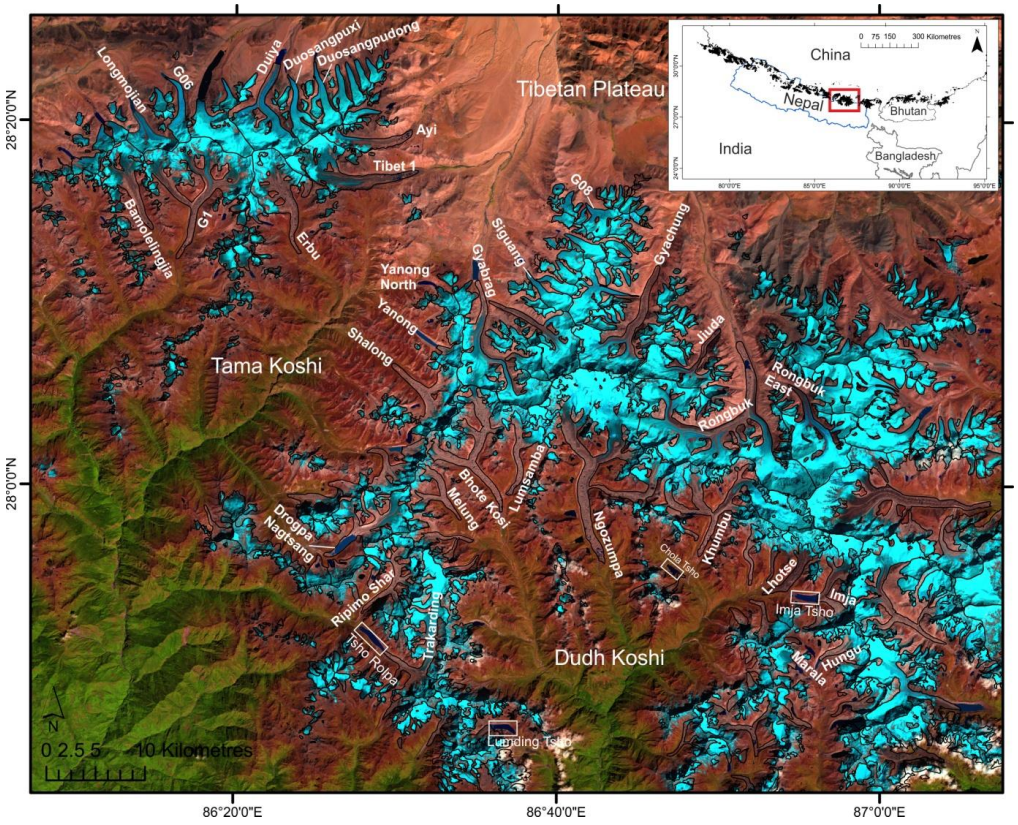

Figure 3.1. The glaciers of the Everest region. Named glaciers are the glaciers we highlight in this study. Major catchments include the Tama Koshi and Dudh Koshi on the southern flank of the Himalaya and the Pumqu river catchment on the northern side of the divide, with glaciers flowing onto the Tibetan Plateau (China). Named glacial lakes are highlighted, although many remain unnamed. Background imagery is a Landsat OLI image from 2014 available from http://earthexplorer.usgs.gov/.

The largest 40 of 278 glaciers in the Dudh Koshi catchment account for 70% of the glacierised area (482 km^2- Bajracharya and Mool, 2009). These glaciers are all partially debris-covered, with debris mantles reaching at least several decimetres in thickness (Rounce and McKinney, 2014; Rowan et al., 2015). Here, the total area of glacier surface covered by debris has increased since the 1960s (Thakuri et al., 2014) and several previous studies have published surface lowering data for the catchment indicating accelerating surface lowering rates over recent decades (e.g. Bolch et al., 2011; Nuimura et al. 2012). We select nine of the largest glaciers (Supplementary table 1) for analysis given that they provide the greatest potential volume of meltwater to downstream areas.

There are a total of 80 glaciers in the Tama Koshi catchment covering a total area of 110 km^2 (Bajracharya et al., 2015). We again selected the largest nine glaciers (Supplementary table 1) for analysis based on relative potential contributions to river flow. The Tama Koshi

is a poorly studied catchment, perhaps best known for the existence of Tsho Rolpa glacial lake, which underwent partial remediation during the 1990s (Reynolds, 1999).

The fourteen glaciers within our sample that flow onto the Tibetan Plateau (Supplementary table 1) all contribute meltwater to the Pumqu river catchment, which covers an area of 545 km^2 (Che et al., 2014). Debris cover is less prevalent on glaciers of the Pumqu catchment, and glacier recession has caused a 19 % of glacier area loss since 1970 (Jin et al., 2005; Che et al., 2014). There is relatively little information on glacier ELAs other than in the Dudh Koshi catchment. In the Dudh Koshi, Asahi et al. (2001) estimated ELAs to be at around 5600 m a.s.l. in the early 2000s. Wagnon et al. (2013) measured annually variable ELAs of 5430–5800 m a.s.l. on the Mera and Polkalde glaciers between 2007 and 2012, Shea et al. (2015) estimate the current ELA to be 5500 m a.s.l., and Gardelle et al. (2013) estimated the ELA to be around 5840 m over the period 2000–2009. In the Pumqu catchment, those in the Rongbuk valley were estimated to be between 5800 and 6200 m a.s.l. for the period 1974–2006 (Ye et al., 2015).

A number of studies have identified an abundance of glacial water bodies in the Everest region. Salerno et al. (2012) identified 170 unconnected glacial lakes (4.28 km^2), 17 proglacial lakes (1.76 km^2) and 437 supraglacial lakes (1.39 km^2) in the Dudh Koshi catchment. Gardelle et al. (2011) identified 583 supraglacial ponds and lakes in an area comparable in coverage to Figure 3.1. Watson et al. (2016) mapped 9340 supraglacial ponds on 8 glaciers of the Dudh Koshi catchment and Rongbuk glacier in the Pumqu catchment. Watson et al. (2016) also show a net increase in ponded area for six of their nine studied glaciers. Some of the largest glacial lakes in this region have also been expanding in recent decades (Sakai et al., 2000; Che et al., 2014; Somos-Valenzuela et al., 2014). This increased meltwater ponding at glacier termini has potential to affect ice dynamics and down-valley meltwater and sediment fluxes (Carrivick and Tweed, 2013) as well as causing a hazard to populations living downstream. Several of the lakes have burst through their moraine dams in previous decades causing rapid and extensive flooding downstream; the best studied outburst floods are those from Nare glacier in 1977 (Buchroithner et al., 1982) and from Dig Tsho in 1985 (Vuichard and Zimmerman, 1987).

We classify nine glaciers from the sample as lacustrine terminating, where the glacier termini and glacial lakes are actively linked. We do not consider either Rongbuk Glacier or Gyabrag Glacier as lacustrine terminating. Gyabrag Glacier is now separated from a large proglacial lake by a large outwash plain and we do not believe the lake can have an influence on the retreat of the glacier. In the case of Rongbuk Glacier, the lake is supraglacial and far up-glacier from its terminal region and thus does not currently influence

the recession of the terminus of the glacier. The expanding Spillway Lake at the terminus of Ngozumpa Glacier (Thompson et al., 2012) is currently of limited depth (Mertes et al., 2016), and is unlikely to affect glacier dynamics until water depth approaches ice thickness, so we also exclude Ngozumpa Glacier from the lacustrine terminating category.

3.4 Data sources

3.4.1 Digital elevation models

Our reference elevation dataset across all three catchments is the Shuttle Radar Topographic Mission (hereafter SRTM) version 3.0, non-void filled, 1 arc second digital elevation model (hereafter DEM). The main objective of the SRTM mission was to obtain single-pass interferometric SAR imagery to be used for DEM generation on a near global scale (56˚S to 60˚ N- 80% of the planet's surface) with targeted horizontal and vertical accuracies of 16 m and 20 m, respectively, although Farr et al. (2007) report horizontal and vertical accuracies of better than 10 m for most regions globally. This dataset was acquired in February 2000 and was released at 30 m resolution in late 2014 (USGS, 2016). The SRTM data we used was acquired by a 5.6 cm C-band radar system.

Our 2014/2015 elevation dataset comprises a number of high resolution (8 m grid) DEMs generated by Ohio State University and distributed online by the Polar Geospatial Centre at the University of Minnesota that provide coverage of an extended area around the Everest region (Table 1). These stereo-photogrammetric DEMs have been generated using a Surface Extraction with TIN-based Search-space Minimization (hereafter SETSM) algorithm from Worldview 1, 2 and 3 imagery (Noh and Howat, 2015). The SETSM algorithm is designed to automatically extract a stereo-photogrammetric DEM from image pairs using only the Rational Polynomial Coefficients (RPCs) as geometric constraints. The geolocation accuracy of RPCs without ground control for Worldview 1 and 2 data is 5 m (Noh and Howat, 2015) which may ultimately result in matching failure. The SETSM algorithm updates RPCs to mitigate this error and produces DEMs with an accuracy of ± 4 m in X, Y and Z directions (Noh and Howat, 2015). SETSM DEMs are gap-filled using a natural neighbour interpolation; we removed these pixels before DEM differencing and the calculation of glacier mass balance.

Table 1.1. Scenes used in glacier outline delineation, ASTER DEM generation, SRTM ice facies mask generation and by the Polar Geospatial Centre in the generation of SETSM DEMs.

Sensor	Scene ID	Date of acquisition	Purpose
Landsat OLI	LC81400412014334LGN00	30/11/2014	Glacier outlines
Landsat ETM+	LE71390412000302SGS00	29/10/2000	Glacier outlines
Landsat ETM+	LE71400402002005SGS00	05/01/2002	Ice facies mask
Landsat ETM+	LE71400412002005SGS00	05/01/2002	Ice facies mask
ASTER	L1A.003:2014050545	29/11/2014	ASTER DEM
Worldview 3	WV03_20150121_10400100076C0700	21/01/2015	SETSM DEM
Worldview 1	WV01_20150504_102001003C5FB900	04/05/2015	SETSM DEM
Worldview 1	WV01_20140115_102001002A289F00	15/01/2014	SETSM DEM
Worldview 1	WV01_20140324_102001002D263400	24/03/2014	SETSM DEM
Worldview 1	WV01_20150204_102001003A5B7900	04/02/2015	SETSM DEM
Worldview 2	WV02_20150202_103001003D4C7900	02/02/2015	SETSM DEM
Worldview 1	WV01_20140218_102001002C5FA100	18/02/2014	SETSM DEM
Worldview 1	WV01_20141022_102001003525D400	22/10/2014	SETSM DEM
Worldview 2	WV02_20141110_1030010039013C00	10/11/2014	SETSM DEM
Worldview 1	WV01_20141129_102001002776B500	29/11/2014	SETSM DEM
Worldview 1	WV01_20140514_102001003001E400	14/05/2014	SETSM DEM

Over two small areas of the Dudh Koshi (over the lower reaches of the Bhote Kosi and Melung glaciers) the SETSM DEMs contained data gaps. To complete coverage of DEMs over these glaciers we generated ASTER DEMs and used the surface to cover elevation bands across these glaciers where no data were available from the SETSM grids. We used ERDAS Imagine (2013) to generate ASTER DEMs with ground control points (GCPs) matched between features in the ASTER imagery and the high resolution imagery available in Google Earth. We used a large number of GCPs (45) and tie points (> 75) to minimise the root mean squared (RMS) error of GCP positions. All SETSM and ASTER DEMs were resampled to a 30 m resolution to match that of the SRTM data before any differencing was carried out.

3.4.2 Glacier outlines

Glacier outlines were downloaded from the Global Land Ice Measurement form Space (GLIMS) Randolph Glacier Inventory (RGI) Version 5.0 (Arendt et al., 2015) and modified for 2000 and 2014 glacier extents based on Landsat scenes closely coinciding in acquisition with the DEM data. Glacier extents from these two epochs were used to calculate area changes. The 2000 Landsat scene was acquired by the Enhanced Thematic Mapper Plus (ETM+) sensor and thus has a single 15 m resolution panchromatic band and six 30 m

multispectral bands. The 2014 scene was acquired by the Operational Land Imager (OLI) sensor and also has a single 15 m panchromatic band as well as eight 30 m multispectral bands. Both scenes were pan-sharpened to match the resolution of the multispectral bands to that of the panchromatic band before glacier outlines were adjusted. Adjustments were limited to correcting changes in glacier frontal position and changes along the lateral margins because of surface lowering.

3.5 Methods

3.5.1 DEM coregistration

We followed the three-step correction process of Nuth and Kääb (2011), through which biases inherent in stereoscopic DEMs can be corrected. We assessed and corrected where necessary for: (i) mismatch in the geo-location of the modern DEMs versus the reference SRTM dataset (in x, y, and z direction); (ii) the existence of an elevation dependant bias, and; (iii) biases related to the acquisition geometry of the data. Each step was taken individually, so that separate error terms could be understood, rather than bundling them together as multiple regression based adjustments as previous studies have done, such as Racoviteanu et al. (2008) and Peduzzi et al (2010), for example. Corrections applied to DEMs where any one of the three biases were present included shifting of DEM corner coordinates, simple vertical shifting through addition or subtraction, and the fitting of linear and polynomial trends depending on the spatial variability of elevation differences across DEMs and through their elevation ranges. Acquisition geometry related biases (along or cross satellite track) were detected in two SETSM strips (Table 3) and both ASTER scenes and were corrected for using linear trends fitted through difference data. DEM co-registration was carried out following the conversion of SETSM elevation data to geoid heights using the Earth Gravitational Model (EGM) 2008 grid available from the National Geospatial-Intelligence Agency.

3.5.2 SRTM DEM correction

Some studies have shown that the SRTM dataset may underestimate glacier surface elevations because of C-band radar wave penetration into snow and ice (Rignot et al., 2001). Kääb et al. (2012) assessed the magnitude of C-band penetration over various test sites in the Himalaya and over different ice facies (clean ice, snow and firn) by extrapolating ICESat Vs SRTM glacier elevation differences back to the SRTM acquisition date, showing penetration estimates of several metres. To account for this bias, we have corrected the SRTM dataset using the penetration estimates of Kääb et al. (2012), after generating a mask

for clean ice, firn and snow cover using the most suitable Landsat ETM+ scenes (Table 1) available around the acquisition date of the SRTM dataset. We applied a correction to the SRTM DEM of +4.8 m over areas of firn/snow, and +1.2 m over areas of clean ice (see supplementary table S2 of Kääb et al. (2012)). We do not apply any penetration correction over debris-covered areas given the uncertainty expressed by Kääb et al. (2012) about the influence of possibly greater than average snowpack depth at the point of ICESat acquisition and the properties of the snowpack at the point of SRTM data acquisition on their penetration estimate.

Berthier et al. (2006) suggested that the extreme topography present in mountain regions is poorly replicated in coarse-resolution DEMs such as the SRTM DEM. Different studies have applied positive or negative corrections to the SRTM DEM (Berthier et al., 2007; Larsen et al., 2007), depending on the severity of the terrain at their respective study sites. Inspection of DEM differences across the study site showed no clear relationship between elevation differences and altitude (see supplementary information Figure 1), thus no elevation dependant correction was applied.

Table 1.2. Mean differences and the standard deviation associated with off-glacier elevation difference data between ASTER, SETSM and SRTM DEMs before and after the DEM correction process. The uncertainty associated with DEM difference data (sum of standard error estimates for each 100 m elevation bin of difference data) is also listed for each SETSM and ASTER DEM.

Sensor	ASTER scene ID	Pre correction mean & StDev stable ground differences Vs SRTM (m)		Post correction mean & StDev stable ground differences Vs SRTM (m)		dh/dt uncertainty (± m a^{-1})
ASTER	L1A.003:2014050545	–64.12	25.99	0.43	11.30	0.47
	SETSM tile					
WV 3	WV03_20150121_10400100076C0700	–6.07	11.54	0.53	6.43	0.25
WV 1	WV01_20150504_102001003C5FB900	–5.68	15.76	–0.43	5.89	0.40
WV 1	WV01_20140115_102001002A289F00	–3.56	9.50	0.50	6.64	0.27
WV 1	WV01_20140324_102001002D263400	–2.21	8.92	0.07	5.90	0.33
WV 1	WV01_20150204_102001003A5B7900	–1.26	17.50	–0.36	5.65	0.31
WV 2	WV02_20150202_103001003D4C7900	–3.80	12.34	–0.03	6.56	0.29
WV 1	WV01_20140218_102001002C5FA100	–2.00	9.80	–0.23	6.71	0.28
WV 1	WV01_20141022_102001003525D400	–9.54	16.50	0.36	6.89	0.35
WV 2	WV02_20141110_1030010039013C00	–2.89	9.83	0.07	5.87	0.15
WV 1	WV01_20141129_102001002776B500	–5.72	8.31	0.16	4.76	0.18
WV 1	WV01_20140514_102001003001E400	–3.51	10.12	–0.26	5.91	0.26

3.5.3 Gap filling and outlier filtering

Once DEMs had been co-registered and corrected for present biases, DEMs were differenced to yield surface elevation change data. To remove outlying values, we firstly excluded obviously incorrect difference values, (exceeding ± 120 m) and then followed the approach of Gardelle et al. (2013) in using the standard deviation of DEM difference data to classify probable outliers. We removed values exceeding 3 standard deviations. Such outlier definitions are justified in areas of shallow slope and high image contrast where DEM quality is generally high (Ragettli et al. 2016), but could be considered lenient where featureless surfaces, for example snow covered areas of accumulation zones, might lead to poor elevation data derivation and limit the accuracy of stereoscopic DEMs. Noh and Howat (2015) show how the iterative approach of the SETSM algorithm and the high spatial and radiometric resolution of WorldView imagery preclude such an issue, and we therefore consider a 3 standard deviation threshold appropriate.

To complete data coverage and allow for glacier mass balance estimates, the filling of data gaps was required. Only small (<~5 x 5 grid cells) gaps were present in DEM difference data over most of the glaciers in our sample, but some larger gaps could be found over areas of steep surface slope, for example high in accumulation zones, or where deep shadows might have been extensive in WorldView imagery. We filled gaps in DEM difference data using median values from the 100 m elevation band in which the data gap was situated (Ragettli et al. 2016).

3.5.4 Hypsometric analyses and elevation range normalisation

Glacier hypsometry, the distribution of glacier area over altitude, is governed by valley shape, relief and ice volume distribution (Jiskoot et al., 2009). It is important for long-term glacier response because it defines the distribution of mass with elevation and thus determines how the glacier responds to changes in elevation-dependent temperature (Furbish and Andrews, 1984). To assess glacier hypsometry, we used the aforementioned glacier outlines and the SETSM DEMs, which offer better data coverage than the non-void filled SRTM dataset, to split these glacier extents into segments covering 100 m elevation ranges, and calculated the area of each segment. We followed the approach of Jiskoot et al. (2009) to categorise each glacier or the population of glaciers in each catchment according to a hypsometric index (HI), where:

$$HI = \frac{(H_{max} - H_{med})}{(H_{med} - H_{min})} \quad (1)$$

and H_{max} and H_{min} are the maximum and minimum elevations of the glacier, and H_{med} the median elevation that divides the glacier area in half (Jiskoot et al., 2009). Glaciers were grouped into five HI categories: 1- HI < –1.5, very top heavy; 2- HI –1.2 to –1.5, top heavy; 3- HI –1.2 to 1.2, equidimensional; 4- HI 1.2 to 1.5, bottom heavy; and 5- HI > 1.5, very bottom heavy. Top heavy glaciers store more ice at higher elevation, for example in broad accumulation zones, whereas bottom heavy glaciers have small accumulation zones and long tongues.

To construct elevation change and glacier hypsometry curves for the 32 glaciers in our sample, we have normalised the elevation range of each glacier following the method of Arendt et al. (2006):

$$H_{norm} = \frac{(H - H_{min})}{(H_{max} - H_{min})} \quad (2)$$

where H_{min} and H_{max} are the elevations of the glacier terminus and the elevation maximum of each glacier. This normalisation process allows the direct comparison of elevation changes and glacier hypsometry regardless of termini elevation. Surface elevation change and glacier hypsometry curves are presented in Figures 3.5 and 3.6.

3.5.5 Mass loss calculations

A conversion factor of 850 kg m^{-3} was used to account for the density of glacier ice for all glaciers in the sample (Huss, 2013). We assigned an additional 7 % to mass loss uncertainty estimates to account for error in the density conversion (Huss, 2013). The mass loss estimates generated for lake-terminating glaciers are slight underestimates because, with no information available on bed topography, we cannot account for ice that has been replaced by water during lake expansion. Mass balance estimates for these glaciers therefore only incorporate aerial mass loss from the 2000 calving front, up-glacier. We also acknowledge that our surface lowering estimates incorporate any upward or downward flow of ice resulting from, for example, compressional flow over a zone of transition from active to inactive ice. We do not quantify emergence velocity as the ice thickness and surface velocity data required to do so (Immerzeel et al. 2014) are not available for an adequate number of glaciers in our sample.

3.5.6 Estimation of ELAs

We follow the approach of Braithwaite and Raper (2010) in using the median altitude of each glacier, information available in the RGI, to estimate the ELA of glaciers in our sample. Such an approach is most appropriate for glaciers in a state of balanced mass budget (Braithwaite and Raper, 2010; Baithwaite, 2015), thus the ELA estimates produced using

this method could be considered an underestimate of modern day ELAs given the negative state of mass balance of the majority of Himalayan glaciers. However, without measured mass balance records of adequate length against which to compare this, or other (Braithwaite, 2015), ELA estimation methods, we take it as the best available approach. This is a method that has previously been employed in the Himalaya (Zhao et al., 2016), although we also note that this method cannot account for the input of avalanched material from steep valley walls- a substantial source of accumulation for Himalayan glaciers (Benn and Lehmkuhl, 2000). To estimate prospective future ELAs in response to temperature increases, we used vertical temperature gradients of –8.5 ^{o}C km^{-1} for the Pumqu catchment (Kattel et al., 2015) and –5.4 ^{o}C km^{-1} for the Dudh Koshi and Tama Koshi catchments (Immerzeel et al., 2014) to calculate prospective ELA shifts given different warming scenarios. We calculated ELAs for projected minimum, mean and maximum temperature increases under the 4 main RCP scenarios outlined in the IPCC AR5 working group report (Collins et al., 2013).

3.6 Uncertainty

3.6.1. DEM differencing uncertainty

Our elevation change uncertainty estimates have been calculated through the derivation of the standard error ($E_{\Delta h}$) - the standard deviation of the mean elevation change- of 100 m altitudinal bands of elevation difference data (Gardelle et al., 2013; Ragettli et al., 2016):

$$E_{\Delta h} = \frac{\sigma_{stable}}{\sqrt{\mathrm{N}}} \quad (3)$$

Where σ_{stable} is the standard deviation of the mean elevation change of stable, off-glacier terrain, and N is the effective number of observations (Bolch et al., 2011). N is calculated through:

$$N = \frac{N_{tot} \cdot PS}{2d} \quad (4)$$

Where N_{tot} is the total number of DEM difference data points, PS is the pixel size and d is the distance of spatial autocorrelation. We follow Bolch et al. (2011) in estimating d to equal 20 pixels (600 m). $E_{\Delta h}$ for each DEM is the sum of standard error estimates of each altitudinal band (Gardelle et al., 2013).

We have also considered whether the different acquisition dates of Worldview imagery (Table 1) has led to the sampling of seasonal glacier surface elevation variations caused by a remnant snowpack (e.g. Berthier et al. 2016). Such a bias should be partly corrected for

during vertical DEM adjustment using off-glacier terrain assuming a similar snowpack thickness on and off-glacier (Wang and Kääb, 2015). Two overlapping SETSM DEMs (ending FA100 and 3C00 in Table 1) have been generated from Worldview imagery acquired before and after the summer monsoon (when glaciers receive most accumulation) of 2014, thus any spatially consistent vertical differences may show a remnant snow pack that would cause an elevation bias. The difference between these two SETSM DEMs over the Bamolelingjia and G1 glaciers is slight (mean 0.69 m, σ 3.81 m), but we cannot be sure that these differences represent a region-wide average. We have incorporated the mean elevation difference of these SETSM DEMs over glacier surfaces (dZ_{season}) into our overall uncertainty budget. We summed different sources of error quadratically to calculate our overall uncertainty ($\sigma_{dh/dt}$) associated with DEM difference data:

$$\sigma_{\mathrm{dh/dt}} = \sqrt{\mathrm{E}_{\Delta \mathrm{h}}^2 + \mathrm{dZ}_{\mathrm{season}}^2} \qquad (5)$$

$\sigma_{dh/dt}$ is then weighted depending on the hypsometry of each glacier, giving a glacier specific measure of elevation change uncertainty that considers the spatially nonuniform distribution of uncertainty (Ragettli et al., 2016).

3.6.2 Glacier area change uncertainty

There are two principal sources of uncertainty in the measurement accuracy of the position of a glacier margin; sensor resolution and the co-registration error between the images acquired at each measurement epoch (Ye et al., 2006; Thakuri et al., 2014). We follow the approach of Ye et al. (2006) to quantify the uncertainty associated with the total area changes documented across our sample of glaciers. We incorporate geolocation accuracy estimates of 10.5 m for Landsat ETM+ imagery and 6.6 m for Landsat OLI imagery (Storey et al., 2014) into the uncertainty budget and suggest the total measurement uncertainty in glacier area between 2000 and 2015 image sets was ± 0.04 km^2 a^{-1}. Area weighted, glacier specific uncertainty estimates are given in Supplementary table 3.

3.7 Results

3.7.1 Glacier mass balance

The mean mass balance of all 32 glaciers in our sample was –0.52 ± 0.22 m w.e. a^{-1} between 2000 and 2015. There is considerable variability in the mass balance of glaciers with different terminus type (Figures 3.3 and 3.4) and in the rates of surface lowering through the altitudinal range of highlighted glaciers (Figures 3.5 and 3.6). The mean mass balance of

glaciers in catchments either side of the orographic divide are not markedly different, however.

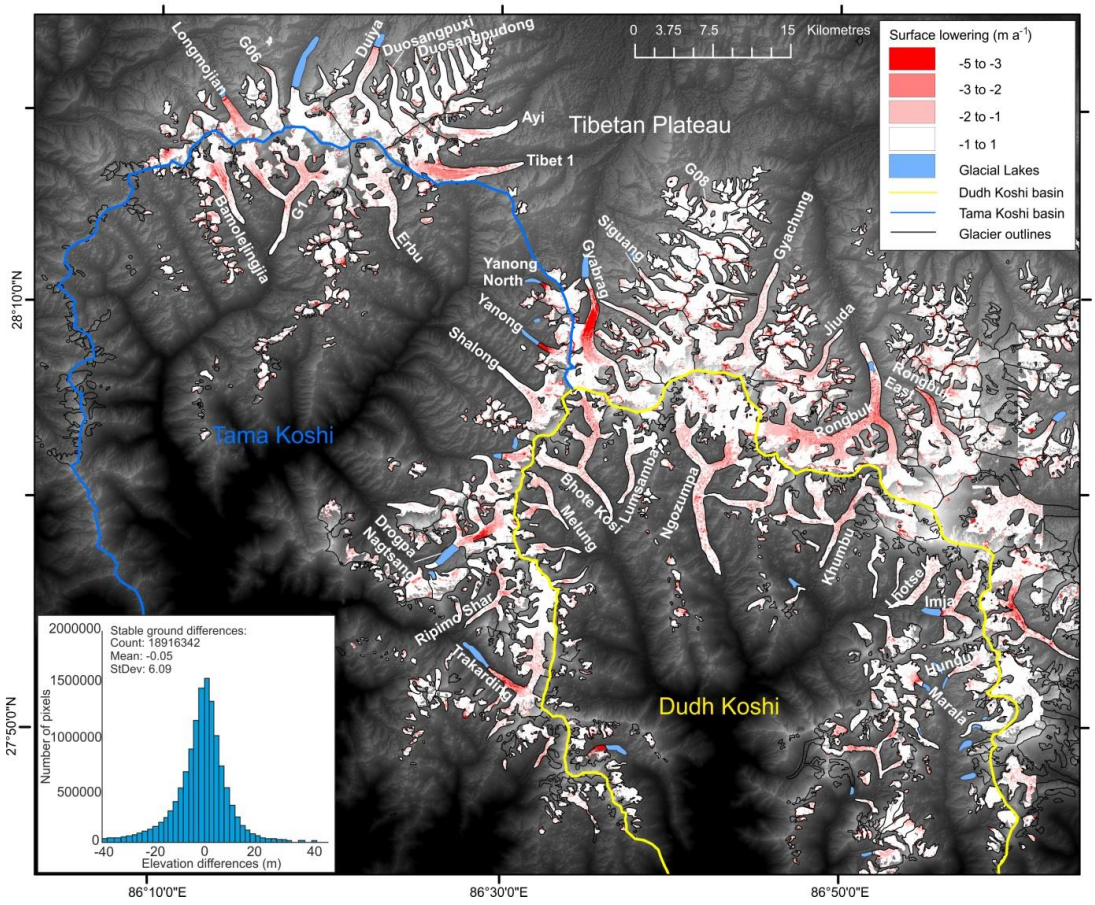

Figure 3.2. Glacier surface elevation change over the study area between 2000 and 2014/15. Also shown is a summary of off-glacier terrain differences. Areas of no data show the ASTER GDEM underlay.

Mean glacier mass balance (including land and lacustrine terminating glaciers) was –0.51 ± 0.22 m w.e. a^{-1} in the Tama Koshi catchment, –0.58 ± 0.19 m w.e. a^{-1} in the Dudh Koshi catchment, and –0.61 ± 0.24 m w.e. a^{-1} for glaciers flowing into the Pumqu catchment over the study period. The mean mass balance of nine lacustrine terminating glaciers was –0.70 ± 0.26 m w.e. a^{-1}. This was 32% more negative than land terminating glaciers (mean mass balance of –0.53 ± 0.21 m w.e. a^{-1}) we include in our sample. The lowest mass loss rates occurred over debris-free glaciers at high altitude (5600 – 6200 m a.s.l) in the Pumqu catchment. The mean mass balance of these glaciers was –0.25 ± 0.22 m w.e. a^{-1} (Supplementary table 2) over the study period. Individual glacier mass balance estimates can be found in the Supplementary Information.

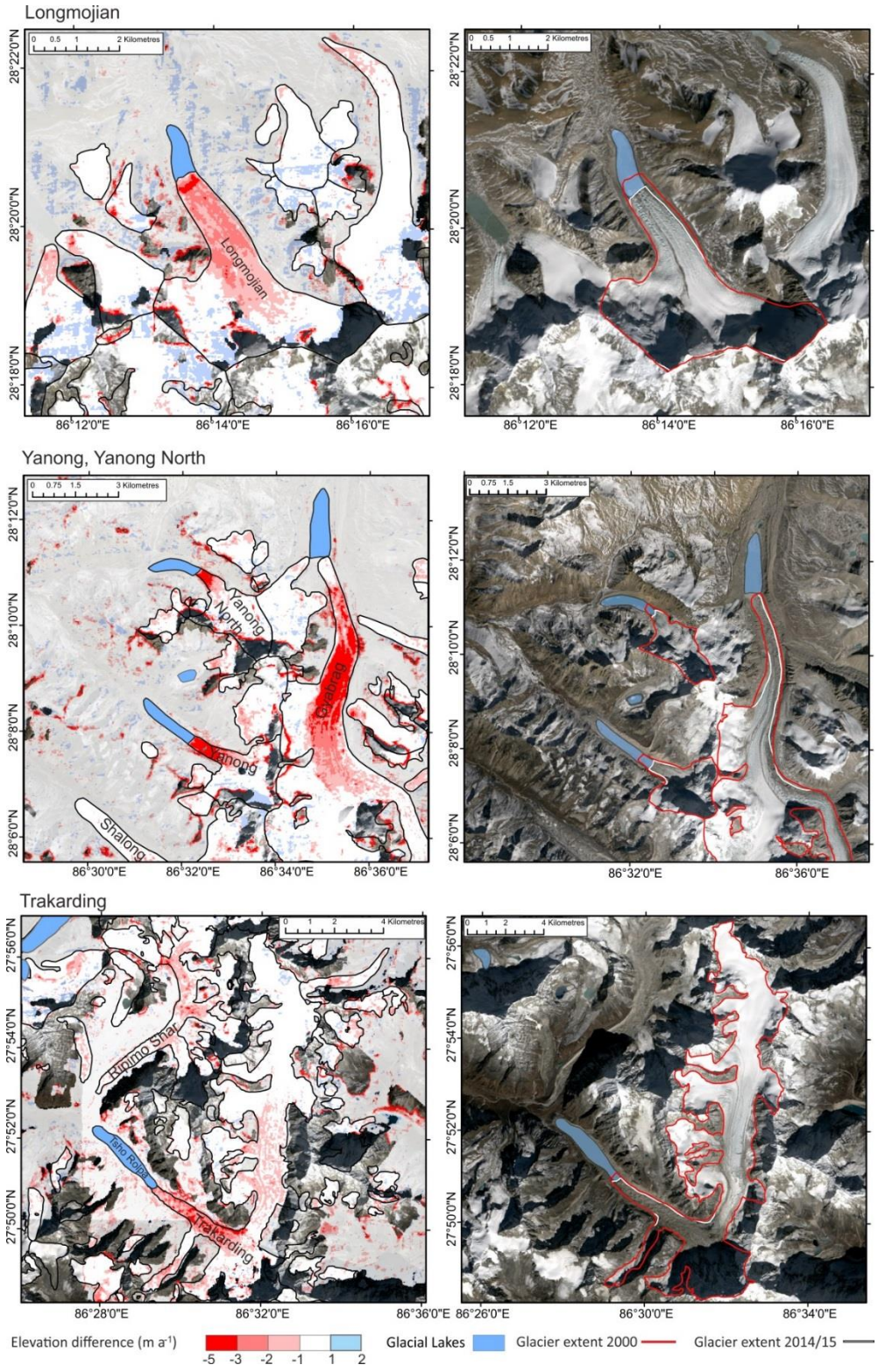

Figure 3.3. Examples of surface elevation change and total area change over the study period on lake-terminating glaciers. Semi-transparent, off-glacier differences are also shown.

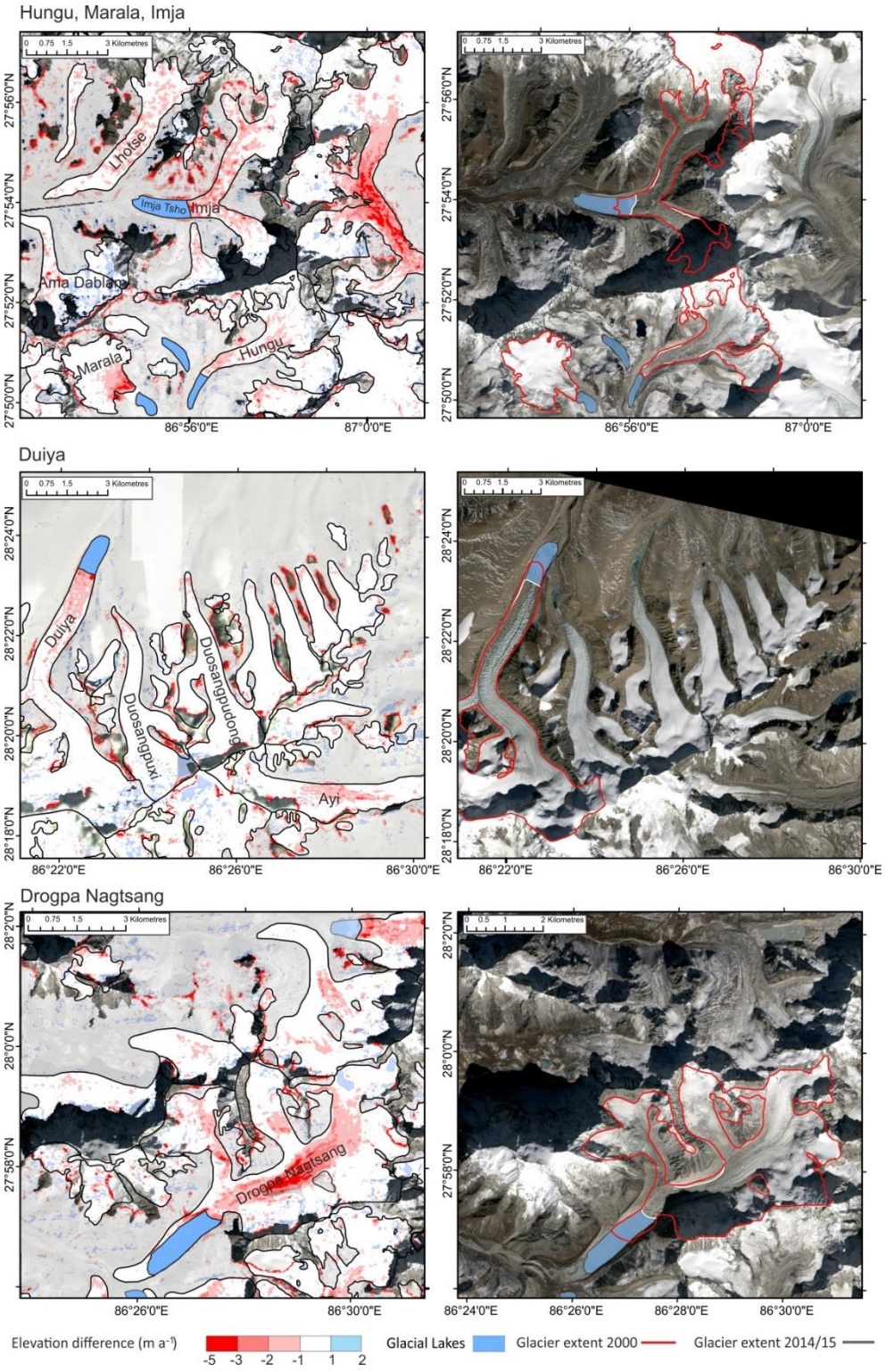

Figure 3.4. Further examples of glacier surface elevation change and total area change over the study period on lake-terminating glaciers. Semi-transparent, off-glacier differences are also shown.

3.7.2 Glacier surface lowering

The altitude at which maximum surface lowering rates occurred differed depending only on glacier terminus type (Figures 3.5 and 3.6). Across all three catchments, substantial surface lowering was pervasive over the middle portions of larger, land terminating glaciers (Figure 3.2). In the Dudh Koshi, surface lowering rates are at their highest (–1.06 ± 0.10 m a^{-1}) around 5200 m a.s.l., although similar surface lowering rates occurred between 5100 and 5300 m a.s.l (Figure 3.5). In the Tama Koshi the highest rates of surface lowering (–1.08 ± 0.12 m a^{-1}) occurred at around 5400 m a.s.l (Figure 5). In the Pumqu catchment, the highest mean surface lowering rates again occurred between 5300 and 5400 m a.s.l.; the mean surface lowering rate at this altitude was –1.62 ± 0.14 m a^{-1} over the study period. Surface lowering rates over glaciers in the Pumqu catchment were higher than those in the Tama Koshi and Dudh Koshi catchments (Figure 3.5) up to 5700 m a.s.l. (–1.24 ± 0.21 m a^{-1} at this altitude). Of note is the surface lowering over clean-ice areas high up on glaciers such as Ngozumpa, Rongbuk, Gyabrag and Bhote Kosi (Figure 3.2). Surface lowering extended into tributary branches and the cirques of these largest glaciers. Individual glaciers showed much greater surface lowering, particularly in the Pumqu catchment. Gyabrag glacier lost an exceptional –3.33 ± 0.28 m a^{-1} between 5300 and 5400 m a.s.l (Figure 3.5).

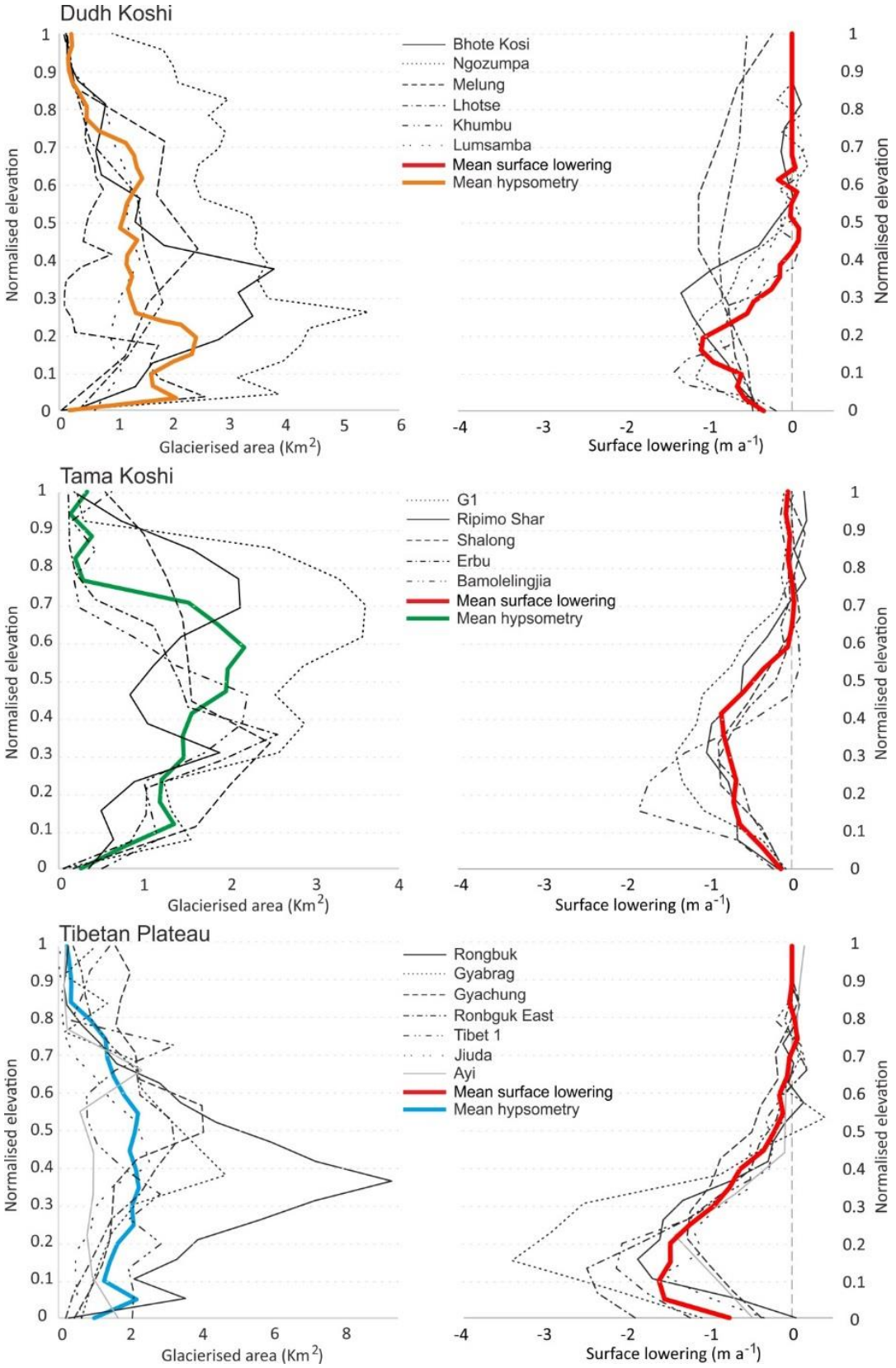

Figure 3.5. Surface elevation change and glacier hypsometry curves for all land-terminating glaciers in the three different catchments of the study area.

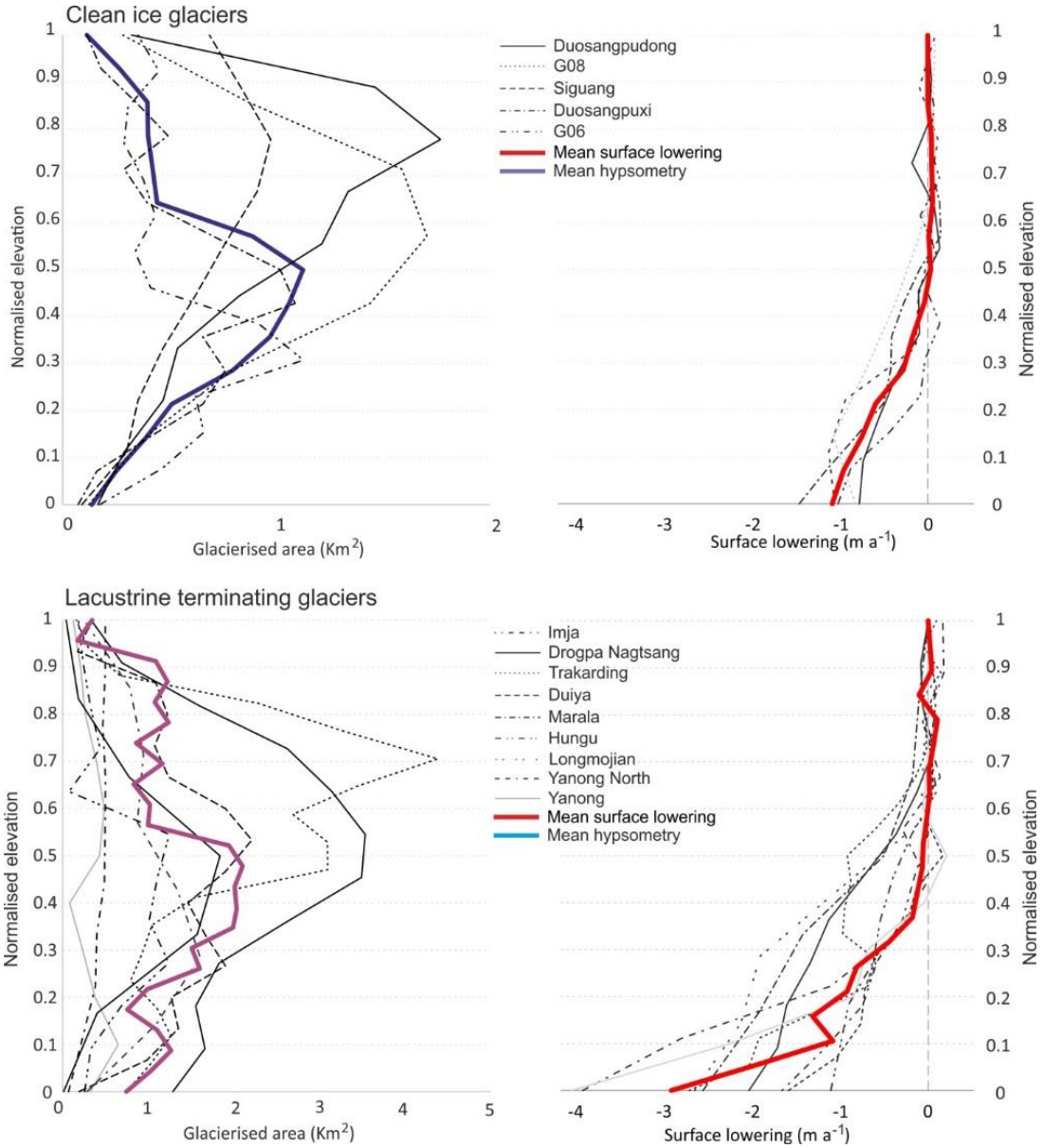

Figure 3.6. Surface lowering and glacier hypsometry curves for clean ice and lake-terminating glaciers in the study area.

The maximum surface lowering rates (–2.79 ± 0.29 m a^{-1}) occurred at the lowest elevations (between 4700 and 4900 m a.s.l) of lacustrine terminating glaciers (Figure 3.6). These nine glaciers all showed a linear surface lowering gradient. We calculate the lowering gradient as surface elevation change per 100 m (m a^{-1}/100 m) vertical elevation change below the ELA. Lacustrine terminating glaciers showed a lowering gradient of 0.30 m a^{-1}/100 m over the study period. The lowering gradient of land terminating glaciers was non-linear. Surface lowering was negligible around the terminus of most land terminating glaciers, with enhanced ice loss occurring further up-glacier where debris cover may have been thin or patchy. Lowering gradients for the area of land terminating glaciers between the ELA and the altitude of maximum ice loss were 0.59, 0.66 and 0.38 m a^{-1}/100 m for glaciers in the

Pumqu catchment, and in the Dudh Koshi and Tama Koshi catchments, respectively. Clean ice glaciers also showed a linear lowering gradient- 0.77 m w.e. a^{-1}/100 m.

3.7.3 Glacier area changes

Two different patterns of ice area loss occurred over the study area during the last 15 years. Lacustrine terminating glaciers and clean ice glaciers all lost ice around their termini/calving fronts (Figures 3.3 and 3.4) as glacial lakes expanded and termini receded. On average, lacustrine terminating glaciers each lost 0.54 ± 0.07 km^2 of ice (3.58% of their total area) over the 15 year study period. Drogpa Nagtsang reduced in size by 2.37 km^2 (9.12 % of its total area: Supplementary table 3) as the associated rapidly-forming lake expanded. Clean ice glaciers lost 0.09 ± 0.03 km^2 of ice (1.31 % of their total area) on average.

Land terminating glaciers lost little area as their surfaces lowered rather than their termini retreating. In the Tama Koshi and Dudh Koshi catchments, and in the Pumqu catchment, land terminating glaciers lost a mean of 0.14 ± 0.12 km^2 (0.50 % of their total area), 0.09 ± 0.13 km^2 (0.60 % of their total area) and 0.41± 0.12 (1.77 % of their total area) of ice, respectively. Over these glaciers, any ice area loss was concentrated up-glacier, where their lateral margins dropped down inner moraine slopes and glacier tongues narrowed slightly.

Overall, our sample of glaciers lost 0.12 ± 0.04 % of their total area per year over the study period. This figure is identical to that of Bolch et al. (2008) who assessed area change over a smaller number of the same glaciers in our sample between 1962 and 2005. The annual area change rate we calculate is lower than those estimated by Thakuri et al. (2014) and references within. Thakuri et al. (2014) calculated a median annual surface area change rate of –0.42 ± 0.06 % a^{-1} in the Dudh Koshi catchment between 1962 and 2011. However, Thakuri et al. (2014) document area change over a number of smaller glaciers that are free of debris cover, and therefore readily advance or retreat in response to climatic change, thus our estimates are not directly comparable.

3.7.4 Glacier hypsometry and approximate ELAs

The distribution of ice with elevation varies widely among the three studied catchments (Figures 3.5 and 3.6). Debris-covered glaciers of the Dudh Koshi catchment and in the Pumqu catchment are typically very bottom heavy, with average HI scores of 2.63 and 2.34, respectively (Supplementary table 1). Glacier hypsometry is concentrated between 4800 and 5500 m (Figure 3.5) for the Dudh Koshi catchment, and between 5600 and 6500 m in the Pumqu catchment. Notable exceptions are Khumbu and Ngozumpa Glaciers which store ice

in broad accumulations zones above 7000 m (Supplementary tables 1 and 2). The majority of glaciers in the Tama Koshi have an equi-dimensional hypsometry (mean HI of 1.14), with most ice stored between 5300 and 5800 m. Glaciers in the Tama Koshi have broader accumulation basins than in the Dudh Koshi catchment, and main glacier tongues are formed of multiple, smaller tributaries flowing from higher altitude in a number of cases (Figure 3.1). The mean hypsometry (Figure 3.6) of lacustrine terminating glaciers shows no distinctive morphology as the sample is composed of glaciers from all three catchments in the study area. Clean ice glaciers have a mean HI of 1.18 and could therefore be summarised as equidimensional, but the morphology of the 5 glaciers we assess is highly variable (see Supplementary table 3). In complete contrast to debris-covered glaciers, their ice is stored at higher mean altitudes on average; primarily between 6000 and 6500 m (Figure 3.6).

We estimate the mean ELA of debris-covered glaciers in the Dudh Koshi and Tama Koshi catchments, and of our selection of glaciers in the Pumqu catchment to be 5477, 5568, and 6037 m a.s.l., respectively. We estimate the mean ELA of the 5 clean-ice glaciers in our sample to be 6216 m. Using those ELAs the accumulation area ratio (AAR) (Dyurgerov et al., 2009) can be estimated for each glacier. We have calculated mean AARs of 0.41, 0.43 and 0.37 for debris-covered glaciers in the Dudh Koshi and Tama Koshi catchments, and in the Pumqu catchment, respectively. The mean AAR of clean ice glaciers in our sample is 0.39.

3.8 Discussion

3.8.1 Variability in rates of ice loss across the orographic divide

The mean mass balance estimates we have derived for glaciers situated in catchments North and South of the main orographic divide are not markedly different. However, the contrast in maximum of surface lowering (Figure 3.5) from glaciers flowing north of the divide and the sustained surface lowering through a broader portion of their elevation range (Figure 3.5) suggests an additional or amplified process has driven glacier change north of the divide over recent decades. In this section we discuss possible topographic and climatic drivers of the difference in the rates of surface lowering across the range divide.

The Indian summer monsoon delivers a large proportion of total annual precipitation (up to 80% of the total annual amount) to the Everest region of Nepal, resulting in high glacier sensitivity to temperature (Fujita, 2008; Sakai et al., 2015). The extreme topography in this region and the location of the orographic divide perpendicular to the prevailing monsoon

result in rainfall peaks that are offset from the maximum elevations, with greatest rainfall occurring to the south of the divide and decreasing to the north across the Everest region (Bookhagen and Burbank, 2010; Wagnon et al. 2013). Around 449 mm a^{-1} of rainfall falls at the Pyramid research station (5000 m a.s.l.) at Khumbu Glacier (Salerno et al., 2015), whereas Dingri on the Tibetan Plateau (4300 m a.s.l.) to the north is much drier with 263 ± 84.3 mm a^{-1} of rainfall annually (Yang et al., 2011). Snowfall may follow a similar across-range gradient to rainfall, although falling snow may be carried further into the range by prevailing winds from the south. However, no reliable measurements of snowfall exist in this region with which to compare these trends. The north-south precipitation gradient across the orographic divide promotes differences in the response of these glaciers to climate change, such that those to the north are relatively starved of snow accumulation (Owen et al., 2009) and exposed to greater incoming radiative fluxes under generally clearer skies. Owen et al. (2009) suggest that this precipitation gradient resulted in greater glacier sensitivity to climate change on the northern slopes of the Himalaya during the Late Quaternary, with asymmetric patterns of ELA rise occurring since the Last Glacial Maximum (LGM).

During the period of this study (2000–2015), mean annual air temperatures have increased and rainfall amounts appear to have decreased in the Everest region (Salerno et al., 2015). At the Pyramid Observatory at Khumbu Glacier in the Dudh Koshi catchment, increases in minimum (+0.07 °C a^{-1}), maximum (+0.009 ° C a^{-1}) and mean (+0.044 ° C a^{-1}) annual air temperatures above 5000 m a.s.l. were observed between 1994 and 2013 (Salerno et al., 2015). At Dingri on the Tibetan Plateau 60 km northeast of Mt. Everest, increases in minimum (+0.034 ° C a^{-1}), maximum (+0.041 ° C a^{-1}) and mean (+0.037 ° C a^{-1}) annual air temperatures occurred over the same period (Salerno et al., 2015). Yang et al. (2011) also show a longer-term increase in the mean annual air temperature at Dingri, as do Shrestha et al. (1999) across the southern flank of the greater Himalaya. Between 1959 and 2007, the mean annual air temperature increased by 0.06 ° C a^{-1}at Dingri (Yang et al., 2011). Shestha et al. (1999) calculated an increase in the mean annual air temperature of 0.057 ° C a^{-1} between 1971 and 1994 across a number of sites in the greater Himalaya.

The snowline altitude also appears to have increased recently on the southern flank of the Himalaya; Thakuri et al. (2014) showed a rapid ascent of the snow-line altitude in the Dudh Koshi between 1962 and 2011 (albeit through documenting transient snowlines from single scenes acquired at each epoch), and Khadka et al. (2014) suggest declining snow cover over the winter and spring months in the glacierised altitudinal ranges of the Tama Koshi catchment, between 2000 and 2009; a factor that may influence accumulation rates. Kaspari et al. (2008) showed decreasing accumulation recorded in an ice core collected from East

Rongbuk Glacier Col (6518 m a.s.l.) on the northern side of Mount Everest between the 1970s and 2001.

We suggest that the north–south orographic precipitation gradient across the main divide may have caused greater surface lowering rates on glaciers in the Pumqu catchment than those glaciers to the south over the study period. We also suggest that measured, contemporary increases in air temperature, observations of increasing snowline altitude and declining accumulation are likely to enhance glacier mass loss across the range in future, but considerable unknowns remain in the temporal evolution of debris cover extent and thickness (Thakuri et al., 2014), the strength of the summer monsoon in coming decades (e.g. Boos et al., 2016), and the expansion or shrinkage of glacial lakes (see section 5.3), all of which could additionally influence future glacier mass balance.

3.8.2 Comparison of mass balance estimates with other studies

Several other studies have generated geodetic mass balance estimates for glaciers of the Everest region over several different time periods. Bolch et al. (2011) generated balance estimates of –0.32 ± 0.08 m w.e. a^{-1} and –0.79 ± 0.52 m w.e. a^{-1} for ten glaciers to the south and west of Mt Everest over the periods 1970-2007 and 2002-2007, respectively. Nuimura et al. (2012) calculated a regional mass balance of –0.45 ± 0.25 m w.e. a^{-1} for 97 glaciers across the region over the period 1992-2008. Kääb et al. (2012) estimated a mass balance of –0.39 ± 0.11 m w.e. a^{-1} for a 3˚ x 3˚ cell centred on the Everest region between 2003 and 2008. Gardelle et al. (2013) calculated a slightly less negative mass balance of –0.26 ± 0.13 m w.e. a^{-1} between 1999 and 2011, although the SRTM penetration correction applied by Gardelle et al. (2013) may have caused bias towards less negative mass balance (Kääb et al. 2012; Barundun et al., 2015). The regional mass balance of –0.52 ± 0.22 m w.e. a^{-1} that we have calculated suggests that the mass loss rates measured by, Nuimura et al. (2012) and Kääb et al. (2012) have been sustained and possibly increased in recent years (Table 1.3), as Bolch et al. (2011) also suggest.

Table 1.3. Mass balance estimates (from geodetic and altimetric studies) for the broader Everest region and comparable sub-regions/ catchments.

Time period and area	Mass balance estimate (m w.e. a^{-1})	Study
Dudh Koshi		
1970-2008	–0.32 ± 0.08	Bolch et al. (2011)
1992-2008	–0.45 ± 0.25	Nuimura et al. (2012)
2000-2015	–0.58 ± 0.19	This study
Pumqu (Tibetan Plateau)		
1974-2006	–0.40 ± 0.27	Ye et al. (2015)
2003-2009	–0.66 ± 0.32	Neckel et al. (2014)
2000-2015	–0.61 ± 0.24	This study
Tama Koshi		
2000-2015	–0.51 ± 0.22	This study
Everest region		
1999-2011	–0.26 ± 0.13	Gardelle et al. (2013)
2003-2008	–0.39 ± 0.11	Kääb et al. (2012)
2000-2015	–0.52 ± 0.22	This study

On the Tibetan Plateau, Neckel et al. (2014) estimated the mass balance of glaciers on the northern side of the orographic divide in the central and eastern Himalaya (their sub-region G) to be –0.66 ± 0.36 m w.e. a^{-1} between 2003 and 2009. The mass balance of glaciers in our sample within the same region was –0.59 ± 0.27 m w.e. a^{-1} between 2000 and 2015. Ye et al. (2015) estimated glacier mass balance to be –0.40 ± 0.27 m w.e. a^{-1} in the Rongbuk catchment between 1974 and 2006, suggesting that glacier ice mass loss rates may have increased over the last decade in this area of the Tibetan Plateau (Table 1.3).

3.8.3 The influence of glacial lakes on glacier mass balance

Only Nuimura et al. (2012) have directly compared mass loss rates of lacustrine and land terminating glaciers in the study area, showing faster surface lowering rates over Imja and Lumding glaciers in the Dudh Koshi catchment. Our data confirm that lacustrine terminating glaciers can indeed lose ice at a much faster rate than land terminating glaciers. The variability in the mass balance of the nine lacustrine terminating glaciers (Figure 3.6) we highlight suggests the fastest mass loss rates occur in the later stages of lake development. Glaciers such as the Yanong and Yanong North, in the Tama Koshi catchment, sit behind large proglacial lakes and are in a state of heavily negative mass balance (–0.76 ± 0.18 and –0.62 ± 0.25 m w.e. a^{-1}, respectively). Their surfaces lowered by 3 m a^{-1} or more over their lower reaches (Figure 3.6) over the study period. These glaciers

are now relatively small and steep and no longer possess a debris-covered tongue, and so may represent the end-product of debris-covered glacier wastage described by Benn et al. (2012). In contrast, glaciers such as Duiya, in the Pumqu catchment, currently has only a small lake at its termini, showed moderate area losses (0.5 km^2, or 4.28% of its total area) and moderately negative mass balance (–0.45 ± 0.13 m w.e. a^{-1}) over the study period. Continued thinning of the terminal regions of glaciers with smaller glacial lakes would lead to a reduction in effective pressure, an increase in longitudinal strain and therefore flow acceleration (Benn et al., 2007). The retreat of the calving front up-valley into deeper bed topography may also increase calving rates (Benn et al., 2007), and a combination of both of these processes would lead to enhanced ice loss. Very little surface velocity data exist for lacustrine terminating debris-covered glaciers. Only Quincey et al. (2009) measured high surface velocities (25 m a^{-1} or more) over Yanong glacier (their Figure 4, panel D), suggesting it is possible for lacustrine terminating glaciers to become more dynamic in the later stages of lake development in the Himalaya. Conversely, Thakuri et al. (2016) have shown flow deceleration of glaciers that coalesce to terminate in Imja Tsho over the period 1992-2014, and suggest that reduced accumulation caused by decreasing precipitation is responsible for diminishing surface flow on this glacier. Clearly, more expansive investigation into the evolving dynamics of lacustrine terminating glaciers in the Himalaya is required if we are to better understand their potential future mass loss.

3.8.4 Glacier stagnation

A number of studies (Luckman et al. 2007; Scherler et al. 2008, 2011; Quincey et al. 2009) have shown how many glaciers in the Everest region appear to be predominantly stagnant, with large parts of the long, debris-covered glacier tongues in the area showing little to no flow. Watson et al. (2016) have documented an increasing number and total area of supraglacial melt ponds over a number of the same glaciers studied by Quincey et al. (2009) in the Dudh Koshi catchment (Khumbu, Ngozumpa, Lhotse, Imja and Ama Dablam), since the early 2000's. Over these glaciers, our data show a very distinctive surface lowering pattern (Figure 3.2), with localised, heterogenous surface lowering appearing to mirror the distribution of large supraglacial ponds and ponds networks. This ice loss pattern is prevalent on the Erbu, Gyachung, Jiuda, Shalong, and G1 glaciers (Figure 3.2), and high resolution imagery available on Google Earth shows that these glaciers also have well developed networks of supraglacial ponds. We would therefore suggest that large parts of the biggest glaciers in the Tama Koshi catchment and on the Tibetan Plateau are also stagnant, and may see increasing supraglacial meltwater storage in the future, similar to that documented by Watson et al. (2016).

3.8.5 Susceptibility of glaciers to future mass loss- ELA ascent in response to warming

The coincidence of maximum surface lowering rates with the altitude of maximum hypsometry in the Dudh Koshi catchment (Figure 3.5) suggests large glacier mass losses in this catchment. Sustained and prolonged mass loss may lead to a bi-modal hypsometry here, with the physical detachment of debris-covered glacier tongues and their high-elevation accumulation zones a possibility (Rowan et al., 2015; Shea et al., 2015). Surface lowering maxima in the Tama Koshi catchment presently occur at a slightly lower elevation range than the main hypsometric concentration, and across lower reaches of glacier tongues in the Pumqu catchment.

Figure 3.7 shows projected AARs, averaged across each catchment, in response to different levels of temperature rise. These predictions are based on published lapse rates (Immerzeel et al., 2014; Kattel et al., 2015) that may be spatially variable and assume no changes in precipitation type or amount, or any variability in the contribution of avalanches to accumulation.

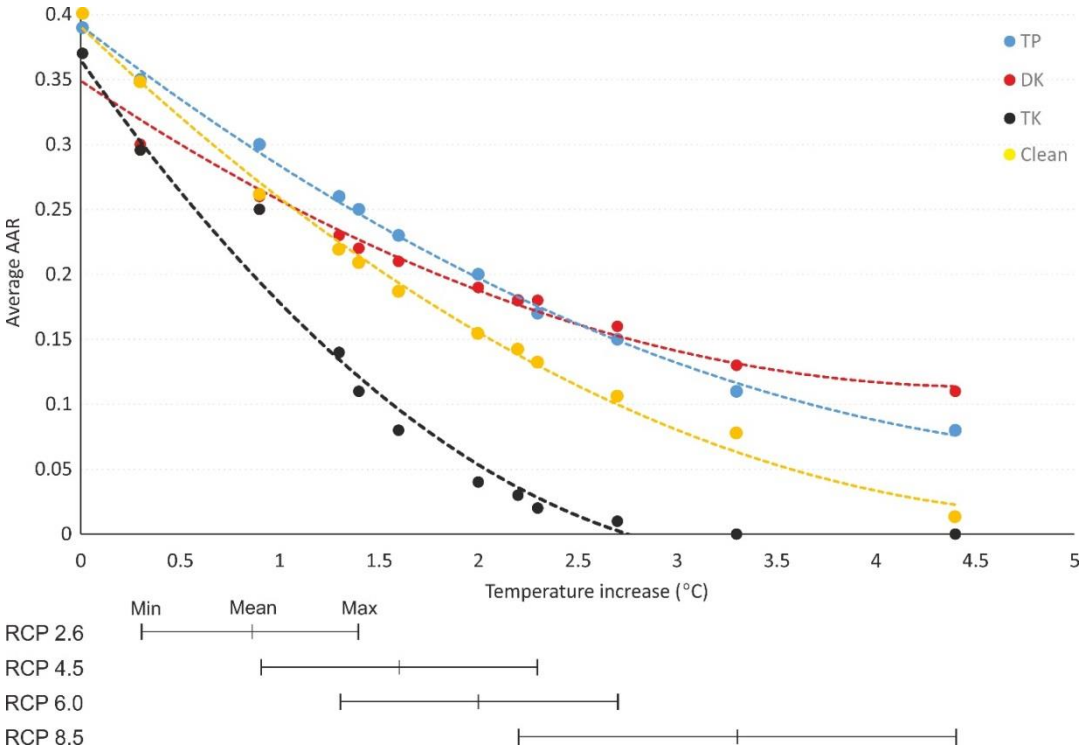

Figure 3.7. Projected AARs (averaged across each catchment) based on different scenarios of temperature increase relative to the present day and accompanying ELA rise. Temperature rise scenarios have been used from the IPCC AR5 Working Group report. TP-

Tibetan Plateau; DK- Dudh Koshi; TK- Tama Koshi; Clean- Clean ice glaciers. Each point represents a projected AAR given minimum, mean or maximum temperature rise under each RCP scenario.

To allow the comparison of our results with similar estimates of other studies (Shea et al., 2015; Rowan et al., 2015), we focus specifically on ELA rise resulting from RCP 4.5 minimum and maximum projected warming of annual air temperatures (+0.9 ºC to +2.3 ºC by 2100). Such temperature increases would cause a rise in ELA of between 165 and 425 m in the Dudh and Tama Koshi catchments, and between 107 and 270 m of ELA ascent over glaciers in the Pumqu catchment . A rise in ELAs would most significantly affect the Tama Koshi catchment glaciers, which currently has the highest catchment averaged AAR- 0.43. RCP 4.5 warming could cause AAR decrease to 0.29 and 0.08, respectively, in the Tama Koshi catchment. The greater altitudinal range and higher accumulation zones of glaciers in the Dudh Koshi catchment and in the Pumqu catchment would dampen the effects of a rise in ELA on glacier mass balance, with AAR adjustment occurring more gradually (Figure 3.7). AARs could decrease to 0.27 or 0.17 in the Dudh Koshi and to 0.29 or 0.18 in the Pumqu catchment. ELA rise in response to this particular warming scenario would mean a 12–30% increase in the total glacierised area below the ELA in the Pumqu catchment , a 24–61 % increase in the Tama Koshi catchment, and a 23-40% increase in the Dudh Koshi catchment. Should more substantial temperature increases occur (> 2 ºC warming), AARs could reduce to zero on a number of individual glaciers, and the ELA could rise to near maximum glacier altitudes in the Tama Koshi catchment. Clean ice glacier AAR adjustment may be rapid given their limited altitudinal range (Figure 3.7).

Glacier AAR is a parameter strongly related to long-term mass balance for typical alpine glaciers (König et al., 2014), although the effect of a diminishing AAR may be dampened on Himalayan glaciers given the large input of avalanche material derived from high surrounding headwalls (Iturrizaga, 2011). Since data on the rates of avalanching in high-mountain environments such as the Himalaya are sparse (Benn and Lehmkuhl, 2001), the impact of predicted AAR reduction remains somewhat uncertain.

3.9 Conclusions

DEM differencing has revealed substantial mass loss from many large, debris-covered glaciers in the central Himalaya over the last 15 years. Geodetic mass balance estimates have been calculated for 32 glaciers across three different catchments around the Everest region. We found similarly negative mass budgets for glaciers flowing onto the southern

flank of the Himalaya, in the Tama Koshi (–0.51 ± 0.22 m w.e. a^{-1}) and Dudh Koshi (–0.58 ± 0.19 m w.e. a^{-1}) catchments, and in the Pumqu catchment (–0.61 ± 0.24 m w.e. a^{-1}).

The division of our sample of glaciers depending on their terminus type shows contrasting mass loss rates between land and lacustrine terminating glaciers. The mean mass balance of nine lacustrine terminating glaciers we assessed was –0.70 ± 0.26 m w.e. a^{-1}, 32% more negative than land terminating glaciers (mean mass balance of –0.53 ± 0.21 m w.e. a^{-1}). The mass balance of nine lacustrine terminating glaciers ranged from –0.91 ± 0.22 m w.e. a^{-1} to –0.45 ± 0.13 m w.e. a^{-1} and we would suggest that glacial lakes in the region are at different stages of expansion. Accelerating mass loss is likely from several of these lacustrine terminating glaciers whose termini will retreat into deeper lake water.

Surface lowering curves show that the maximum lowering rate (–1.62 ± 0.14 m a^{-1} between 5300 and 5400 m.a.s.l.) of glaciers in the Pumqu catchment was well above the maximum lowering rate of glaciers flowing south of the orographic divide (–1.06 ± 0.10 m a^{-1} between 5200 and 5300 m a.s.l. in the Dudh Koshi catchment, –1.08 ± 0.12 m a^{-1} between 5200 and 5300 m a.s.l. in the Tama Koshi catchment), and that glaciers in the Pumqu catchment are losing ice over a much broader altitudinal range than their south-flowing counterparts. We suggest that the across-range contrast in annual precipitation amount, combined with rising mean air temperatures over recent decades may have caused greater ice loss rates from the north flowing glaciers.

Predicted warming in the Everest region will lead to increased ELAs and, depending on glacier hypsometry, substantial increases in the size of ablation areas. We show that glaciers of the Tama Koshi catchment will see the greatest reduction in glacier AAR due to their equidimensional hypsometry and more limited elevation range in comparison to glaciers of the Dudh Koshi or in the Pumqu catchment. Warming of +0.9 ^{o}C to +2.3 ^{o}C by 2100 (IPCC RCP 4.5) would decrease glacier AAR to 0.29 or 0.08 in the Tama Koshi catchment, 0.27 or 0.17 in the Dudh Koshi catchment, and 0.29 or 0.18 in the Pumqu catchment , respectively.

Our findings are important for two reasons. First, they suggest that glacial lake growth and current glacial lake expansion that has been documented across the Himalaya could be accompanied by amplified glacier mass loss in the near future. Second, they show that glacier AAR adjustment in response to predicted warming across the Himalaya could be spatially very variable, complicating the prediction of future glacier meltwater runoff contribution from river catchments across the region.

Author contribution

OK, DQ and JC designed the study. OK carried out all data processing and analysis. OK, DQ, JC and AR wrote the paper.

Acknowledgements

SETSM DEMs are available for download from http://www.pgc.umn.edu/elevation. The SRTM dataset is available from https://lta.cr.usgs.gov/SRTM1Arc. EGM2008 gridded data is available from http://earth-info.nga.mil/GandG/wgs84/gravitymod/egm2008/egm08_gis.html. OK is a recipient of a NERC DTP PhD studentship. We are grateful for the comments of Benjamin Robson for his comments on an early version of the paper, and for guidance on the use of SETSM data from Ian Howat. We finally thank Tobias Bolch, Joseph Shea and an anonymous reviewer for their thorough and constructive assessments of the manuscript.

References

Arendt, A., Echelmeyer, K., Harrison, W., Lingle, C., Zirnheld, S., Valentine, V., Ritchie, B. and Druckenmiller, M.: Updated estimates of glacier volume changes in the western Chugach Mountains, Alaska, and a comparison of regional extrapolation methods, J Geophys Res-Earth, 111 (F3), 2006.

Arendt, A., Bliss, A., Bolch, T., Cogley, J. G., Gardner, A. S., Hagen, J.-O., Hock, R., Huss, M., Kaser, G., Kienholz, C., Pfeffer, W. T., Moholdt, G., Paul, F., Radić, V., Andreassen, L., Bajracharya, S., Barrand, N.E., Beedle, M., Berthier, E., Bhambri, R., Brown, I., Burgess, E., Burgess, D., Cawkwell, F., Chinn, T., Copland, L., Davies, B., De Angelis, H., Dolgova, E., Earl, L., Filbert, K., Forester, R., Fountain, A. G., Frey, H., Giffen, B., Glasser, N. F., Guo, W. Q., Gurney, S., Hagg, W., Hall, D., Haritashya, U. K., Hartmann, G., Helm, C., Herreid, S., Howat, I., Kapustin, G., Khromova, T., König, M., Kohler, J., Kriegel, D., Kutuzov, S., Lavrentiev, I., LeBris, R., Liu, S. Y., Lund, J., Manley, W., Marti, R., Mayer, C., Miles, E. S., Li, X., Menounos, B., Mercer, A., Mölg, N., Mool, P., Nosenko, G., Negrete, A., Nuimura, T., Nuth, C., Pettersson, R., Racoviteanu, A., Ranzi, R., Rastner, P., Rau, F., Raup, B., Rich, J., Rott, H., Sakai, A., Schneider, C., Seliverstov, Y., Sharp, M., Sigurðsson, O., Stokes, C., Way, R. G., Wheate, R., Winsvold, S., Wolken, G., Wyatt, F., Zheltyhina, N. Randolph Glacier Inventory – A Dataset of Global Glacier Outlines: Version 5.0. Global Land Ice Measurements from Space, Boulder Colorado, USA. Digital Media, 2015.

Asahi, K. Inventory and recent variations of glaciers in the eastern Nepal Himalayas. Journal of the Japanese Society of Snow and Ice, 63, 159-169, 2001.

Bajracharya, S. R., Maharjan, S. B., Shrestha, F., Guo, W., Liu, S., Immerzeel, W. & Shrestha, B. The glaciers of the Hindu Kush Himalayas: current status and observed changes from the 1980s to 2010. International Journal of Water Resources Development, 31, 161-173, 2015.

Bajracharya, S. R. & Mool, P. Glaciers, glacial lakes and glacial lake outburst floods in the Mount Everest region, Nepal. Annals of Glaciology, 50, 81-86, 2009.

Barundun, M., Huss, M., Sold, L., Farinotti, D., Azisov, E., Salzmann, N., Usubaliev, R., Merkushkin, A. and Hoelzle, M.: Re-analysis of seasonal mass balance at Abramov glacier 1968–2014, Journal of Glaciology, 61(230), 1103–1117, doi:10.3189/2015JoG14J239, 2015.

Benn, D.I., Lehmkuhl, F. Mass balance and equilibrium line altitudes of glaciers in high mountain environments. Quaternary International 65/66, 15–29. 2000.

Benn, D. I., Kirkbride, M.P., Owen, L.A. & Brazier, V. Glaciated valley landsystems. In: Evans, D.J.A. (Ed.), Glacial Landsystems. Arnold, pp. 372–406, 2003.

Benn, D. I., Warren, C. R. & Mottram, R. H. Calving processes and the dynamics of calving glaciers. Earth-Science Reviews, 82, 143-179, 2007.

Benn, D. I., Bolch, T., Hands, K., Gulley, J., Luckman, A., Nicholson, L. I., Quincey, D., Thompson, S., Toumi, R. & Wiseman, S. Response of debris-covered glaciers in the Mount Everest region to recent warming, and implications for outburst flood hazards. Earth-Science Reviews, 114, 156-174, 2012.

Berthier, E., Arnaud, Y., Kumar, R., Ahmad, S., Wagnon, P. & Chevallier, P. Remote sensing estimates of glacier mass balances in the Himachal Pradesh (Western Himalaya, India). Remote Sensing of Environment, 108, 327-338, 2007.

Berthier, E., Arnaud, Y., Vincent, C. & Remy, F. Biases of SRTM in high-mountain areas: Implications for the monitoring of glacier volume changes. Geophysical Research Letters, 33, 2006.

Berthier, E., Scheifer, E., Clarke, G. K. C., Menounos, B. & Remy, F. Contribution of Alaskan glaciers to sea-level rise derived from satellite imagery. Nature Geoscience, 3, 92-95, 2010.

Berthier, E., Cabot, V., Vincent, C. & Six, D. Decedal region-wide and glacier wide mass balances derived from multi-temporal ASTER satellite digital elevation models. Validation over the Mont-Blanc area. Frontiers in Earth Science, 4. Doi 10.3389/feart.2016.00063, 2016.

Bhutiyana, M.R. Kale, V.S. & Pawar, N.J. Climate change and the precipitation variations in the northwestern Himalaya: 1866-2006. International Journal of Climatology, 30, 535-548, 2010.

Bolch, T., Kulkarni, A., Kääb, A., Huggel, C., Paul, F., Cogley, J. G., Frey, H., Kargel, J. S., Fujita, K., Scheel, M., Bajracharya, S. & Stoffel, M. The State and Fate of Himalayan Glaciers. Science, 336, 310-314, 2012.

Bolch, T., Pieczonka, T. & Benn, D. I. Multi-decadal mass loss of glaciers in the Everest area (Nepal Himalaya) derived from stereo imagery. Cryosphere, 5, 349-358, 2011.

Bollasina, M. A., Ming, Y. & Ramaswamy, V. Anthropogenic Aerosols and the Weakening of the South Asian Summer Monsoon. Science, 334, 502-505, 2011.

Bookhagen, B. & Burbank, D. Towards a complete Himalayan hydrologic budget: The spatiotemporal distribution of snow melt and rainfall and their impact on river discharge. Journal of Geophysical Research, 115, p.F03019.

Boos, W. R. & Storelvmo, T. Near-linear response of mean monsoon strength to a broad range of radiative forcings. Proceedings of the National Academy of Sciences, 113, 1510-1515, 2016.

Buchroithner, M. F., Jentsch, G. & Wanivenhaus, B. Monitoring of recent geological events in the Khumbu area (Himalaya, Nepal) by digital processing of landsat MSS data. Rock mechanics, 15, 181-197, 1982.

Carrivick, J. L., & Tweed, F. S. Proglacial lakes: character, behaviour and geological importance. Quaternary Science Reviews, 78, 34-52, 2013.

Che, T., Xaio, L. & Liou, Y.-A. Changes in Glaciers and Glacial Lakes and the Identification of Dangerous Glacial Lakes in the Pumqu River Basin, Xizang (Tibet). Advances in Meteorology, 2014, 8, 2014.

Cherkasov, P. & Ahmetova, G.S. Ice flow and mass continuity of Shumsky Glacier in the Djungarski Alatau Range of Kazakhstan, Central Asia. Journal of Geophysical Research, 101, 12913-12920, 1996.

Collins, M., R. Knutti, J. Arblaster, J.-L. Dufresne, T. Fichefet, P. Friedlingstein, X. Gao, W.J. Gutowski, T. Johns, G. Krinner, M. Shongwe, C. Tebaldi, A.J. Weaver and M. Wehner, 2013: Long-term Climate Change: Projections, Commitments and Irreversibility. In: Climate Change 2013: The Physical Science Basis. Contribution of Working Group I to the Fifth Assessment Report of the Intergovernmental Panel on Climate Change [Stocker, T.F., D. Qin, G.-K. Plattner, M. Tignor, S.K. Allen, J. Boschung, A. Nauels, Y. Xia, V. Bex and P.M. Midgley (eds.)]. Cambridge University Press, Cambridge, United Kingdom and New York, NY, USA.

Cherkasov, P. & Ahmetova, G.S. Ice flow and mass continuity of Shumsky Glacier in the Djungarski Alatau Range of Kazakhstan, Central Asia. Journal of Geophysical Research, 101, 12913-12920, 1996.

Dyurgerov, M., Meier, M. F. & Bahr, D. B. A new index of glacier area change: a tool for glacier monitoring. Journal of Glaciology, 55, 710-716, 2009.

Farr, T.G., Rosen, P.A., Carop, E., Crippen, R., Duren, R., Hensley, S., Korbick, M., Paller, M., Rodriguez, E., Roth, L., Seal, D., Shaffer, S., Shimada, J., Umland, J., Werner, M., Oskin, M., Burbank, D. & Alsdorf, D. The Shuttle Radar Topography Mission. Reviews of Geophysics, 45. doi:10.1029/2005RG000183, 2007.

Farinotti, D., Huss, M., Bauder, A., Funk, M. & Truffer, M. A method to estimate the ice volume and ice-thickness distribution of alpine glaciers. Journal of Glaciology, 55, 191, 2009.

Frey, H., Machguth, H., Huss, M., Huggel, C., Bajracharya, S., Bolch, T., Kulkarni, A., Linsbauer, A., Salzmann, N. & Stoffel, M. Estimating the volume of glaciers in the Himalayan-Karakoram region using different methods. The Cryosphere, 8, 2313-2333, 2014.

Furbish, D.J. & Andrews, J.T. The use of hypsometry to indicate long term stability and response of valley glaciers to changes in mass transfer. Journal of Glaciology, 30, 105, 199-211, 1984.

Fujita, K.: Effect of precipitation seasonality on climatic sensitivity of glacier mass balance, Earth and Planetary Science Letters, 276, 14–19, doi:10.1016/j.epsl.2008.08.028, 2008.

Gardelle, J., Arnaud, Y. & Berthier, E. Contrasted evolution of glacial lakes along the Hindu Kush Himalaya mountain range between 1990 and 2009. Global and Planetary Change, 75, 47-55, 2011.

Gardelle, J., Berthier, E. and Arnaud, Y.: Slight mass gain of Karakorum glaciers in the early 21st century, Nat Geosci, 5(5), 322–325, doi:10.1038/ngeo1450, 2012.

Gardelle, J., Berthier, E., Arnaud, Y. & Kääb, A. Region-wide glacier mass balances over the Pamir-Karakoram-Himalaya during 1999-2011. Cryosphere, 7, 1263-1286, 2013.

Hambrey, M. J., Quincey, D. J., Glasser, N. F., Reynolds, J. M., Richardson, S. J. & Clemmens, S. Sedimentological, geomorphological and dynamic context of debris-mantled glaciers, Mount Everest (Sagarmatha) region, Nepal. Quaternary Science Reviews, 27, 2361-2389, 2008.

Huss, M.: Density assumptions for converting geodetic glacier volume change to mass change, The Cryosphere, 7, 877-887, doi:10.5194/tc-7-877-2013, 2013.

Huss, M., Bauder, A., Funk, M. & Hock, R. 2008. Determination of the seasonal mass balance of four Alpine glaciers since 1865. Journal of Geophysical Research: Earth Surface, 113, doi:10.1029/2007JF000803, 2008.

Huss, M. & Farinotti, D. Distributed ice thickness and volume of all glaciers around the globe, Journal of Geophysical Research, 117, F04010, doi:10.1029/2012JF002523, 2012.

Huss, M. & Hock, R. A new model for global glacier change and sea-level rise. Frontiers in Earth Science, 3, 2015.

Immerzeel, W. W., Van Beek, L. P. H. & Bierkens, M. F. P. Climate Change Will Affect the Asian Water Towers. Science, 328, 1382-1385, 2010.

Immerzeel, W.W., Kraaijenbrink, M. Shea, J.M., Shrestha, A.B., Pellicciotti, F., Bierkens, M.F.P. & de Jong, S.M. High-resolution monitoring of Himalayan glacier dynamics using unmanned aerial vehicles. Remote Sensing of Environment, 150, 93-103, 2014.

Jin, R., Li, X., Che, T., WU, L. & Mool, P. Glacier area changes in the Pumqu river basin, Tibetan Plateau, between the 1970s and 2001. Journal of Glaciology, 51, 607-610, 2005.

Jiskoot, H., Curran, C. J., Tessler, D. L. & Shenton, L. R. Changes in Clemenceau Icefield and Chaba Group glaciers, Canada, related to hypsometry, tributary detachment, length, slope and area & aspect relations. Annals of Glaciology, 50, 133-143, 2009.

Kääb, A. Combination of SRTM3 and repeat ASTER data for deriving alpine glacier flow velocities in the Bhutan Himalaya. Remote Sensing of Environment, 94, 463-474, 2005.

Kääb, A., Berthier, E., Nuth, C., Gardelle, J. & Arnaud, Y. Contrasting patterns of early twenty-first-century glacier mass change in the Himalayas. Nature, 488, 495-498, 2012.

Kääb, A., Treichler, D., Nuth, C. and Berthier, E., 2015. Brief Communication: Contending estimates of 2003–2008 glacier mass balance over the Pamir–Karakoram– Himalaya. The Cryosphere, 9(2), pp.557-564, 2015.

Kapnick, S. B., Delworth, T. L., Ashfaq, M., Malyshev, S. & Milly, P. C. D. Snowfall less sensitive to warming in Karakoram than in Himalayas due to a unique seasonal cycle. Nature Geosci, 7, 834-840, 2014.

Kaspari, S., Hooke, R. LeB., Mayewski, P.A., Kang, S.C., Hou, S.G. & Qin, D.H. Snow accumulation rate on Qomolangma (Mount Everest), Himalaya: synchroneity with sites across the Tibetan Plateau on 50-100 year timescales. Journal of Glaciology, 54, 185, 343-352. Doi: 10.3189/002214308784886126, 2008.

Kattel, D. B., Yao, T., Yang, W., Gao, Y. & Tian, L. Comparison of temperature lapse rates from the northern to the southern slopes of the Himalayas. International Journal of Climatology, 35, 4431-4443, 2015.

Khadka, D., Babel, M. S., Shrestha, S. & Tripathi, N. K. Climate change impact on glacier and snow melt and runoff in Tamakoshi basin in the Hindu Kush Himalayan (HKH) region. Journal of Hydrology, 511, 49-60, 2014.

König, M., Nuth, C., Kohler, J., Moholdt, G. & Pettersen, R. A digital glacier database for svalbard. In: Kargel, S. J., Leonard, J. G., Bishop, P. M., Kääb, A. & Raup, H. B. (eds.) Global Land Ice Measurements from Space. Berlin, Heidelberg: Springer Berlin Heidelberg, 2014.

Larsen, C. F., Motyka, R. J., Arendt, A. A., Echelmeyer, K. A. & Geissler, P. E. Glacier changes in southeast Alaska and northwest British Columbia and contribution to sea level rise. Journal of Geophysical Research: Earth Surface, 112, F01007, 2007.

Luckman, A., Quincey, D. & Bevan, S. The potential of satellite radar interferometry and feature tracking for monitoring flow rates of Himalayan glaciers. Remote Sensing of Environment, 111, 172-181, 2007.

Lutz, A. F., Immerzeel, W. W., Gobiet, A., Pellicciotti, F. & Bierkens, M. F. P. Comparison of climate change signals in CMIP3 and CMIP5 multi-model ensembles and implications for Central Asian glaciers. Hydrol. Earth Syst. Sci., 17, 3661-3677, 2013.

Mertes, J. R., Thompson, S. S., Booth, A. D., Gulley, J. D., & Benn, D. I. A conceptual model of supraglacial lake formation on debris-covered glaciers based on GPR facies analysis, Earth Surf. Proc. Land., 42, 903–914, https://doi.org/10.1002/esp.4068, 2016.

Neckel, N., Kropacek, J., Bolch, T., and Hochschild, V.: Glaciervmass changes on the Tibetan Plateau 2003–2009 derived from ICESat laser altimetry measurements, Environ. Res. Lett., 9, 014009, doi:10.1088/1748-9326/9/1/014009, 2014.

Noh, M. J. & Howat, I. M. Automated stereo-photogrammetric DEM generation at high latitudes: Surface Extraction with TIN-based Search-space Minimization (SETSM) validation and demonstration over glaciated regions. GIScience & Remote Sensing, 52, 198-217, 2015.

Nuimura, T., Fujita, K., Yamaguchi, S. & Sharma, R. R. Elevation changes of glaciers revealed by multitemporal digital elevation models calibrated by GPS survey in the Khumbu region, Nepal Himalaya, 1992-2008. Journal of Glaciology, 58, 648-656, 2012.

Nuth, C. & Kääb, A. Co-registration and bias corrections of satellite elevation data sets for quantifying glacier thickness change. Cryosphere, 5, 271-290, 2011.

Nuth, C., Kohler, J., Aas, H. F., Brandt, O. & Hagen, J. O. Glacier geometry and elevation changes on Svalbard (1936-90): a baseline dataset. In: SHARP, M. (ed.) Annals of Glaciology, Vol 46, 2007. Cambridge: Int Glaciological Soc, 2007.

Owen, L.A. Robinson, R., Benn, D.I., Finkel, R.C., Davis, N.K., Yi, C., Putkonen, J., Li, D. & Murray, A.S. Quaternary glaciation of Mount Everest. *Quaternary Science Reviews*, 28(15-16), pp.1412–1433, 2009.

Pellicciotti, F., Stephan, C., Miles, E., Herreid, S., Immerzeel, W. W. & Bolch, T. Mass-balance changes of the debris-covered glaciers in the Langtang Himal, Nepal, from 1974 to 1999. Journal of Glaciology, 61, 373-386, 2015.

Pepin, N., Bradley, R.S., Diaz, H.F., Baraer, M., Caceres, E.B., Forsythe, N., Fowler, G., Greenwood, M.Z., Hashmi, X.D., Liu, J.R., Miller, K., Ning, A., Ohmura, E., Palazzi, I., Rangwala, W., Schöner, I., Seversky, M., Shahgedanova, M., Wang, S.N. Williamson, N. & Yang, D.Q. Elevation-dependent warming in mountain regions of the world. Nature Clim. Change, 5, 424-430, 2015.

Pope, A. Willis, I.C., Palsson, F., Arnold, N.S., Rees, G., Bjornsson, H. & Grey, L. Elevation change, mass balance, dynamics and surging of Langjökull, Iceland from 1997 to 2007, Journal of Glaciology, 62(233), 497-511, doi: 10.1017/jog.2016.55, 2016.

Quincey, D. J., Luckman, A. & Benn, D. Quantification of Everest region glacier velocities between 1992 and 2002, using satellite radar interferometry and feature tracking. Journal of Glaciology, 55, 596-606, 2009.

Quincey, D. J., Richardson, S. D., Luckman, A., Lucas, R. M., Reynolds, J. M., Hambrey, M. J. & Glasser, N. F. Early recognition of glacial lake hazards in the Himalaya using remote sensing datasets. Global and Planetary Change, 56, 137-152, 2007.

Ragettli, S., Bolch, T., and Pellicciotti, F.: Heterogeneous glacier thinning patterns over the last 40 years in Langtang Himal, Nepal, The Cryosphere, 10, 2075-2097, doi:10.5194/tc-10-2075-2016, 2016.

Rankl, M. & Braun, M.: Glacier elevation and mass changes over the central Karakoram region estimated from TanDEM-X and SRTM/X-SAR digital elevation models, Annals of Glaciology, 51(71), 273–280, doi:10.3189/2016AoG71A 024, 2016.

Reynolds, J.M. Glacial hazard assessment at Tsho Rolpa, Rolwaling, Central Nepal. Quaterly Journal of Engineering Geology and Hydrogeology, 32, 209-214, 1999.

Rignot, E., Echelmeyer, K. & Krabill, W. Penetration depth of interferometric synthetic-aperture radar signals in snow and ice. Geophysical Research Letters, 28, 3501-3504, 2001.

Rounce, D. R. & McKinney, D. C. Debris thickness of glaciers in the Everest area (Nepal Himalaya) derived from satellite imagery using a nonlinear energy balance model. The Cryosphere, 8, 1317-1329, 2014.

Rowan, A. V., Egholm, D. L., Quincey, D. J. & Glasser, N. F. Modelling the feedbacks between mass balance, ice flow and debris transport to predict the response to climate change of debris-covered glaciers in the Himalaya. Earth and Planetary Science Letters, 430, 427-438, 2015.

Rupper, S., Schaefer, J.M., Burgener, L.K., Koenig, L.S., Tsering, K. & Cook, E.R. Sensitivity and response of Bhutanese glaciers to atmospheric warming. *Geophysical Research Letters*, 39(19), p.L19503, 2012.

Sakai, A., Chikita, K. & Yamada, T. Expansion of a moraine-dammed glacial lake, Tsho Rolpa, in Rolwaling Himal, Nepal Himalaya. Limnology and Oceanography, 45, 1401-1408, 2000.

Sakai, A., Nuimura, T., Fujita, K., Takenaka, S., Nagai, H. and Lamsal, D.: Climate regime of Asian glaciers revealed by GAMDAM glacier inventory, The Cryosphere, 9(3), 865–880, doi:10.5194/tc-9-865-2015, 2015.

Salerno, F., Thakuri, S., D'Agata, C., Smiraglia, C., Manfredi, E.C., Viviano, G. & Tartari, G. Glacial lake distribution in the Mount Everest Region: Uncertainty of measurement and conditions of formation. Global and Planetary Change, 92-93, 30-39, 2012.

Salerno, F., Guyennon, N., Thakuri, S., Viviano, G., Romano, E., Vuillermoz, E., Cristofanelli, P., Stocchi, P., Agrillo, G., Ma, Y. & Tartari, G. Weak precipitation, warm winters and springs impact glaciers of south slopes of Mt. Everest (central Himalaya) in the last 2 decades (1994–2013). The Cryosphere, 9, 1229-1247, 2015.

Scherler, D., Leprince, S. & Strecker, M. R. Glacier-surface velocities in alpine terrain from optical satellite imagery - Accuracy improvement and quality assessment. *Remote Sensing of Environment*, 112, 3806-3819, 2008.

Scherler, D., Bookhagen, B. & Strecker, M.R. Hillslope-glacier coupling: The interplay of topography and glacial dynamics in High Asia. Journal of Geophysical Research, 116, doi:10.1029/2010JF001751, 2011.

Shea, J.M., Immerzeel, W.W., Wagnon, P., Vincent, C. and Bajracharya, S. Modelling glacier change in the Everest region, Nepal Himalaya. The Cryosphere, 9(3), pp.1105-1128, 2015.

Shrestha, A. B., Wake, C. P., Mayewski, P. A. & Dibb, J. E. Maximum temperature trends in the Himalaya and its vicinity: An analysis based on temperature records from Nepal for the period 1971-94. Journal of Climate, 12, 2775-2786, 1999.

Somos-Valenzuela, M. A., Mckinney, D. C., Rounce, D. R. & Byers, A. C. Changes in Imja Tsho in the Mount Everest region of Nepal. Cryosphere, 8, 1661-1671, 2014.

Thakuri, S., Salerno, F., Smiraglia, C., Bolch, T., D'Agata, C., Viviano, G. & Tartari, G. Tracing glacier changes since the 1960s on the south slope of Mt. Everest (central Southern Himalaya) using optical satellite imagery. Cryosphere, 8, 1297-1315, 2014.

Thakuri, A., Salerno, F., Bolch, T., Guyennon, N. & Tartari, G. Factors controlling the accelerated expansion of Imja Lake, Mount Everest region, Nepal. Annals of Glaciology, 57(71), doi: 10.3189/2016AoG71A063, 2016.

USGS. 2016. *Shuttle Radar Topography Mission (SRTM) 1 Arc-Second Global*. [ONLINE] Available at: https://lta.cr.usgs.gov/SRTM1Arc. [Accessed 08 March 2016]

Vuichard, D. & Zimmerman, M. The 1985 Catastrophic Drainage of a Moraine-Dammed Lake, Khumbu Himal, Nepal: Cause and Consequences. Mountain Research and Development, 7, 91-110, 1987.

Wagnon, P., Vincent, C., Arnaud, Y., Berthier, E., Vuillermoz, E., Gruber, S., Ménégoz, M., Gilbert, A., Dumont, M., Shea, J.M. and Stumm, D. Seasonal and annual mass balances of Mera and Pokalde glaciers (Nepal Himalaya) since 2007. Cryosphere, 7(6), pp.1769-1786, 2013.

Watson, C.S. Quincey, D.J, Carrivick, J.L. and Smith, M.W. The dynamics of supraglacial ponds in the Everest region, central Himalaya. Global and Planetary Change, 142, 14-27, 2016.

Yang, X., Zhang, T., Qin, D., Kang, S. & Qin, X. Characteristics and Changes in Air Temperature and Glacier's Response on the North Slope of Mt. Qomolangma (Mt. Everest). Arctic, Antarctic, and Alpine Research, 43, 147-160, 2011.

Ye, Q., Kang, S., Chen, F. & Wang, J. Monitoring glacier variations on Geladandong mountain, central Tibetan Plateau, from 1969 to 2002 using remote-sensing and GIS technologies. Journal of Glaciology, 52, 179, 537-545, 2006.

Ye, Q., Bolch, T., Naruse, R., Wang, Y., Zong, J., Wang, Z., Zhao, R., Yang, D. & Kang, S. Glacier mass changes in Rongbuk catchment on Mt. Qomolangma from 1974 to 2006 based on topographic maps and ALOS PRISM data. Journal of Hydrology, 530, 273-280, 2015.

Chapter 4

Contrasting geometric and dynamic evolution of lake and land-terminating glaciers in the central Himalaya

Owen King[1], Amaury Dehecq[2], Duncan Quincey[1], Jonathan Carrivick[1]

Manuscript published in Global and Planetary Change, doi.org/10.1016/j.gloplacha.2018.05.006

4.1 Abstract

The impact of glacial lake development on the evolution of glaciers in the Himalaya is poorly quantified, despite the increasing prevalence of supraglacial and proglacial water bodies throughout the region. In this study we examine changes in the geometry, velocity and surface elevation of nine lake-terminating and nine land-terminating glaciers in the Everest region of the central Himalaya over the time period 2000 to 2015. The land-terminating glaciers we examined all decelerated (mean velocity change of -0.16 to -5.60 m a^{-1} for different glaciers), thinned most in their middle reaches, and developed a more gently sloping surface (-0.02 to -0.37˚ change) down-glacier over the period 2000-2015. The lake-terminating glaciers we examined all retreated (0.46 to 1.42 km), became steeper (0.04 to 8.68° change), and showed maximum thinning towards their termini, but differed in terms of their dynamics, with one group of glaciers accelerating (mean speed-up of 0.18 to 8.04 m a^{-1}) and the other decelerating (mean slow-down of -0.36 m a^{-1} to -8.68 m a^{-1}). We suggest that these two scenarios of glacier evolution each represent a different phase of glacial lake expansion; one that is accompanied by increasingly dynamic glacier behaviour and retreat, and a phase where glacial lakes have little impact on glacier behaviour that may precede or follow the phase of active retreat. Our observations are important because they quantify the interaction of glacial lake expansion with glacier ice mass loss, and show that increased glacier recession should be expected where a glacial lake has begun to develop.

Key words: Glacial lakes, Himalaya, Glacial lake outburst floods, Digital Elevation Model, Glacier velocity

4.2 Introduction

The number and size of proglacial (moraine- and ice-dammed) lakes has increased dramatically across the Hindu Kush Karakoram Himalaya (HKKH) in recent decades (Zhang et al., 2015; Nie et al., 2017), and their expansion has been associated with areal and volumetric reductions in glacier extent (Basnet et al., 2013; King et al., 2017; Wang et al., 2017). The presence of a glacial lake may be indicative of a glacier in its most advanced state of recession (Sakai and Fujita, 2010; Benn et al., 2012), thus glacial lakes may become populous in high mountain regions as precipitation and temperature changes continue. Glacial lakes are particularly likely to form where substantial moraine dams have been constructed during glacial maxima (Benn et al., 2012). Ice mass loss rates from marine- and lake-terminating glaciers have been shown to be elevated above their land-terminating counterparts elsewhere in the world (Truffer and Motyka, 2016; Willis et al., 2012; McNabb and Hock, 2014; Tsutaki et al., 2016; Melkonian et al., 2016), and their flow characteristics have been found to be contrasting (Willis et al., 2012; Burgess et al., 2013). If simulations of Himalayan glacier evolution over coming decades are to be robust, it is therefore imperative that we improve our understanding of the response of Himalayan glaciers to glacial lake growth.

At present, knowledge of Himalayan glacial lakes and their impact on the dynamics of their host glaciers remains relatively limited. Nie et al. (2017) documented 2.7, 51.7 and 366.6 % increases in the total area of glacier fed but unconnected, proglacial and supraglacial lakes, respectively, between 1990 (n = 4549) and 2015 (n = 4950) across the entire HKKH. Reynolds et al. (2000), Quincey et al. (2007), and Sakai and Fujiuta (2010) identified a set of glacier surface characteristics conducive to supraglacial lake formation. They suggested that meltwater ponding and pond coalescence is most likely where the glacier surface has a surface gradient of less than 2˚and a negligible velocity, with steeper, faster glacier surfaces liable to meltwater runoff and/or fracturing that would promote meltwater drainage. Thakuri et al. (2016) examined the evolution of one lake-terminating glacier in the Everest region-Imja Tsho, showing an increased surface lowering rate, but decreased surface velocity over Imja and Lhotse Shar Glaciers between 2001 and 2014 and 1992/93 to 2013/14, respectively. King et al. (2017) generated glacier mass balance estimates for 32 glaciers in the Everest region of the Himalaya over the period 2000 to 2015 and showed 32 % greater mass loss from lake-terminating glaciers when compared with land-terminating glaciers. King et al. (2017) also show amplified surface lowering rates and opposing surface lowering gradients over lake versus land-terminating glaciers.

Glacial lakes present a considerable hazard to communities downstream due to their susceptibility to catastrophic drainage and the release of a glacial lake outburst flood (GLOF) (Fujita et al., 2013). Carrivick and Tweed (2016) compiled a record of 216 glacier flood events from 78 different sites in central Asia (since ~1500 AD) and ranked central Asian countries as most susceptible in a damage index considering recorded deaths, evacuations, and property and infrastructure destruction and disruption. In a region-wide study of glacial lake growth in the Himalaya, Nie et al. (2017) identified 118 rapidly expanding lakes that may be a priority for risk assessment. Rounce et al. (2017) identified 131 glacial lakes in Nepal with an area of greater than 0.1 km^2, and attempted to categorise glacial lakes based on their outburst probability, and considered the effects of lake expansion on the likelihood of lake failure. Rounce et al. (2017) classified 11 'very high risk' lakes and 31 'high risk' lakes. Rounce et al. (2017) identified Imja Tsho (in the Everest region) as a lake that will become increasingly hazardous, citing lake expansion towards more avalanche prone terrain as the primary factor increasing the chance of an outburst flood occurring. Using an alternative hazard assessment framework, ICIMOD (2011) identified 49 hazardous, and 21 critically hazardous glacial lakes (out of 1466) in Nepal. Concern over the hazard posed by glacial lakes has seen major remediation efforts to stabilise moraine dams and lower lake levels at several sites in recent decades (Reynolds, 2000; Rounce et al., 2017), underlining the importance of understanding their likely evolution as climate in the region continues to change (Sakai and Fujita, 2010; Yang et al., 2011; Salerno et al., 2015).

In this study we examine the evolution of nine lake-terminating and nine land-terminating glaciers in the Everest region of the central Himalaya, which is a region that has experienced a 20 % increase in lake area from 2000 to 2009 (Gardelle et al., 2011). The primary research question we pose is whether changes in glacier velocity, geometry, and rates of mass loss over the period 2000 to 2015 differ based on terminus type. We use observations of surface dynamics and morphology to examine the processes that may be driving glacier change in this region. Finally, we demonstrate how these data can be used to highlight glaciers that are preconditioned for glacial lake formation or lake expansion in the imminent future.

4.3 Study area

Glaciers of the Everest region (Figure 1) can be broadly grouped into three categories:

1. Large land-terminating glaciers flowing down from mountain massifs such as Everest, Lhotse, Cho Oyu and Makalu (all >8000 m a.s.l.) that terminate on land and account for the

greatest portion of glacierised area. These glaciers vary in length, ranging from 1-2 km to more than 10 km long. These glaciers are flanked by large Little Ice Age (LIA) moraines and are mantled by debris layers up to several metres in thickness (Nakawo et al., 1986, 1999).

2. Lake-terminating glaciers that vary in size and surface cover. Lake areas vary from less than 1 km^2 to nearly 4 km^2, debris-cover ranges from 0-100%, and glacier length ranges from 3-12 km. The majority of glacial lakes are proglacial, although large supraglacial lakes have recently developed on Rongbuk and Drogpa Nagtsang glaciers (Figure 1).

3. Numerous smaller, clean ice glaciers located at high elevation (>5000 m a.s.l.), mostly north of the orographic divide in the Everest region. These glaciers do not typically host glacial lakes and have only retreated a small amount from their LIA limits. We do not focus on glaciers of this type in this study.

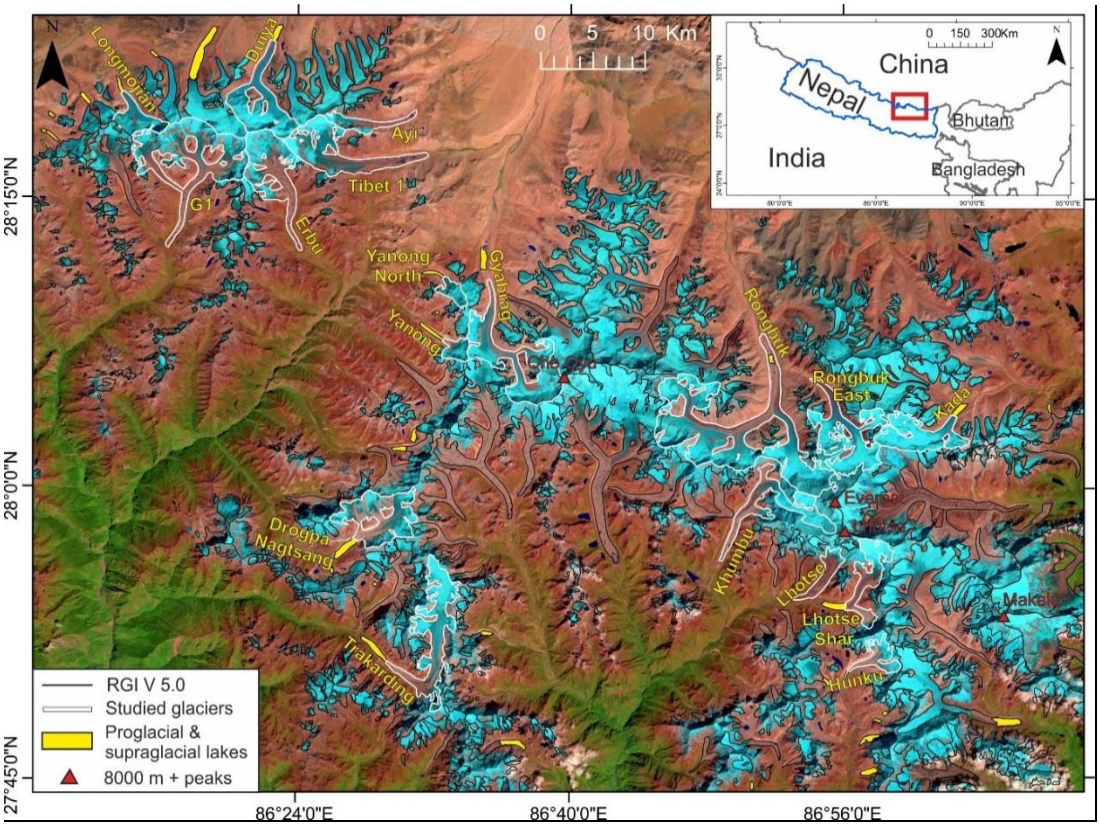

Figure 4.1. The Everest region of the central Himalaya. Black glacier outlines show the extent of the RGI version 5.0, whereas white glacier outlines mark the glaciers we focus on in this study. Pro- and supraglacial lakes are also marked, along with mountain peaks above 8000 m in the area. Background imagery is a Landsat OLI image from 2014 available from http://earthexplorer.usgs.gov/

The nine glaciers we classify as lake-terminating are Imja/ Lhotse Shar, Yanong, Yanong North, Kada, Drogpa Nagtsang, Trakarding, Longmojian, Duiya and Hunku glaciers (Figure 1, Table S1). These glaciers all have well-developed glacial lakes which are dammed by a full moraine loop, and lose mass through calving as well as melt (Benn et al., 2001; Somos-Valenzuela et al., 2014). We do not classify glaciers that host supraglacial lakes as lake-terminating as we cannot be certain of the depth of these lakes and whether they are directly influencing glacier behaviour. The nine land-terminating glaciers we assess are G1, Erbu, Tibet 1, Ayi, Gyabrag, Rongbuk, Rongbuk East, Khumbu and Lhotse glaciers (Figure 1). Glacier attributes for both lake- and land-terminating glaciers can be found in Supplementary Table 1.

4.4 Methods and data

4.4.1 Data sources

Glacier surface velocity data were generated by tracking surface features in a series of Landsat 7 (ETM+) and 8 (OLI) panchromatic images (both 15 m spatial resolution) (c.f. Dehecq et al., 2015). First, individual displacement fields were generated at 120 m resolution for all pairs of images separated by approximately 1 year (between 352 and 384 days) using orientation correlation (Fitch et al., 2002) with a correlation window of 16 x 16 pixels, and divided by the pair time span to derive as close to annual velocity fields as the imagery archive allows. Second, velocity fields for a similar period of time were stacked together by taking the median value of the velocity stack in each pixel. For this study, stacks of velocity fields were generated for the period 1999 to 2003 (Landsat ETM+) and 2013 to 2015 (Landsat OLI). Uncertainty is estimated at each pixel based on the number and median absolute deviation of the velocity estimates, using a relationship that is calibrated using off-ice measurements (Dehecq et al., 2015). The median uncertainty associated with velocity measurements is ± 1.93 (1999/03) and ±1.22 (2013/15) m a^{-1} over stable, off-glacier areas and ± 2.71 (1999/03) and ± 1.61 (2013/15) m a^{-1} over glacier surfaces.

Glacier surface lowering and glacier geometry data were derived from the DEM time series presented in King et al. (2017). DEMs in this time series included the Shuttle Radar Topographic Mission (SRTM) 1 arc sec DEM and multiple Surface Extraction with TIN-based Search-space Minimization (SETSM) derived DEMs produced by Ohio State University and distributed online by the Polar Geospatial Center at the University of Minnesota following the approach of Noh and Howat (2015). The SRTM DEM was generated by interferometry using data acquired in February 2000, and the SETSM photogrammetric DEMs were generated from optical stereo (WorldView, 1, 2 and 3)

imagery spanning the period 15/01/2014 to 04/05/2015. Previous studies have suggested that the SRTM dataset may underestimate glacier surface elevations because of the penetration of C-band radar waves into snow and ice (Rignot et al., 2001). To account for this bias, we generated a clean ice, firn and snow cover mask using a Landsat ETM+ scene (05/01/2002) acquired close to the date of the SRTM, and applied elevation corrections of +4.8 m over areas of firn/snow, +1.2 m over areas of clean ice and no correction over debris covered glacier surfaces, following the approach of Kääb et al. (2012) and King et al. (2017). The two DEM sets were coregistered following the approach of Nuth and Kääb (2012) where geolocation errors, along or cross track tilts and elevation dependant biases were corrected for, if present. King et al. (2017) give a thorough description of the DEM coregistration and correction process, along with the methods used to estimate surface elevation change uncertainty budgets. The estimated uncertainty (standard error over off-glacier areas) associated with elevation change data is glacier dependant due to area (glacier hypsometry) weighting, but ranges from ± 0.14 to ± 0.39 m a^{-1}.

Additional datasets included the Randolph glacier inventory (RGI) version 5.0 (Bajracharya et al., 2014) and Level-1 terrain processed Landsat imagery from Landsat TM, ETM+ and OLI sensors. A full scene list is included in supplementary information (Table S2). RGI data provided glacier extent information for clipping of glacier surface elevation and glacier surface velocity data. Landsat TM, ETM+ and OLI archive data were used to document lake-terminating glacier ice front locations over the period 1989-2015.

4.4.2 Glacier surface geometry assessment and glacier velocity profiles

In contrast to previous studies, which have either measured surface slope from a fixed point at the glacier terminus (e.g. Quincey et al., 2007), or from a fixed point at the front of a distance bin (Miles et al., 2016), we chose to fit a line through ‘average’ glacier surface elevation profiles over 750 m bin lengths. ‘Average’ surface elevation profiles were calculated as the mean surface elevation taken from manually delineated flow-parallel profiles spaced 100 m apart, including the glacier centreline (n = 3 or 5 depending on glacier width) across the glacier surface (see figure S1 for an example). The comparison of slope estimates from a variety of bin lengths (250, 500, 750, and 1000 m) showed 750 m to be the ideal bin length that characterised general undulations in glacier surface topography; shorter or longer bin lengths produced noisy or artificially smoothed glacier surface gradient estimates, respectively (Figure S2).

We followed a similar flow line average approach to summarise glacier velocity data over the study period (Figure S1). Again, we calculated mean glacier velocity from flow-parallel profiles spaced 100 m apart across the glacier surface. This approach was preferred to using a centreline velocity in isolation as this cannot account for cross-glacier fluctuations caused by drag at the ice margins. We applied this approach to both velocity stacks (1999 to 2003 and 2013 to 2015) to allow the calculation of velocity differences over the study period.

We limited our analysis of glacier geometry change and surface velocity fluctuations to below the median altitude of each glacier, which we have used as a proxy of the equilibrium line altitude (ELA) (Braithwaite and Raper, 2009), as the impact of lake development is likely to be most profound in this part of each glacier (Sakai et al., 2015). This approach also limited analyses to areas where data quality was highest, with DEM extraction and feature tracking performing poorly in areas of low-contrast and textureless terrain, such as snow-covered glacier accumulation zones.

4.4.3 Glacier front position delineation

The calving fronts of lake-terminating glaciers were delineated manually from scenes contained in the Landsat TM, Landsat ETM+ and Landsat OLI archives using ArcMap GIS software. We mapped ice front positions over the period 1989 to 2015 (Table S2). Variations in frontal position were calculated following the box method proposed by Moon and Joughin (2008), where average front position change is derived by dividing the total area of a polygon including the calving front by the width of a fixed reference profile in the up-glacier direction. Glacial lake area was attained following the approach of studies such as Nie et al. (2017) to classify water bodies in Landsat TM, ETM+ and OLI scenes using the Normalised Difference Water Index.

The uncertainty associated with the measurement of the position of a glacier front using repeat imagery is composed of image co-registration error and delineation errors (Ye et al., 2006). We follow the method of Ye et al. (2006) to estimate glacier front position uncertainty, incorporating the pixel resolution (30 m for Landsat TM and 15 m for Landsat ETM+ and Landsat OLI scenes) and registration error, taken as the Geometric Root Mean Square Error (GRMSE) value provided in the image metadata, into the error budget. Consequently, uncertainty in calculating the mean front position change was ± 0.008 km a^{-1} across all epochs, ranging from ± 0.002 to ± 0.018 km a^{-1} for different time periods and across different image pairs. We followed the approach of Fujita et al. (2009) to estimate the uncertainty associated with glacial lake area, and assume that the perimeter of the glacial lake has been identified to within ½ a single pixel. Mean lake area uncertainty across all

time periods and scenes was ± 0.08 km^2, and ranged from ± 0.04 to ± 0.19 km^2 depending on scene resolution.

4.4.4 Debris cover extent mapping

To quantify the extent of debris cover over our sample of glaciers we first generated a clean ice, firn and snow mask using a Landsat OLI scene and band ratio ($(\frac{\text{OLI Band 4}}{\text{OLI Band 6}})$ and a manually set threshold) techniques following the approach Paul et al. (2016). We then used this mask to eliminate non-debris covered glacier areas from the RGI inventory, leaving a mask of only debris-covered glacier area.

4.5 Results

4.5.1 Glacier geometry and glacier geometry change

All land-terminating glaciers exhibited a reduction in surface slope values in the down-glacier direction and therefore have a concave surface profile (Figures 2 and 3). The surface slope did not exceed 8° in any case below ELAs, and 5 of the 9 glaciers we assessed had large portions of less than 2° slope. All of the land-terminating glaciers showed a distinct trend in surface gradient change. The upper reaches of the ablation zone of land-terminating glaciers steepened, whilst the gradient of their lower reaches reduced (Figures 2 and 3). The transition from slight surface steepening to surface gradient reduction occurred at or close to the zone where debris cover became prevalent on each glacier. Mean surface gradient change was effectively zero as a result (-0.03˚across the nine glaciers), but ranged from +1˚ (Rongbuk East and Ayi glaciers) to -4˚(Gyabrag Glacier).

Five of the nine lake-terminating glaciers showed increasing surface slope down glacier and thus exhibited a convex down-glacier profile (Figures 4 and 5). The remaining four lake-terminating glaciers showed either a linear or concave-down profile. Broadly speaking, lake-terminating glaciers were steeper than land-terminating glaciers, with some showing sections of > 20° slope. The style of geometry change shown by lake-terminating glaciers contrasted with that of land-terminating glaciers. Of the nine lake-terminating glaciers we studied, 5 showed pervasive increases in surface gradient throughout the length of their ablation zones (glaciers shown in Figure 4). A mean of 1.37˚of surface steepening occurred over these 5 glaciers (ranging from 0.33 to 2.35° for individual bins). Surface steepening was most substantial within 1 to 2 km of glacier calving fronts. Slight glacier surface steepening (mean 0.25˚) occurred on the other four lake-terminating glaciers we assessed (Drogpa Nagtsang, Hunku, Longmojian and Trakarding glaciers; Figure 5), and they displayed the same down-glacier trend in geometry change as the land-terminating glaciers.

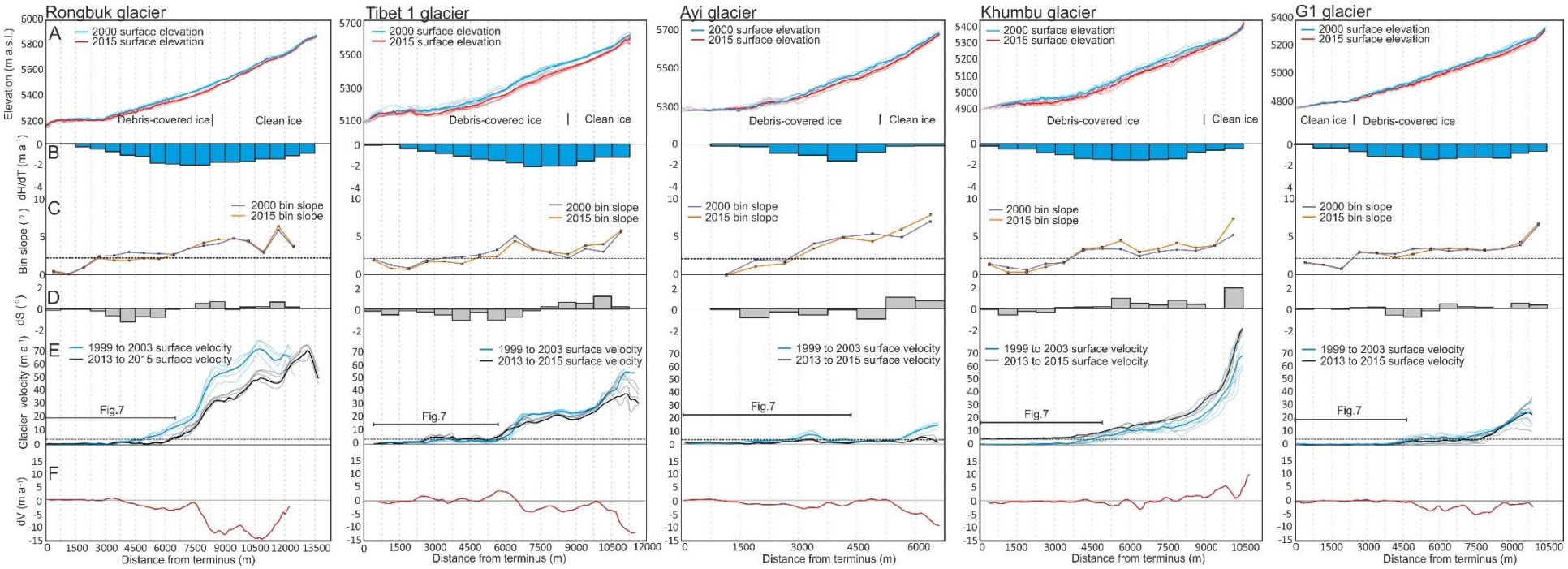

Figure 4.2. Surface elevation (A), surface elevation change (dH/dT) (B), surface slope (C), surface slope change (dS) (D), surface velocity (E) and surface velocity change (dV) (F) of five land-terminating glaciers in the study area. The coverage of high-resolution satellite imagery shown in Figure 7 is marked on velocity difference panels. Thresholds of surface slope (2˚) and surface velocity (4 m a^{1}) required for surface meltwater ponding are also marked.

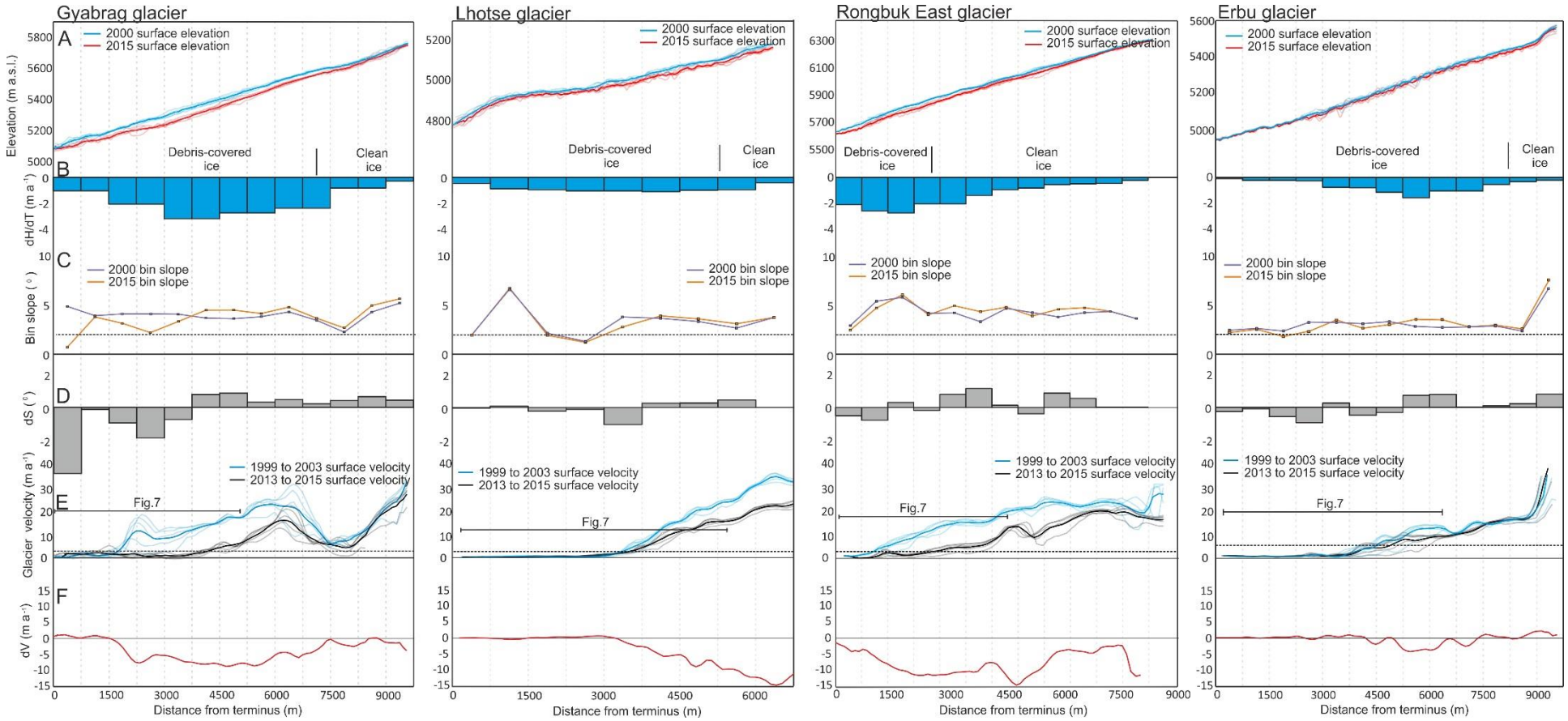

Figure 4.3. Surface elevation (A), surface elevation change (dH/dT) (B), surface slope (C), surface slope change (dS) (D), surface velocity (E) and surface velocity change (dV) (F) of four land-terminating glaciers in the study area. The coverage of high-resolution satellite imagery shown in Figure 7 is marked on velocity difference panels. Thresholds of surface slope (2 ˚) and surface velocity (4 m a^1) required for surface meltwater ponding are also marked.

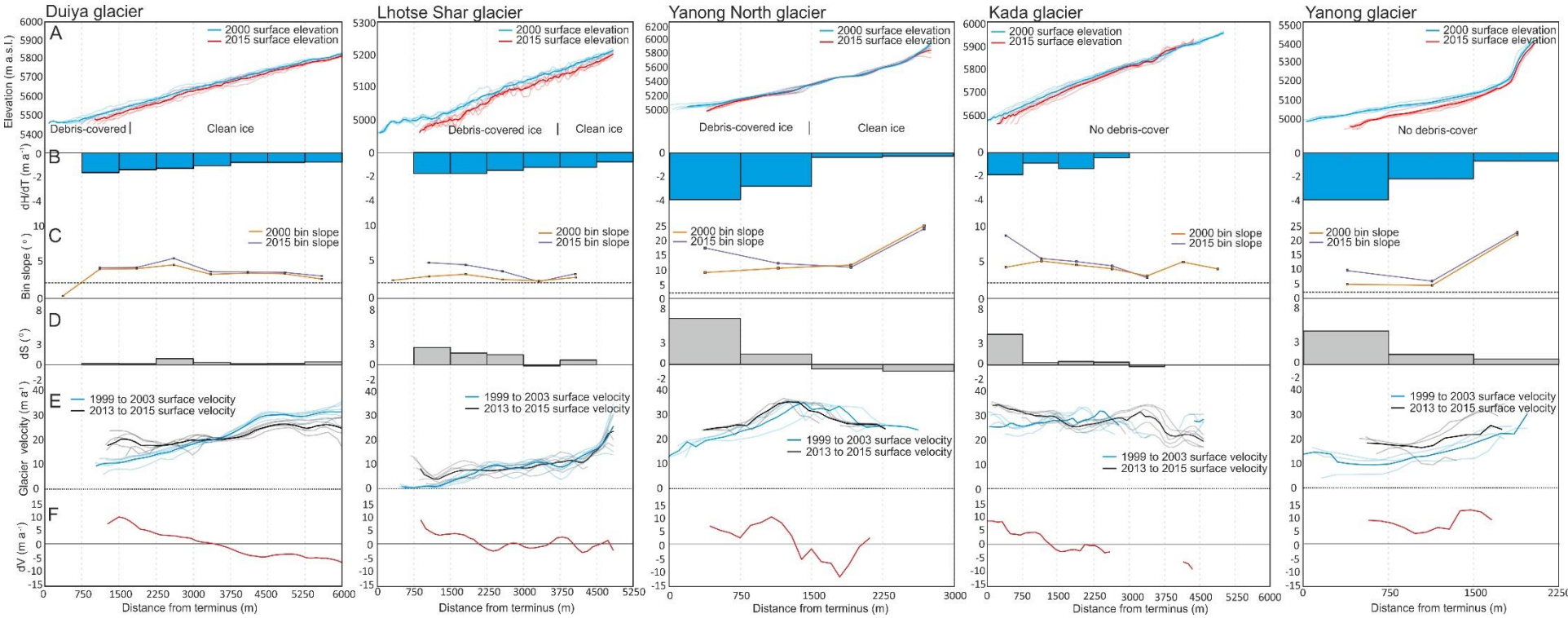

Figure 4.4. Surface elevation (A), surface elevation change (dH/dT) (B), surface slope (C), surface slope change (dS) (D), surface velocity (E) and surface velocity change (dV) (F) of five lake-terminating glaciers in the study area. The coverage of high-resolution satellite imagery shown in Figure 7 is marked on velocity difference panels. Thresholds of surface slope (2˚) and surface velocity (4 m a^1) required for surface meltwater ponding are also marked.

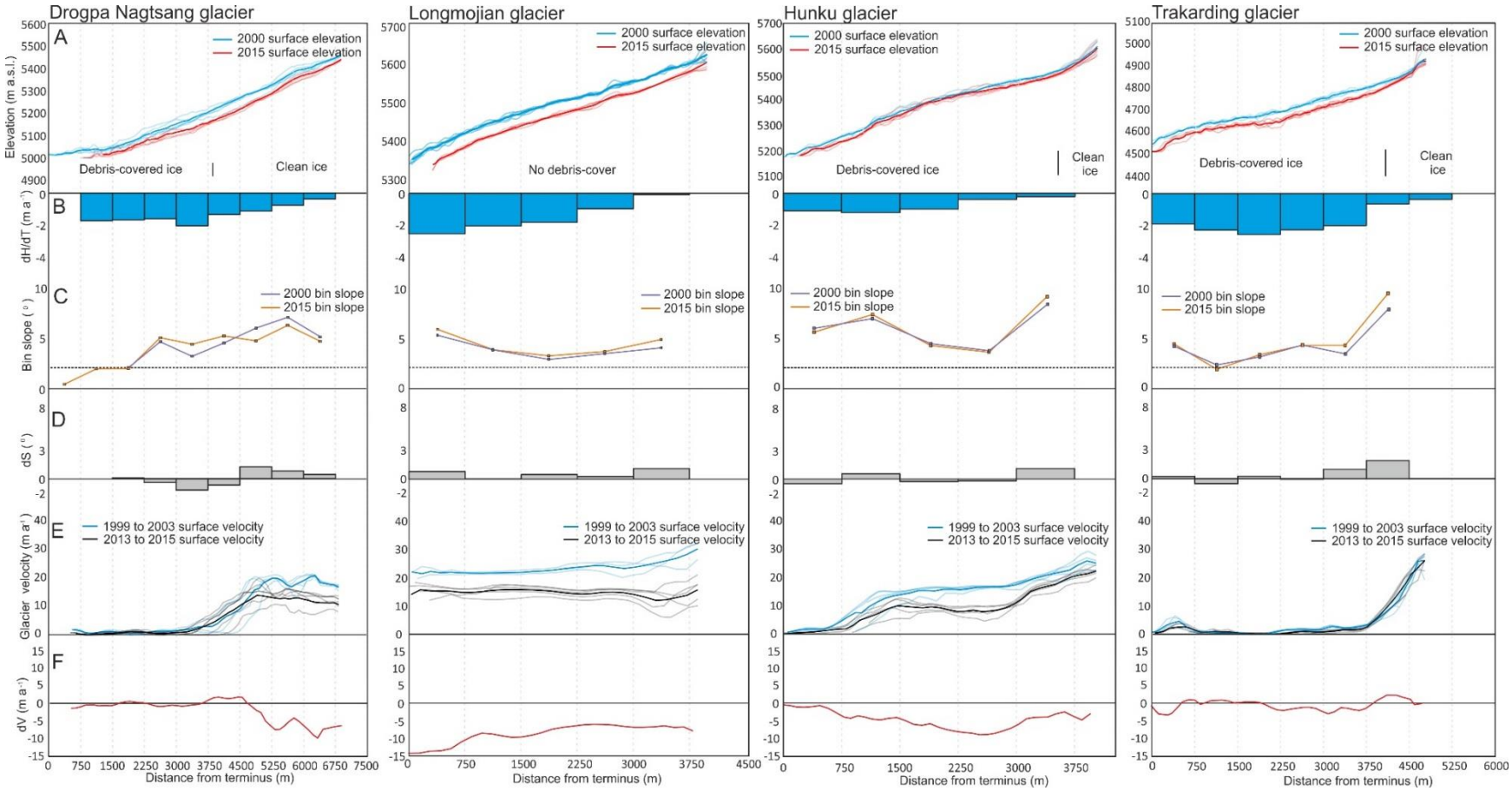

Figure 4.5. Surface elevation (A), surface elevation change (dH/dT) (B), surface slope (C), surface slope change (dS) (D), surface velocity (E) and surface velocity change (dV) (F) of four lake-terminating glaciers in the study area. The coverage of high-resolution satellite imagery shown in Figure 7 is marked on velocity difference panels. Thresholds of surface slope (2 ˚) and surface velocity (4 m a^1) required for surface meltwater ponding are also marked.

4.5.2 Glacier velocity and glacier velocity change

Large portions of land-terminating glaciers were either stationary or flowing at a rate below the level of detection of the feature tracking algorithm (Figures 2 and 3). Across the nine land-terminating glaciers, a mean of 37% of their total length was flowing at or less than 4 m a^{-1}. In contrast, seven of the nine lake-terminating glaciers showed active flow throughout their length, with Drogpa Nagtsang and Trakarding glaciers being the exceptions to this rule. Lhotse Shar Glacier showed little to no flow around its calving front between 1999 and 2003, but showed velocities of ~10 m a^{-1} in the 2013 to 15 velocity stack over the same area. Those lake-terminating glaciers that do show active flow throughout were flowing as fast at their terminus as at the approximate ELA.

Comparison of the two velocity stacks (from 1999 to 2003 and from 2013 to 2015) revealed substantial changes in ice velocities over the study period. Land-terminating glaciers decelerated over large portions of their lower reaches (Figures 2 and 3). Mean, ablation zone velocity reduction was -2.31 m a^{-1} (ranging from -0.16 m a^{-1} to -5.60 m a^{-1} for individual glaciers) for the nine land-terminating glaciers. This represents a 34% reduction in flow rates below the median altitude of land-terminating glaciers. In specific areas glacier velocity change of more than -10 m a^{-1} was detected, the location of which varied between glaciers (Figures 2 and 3).

Five of the nine lake-terminating glaciers (all shown in Figure 4) showed increased surface velocities over their lower reaches over the study period. Mean, ablation zone velocity change was 2.67 m a^{-1}, ranging from 0.18 m a^{-1} to 8.04 m a^{-1} for individual glaciers, but all five of these glaciers showed more substantial (10 m a^{-1} or more) acceleration towards their termini. These changes represent a 24% acceleration in flow rates below the median altitude of these five lake terminating glaciers.

The other four lake-terminating glaciers (shown in Figure 5) decelerated over their ablation zones over the study period. Mean, ablation zone wide velocity change was -3.92 m a^{-1} (ranging from -0.36 m a^{-1} to -8.68 m a^{-1} for individual glaciers) for these four glaciers, a 34% reduction in flow rates below the median altitude. Again, maximum velocity change reached -10 m a^{-1} or more on three of these glaciers (Figure 5).

Flow acceleration and deceleration caused opposing strain rates over the lower reaches of lake-terminating glaciers. Longitudinal strain rates ($\frac{dv}{dx}$), averaged over the lowermost one kilometre of each glacier, using the 2013-2015 velocity dataset (Table 1), were positive (ranging from 0.03 to 0.06 a^{-1}), and flow was therefore extensional, over the five glaciers

that accelerated over the study period. Strain rates were negative (ranging from -0.01 to -0.05 a^{-1}), and thus flow was compressional, over the terminal zone of the four glaciers that decelerated over the study period.

Table 4.1. Mean ablation zone velocity change, ice front position change, glacier geometry (surface slope) and terminal zone strain rate for lake-terminating glaciers. Terminal strain estimates are a mean value taken over the lowermost one kilometre of each glacier. Italicised values and glaciers are shown in figure 5, whereas plain text values and glaciers are shown in figure 4.

Glacier	Ablation zone velocity change ($m\ a^{-1}$)	Mean ice front position change rate 1989-2015 ($m\ a^{-1}$)	Mean change in slope (degrees)	Terminal strain rate (a^{-1})	Ice front width change (m)
Drogpa Nagtsang	*-1.96*	*-64.07**	*0.04*	*-0.01*	*-14*
Longmojian	*-8.68*	*-13.98*	*0.41*	*-0.05*	*70*
Hunku	*-4.64*	*6.87*	*0.10*	*-0.01*	*-7*
Trakarding	*-0.40*	*-21.34*	*0.43*	*-0.01*	*-93*
Mean	***-3.92***	***-23.13***	***0.25***	***-0.02***	***-11***
Duiya	0.18	-33.62	0.33	0.06	-54
Yanong North	2.87	-21.99	2.13	0.06	31
Lhotse Shar	0.63	-30.19	0.95	0.03	227
Kada	1.63	-29.92	1.10	0.05	29
Yanong	8.04	-46.40	2.35	0.06	-68
Mean	**2.67**	**-32.42**	**1.37**	**0.05**	**33**

*Drogpa Nagtsang ice front position rates measured from 1996-2015.

4.5.3 Lake-terminating glacier ice front position and lake expansion

All but one of the lake-terminating glaciers showed substantial cumulative ice front retreat between 1989 and 2015, ranging from 460 m to 1420 m (Figure 6). Drogpa Nagtsang showed the largest ice front retreat (Figure S2) despite the relatively recent formation of the lake (late 1980s). Some lake-terminating glaciers (Longmojian, Yanong North, Duiya) showed steady retreat rates, some (Trakarding, Yanong) showed a reduction in retreat rate, and some (Lhotse Shar, Kada, Drogpa Nagtsang) showed an increase in retreat rate. Mean retreat rates ranged between -14 ± 3 m a^{-1} (Longmojian) to -64 ± 5 m a^{-1} (Drogpa Nagtsang) over the study period. Hunku Glacier is unique in having sustained a consistent ice front position between 1989 and 2015 (Figure 6a).

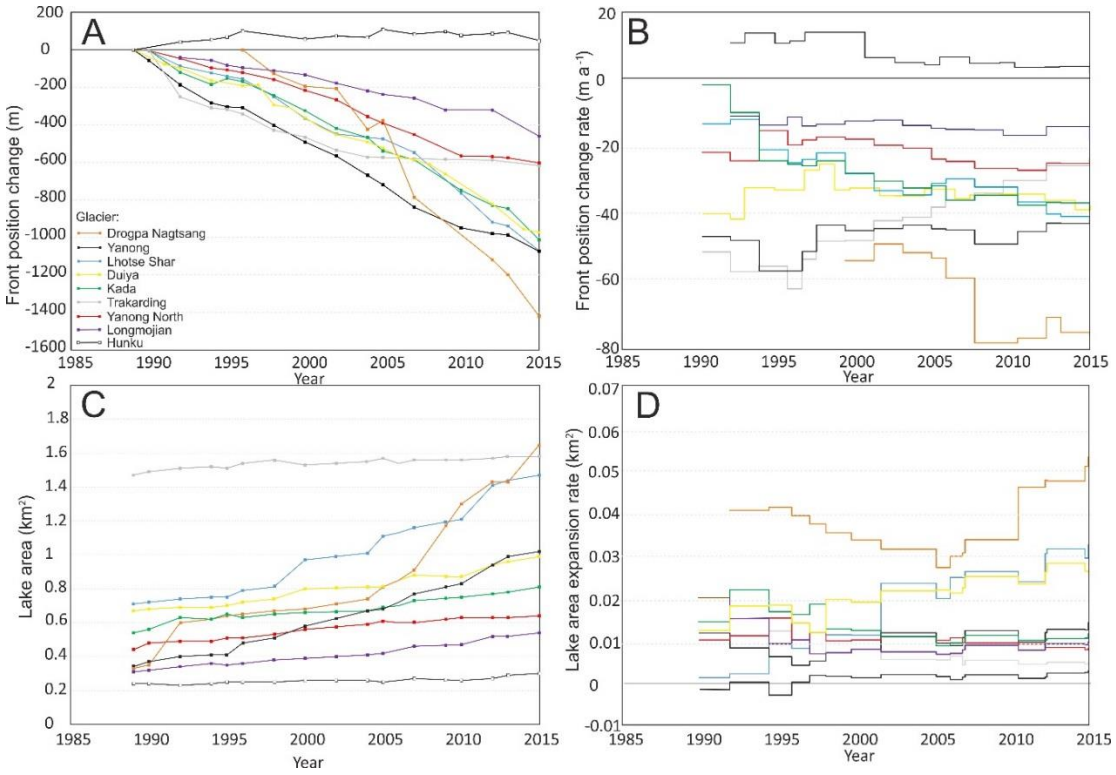

Figure 4.6. A) Cumulative ice front; B) Ice front retreat rate; C) Lake area increase; and D) Lake area expansion rates for the 9 glaciers hosting lakes over the period 1989-2015.

Glacial lake area ranged from 0.24 ± 0.06 km^2 (Hunku Glacier lake) to 1.47 ± 0.19 km^2 (Tsho Rolpa, hosted by Trakarding Glacier) in 1989, and from 0.31 ± 0.06 km^2 (Hunku Glacier lake) to 1.72 ± 0.17 km^2 (Drogpa Nagtsang Glacier lake) in 2015. Glacial lake expansion rates again varied between glaciers, with some lakes (hosted by Drogpa Nagtsang, Lhotse Shar, Duiya and Yanong glaciers) expanding at increasing rates, some lakes (hosted by Hunku, Longmojian, Kada and Yanong glaciers) expanding at a steady rate, and one lake, hosted by Trakarding glacier, expanding at a diminishing rate (Figure 6d).

The change in ice front widths that occurred alongside ice front retreat was highly variable over the study period (Table 1). The ice front width of five of the nine lake-terminating glaciers (Duiya, Yanong, Drogpa Nagtsang, Trakarding and Hunku glaciers) reduced by between –7 to -93 m over the study period. Ice front widening ranged from 29 to 227 m on the other four (Lhotse Shar, Kada, Yanong North and Longmojian) lake-terminating glaciers.

4.6 Discussion

There are clear differences in the evolving geometry and velocity of land- and lake-terminating glaciers in the Everest region. These contrasts suggest that very different processes have been operating on these glaciers of different terminus type throughout the study period.

4.6.1 Land-terminating glacier dynamics

The changes in the velocity and geometry of the land-terminating glaciers we have assessed were remarkably consistent, with all nine land-terminating glaciers experiencing similar surface geometry and velocity adjustments over the study period (Figures 2 and 3). The reduced surface velocities we measured over the lower reaches of land-terminating glaciers (Figures 2 and 3) suggests a longitudinally compressional flow regime exists here, which would have resulted in positive vertical ice motion and therefore surface elevation increases up-glacier of stagnant ice (Rounce et al., 2018). However, the highest thinning rates we measured occurred in areas proximal to stagnant ice where surface velocities declined (Figures 2 and 3). Areas of the most substantial velocity reductions were coincident with the clean ice- debris covered transition zone of each land-terminating glacier, where debris thicknesses are commonly only a few centimetres (Nakawo et al., 1986; Rounce et al., 2018). Under such a thin debris layer, melt rates can be elevated above that of debris-free ice (Østrem, 1959; Nicholson and Benn, 2006; Evatt et al., 2015), and appear to have been of a sufficient magnitude to counter the vertical component of ice flux divergence and resulted in substantial surface lowering. The slight increases in surface gradient we have documented across the clean ice- debris covered boundary on each glacier (Figures 2 and 3) have therefore occurred because surface lowering rates are elevated above that of clean ice in this zone of thin debris. Closer to glacier termini, the impact of both sub-debris melt and ice flux divergence is less substantial (Rounce et al., 2018) as debris thickness increases and ice flow is negligible, but surface lowering and surface gradient reductions still occurred (Figures 2 and 3). This is presumably because of the impact of much expanded supraglacial pond and ice cliff networks on land-terminating glaciers in the area (Watson et al., 2016; 2017), which act as hot-spots of melt on debris covered glaciers.

The reduction of surface gradients (Figures 2 and 3) and prolonged ice thinning on glaciers in the Everest region (*cf.* Bolch et al., 2011) will have led to a reduction in driving stress (Cuffey and Paterson, 2010; Benn et al., 2012) and therefore glacier velocities, not just over our study period, but also during preceding decades. Figures 2 and 3 show that this process has clearly been in operation on the lower reaches of land-terminating glaciers in the

Everest region; large areas display little or no flow up to several kilometres from their termini, surface gradients are low across these stagnant areas (Figures 2 and 3)., and the greatest differences in surface velocity were seen on glaciers (Gyabrag and Rongbuk) with the greatest percentage decrease in surface gradient (Figures 2 and 3). Thakuri et al. (2014) show a 17.1 ± 3.1% increase in the total area of debris covered ice in the Everest Region since the 1960's, which has predominantly occurred as an up-glacier migration of the debris covered-clean ice transition zone. The debris mantle on this part of a debris covered glacier is thin (Rounce and McKinney, 2014), thus surface lowering is amplified and the longitudinal surface gradient has reduced (Figures 2 and 3). Continued expansion of the debris cover up-glacier could therefore also cause areas of reducing surface slope to spread, with consequent further reductions in ice flow.

An additional process that may be contributing to glacier deceleration is a reduction in accumulation and therefore a reduction in ice flux to lower elevations (e.g. Benn et al., 2012; Nuimura et al., 2011; Heid and Kääb, 2012). Increased snow line altitudes (Thakuri et al., 2014), decreasing precipitation (Salerno et al. 2015) and reduced accumulation between 1970 and 2001 detected in an ice core on the northern side of the orographic divide in the Everest region (Kaspari et al., 2008) could all be taken as evidence of reduced accumulation over our study period. However, a change in accumulation would only immediately impact on the upper reaches of each glacier, and would take time to propagate down to the ablation zone, where we have documented the most substantial changes in glacier velocity and geometry. Knowledge of the response time of Himalayan glaciers to perturbations in accumulation is currently relatively limited. Scherler et al. (2011) estimated the response time of 286 glaciers across the Himalaya, some of which were debris covered and some of which were devoid of debris cover. Scherler et al. (2011) found that the neither the response time nor the climate sensitivity of debris covered glaciers could be estimated using the same attributes as clean ice glaciers (e.g. Leclercq and Oerlemans, 2010), and suggest that the impact of an insulating debris layer on terminus retreat rates precludes their use as indicators of recent climate change. Banerjee and Shankar (2013) suggested that debris covered glaciers may exhibit a > 100 year 'stationary period' in response to a warming climate and associated ELA increase, with little to no terminus retreat occurring during this period. Of the nine land-terminating glaciers shown in Figures 2 and 3, eight are stationary over their lower reaches, and have been since at least the date of our first velocity observations (1999). Thakuri et al. (2014) also documented little (-6.1 ± 0.2 m a^{-1}) ice front retreat over land-terminating glacier in the Everest region over the period 1962 to 2011. However, without more temporally extensive observations of glaciers length variations and glacier velocity, it is difficult to suggest how long these glaciers may have been in the

stationary state suggested by Banerjee and Shankar (2013), and how close they may be to a different mode of response to continued warming.

4.6.2 Lake-terminating glacier dynamics

The velocity and geometry change data we have generated for lake-terminating glaciers can be separated into two distinct groups (Figures 4 and 5). The increased velocity of the five lake-terminating glaciers shown in Figure 4, and the associated expansion of the glacial lakes they host (Figure 6), suggests a link between lake expansion and glacier behaviour in these 5 cases. Conversely, the flow velocity deceleration of the four lake-terminating glaciers shown in Figure 5 suggests glacial lake expansion may not have significantly impacted their dynamics over the study period. These observations suggest two contrasting sets of processes have been in operation on lake-terminating glaciers in the Everest region over the last 15 years.

The two main components of frontal ablation on marine- and lake-terminating glaciers are mechanical calving and the subaqueous melt of the ice front in contact with water (Carrivick and Tweed, 2013). Either of these melt components can be the dominant factor in ice front position retreat across different water terminating glaciers in both space and time (Truffer and Motyka, 2016). The magnitude of subaqueous melt depends primarily on the temperature of the proglacial water body and its salinity. Small, proglacial lakes are typically much cooler than water in a coastal, marine setting (Chikita, 2007; Truffer and Motyka, 2016), and there is little density contrast between glacial meltwater and the freshwater of the proglacial water body to drive the circulation of water and enhance subaqueous melt. Indeed, Trussel et al. (2013) found that on one Alaskan, lake-terminating glacier (Yakutat Glacier), the observed thinning could be entirely explained by surface melt, and that there was no contribution from subaqueous melt. Data on the temperature and structure of the proglacial lakes in our study area are limited. Chikita (2007) show a water temperature of 2-3˚C for much of the water column in Imja Tsho and Tsho Rolpa with only a shallow (~20 m of a total water depth of 120 m or more for both lakes) layer of warmer water (3-6˚C) towards the surface of the lake. These temperatures are similar to those of the lake at the front of Yakutat Glacier (water temperatures of between 0.5-1.5˚C- Trussel et al., 2013), and we therefore suggest that such conditions cannot reasonably account for the mass loss rates that have been detected on these glaciers (King et al., 2017). It is likely that the warm surface layer documented by Chikita (2007) and wind driven water currents (Sakai et al., 2009) would drive the development of a thermal notch as has been documented on other lake-terminating glaciers (Warren and Kirkbride, 2003; Trussel et al., 2013), but

only over a limited vertical extent. We therefore focus the following discussion of lake-terminating glacier retreat on the impact of mechanical calving on these glaciers.

The acceleration of the five lake-terminating glaciers shown in Figure 4, and their sustained or accelerating ice front retreat rates (Figure 6), suggests a link between lake development and glacier behaviour in these 5 cases over the last 15 years. Benn et al. (2007) outline three models of water-terminating glacier behaviour, the third of which, which considers both lateral and basal drag as the dominant resisting stress to ice flow, is most appropriate for the topographically constrained glaciers we have assessed in this study. The model of Benn et al. (2007) is applicable to glaciers that have developed a lake of sufficient depth to interact with the glacier at its bed. In this model, dynamic water-terminating glacier retreat is triggered by an imposed thinning (an increase in surface melt, for example) that alters the level of effective pressure- the difference between ice overburden pressure and water pressure. Decreasing effective pressure causes ice flow acceleration and a positive feedback ensues between acceleration, increased longitudinal strain, dynamic thinning and calving retreat. Calving retreat becomes dominant because extensional flow causes the deepening of crevasses in the terminal zone of each glacier, and because thinning reduces the freeboard level (the height of the glacier surface above lake level), increasing the likelihood that crevasses will reach the waterline. The strength of this feedback differs depending on the magnitude of resisting stresses (lateral and basal drag), particularly where the glacier is grounded, with the maximum attainable glacier velocity being lower where resisting stresses are high, and vice versa. The magnitude of the feedback between these processes can also be moderated by surface gradient (Benn et al., 2007).

We have documented the occurrence of a number of the processes that combine to set up the positive feedback proposed by Benn et al. (2007) to drive increased ice loss on lake-terminating glaciers. The five lake-terminating glaciers shown in Figure 4 have experienced substantial terminal zone thinning (shown here and in Bolch et al., 2011; Nuimura et al., 2012), flow acceleration (Figure 4) and increased longitudinal strain (Table 1), and sustained or accelerating ice front retreat rates over the last 26 years (Figure 6). We therefore suggest that the set of processes incorporated into the model of Benn et al. (2007) are in operation on some Himalayan lake-terminating glaciers, as has been inferred on lake-terminating glaciers in other glacierised regions (Muto and Furaya, 2013; Robertson et al., 2013; Sakakibara et al., 2014; Chernos et al., 2016). The variability in cumulative glacier front retreat and glacier front retreat rates we show in Figure 6, and the broad range of mass balance estimates generated for lake-terminating glaciers by King et al. (2017), likely reflects the variable response of glaciers depending on their topographic setting (i.e. valley

morphology), width and surface slope- all factors that influence levels of basal and lateral drag (Pementel et al., 2010; Adhikari and Marshall., 2012).

The slowdown of the four lake-terminating glaciers shown in Figure 5 suggests glacial lake expansion may not have been the dominant factor in their evolving dynamics over our study period, despite the physical link between each lake and its host glacier. Three of these four glaciers (Trakarding, Hunku and Longmojian) have hosted glacial lakes since at least the 1970's (Sakai et al., 2000; Bajracharya et al., 2007), and may have been thinning, like other glaciers in the Everest region (Bolch et al., 2011), over a similar timescale, including our study period (King et al., 2017). The deceleration of these three glaciers may therefore be a result of a reduction in driving stress and increased resistive stresses (lateral and basal drag) as the terminal zone of these glaciers narrowed (Table 1) in association with thinning (Pementel et al., 2010; Adhikari and Marshall., 2012). Reduced ice flow, combined with increased resistive stresses, would have reduced levels of longitudinal stretching, transverse crevassing and therefore calving, when compared with formerly elevated surface velocities (Benn et al., 2012). The diminishing ice front retreat rate of Trakarding Glacier may be evidence of this process. The less substantial terminus proximal surface lowering on Trakarding and Hunku glaciers over the study period likely indicates that surface melt is now the dominant ice loss process, rather than calving and dynamic ice front retreat.

The behaviour of Drogpa Nagtsang cannot be explained by these same processes given the relatively recent formation of its lake (Figure 6). In this case, the lake that has developed may still be supraglacial, and is therefore too shallow (or the glacier still too thick) to initiate more dynamic glacier behaviour. Until this glacier thins, or the lake melts through the remaining glacier ice, flow acceleration through an adjustment of effective pressure will not occur. The changes in glacier velocity and geometry we have observed for this glacier (Figure 5) are more akin to those of a land-terminating glacier, as would be the case on other glaciers that have recently developed lakes that are yet to influence their dynamics.

4.6.3 Preconditioning of glacier surfaces for lake development- can lake formation be predicted?

Previous studies have suggested that under particular geometric and dynamic conditions surface melt ponds are likely to coalesce, enabling glacial lakes to form. Quincey et al. (2007) and Reynolds et al. (2000) suggested that meltwater ponding and coalescence is most likely to occur where glacier surfaces are of less than 2˚slope and effectively 'stagnant'. If a glacier surface is steeper than this threshold or flowing actively, meltwater will continue to

drain down-glacier, or crevasse formation (from active flow) will provide pathways for englacial meltwater rerouting, most likely towards the edge of a glacier, where lateral drag causes enhanced strain and ice surface fracturing (Cuffey and Paterson, 2010). Using the criteria of Quincey et al. (2007) and Reynolds et al. (2000) we are able to assess whether any of the land-terminating glaciers we have examined are primed for glacial lake development.

Figure 7 shows the terminal regions of the nine land-terminating glaciers depicted in Figures 2 and 3. Of these glaciers, five (those in Figure 2) show substantial supraglacial pond formation (water bodies of <20,000 m^2 area), or, in the case of Rongbuk Glacier, supraglacial lake formation (Watson et al., 2016). These glaciers showed large areas of < 2˚ slope and negligible ice flow in the first epoch of our DEM and velocity time series, and an expanded area of the same conditions at the end of our study period. Watson et al. (2016) documented substantial increases in the ponded area of some of these glaciers over our study period, as did Chen et al. (2014) for the supraglacial lake on Rongbuk Glacier, so it is likely that these glaciers are already in the early stages of glacial lake development. Continued sub-debris melt in the middle reaches of these glaciers would further decrease the surface gradient and provide meltwater, both aiding supraglacial pond and lake expansion.

Four of the nine land-terminating glaciers we studied (shown in Figure 3) fail to meet one or both of the criteria proposed by Quincey et al. (2007) and Reynolds (2000) (Figure 7), and have not experienced pond coalescence. Gyabrag Glacier (Figure 7 panel G) showed surface gradient values greater than the 2° threshold (mean of 4.03°) required for effective meltwater ponding. Rongbuk East (Figure 7 panel F) showed substantial ice flow to its terminus (Figure 3c), as well as being too steep (mean 4.15°) for water to collect. Small areas of Lhotse and Erbu glaciers meet the velocity and surface gradient thresholds (Figures 3b & d), and some ponding is evident on these glaciers (Figure 7, panels H & I). Lhotse and Erbu glaciers may therefore be in the early stages of pond coalescence, and further surface lowering will aid water ponding here. Collectively, these observations suggest the criteria outlined by Quincey et al. (2007) and Reynolds (2000) are appropriate as a first-pass method to identify glaciers that may or may not be susceptible to glacial lake formation.

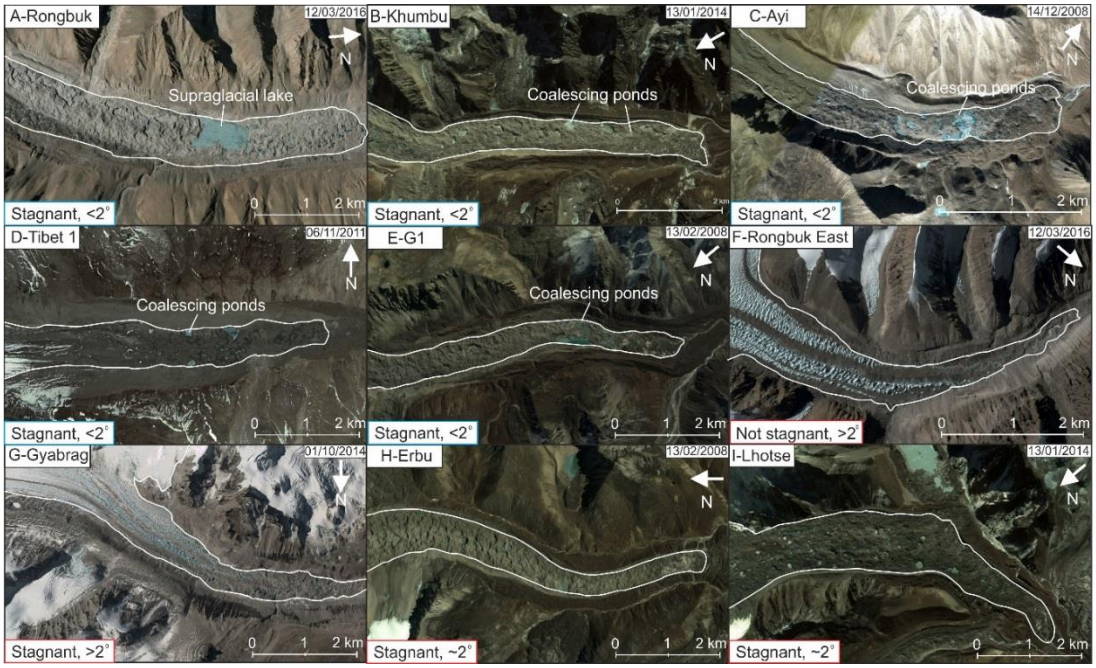

Figure 7. Satellite imagery (Geoeye, Worldview) of the terminal areas of land-terminating glaciers we focus on in this study. Panels A-E are of glaciers that meet the criteria required for glacial lake formation, whereas panels F-I show glaciers that do not meet these criteria.

4.6.4 Implications of lake-terminating glacier retreat

We have shown here how different ice mass loss processes may drive the evolution of lake and land-terminating glaciers in the Himalaya. Lake-terminating glaciers experience different phases of retreat and ice loss as the lake they host expands. Initially, a phase of lake expansion may occur that is not accompanied by amplified glacier mass loss. As the lake level rise or the host glacier thins, calving can occur, front retreat rates may accelerate, the glacier surface profile steepens, and ice flow rates increase. Towards the later stages of lake growth, after a sustained period of ice front retreat and glacier thinning, which reduce driving stresses and increase resisting stresses (lateral and basal drag) due to glacier narrowing (e.g. Adhikari and Marshall, 20120), lake-terminating glaciers slowdown and their retreat rate diminishes. As the total number of glacial lakes seems to be increasing, not just in the Everest Region, but across the Himalaya (Zhang et al., 2015; Nie et al., 2017), it can be inferred that glacial lake expansion will serve to amplify the future mass loss of their host glaciers. Similar observations of amplified ice loss from lake terminating glaciers have been made elsewhere in the Himalaya. For example, Basnett et al. (2013) examined the area loss of 38 glaciers in the Sikkim Himalaya, India, from 1990-2014, and found that the total area loss of the 23 lake-terminating glaciers in their sample was five times greater than the total area loss of land terminating glaciers. Wang et al. (2017) observed similarly amplified

retreat rates of lake terminating glaciers (six times higher) when compared with land terminating glaciers in the Hengduan Shan region of the southeastern Tibetan Plateau from 1990-2014.

It is unclear how long it takes for lake growth to initiate more dynamic glacier behaviour. The development of the large (1.38 km^2) supraglacial lake on Drogpa Nagtsang Glacier has been rapid (Figure 6), but there is no evidence for a resulting effect on the glacier velocity or geometry. Similarly, Rongbuk Glacier has developed a large (0.48 km^2) supraglacial lake since the early 1990s (Chen et al., 2014), but the glacier is stagnant over the area the lake occupies, and the gradient of its lower reaches has reduced as the lake has persisted. Without detailed ice thickness and multi-temporal lake bathymetry datasets, which are both sparse in the Everest region and across the Himalaya as a whole, predictions of when supraglacial lake growth may impact ice dynamics are obviously difficult to make, and may be glacier specific, depending on deepening rates of individual lakes.

Once a full-depth lake has developed and has begun to impact on glacier velocities and thinning rates, the duration of amplified ice mass loss will depend on the spatial extent of enhanced thinning and the magnitude of acceleration. This study has shown that substantial glacier length reductions could occur over a few decades. Although the front retreat rates we show (Figure 6) may seem moderate, the cumulative total front retreat on the nine lake-terminating glaciers in our sample accounted for an average glacier length reduction of almost 20% (ranging from 11-41%) over 25 years. Throughout this period of ice front retreat, surface lowering rates over the terminal regions of lake-terminating glaciers may be more than double those of neighbouring land-terminating glaciers (King et al., 2017), and this impacts on the mass balance of each lake-terminating glacier (Bolch et al., 2011; King et al., 2017). The scale of ice loss is also likely to be large on Himalayan glaciers that have especially low surface gradients, as the presence of a glacial lake pins the glacier terminus to a certain altitude and precludes the stabilising feedback of the glacier retreating to a higher altitude (Truffer and Motyka, 2016). Glaciers with long ablation zones of a similar altitude, such as those shown in Figure 2, will therefore have to retreat substantially up-valley before they can separate vertically from their glacial lake.

The expansion of a glacial lake heightens GLOF hazard directly because; 1) glacial lake expansion increases the area into which mass movements (from both the host glacier and surrounding terrain) can enter and form an overtopping wave, and 2) an increase in lake volume increases lake depth and hence the water burden pressure on the terminal moraine dam. An increase in the calving flux or frequency of large calving events may also lead to

more frequent wave or overtopping events (Fujita et al., 2013; Westoby et al, 2014). Gardelle et al. (2011) documented a 20 % increase in the area of glacial lakes in the Everest region over the period 2000-2009, and our ice front position data shows that this trend has continued through to 2015. Rounce et al. (2017) modelled potential lake expansion and mass-movement trajectories in the Everest region and showed that Imja Tsho could become more hazardous as the lake becomes more proximal to avalanche prone terrain up-valley. The same scenario can be envisaged for other glacial lakes, particularly those that have formed on glaciers fed by steep headwalls and whose primary source of accumulation if from avalanches, as is common in the Himalaya (Benn and Lehmkuhl, 2001; Iturrizaga, 2011).

4.6.5 Outlook

A number of recent modelling studies (e.g. Rowan et al., 2015; Shea et al., 2015; Anderson and Anderson, 2016) have successfully replicated the changes in geometry and velocity of Himalayan land-terminating glaciers in a state of negative mass balance that we describe above. However, the complete contrast in the evolution of lake-terminating glaciers demands a modified approach be taken to simulate their behaviour under different climate scenarios. The similarity of the velocity and thinning regimes predicted by the modelling work of studies such as Benn et al. (2007) with the data we present here suggests that many elements of lake-terminating glacier behaviour in the Himalaya can be predicted. The calculation of the time taken for a full depth lake to form and the accommodation space available for a glacial lake is currently limited by a paucity of well-constrained glacier bed topography and ice thickness data, both of which may be suitable foci for future work in the region. Where a glacier is already hosting a glacial lake, measurements of lake bathymetry (e.g.Yamada, 1998; Somos-Valenzuela et al., 2014) are important as, alongside the down-glacier velocity gradient, the difference between ice thickness and water depth is considered a primary control on lake-terminating glacier terminus position (Benn et al., 2007). Detailed measurements of glacial lake depth are currently only available for Imja Tsho in our study area. Comparison of the bathymetric surveys presented by Chikita (2007), Fujita et al. (2009) and Somos-Valenzuela et al. (2014) suggests up to 30 m of deepening in this lake between 1996/1997 and 2012, which may have been a large contributing factor in the dynamic changes of its host glacier (Lhotse Shar Glacier) that we have shown.

4.7 Conclusions

Analysis of a time series of DEMs and glacier surface velocity data has revealed contrasting geometric and dynamic evolution of lake- and land-terminating glaciers in the Everest region of the Central Himalaya over the last 15 years. Land-terminating glaciers showed similar thinning patterns, changes in surface gradient and changes in velocity. These glaciers thinned most close to the debris-clean ice transition zone, became shallower over their lower reaches and decelerated over the study period. Lake-terminating glacier behaviour can be characterised by two distinct groups. Five of the nine lake-terminating glaciers we assessed showed increased surface velocities alongside enhanced terminal thinning and increased surface gradients. These five glaciers show steady or increasing ice front retreat rates. The remaining four lake-terminating glaciers showed low magnitude glacier surface steepening, reduced glacier surface velocities and steady or diminishing ice front retreat rates. We suggest that this contrasting lake-terminating glacier behaviour represents two different phases of glacier-lake interaction; one where a dynamic link exists between lake expansion and glacier mass loss, with a positive feedback operating between decreasing effective pressure, increased ice velocities, enhanced thinning and longitudinal strain, enhancing mass loss. The other is representative of either an early phase of lake development, during which a glacial lake does not substantially impact on its host glaciers dynamics, or a late stage where a glacier begins to disconnect from the lake it hosts. During either of these stages, changes in glacier velocity or geometry will be more akin to those of a land-terminating glacier.

The timeline of lake development and coincident glacier retreat remains uncertain, but we have documented substantial ice front retreat over a few decades in the Everest region of the central Himalaya. An improved understanding of the bed topography and ice thickness of glaciers primed for lake development would undoubtedly aid efforts to model future lake-terminating glacier behaviour. In their absence, glacier geometry and glacier velocity data can at least be used as a first-pass tool to identify glaciers that are preconditioned for lake development. These data may serve as early warning for those living and working in the region who may need to adapt to an increasing hazard over coming decades, but additionally, they may also be used by numerical modellers aiming to simulate glacier evolution under varying climatic scenarios, as the need to consider glacier-lake interactions becomes increasingly pertinent.

Acknowledgements

OK is a recipient of a NERC SPHERES DTP PhD studentship (grant award NE/L002574/1). AD was supported by funding from the NASA Cryosphere program. The research was conducted at the Jet Propulsion Laboratory, California Institute of Technology under contract with the National Aeronautics and Space Agency.

References

Adhikari S, Marshall SJ. 2012. Parameterization of lateral drag in flowline models of glacier dynamics. Journal of Glaciology. 58(212): 1119–1132, doi:/10.3189/2012JoGG12J018.

Anderson, L.S. & Anderson, R. 2016. Modeling debris-covered glaciers: response to steady debris deposition. The Cryosphere. 10, 1105-1124, doi:10.5194/tc-10-1105-2016.

Bajracharya, S. R., Mool, P. K., and Shrestha, B. R.: Impact of Climate Change on Himalayan Glaciers and Glacial Lakes: Case Studies on GLOF and Associated Hazards in Nepal and Bhutan, International Centre for Integrated Mountain Development (ICIMOD), Kathmandu, 2007.

Bajracharya, Samjwal (submitter); Shrestha, Finu; Bajracharya, Samjwal; Maharjan, SB; Guo, Wanqin (analyst(s)), 2014. GLIMS Glacier Database. Boulder, CO. National Snow and Ice Data Center. http://dx.doi.org/10.7265/N5V98602.

Banerjee, A., & Shankar, R. 2013. On the response of Himalayan glaciers to climate change. Journal of Glaciology. 59(215), 480-490. doi:10.3189/2013JoG12J130.

Basnet, S., Kulkarni, A.V. & Bolch, T. 2013. The influence of debris cover and glacial lakes on the recession of glaciers in Sikkim Himalaya, India. Journal of Glaciology. 59 (218), doi.org/10.3189/2013JoG12J184.

Benn, D.I., Lehmkuhl, F. 2000. Mass balance and equilibrium line altitudes of glaciers in high mountain environments. Quaternary International, 65/66, 15–29, doi.org/10.1016/S1040-6182(99)00034-8.

Benn, D.I., Wiseman, S. & Hands, K.A. 2001. Growth and drainage of supraglacial lakes on debris-mantled Ngozumpa Glacier, Khumbu Himal, Nepal. Journal of Glaciology, 47 (159), 626-638, doi.org/10.3189/172756501781831729.

Benn, D. I., Bolch, T., Hands, K., Gulley, J., Luckman, A., Nicholson, L. I., Quincey, D., Thompson, S., Toumi, R. & Wiseman, S. 2012. Response of debris-covered glaciers in the

Mount Everest region to recent warming, and implications for outburst flood hazards. Earth-Science Reviews (114), 156-174, doi.org/10.1016/j.earscirev.2012.03.008.

Benn, D.I., Hulton, N.R.J. & Mottram, R.H. 2007. 'Calving laws', 'sliding laws' and the stability of tidewater glaciers. Annals of Glaciology (46), doi.org/10.3189/172756407782871161.

Bolch, T., Pieczonka, T., and Benn, D. I. Multi-decadal mass loss of glaciers in the Everest area (Nepal Himalaya) derived from stereo imagery. The Cryosphere (5) 349–358, doi.org/10.5194/tc-5-349-2011, 2011.

Braithwaite, R. J. and Raper, S. C. B. 2009. Estimating equilibrium-line altitude (ELA) from glacier inventory data. Annals of Glaciology (50), 127–132, doi.org/10.3189/172756410790595930.

Burgess, E., Forster, R.E. & Larsen, C.F. 2013. Flow velocities of Alaskan glaciers. Nature Communications, 4:2146, doi.org/10.1038/ncomms3146.

Carrivick, J.L., & Tweed, F.S. 2013. Proglacial lakes: character, behaviour and geological importance. Quaternary Science Reviews (78), 34-52, doi.org/10.1016/j.quascirev.2013.07.028.

Carrivick, J.L., & Tweed, F.S. 2016. A global assessment of the societal impacts of glacier outburst floods. Global and Planetary Change (144), 1-16, doi.org/10.1016/j.gloplacha.2016.07.001.

Chen, W., Doko, T., Liu, C., Ichinose, T., Fukui, H., Feng, Q. & Gou, P. 2014. Changes in Rongbuk Lake and Imja lake in the Everest region of Himalaya, The international archives of the Photogrammetry, Remote Sensing and Spatial Information Sciences, Volume XL-2, ISPRS Technical Commission II Symposium, doi.org/10.5194/isprsarchives-XL-2-259-2014.

Chernos, M., Koppes, M. & Moore, R.D. 2016. Ablation from calving and surface melt at lake-terminating Bridge Glacier, British Columbia, 1984-2013. The Cryosphere (10), 87-102, doi.org/10.5194/tc-10-87-2016.

Chikita, K.A. 2007. Topographic effects on the thermal structure of Himalayan glacial lakes: Observations and numerical simulation of wind. Journal of Asian Earth Sciences (30), 344-352, doi.org/10.1016/jseas.2006.10.005.

Cuffey, K.H. & Paterson, W.S.B. 2010. The Physics of Glaciers, 4th ed. Elsevier, Burlington.

Dehecq, A., Gourmelen, N. & Trouve, E. 2015. Deriving large-scale glacier velocities from a complete satellite archive: Application to the Pamir-Karakoram-Himalaya. Remote Sensing of Environment (162), 55-66, doi.org/10.1016/j.rse.2015.01.031.

Evatt, G., Abrahams, I., Heil, M., Mayer, C., Kingslake, J., Mitchell, S., Fowler, A.C. & Clark, C. 2015. Glacial melt under a porous debris layer. Journal of Glaciology, 61(229), 825-836. doi:10.3189/2015JoG14J235.

Fitch, A.J., Kadyrov, A., Christmas, W.J. & Kitller, J. 2002. Orientation correlation. Proceedings of the British Machine Conference (pp.11.1-11.10). BMVA Press, doi.org/10.5244/C.16.11.

Fujita, K., Sakai, A., Nuimura, T., Yamaguchi, S., and Sharma, R. R. 2009. Recent changes in Imja Glacial Lake and its damming moraine in the Nepal Himalaya revealed by in situ surveys and multi-temporal ASTER imagery. Environmental Research Letters (4), 1–7, doi.org/10.1088/1748-9326/4/4/045205.

Fujita K, Sakai A, Takenaka S, Nuimura T, Surazakov AB, Sawagaki T, Yamanokuchi T. 2013. Potential flood volume of Himalayan glacial lakes. Natural Hazards and Earth System Sciences, 13(7), 1827-1839, doi:10.5194/nhess-13-1827-2013.

Gardelle, J., Arnaud, Y. & Berthier, E. 2011. Contrasted evolution of glacial lakes along the Hindu Kush Himalaya mountain range between 1990 and 2009. Global and Planetary Change (75), 47-55,doi.org/10.1016/j.gloplacha.2010.10.003.

Heid, T. & Kääb, A. 2012. Repeat optical satellite images reveal widespread and long term decrease in land-terminating glacier speeds. The Cryosphere (6), 467-478, doi.org/10.5194/tc-6-467-2012.

Itturizaga, L. 2011. Trends in 20th century and recent glaciers fluctuations in the Karakoram Mountains. Zeischrift für Geomorphologie (55), 205-231, doi.org/10.1127/0372-8854/2011/0055S3-0059.

International Centre for Integrated Mountain Development (ICIMOD). Glacial Lakes and Glacial Lake Outburst Floods in Nepal; ICIMOD: Kathmandu, Nepal, 2011.

Kaspari, S., Hooke, R. LeB., Mayewski, P.A., Kang, S.C., Hou, S.G. & Qin, D.H. 2008. Snow accumulation rate on Qomolangma (Mount Everest), Himalaya: synchroneity with sites across the Tibetan Plateau on 50-100 year timescales. Journal of Glaciology, 54 (185), 343-352, doi.org/10.3189/002214308784886126.

King, O., Quincey, D.J., Carrivick, J.L. & Rowan, A.V. 2017. Spatial variability in mass loss of glaciers in the Everest region, central Himalayas, between 2000 and 2015. The Cryosphere (11), 407-426, doi.org/10.5194/tc-11-407-2017.

McNabb, R.W., & Hock, R. 2014. Alaska tidewater glacier terminus positions, 1948-2012. Journal of Geophysical Research: Earth Surface (119), 153-167, doi.org/10.1002/2013JF002915.

Melkonian, A., Willis, M.K. & Pritchard, M.E. 2016. Stikine icefield mass loss between 2000 and 2013/2014. Frontiers in Earth Science, 4 (89), doi.org/10.3389/feart.2016.0089.

Miles, E.S., Willis, I, C., Arnold, N.S., Steiner, J. & Pellicciotti, F. 2016. Spatial, seasonal and interannual variability of supraglacial ponds in the Langtang Valley, 1999-2013. Journal of Glaciology, 63 (237), 88-105, doi.org/10.1017/jog.2016.120.

Moon, T. & Joughin, I. 2008. Changes in ice front position on Greenland's outlet glaciers from 1992 to 2007. Journal of Geophysical Research (113), F02022, doi.org/10.1029/2007JF000927.

Muto, M. & Furaya, M. 2013. Surface velocities and ice-front positions of eight major glaciers in the Southern Patagonian Ice Field, South America, from 2002 to 2011. Remote Sensing of Environment (139), doi.org/10.1016/j.rse.2013.07.034.

Nakawo M, Iwata S, Watanabe O. & Yoshida M. 1986. Processes which distribute supraglacial debris on the Khumbu Glacier, Nepal Himalaya. Annals of Glaciology, 8, 129-131.

Nakawo M, Yabuki H. & Sakai A. 1999. Characteristics of Khumbu Glacier, Nepal Himalaya: recent change in the debris-covered area. Annals of Glaciology, 28, 118-122, doi:10.3189/172756499781821788.

Noh, M. J. and Howat, I. M. 2015. Automated stereo-photogrammetric DEM generation at high latitudes: Surface Extraction with TIN-based Search-space Minimization (SETSM) validation and demonstration over glaciated regions. Remote Sensing (52), 198–217, doi.org/10.1080/15481603.2015.1008621.

Nie, Y., Sheng, Y., Liu, Q., Liu, L., Liu, S., Zhang, Y. & Song, C. 2017. A regional-scale assessment of Himalayan glacial lake changes using satellite observations from 1990-2015. Remote sensing of Environment (189), 1-13, doi.org/10.1016/j.rse.2016.11.008.

Nuimura T, Fujita K, Fukui K, Asahi K, Aryal R. & Ageta Y. 2011. Temporal changes in elevation of the debris-covered ablation area of Khumbu Glacier in the Nepal Himalaya since 1978. Arctic, Antarctic, and Alpine Research, 43(2), 246-255, doi:10.1657/1938-4246-43.2.246.

Nuimura T, Fujita K, Yamaguchi S. & Sharma RR. 2012. Elevation changes of glaciers revealed by multitemporal digital elevation models calibrated by GPS survey in the Khumbu region, Nepal Himalaya, 1992–2008. Journal of Glaciology, 58(210), 648-656, doi:10.3189/2012JoG11J061.

Nuth, C. & Kääb, A. 2011. Co-registration and bias corrections of satellite elevation data sets for quantifying glacier thickness change. The Cryosphere (5), 271-290, doi.org/10.5194/tc-5-271-2011.

Østrem, G. 1959. Ice Melting under a Thin Layer of Moraine, and the Existence of Ice Cores in Moraine Ridges. Geografiska Annaler (41), 228–230, doi.org/10.1080/20014422.1959.11907953.

Paul, F. Winsvold, S.H., Kääb, A. Nagler, T. Schwaizer, G. 2016. Glacier Remote Sensing Using Sentinel-2. Part II: Mapping Glacier Extents and Surface Facies, and Comparison to Landsat 8. Remote Sensing, 8(7), p. 575, doi.org/10.3390/rs8070575.

Pementel S, Flowers GE, Schoof CG. 2010. A hydrologically coupled higher-order flow-band model of ice dynamics with a Coulomb friction sliding law. Journal of Geophysical Research (115), doi.org/10.1029/ 2009JF001621.

Quincey, D. J., Richardson, S. D., Luckman, A., Lucas, R. M., Reynolds, J. M., Hambrey, M. J. & Glasser, N. F. 2007. Early recognition of glacial lake hazards in the Himalaya using remote sensing datasets. Global and Planetary Change (56), 137-152, doi.org/10.1016/j.gloplacha.2006.07.013.

Reynolds, J.M. On the formation of supraglacial lakes on debris-covered glaciers. In: Nakawo, M., Raymond, C.F., Fountain, A. 2000. (Eds), Debris-Covered Glaciers.

Proceedings of a Workshop held at Seatlle, Washington, U.S.A., September 2000, Oxford. IAHS Publication, vol. 264, pp. 153-4161.

Rignot, E., Echelmeyer, K. & Krabill, W. 2001. Penetration depth of interferometric synthetic-aperture radar signals in snow and ice. Geophysical Research Letters, (28), 3501-3504, doi.org/10.1029/2000GL012484.

Robertson, C.M., Brook, M.S., Holt, K.A., Fuller, I. & Benn, D.I. 2013. Calving retreat and proglacial lake growth at Hooker Glacier, Southern Alps, New Zealand. New Zealand Geographer (69), 14-25, doi.org/10.1111/nzg.12001.

Rounce, D. R. & McKinney, D. C. 2014. Debris thickness of glaciers in the Everest area (Nepal Himalaya) derived from satellite imagery using a nonlinear energy balance model. The Cryosphere (8), 1317-1329, doi.org/10.5194/tc-8-1317-2014.

Rounce, D.R., Watson, C.S. & McKinney, D.C. 2017. Identification of hazard and risk for glacial lakes in Nepal Himalaya using satellite imagery from 2000-2015. Remote Sensing 9 (654), doi.org/10.3390/rs9070654.

Rounce, D. R., King, O., McCarthy, M., Shean, D. E. & Salerno, F. 2018. Quantifying debris thickness of debris-covered glaciers in the Everest region of Nepal through inversion of a sub-debris melt model. Journal of Geophysical Research: Earth Surface, 123, doi.org/10.1029/2017JF004395

Rowan, A. V., Egholm, D. L., Quincey, D. J. & Glasser, N. F. 2015. Modelling the feedbacks between mass balance, ice flow and debris transport to predict the response to climate change of debris-covered glaciers in the Himalaya. Earth and Planetary Science Letters (430), 427-438, doi.org/10.1016/j.epsl.2015.09.004.

Sakakibara, D. & Sugiyama, S. 2014. Ice-front variations and speed changes of calving glaciers in the Southern Patagonia Icefield from 1984 to 2011. Journal of Geophysical Research: Earth Surface (119), 2541-2554, doi.org/ 10.1002/2014JF003148.

Sakai A, Nishimura K, Kadota T,. & Takeuchi N. 2009. Onset of calving at supraglacial lakes on debris covered glaciers of the Nepal Himalayas. Journal of Glaciology, 55(193), 909-917, doi:10.3189/002214309790152555, 2009

Sakai A, & Fujita K. 2010. Formation conditions of supraglacial lakes on debris-covered glaciers in the Himalayas. Journal of Glaciology, 56(195), 177-181, doi:10.3189/002214310791190785, 2010

Sakai A, Nuimura T, Fujita K, Takenaka S, Nagai H. & Lamsal D. 2015. Climate regime of Asian glaciers revealed by GAMDAM Glacier Inventory. The Cryosphere, 9(3), 865-880, doi:10.5194/tc-9-865-2015.

Salerno, F., Guyennon, N., Thakuri, S., Viviano, G., Romano, E., Vuillermoz, E., Cristofanelli, P., Stocchi, P., Agrillo, G., Ma, Y., and Tartari, G. 2015. Weak precipitation, warm winters and springs impact glaciers of south slopes of Mt. Everest (central Himalaya) in the last 2 decades (1994–2013). The Cryosphere (9), 1229–1247, doi.org/10.5194/tc-9-1229-2015.

Shea, J.M., Immerzeel, W.W., Wagnon, P., Vincent, C., Bajracharya, S., 2015. Modelling glacier change in the Everest region, Nepal Himalaya. The Cryosphere 9, 1105–1128. https://doi.org/10.5194/tc-9-1105-2015.

Somos-Valenzuela, M. A., Mckinney, D. C., Rounce, D. R. & Byers, A. C. 2014. Changes in Imja Tsho in the Mount Everest region of Nepal. The Cryosphere (8), 1661-1671, doi.org/10.5194/tc-8-1661-2014.

Thakuri, S., Salerno, F., Smiraglia, C., Bolch, T., D'Agata, C., Viviano, G. & Tartari, G. 2014. Tracing glacier changes since the 1960s on the south slope of Mt. Everest (central Southern Himalaya) using optical satellite imagery. The Cryosphere (8), 1297-1315, doi.org/10.5194/tc-8-1297-2014.

Thakuri, A., Salerno, F., Bolch, T., Guyennon, N. & Tartari, G. 2016. Factors controlling the accelerated expansion of Imja Lake, Mount Everest region, Nepal. Annals of Glaciology, 57(71), doi.org/ 10.3189/2016AoG71A063.

Thompson, S. S., Benn, D. I., Dennis, K., and Luckman, A. 2012 A rapidly growing moraine-dammed glacial lake on Ngozumpa Glacier, Nepal. Geomorphology (145), 1–11, doi.org/10.1016/j.geomorph.2011.08.015.

Truffer, M. & Motyka, R.J. 2016. Where glaciers meet water: Subaqueous melt and its relevance to glaciers in various settings. Reviews of Geophysics (54), 220-239, doi.org/10.1002/2015RG000494.

Trüssel, B., Motyka, R.J., Truffer, M. & Larsen, C.F. 2013. Rapid thinning of lake-calving Yakutat Glacier and the collapse of the Yakutat Icefield, southeast Alaska, USA. Journal of Glaciology, 59 (213), doi.org/10.3189/2013J0G12J081.

Tsutaki. S., Sugiyama, S., Sakakibara, D. & Sawagaki, T. 2016. Surface elevation changes during 2007-13 on Bowdoin and Tugto Glaciers, northwestern Greenland. Journal of Glaciology, 62 (236), 1083-1092, doi.org/10.1017/jog.2016.106.

Van der Veen, C.J. 2002. Calving glaciers. Progress in Physical Geography, 26 (1), 96-122, doi.org/10.1191/0309133302pp327ra.

Warren, C.R & Kirkbride, M.P. 2003. Calving speed and climatic sensitivity of New Zealand lake-calving glaciers. *Annals of Glaciology* (36), 173-178, doi.org/10.3189/172756403781816446.

Watson, C.S. Quincey, D.J. Carrivick, J.L. and Smith, M.W. 2016. The dynamics of supraglacial ponds in the Everest region, central Himalaya. *Global and Planetary Change (142)*, 14-27, doi.org/10.1016/j.gloplacha.2016.04.008.

Watson, C.S., Quincey, D.J., Carrivick, J.L. & Smith, M.W. 2017. Ice cliff dynamics in the Everest region of the central Himalaya, Geomorphology, 278, 238-251, doi.org/10/106/j.geomorph.2016.11.017.

Westoby, M.J., Glasser, N.F., Hambrey, M.J., Brasington, J., Reynolds, J.M. & Hassan, M.A.A.M. 2014. Reconstructing historic Glacial Lake Outburst Floods through numerical modelling and geomorphological assessment: Extreme events in the Himalaya. Earth Surface Processes and Landforms (39), 1675-1692, doi.org/10.1002/esp.3617.

Willis, M.J., Melkonian, A.K., Pritchard, M.E. & Ramage, J.M. 2012. Ice loss rates at the Northern Patagonian Icefield derived using a decade of satellite remote sensing. Remote Sensing of Environment, (117), doi.org/10.1016/j.rse.2011.09.017).

Yang, X., Zhang, T., Qin, D., Kang, S. & Qin, X. 2011. Characteristics and Changes in Air Temperature and Glacier's Response on the North Slope of Mt. Qomolangma (Mt. Everest). Arctic, Antarctic, and Alpine Research (43), 147-160, doi.org/stable/41240408.

Ye, Q., Kang, S., Chen, F. & Wang, J. 2006. Monitoring glacier variations on Geladandong mountain, central Tibetan Plateau, from 1969 to 2002 using remote-sensing and GIS technologies. Journal of Glaciology (179), doi.org/10.3189/17275650678182839.

Zhang, G., Yao, T., Xie, H., Wang, W. & Yang, W. 2015. An inventory of glacial lakes in the Third Pole region and their changes in response to global warming. Global and Planetary Change (131), 148-157, doi.org10.1016/j.gloplacha.2015.05.013.

Chapter 5

Quantifying the morphometric evolution of Himalayan debris covered glaciers using fine resolution digital elevation models.

Owen King, Andy G.D. Turner, Duncan J. Quincey, Jonathan L. Carrivick

Manuscript prepared for submission to ‘Geomorphology’.

5.1 Abstract

Debris covered glaciers in the central Himalaya have now experienced several decades of sustained ice loss, predominantly through glacier surface lowering. Glacier surfaces of low longitudinal gradient but locally complex topography have developed in response to ice loss, and profound changes in supraglacial hydrology have been observed over many slow-flowing parts of debris covered glaciers. In this study we examine the role of supraglacial hydrological features on ablation for six debris covered glaciers in the Everest region of the central Himalaya, and quantify the impact of ice loss on the topographic characteristics of these glaciers in recent decades. Specifically, we use SfM-MVS DEMs of fine spatial and temporal resolution to quantify the contemporary contribution of ice cliff and supraglacial pond expansion to overall mass loss (13.2% area, 35% mass loss) from the stagnant area of Khumbu glacier. Across 6 debris covered glaciers in the region we also developed a metric of glacier surface relief to examine the impact of multi-decadal ice loss on glacier surface topographic characteristics. We find three common changes in glacier surface topography, 1) the up- and down-glacier expansion of surface topography of high relief in response to ice cliff and supraglacial pond network expansion, 2) the up-glacier expansion of glacier surface topography of high local relief that may be caused by differential sub-debris melt beneath thin debris and, 3) the terminus-proximal reduction of topographic relief over glaciers with a coupled supraglacial-proglacial hydrological system. The development of a more pitted glacier surface has important implications for glacier surface water storage and also the energy balance of a debris covered glacier surface, both of which could exacerbate future ice loss.

Key words: debris covered glacier, glacier metrics, structure from motion

5.2 Introduction

The Himalaya contains the greatest terrestrial ice mass outside the Polar Regions, comprising more than 20,000 glaciers and a total area of 40,775 km^2 (Frey et al., 2014). Between 14-18% of the total glacier surface area is covered by supraglacial debris (Kääb et al., 2012), although debris cover varies considerably across different glacierised catchments. In some parts of the Himalaya debris cover expansion has been documented in recent decades (Herried et al., 2015). Thakuri et al. (2014) showed a 17.6 ± 3.1% increase in debris covered area on a subset of glaciers in the Everest region between 1962 and 2011.

The presence of a debris mantle complicates the response of a glacier to climatic change (Rowan et al., 2015; Anderson and Anderson, 2016) because it influences the downward flux of energy that is available for melt at the glacier surface. Melt can either be enhanced by a thin layer of surface debris that preferentially, due to its lower albedo, absorbs and transmits incident solar radiation to ice beneath; or melt can be inhibited by a thick layer of debris that stores and re-emits incoming energy with only a small portion reaching the ice surface below (Østrem, 1959; Nicholson and Benn, 2006). Consequently, many debris-covered glaciers persist at altitudes no longer occupied by clean ice glaciers (Rowan et al., 2015).

Spatial variability in melt rates leads to the development of a suite of surface topographic features not commonly found on debris-free glaciers. This topographic development is important because of its potential to impact on the energy balance at the surface of the glacier, and therefore the magnitude of surface ablation (Brock et al., 2006; Cathles et al., 2011; Quincey et al., 2017). In areas where debris cover is thick, ice loss is focused in specific areas of ice cliff and supraglacial pond growth (Watson et al., 2017b), with up to 40% of melt occurring over just 5% of the total glacier area (Thompson et al., 2016). The development of a complex glacier surface topography on debris covered ice can also heavily impact the supraglacial hydrology of debris covered glaciers. Differential melt, ice cliff backwasting and supraglacial pond development creates more accommodation space for the storage of supraglacial meltwater, thus they may play an important role in modulating freshwater runoff and quality in the Himalaya (Irvine-Fynn et al., 2017). Should a supraglacial pond network persist, particularly over glacier surfaces of low slope and low velocity, pond coalescence and ultimately glacial lake development may occur (Quincey et al., 2007; King et al., 2018). Floods from glacial lakes can travel many hundreds of kilometres downstream, and have been responsible for the loss of life in the Himalaya (Carrivick and Tweed, 2016). The presence of a lake at a glacier terminus may also exacerbate glacier retreat and ice mass loss (King et al., 2017).

Despite the importance of glacier surface morphology as a control on melt, supraglacial hydrology, hazard development and ultimately meltwater yield, there remains little knowledge of how ice surface topography evolves over decadal timescales, particularly during periods of rapid ice loss. In this study we therefore aim to examine the topographic evolution of debris covered glacier surfaces in the Everest region of the Himalaya over the last 32 years by analysing two sets of fine-resolution DEMs, derived from aerial photography and WorldView-2 satellite imagery. Specifically, we develop a surface metric that examines the local variability in glacier surface topography. We also examine changes in the glacier surface at a high temporal resolution using SfM-MVS derived DEMs that reveal the dominant melt processes operating at the surface of one of the debris covered glaciers in our sample on an annual timescale. Using these datasets, we aim to identify the processes driving glacier surface morphology change in the area, and to examine how their spatial extent and concentration has altered in recent decades.

5.3 Study site

We focus our study on six glaciers located in the Everest region of the Nepal Himalaya (Figure 5.1). Khumbu Glacier is the largest glacier we study, and originates in the Western Cwn below Mt Everest. The glacier initially flows west, before turning to flow south below its icefall. In 2011, 24 % of the surface of Khumbu Glacier was covered by debris, whereas in 1962, 15% of the glacier was covered by a debris layer (Thakuri et al., 2014). The debris layer increases in thickness down-glacier, from a few cm near the base of its icefall, to more than 2 m near its terminus (Rounce et al., 2015; Rowan et al., 2015; Rounce et al., 2018). An extensive network of supraglacial ponds and ice cliffs exists over the lower 6 km of the glacier (Watson et al., 2016). Between November 2009 and February 2015, Khumbu Glacier gained 99,889 m^2 of ponded area (Watson et al., 2016), and the number of ice cliffs present in its ablation zone increased from 436 to 520 (Watson et al., 2017a). Bolch et al. (2011) showed increasing surface lowering rates over the lower reaches of the glacier using a time series of DEMs spanning the period 1962-2007. The moderate resolution of their DEMs precluded the attribution of enhanced surface lowering to a developing network of cliffs and ponds, but the pattern of surface lowering they show is similar to that caused by cliff and pond expansion that has been documented on the nearby Ngozumpa Glacier (c.f. Thompson et al., 2016).

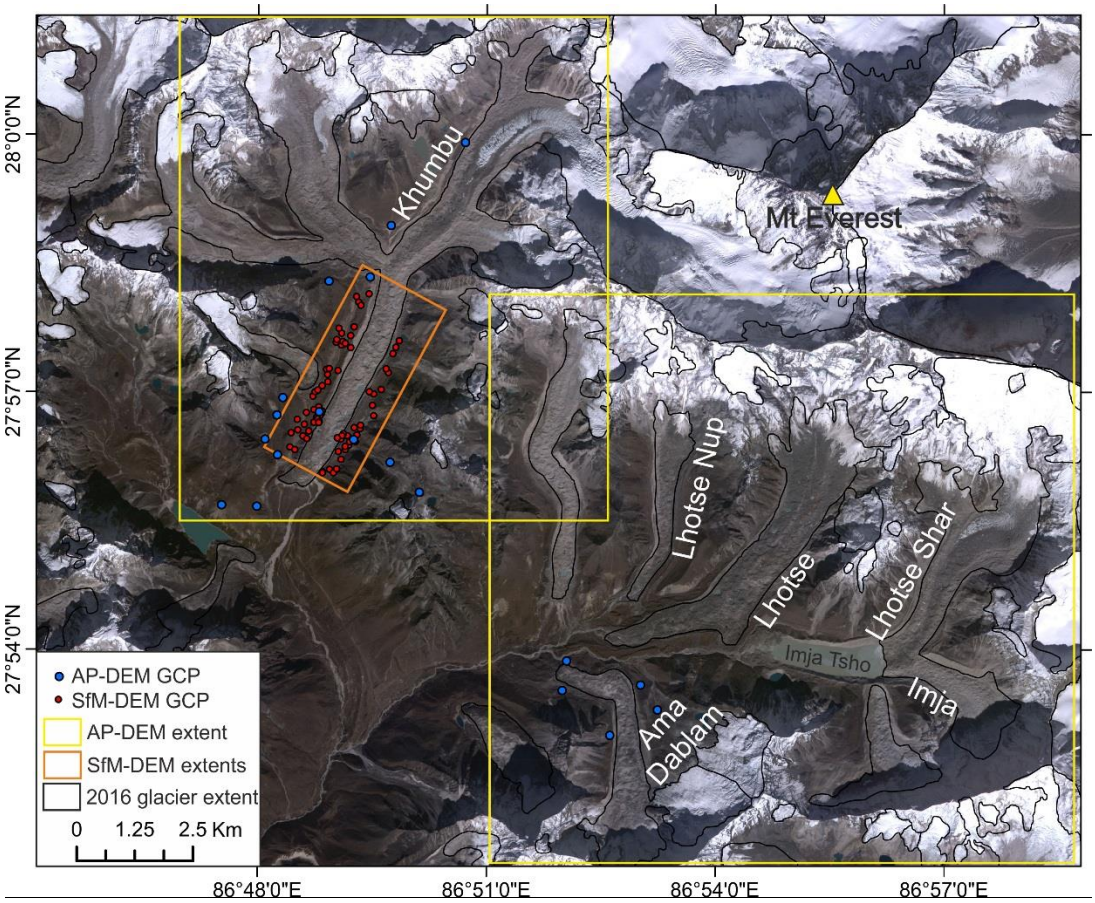

Figure 5.1. The six glaciers we focus on in this study, and the extent of the DEM datasets. WV-DEM coverage is complete for the entire study area and is therefore not shown on the figure. Background image is a RapidEye scene captured in April 2015.

Lhotse Nup and Lhotse Glaciers flow south from the foot of the Lhotse/Nuptse Massif (8516 & 7861 m a.s.l., respectively). These glaciers are 5.1 and 7.1 km in length and show substantial debris cover that has also expanded in recent decades. Thakuri et al. (2014) estimated debris cover extent to be 31 and 36%, respectively for these two glaciers in 1962, and 40 and 42% in 2011. A large proportion of their ice mass input likely comes from avalanching (Benn and Lehmkuhl, 2001). Watson et al. (2016) documented slight increases in ponded area on Lhotse and Lhotse Nup Glaciers (expansion of 25341 m^2 and 7524 m^2) between November 2009 and February 2015. Both of these glaciers hosted a similar number of ice cliffs in 2009 (Lhotse- 299, Lhotse Nup- 59) and 2015 (Lhotse- 293, Lhotse Nup- 71) (Watson et al., 2017a).

Lhotse Shar and Imja Glaciers coalesce before terminating into Imja Tsho - a lake that has been expanding since the early 1960s (Solomos-Valenzuela et al., 2014). Thakuri et al. (2014) treated the two glaciers as one system, and show a slight (2%) increase in debris

cover area between 1962 and 2011. Watson et al. (2016, 2017a) documented a decrease in the number of ice cliffs (459 to 289 on Lhotse Shar, 168 to 122 on Imja) and total ponded area (–56634 m^2 and –6050 m^2) for Lhotse Shar and Imja glaciers between 2009 and 2015. King et al. (2018) showed increased velocities over the lower reaches of Lhotse Shar Glacier over the period 2000-2015, and suggested that the expansion of Imja Tsho may be influencing glacier dynamics.

Ama Dablam Glacier flows north from the eastern flank of Ama Dablam (6812 m a.s.l.). Unlike the glaciers on the opposing valley side (Lhotse, Lhotse Nup and Nuptse Glaciers), Ama Dablam Glacier flows down from a broad, clean ice accumulation zone that feeds a short (4.3 km) debris covered ablation zone. This debris covered tongue comprised 26% of total glacier area in 2011 (Thakuri et al., 2014). This section of the glacier has thinned and retreated since the 1970s (Bolch et al., 2011).

Table 3.1. Attributes of glaciers studied. Glacier ID and elevation information extracted from RGI V6.0. Debris cover extent from 2015.

Glacier ID	Glacier name	Length	Area	Min elev	Max elev	Range	Debris cover (%)
G086917E27925N	Lhotse	7.1	6.9	4821	6082	1261	42
G086820E27978N	Khumbu	15.7	39.5	4915	8062	3147	24
G086949E27913N	Lhotse Shar	6.5	7.01	5021	7998	2977	27
G086949E27913N	Imja	3.71	8.29	5019	8000	2981	35
G086889E27929N	Lhotse Nup	5.1	3.89	4979	5470	491	40
G086882E27875N	Ama Dablam	6.25	5.51	4761	6170	1409	26

5.4 Methods

5.4.1 DEM generation

Our analyses are based on DEMs generated using three different approaches: stereo photogrammetry using aerial photographs (hereafter AP-DEM), stereo photogrammetry using WorldView satellite imagery (hereafter WV-DEM), and Structure from Motion (SfM) with Multi-View Stereo (MVS) (hereafter SfM-DEM) using close range terrestrial photographs. WV-DEMs were generated from several pairs of WorldView-1 and WorldView-2 imagery using the Surface Extraction with TIN-based Search-Space Minimization (SETSM) algorithm described by Noh and Howat (2015). The WorldView

scenes were captured on the 21st March 2016 over the Imja Valley. The WV-DEM covering the Khumbu valley is a composite of two DEMs, one derived from imagery acquired on the 31st Jan 2015 and one acquired from imagery acquired on the 2nd February 2015. We assumed that no substantial surface elevation change occurred in the Khumbu valley during the two day gap between the acquisition dates and mosaicked the two DEMs. The SETSM algorithm used to generate the WV-DEMs uses only the Rational Polynomial Coefficients (RPCs) as geometric constraints, the geolocation accuracy of which is 5 m (Noh and Howat, 2015). RPCs are updated by the SETSM algorithm to increase the geolocation accuracy of DEMs to ±4 m in X, Y and Z directions. WV-DEMs were generated at 2 m ground resolution.

SfM-MVS DEMs were generated following three detailed terrestrial photographic surveys of the ablation zone of the Khumbu Glacier, from the icefall in the middle of the glacier to the terminus in October 2015, May 2016 and May 2017. These surveys were completed by traversing moraine ridges and elevated routes along valley sides and taking photos of the surface of the glacier and its lateral morainic troughs at regular intervals (approximately every 30 metres). All three surveys were conducted using the same survey route, and all contained a very similar number of photographs (~1300 in each survey). We used Agisoft Photoscan (version 1.3.4) to carry out the processing steps required in a standard SfM-MVS workflow (e.g. Smith et al, 2015). Camera alignment and sparse point cloud generation were carried out and only points with a reprojection error of <1.5 were retained. Field-derived GCPs (see section 5.4.2) were identified and placed in photographs from each epoch (October 2016, May 2016 and May 2017). The mean GCP Root Mean Square error (RMSE) was 0.25 m (n = 25) in the October 2015 survey, 0.26 m (n = 27) in the May 2016 survey, and 0.25 m (n = 25) in the May 2017 survey. Dense point clouds were produced using PhotoScan's MVS algorithm and were cleaned manually to remove obvious blunders. We used the Topographic Point Cloud Analysis Toolkit (ToPCAT) (Brasington et al., 2012) to decimate and rasterise the resulting point cloud, setting a minimum point density of $10/m^2$ to produce a 2 m resolution DEM from each time period.

The AP-DEM was derived from fine resolution (0.5 m ground resolution) aerial photographs acquired in 1984 using a Wild RC-10 camera (Washburn, 1989). We used 7 images from the Bradford Washburn aerial photo set, purchased from Swissphoto and scanned at 1693 dpi from the original diapositives. DEM processing was carried out using Leica Photogrammetry suite (LPS) within a frame camera geometric model setup and 2 m DEMs were produced, matching the resolution of the WV & SfM DEMs. Aerial photograph pairs were processed separately for the Khumbu and Imja valleys due to insufficient overlap between image pairs at the edges of each valley for a single composite DEM to be

generated. The outer limits of each of the AP-DEMs fell over Nuptse Glacier, and this glacier has not been included in further analyses because of poor data quality in the perhipheral areas of the two AP-DEMs. Seventeen evenly spread GCPs were used in the Khumbu valley AP-DEM generation, and nine in the Imja valley AP-DEM generation.

5.4.2 Ground control

The geolocation of our AP-DEM and SfM DEMs was fixed using an extensive set of GCPs collected in the Khumbu and Imja valleys. We collected 70 spot height measurements of stable features (mostly large boulders) easily distinguished in both the terrestrial photographic surveys from each epoch, and the aerial photographs (Figure 5.1). We used two Leica GS10 differential GPS (dGPS) units to collect GCPs. One dGPS unit was deployed as a temporary base station over the duration of the October 2015 survey, with the other used as a rover to collect GCPs. Each GCP was occupied in static mode for a minimum of 10 minutes. We used base station data from the permanent Syangboche station (approximately 20 km from the Khumbu) to resolve the position of our temporary base station at the Khumbu, and then used this location as a fixed reference against which we could adjust the location of our GCPs. All dGPS data processing was completed using Leica Geoffice software, and the mean 3-D positional uncertainty of the 70 GCPs used in AP-DEM and SfM-DEM processing was 5.1 mm.

5.4.3 DEM coregistration and bias removal

A substantial cross-track tilt was present in the AP-DEM covering the Imja Valley, likely because of the clustering of GCPs in one section of the model. Initial differencing of the AP-DEMs against the WV-DEMs also revealed a misalignment between these DEM sets. We eliminated co-registration error between the AP-DEM and WV-DEMs by following the methods of Nuth and Kääb (2011). We used the WV-DEM as the master DEM during the co-registration process because of its greater coverage of the study area compared to SfM-DEMs. The cross-track tilt was removed from the Imja Valley AP-DEM using a grid of DEM x-coordinates and a linear regression relationship taken from the difference data between the AP-DEM and WV-DEM. The mean and standard deviation of off-glacier AP-DEM-WV-DEM elevation differences was –0.66 & 8.36 m for the Imja valley, and –0.39 & 7.14 m for the Khumbu valley following co-registration and de-tilting.

5.4.4 Topographic classification of glacier surfaces

Features of locally variable surface relief are ubiquitous on debris covered glaciers. Ice cliff complexes are easily distinguished from the surrounding, undulating topography of the

glacier surface, and from supraglacial ponds, by their contrasting slope or vertical relief. DEMs of sufficiently fine resolution to capture small-scale temporal variability in surface topography can therefore be interrogated to distinguish such features using automatic algorithms, and the distribution and density of such features examined in both space and time. The extent of such features can be quantified from optical imagery, but may be time consuming because of the requirement of manual digitisation (in the case of ice cliffs – Watson et al., 2017a), and may be somewhat complicated by spatially homogenous spectral characteristics of the debris mantled surface.

To assess whether glacier surface features could be identified using fine resolution topographic datasets, we developed a Statistical Measure of Relief (hereafter SMR) metric to summarise the local relief of a subset region of the glacier, as after a series of trial analyses we found that this parameter was the best to distinguish ice cliffs and supraglacial ponds from neighbouring, gently undulating glacier surface topography. The SMR metric is a sum of the negative elevation differences within a specified diameter circular window, relative to a central cell within that window. We produced such a metric using 4 cell, 8 cell and 16 cell windows, and assessed which produced the most realistic estimate of local relief (Supplementary Figures 6 and 7) associated with ice cliff features, and which was able to distinguish the most accurate extent of such features, using a RapidEye (2 m resolution) scene from 2015, and the photographs used to generate SfM models as reference (Supplementary Figure 6). The 8 cell window was deemed most appropriate for identifying features with sharp changes in relief (ice cliffs), as well as more gentle breaks in glacier surface topography. The 4 cell window was too constrained to identify features of moderate relief (reclined ice cliffs), and the 16 cell window yielded estimates of surface relief that were an order of magnitude too large to be representative of individual ice cliffs (1000s m of relief), as well as smoothing features of high relief beyond their actual extent (Supplementary Figure 6). Our analyses was therefore focused on metric grids produced using an 8 cell window on both the 1984 and 2015 DEMs, an example of which is given in Figure 5.2.

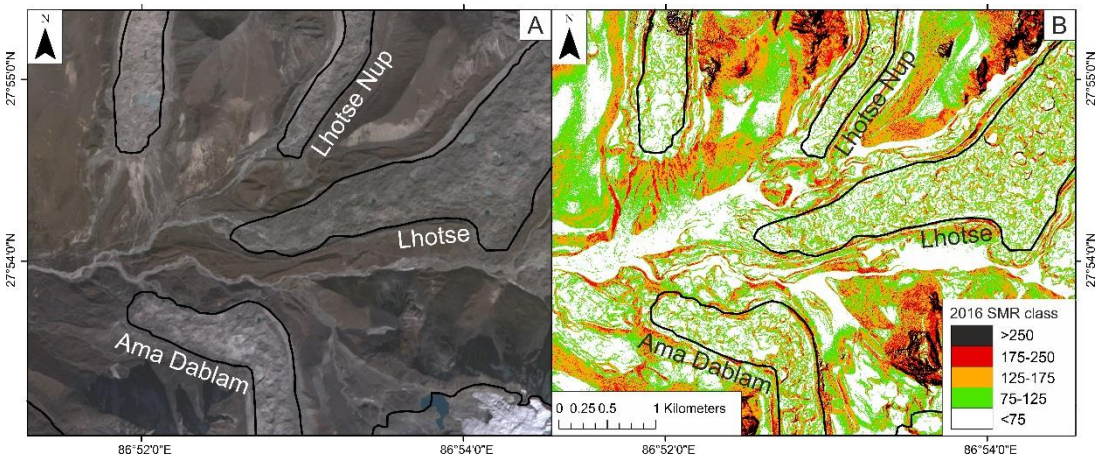

Figure 5.2. An example of the SMR metric classes over the terminal regions of Lhotse, Lhotse Nup and Ama Dablam glaciers, and a RapidEye (left) scene of the same area (17th Nov. 2017).

To assess the variability of glacier surface characteristics in both space and time, we split the SMR metric into categories, in essence a topographic classification of the glacier surface. Categories were defined for the supraglacial environments that particular thresholds of negative elevation differences best represented based on visual analysis, again using RapidEye imagery and SfM surveys as reference. SMR values of <75 m were interpreted as representing gently undulating, debris covered or, near some glacier termini, soil mantled areas; values of 75-125 m were interpreted as representing debris covered glacier surfaces of sufficient relief to allow debris slumping; values of 125-175 m were interpreted as representing ice cliff flanks, and values of 175 m or greater were interpreted to be associated with ice cliff faces. Herein, SMR metric values of <75 m are referred to as SMR_{75}, 75-125 m as $SMR_{75\text{-}125}$, 125-175 as $SMR_{125\text{-}175}$ and >175 m as SMR_{175}. The total area occupied by different classes was calculated for 500 m distance bins along each glacier and compared for the AP- and WV-DEMs. Supraglacial ponds were removed from analyses using pond extent data from Watson et al. (2017a), which were coincident with our study period.

5.4.5 Additional data sources

We combined the fine resolution DEMs and glacier surface metric data with datasets of glacier velocity and supraglacial pond extent generated by Dehecq et al. (2015), Watson et al. (2016) and Watson et al. (in revision) for the Everest region. Glacier surface velocity data were generated by tracking surface features in a series of Landsat 7 (ETM+) and 8 (OLI) panchromatic images (see Dehecq et al., 2015 for more details) over the period 2013-2015. Multiple velocity fields from this period were combined using a median value for each pixel to give an average velocity field that coincided with the date of our contemporary

DEM sets. The supraglacial pond extent datasets of Watson et al. (2016) and Watson et al. (in review) were generated using a combination of Object Based Image Analysis (OBIA) and manual digitisation of WorldView 1 & 2, GeoEye, Pleaideas and QuickBird imagery. The pond extents of Watson et al. (2016) cover several time periods, and we used the most recent pond extents (2013-2015) for each glacier in our study. We also generated supraglacial pond extents from the 1984 aerial photographs using the same OBIA approach as Watson et al. (2016).

5.5 Results

5.5.1 Multi-decadal ice loss

The differencing of the AP-DEM and WV-DEMs shows the substantial ice loss from each glacier over the study period (Figure 5.3). Table 3.2 shows mean surface lowering and annual surface lowering rates for the debris covered and clean ice portions of each glacier over the 31/32 year period between the AP-DEM and WV-DEMs. The AP-DEM covers approximately 44% of the Khumbu Glacier.

Land-terminating glaciers (Khumbu, Lhotse, Lhotse Nup and Ama Dablam) showed most substantial surface lowering several kilometres up-glacier (Figure 5.4). In the case of Khumbu Glacier, maximum surface lowering (~75 m) occurred close to the clean ice-debris covered transition zone below the location of Everest base camp. Surface lowering was slight immediately below this glacier's icefall. In the case of Lhotse, Ama Dablam, and Lhotse Nup Glaciers, surface lowering was most substantial (mean of –18.8, –24.18 and –19.12 m within 1 km of the debris-clean ice transition, maximum of ~ –65 m on each glacier) immediately below the steep headwall and avalanche debris cones present on each glacier (Figure 5.4). Surface lowering was minimal in the terminal region of Khumbu Glacier (mean of –5.65 m within 1 km of the terminal moraine). Lhotse, Ama Dablam and Lhotse Nup glaciers did show slight surface lowering in their terminal regions (mean of –11.03, –10.62 & –8.36 m within 1 km of glacier termini). Five of the six glaciers showed surface lowering in clean ice areas above the extent of debris cover, and only Khumbu Glacier showed any positive elevation change close to its ELA (its icefall). Ice surface elevation increases here were 5-10 m, although DEM coverage was not complete over the area.

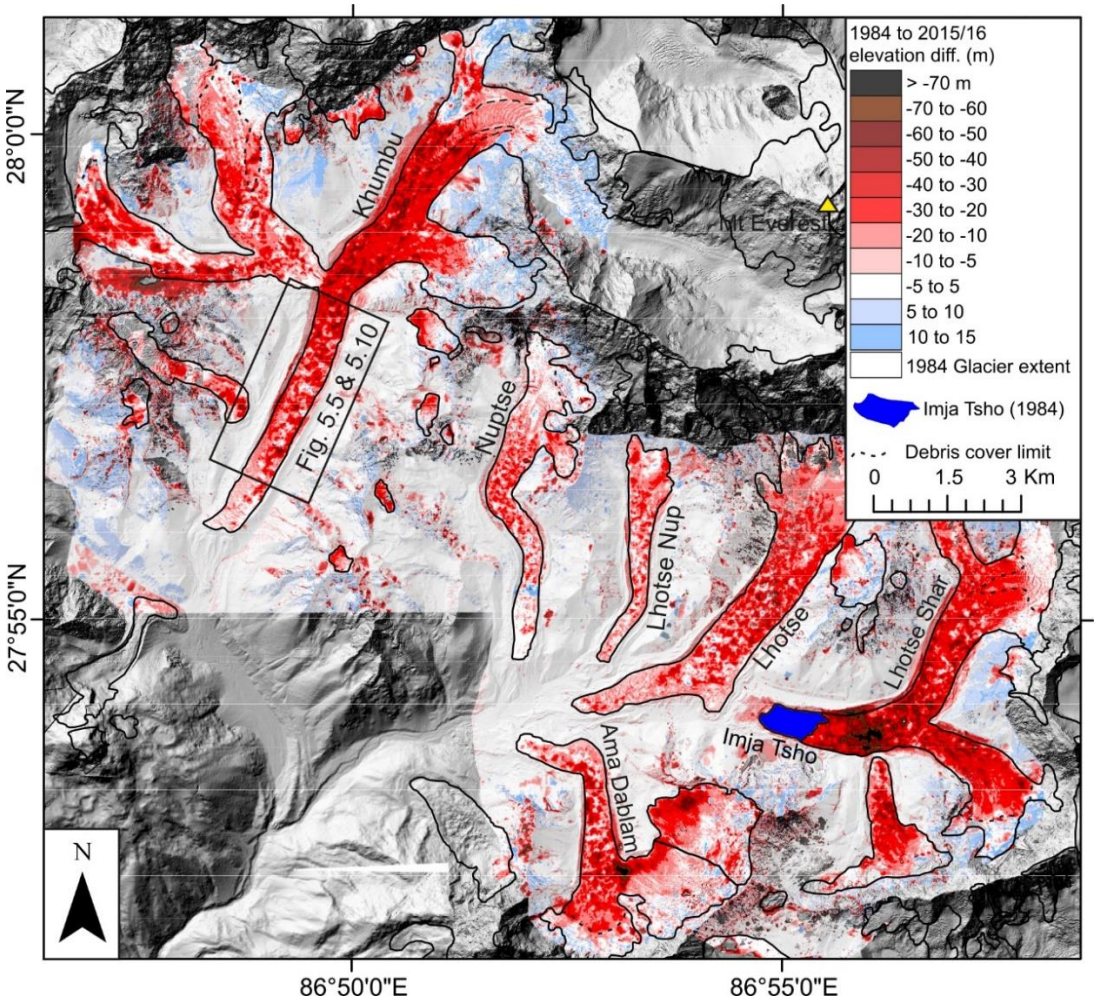

Figure 5.3. The difference in surface elevation calculated by differencing the AP-DEM (1984) and WV-DEMs (2015/16). Inset shows the subset area covered by SfM-MVS DEMs in Figures 5.5 & 5.10.

The lake-terminating Lhotse Shar/ Imja Glacier complex shows a reversed surface lowering gradient when compared with land-terminating glaciers (Figure 5.4). The surface of this glacier lowered most (~85 m) over the area through which Imja Tsho expanded over the study period. The surface lowering measured here comprises the elevation change between the glacier surface and the new lake level, and much more ice may have been lost below the waterline. Surface lowering rates on the Lhotse Shar/ Imja Glacier complex decreased slightly in an up-glacier direction, but was most substantial out of all the glaciers in our sample (Table 3.2). Surface lowering over clean ice areas of all of the glaciers in our sample was reduced when compared with debris covered ice (Table 3.2).

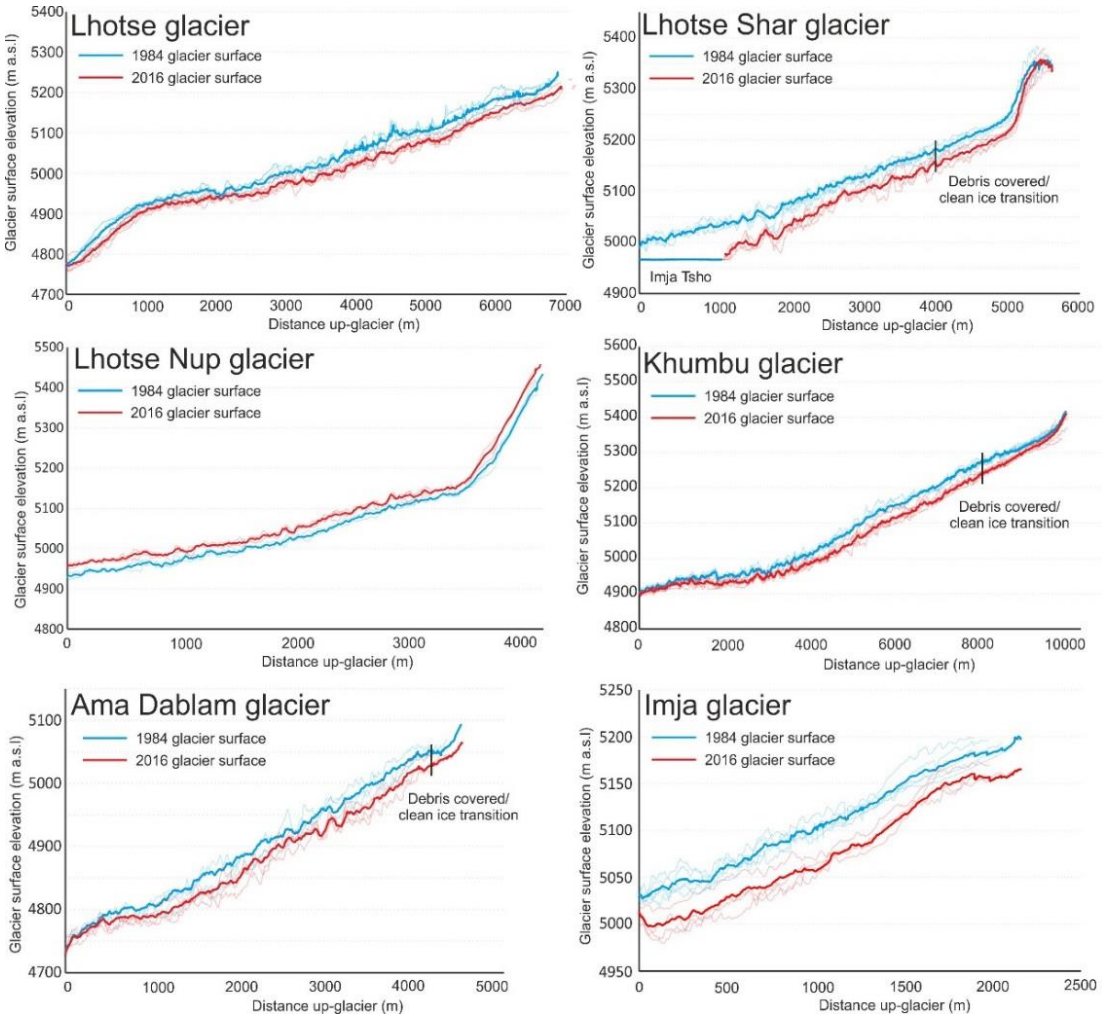

Figure 5.4. Glacier surface elevation profiles taken from AP- and WV-DEMs. Semi-transparent lines are flow-parallel surface elevation profiles spaced 100 m apart across each glaciers surface, and the opaque elevation profiles represent a mean of flowline-parallel profiles. Locations of debris covered- clean ice transition are also shown.

Table 3.2. Changes in the debris covered area on each glacier, along with estimates of total surface lowering, and surface lowering rates, for clean and debris covered ice over the study period.

Glacier	**1984 debris covered area (km ^{2})**	**2016 debris covered area (km ^{2})**	**Δ debris cover area (km^2)**	**Mean debris covered area dh (m)**	**Mean debris covered area dh/dt (m a^{-1})**	**Mean clean ice dh (m)**	**Mean clean ice area dh/dt (m a^{-1})**	**Δ pond area (m^2)**
Khumbu	8.20	8.52	0.32	–22.75	–0.77	–14.49	–0.48	129632
Lhotse Nup	1.66	1.72	0.06	–12.63	–0.41	–10.81	–0.35	18651
Lhotse	6.02	6.30	0.28	–17.82	–0.58	–7.93	–0.26	35368
Lhotse Shar	6.73	6.04	0.69	–26.46	–0.86	–11.38	–0.38	10943
Imja	1.23	1.47	0.24	–31.87	–0.99	–6.85	–0.21	–2655
Ama Dablam	2.51	2.69	0.18	–20.11	–0.66	–13.15	–0.43	–15233

5.5.2 Contemporary ice loss

The differencing of the SfM-DEMs against the WV-DEM (Figure 5.5) revealed the contemporary pattern of ice loss from the surface of the Khumbu Glacier, the pattern of which is contrasting to that on a decadal timescale (Figure 5.3). We focus our analyses of the SfM-DEM difference data on a subset shown in Figure 5.3, because this area is constrained with the best ground control data, and possesses the best photographic coverage. The SfM-DEMs primarily cover the stagnant portion of the glacier. Figure 5.5 shows the evolution of the glacier surface from the end of January 2015 to May 2017. Surface lowering, and therefore ice loss, was concentrated where supraglacial ponds and ice cliffs expanded over the study period. Using supraglacial pond and ice cliff extents from Watson et al. (2016, 2017a), we estimate that pond expansion and cliff retreat accounted for 35% of ice loss over the period Jan 15 to Oct 15, despite occupying just 13.2 % of the subset area of the glacier. The mean backwasting rate (calculated by dividing the total area of surface lowering associated with each cliff by cliff length) of the ice cliffs present in the subset area shown in Figure 5.3 was 13.51 m a^{-1}, ranging from 6.43-18.55 m a^{1}. Cliff expansion affected 8.7% of the glacier surface in the subset area (~118,000 m^2 of 1,350,000 m^2 subset) over our 2 year 4 month study period. The same rate of cliff expansion would result in a complete turnover of the glacier surface in just under 26 years in this subset region.

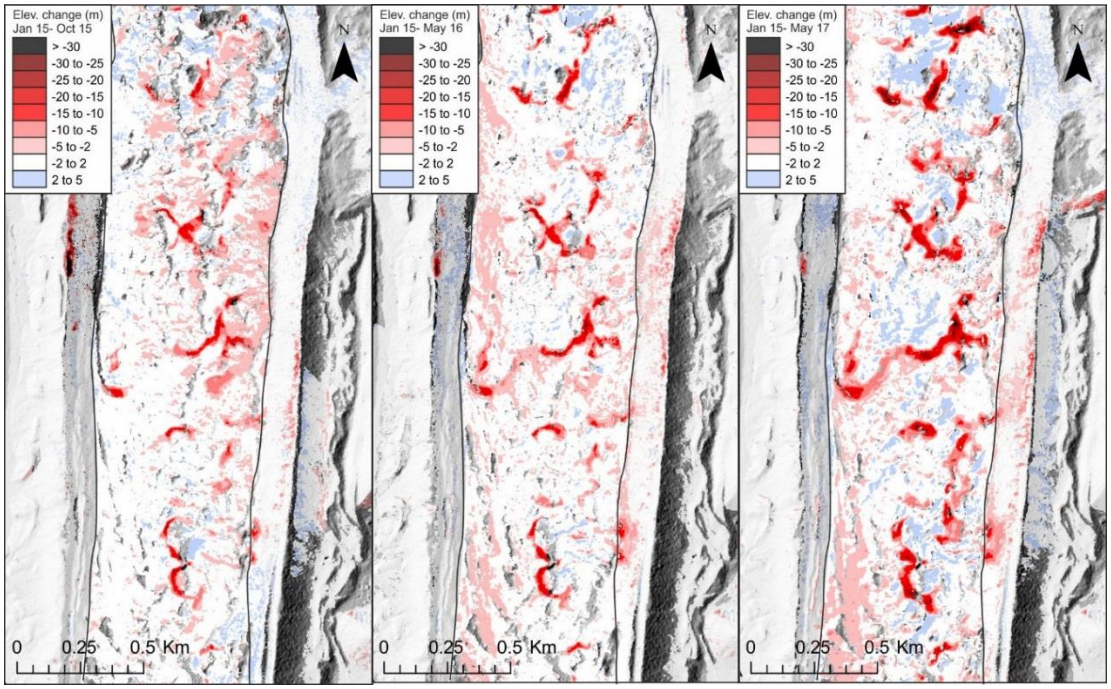

Figure 5.5. The difference in surface elevation between the WV-DEM (Jan 2015) and SfM-DEMs acquired in October 2015, May 2016 and May 2017.

5.5.3 Topographic classification of glacier surfaces

The contribution of each topographic class to the total glacier surface area varied substantially with distance up-glacier on four of the five glaciers we assessed. The lowermost 1 km of Khumbu, Lhotse Nup and Ama Dablam Glaciers were mostly (~60%) composed of SMR_{75} in both time periods. The area covered by SMR_{75} decreased to as little as 30%, 3-5 from the terminus of each of these glaciers. In both time periods, the proportion of glacier surfaces covered by $SMR_{75\text{-}125}$ to SMR_{175} peaked in the middle reaches of Khumbu, Lhotse Nup, Lhotse and Ama Dablam Glaciers (panels B, C and D in Figures 5.6, 5.7 and 5.8), but were generally limited to less than 30% of the total glacier surface area. SMR_{175} accounted for >10% of glacier area on all four of these glaciers, but did cover the greatest area in the middle reaches of each glacier.

In contrast to the other four glaciers, the proportion of the surface of Lhotse Shar and Imja Glaciers covered by SMR_{75} increased up-glacier. On both of these glaciers, the area covered by SMR_{75}increased from ~40% of glacier area within a bin at their termini, to ~60% at the debris-clean ice transition. The percentage of glacier area covered by $SMR_{75\text{-}125}$ to SMR_{175} decreased with distance from the termini of Lhotse Shar and Imja Glaciers (Figure 5.8).

5.5.4 Multi decadal topographic evolution of glacier surfaces

Substantial changes occurred in the surface topography of all of the glaciers we assessed between 1984 and 2015/16. Changes in the area covered by different topographic classes occurred in the terminal regions of some glaciers, as well as towards the debris-clean ice transition zone. Figures 5.6, 5.7 and 5.8 show the contribution of SMR_{75}, $SMR_{75\text{-}125}$, $SMR_{125\text{-}175}$ & SMR_{175} to total glacier surface area in both 1984 and 2015/2016, as well as the change in the cover of each topographic class over the study period.

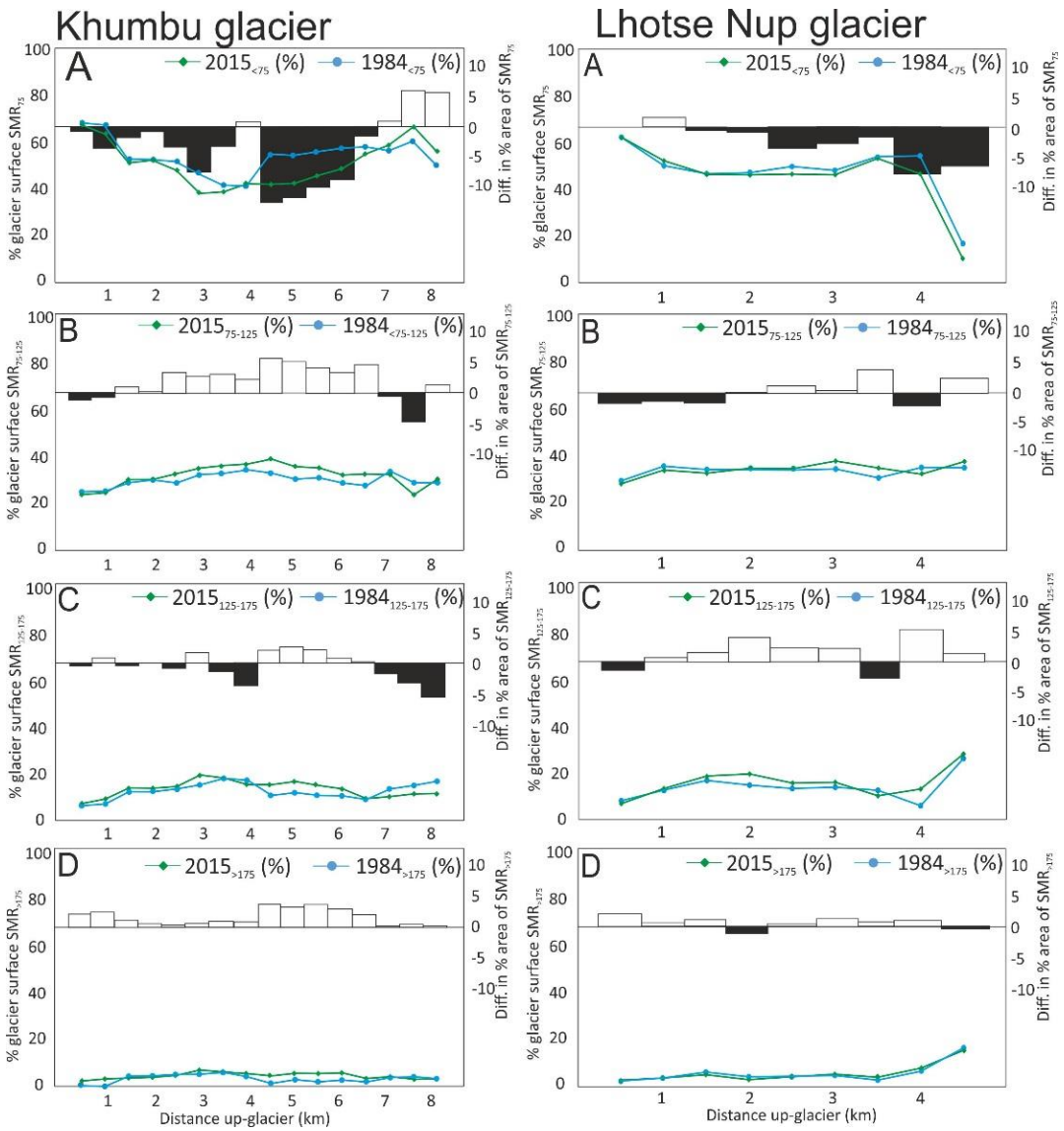

Figure 5.6. Percentage of glacier surface area made up of different classes of topography distinguished by the sum of negative elevation differences in a local (8 pixel) area for Khumbu and Lhotse Nup Glaciers. Also shown is the change in the area covered by different topographic classes over the period 1984-2015/16. SMR_{75} (A) represents gently undulating, debris covered glacier surfaces, $SMR_{75\text{-}125}$ (B) represents debris covered areas of

sufficient slope to allow debris slumping, $SMR_{125-175}$ (c) represents ice cliff flanks & SMR_{175} (D) represents ice cliff faces.

Khumbu Glacier showed a substantial reduction in the area covered by SMR_{75} over the study period. Over the entire debris covered area, the area of this class reduced by 8.7%. The greatest reductions in SMR_{75} occurred between 4-6.5 km up-glacier on Khumbu Glacier. Concomitant increases in SMR_{75-125} to SMR_{175} occurred in the lower reaches of Khumbu Glacier (Figure 5.6), with the most substantial increases occurring >4.5 km up-glacier. The surface of Lhotse Nup Glacier evolved in a similar way to that of Khumbu Glacier. The proportion of this glacier's surface made up of SMR_{75} reduced over the study period (4.5% reduction), with the largest reductions occurring greater than 2.5 km up-glacier. Modest increases in SMR_{75-125} to SMR_{175} occurred high up on this glacier, but increases in total class area were generally limited to ~5% or less (Figure 5.6).

The lower reaches of Lhotse and Ama Dablam Glaciers showed contrasting surface topography change when compared to Khumbu and Lhotse Nup Glaciers. There were 3.8 and 13.2% increases in SMR_{75} within ~2.5 km of the terminus of Lhotse and Ama Dablam Glaciers. There were slight decreases in the area covered by SMR_{75-125} to SMR_{175} in the terminal regions of Lhotse and Ama Dablam Glaciers (Figure 5.7). The middle and higher reaches of Lhotse and Ama Dablam Glaciers showed decreases in SMR_{75}, akin to Khumbu and Lhotse Nup Glaciers. Associated increases in SMR_{75-125} to SMR_{175} occurred greater than 3 km up-glacier on these glaciers (Figure 5.7), although total area changes were limited to <5% for each 500 m band.

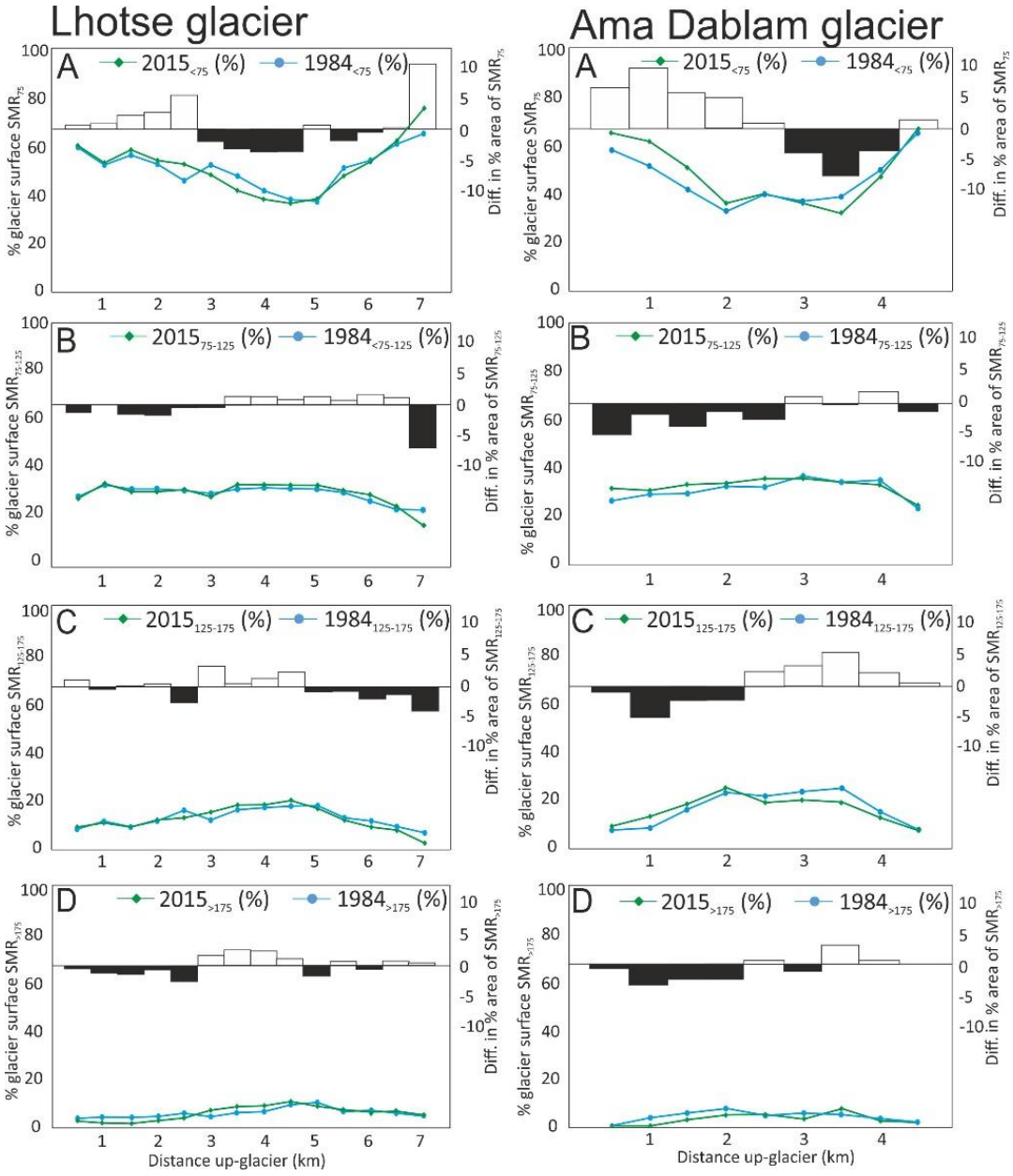

Figure 5.7. The percentage of glacier surface area made up of different classes of topography distinguished by the sum of negative elevation differences in a local (8 pixel) area for Lhotse and Ama Dablam Glaciers. Also shown is the change in the area covered by different topographic classes over the period 1984-2015/16. SMR_{75} (A) represents gently undulating, debris covered glacier surfaces, $SMR_{75\text{-}125}$ (B) represents debris covered areas of sufficient slope to allow debris slumping, $SMR_{125\text{-}175}$ (c) represents ice cliff flanks & SMR_{175} (D) represents ice cliff faces.

The area covered by SMR_{75} increased substantially on Lhotse Shar Glacier, but over a greater area than on Lhotse or Ama Dablam Glaciers. Increases in the area of SMR_{75} extended to 3 km from the calving front of Lhotse Shar Glacier (Figure 5.8), with a 19.6% increase in this class occurring over the study period. The area covered by $SMR_{125\text{-}175}$ and

SMR_{175} decreased within the same 3 km of the glacier terminus (Figure 5.7). Imja Glacier also showed a decreased area of SMR_{175} close to its terminus (within 1.5 km), but less distinctive changes occurred elsewhere on this glacier (Figure 5.8).

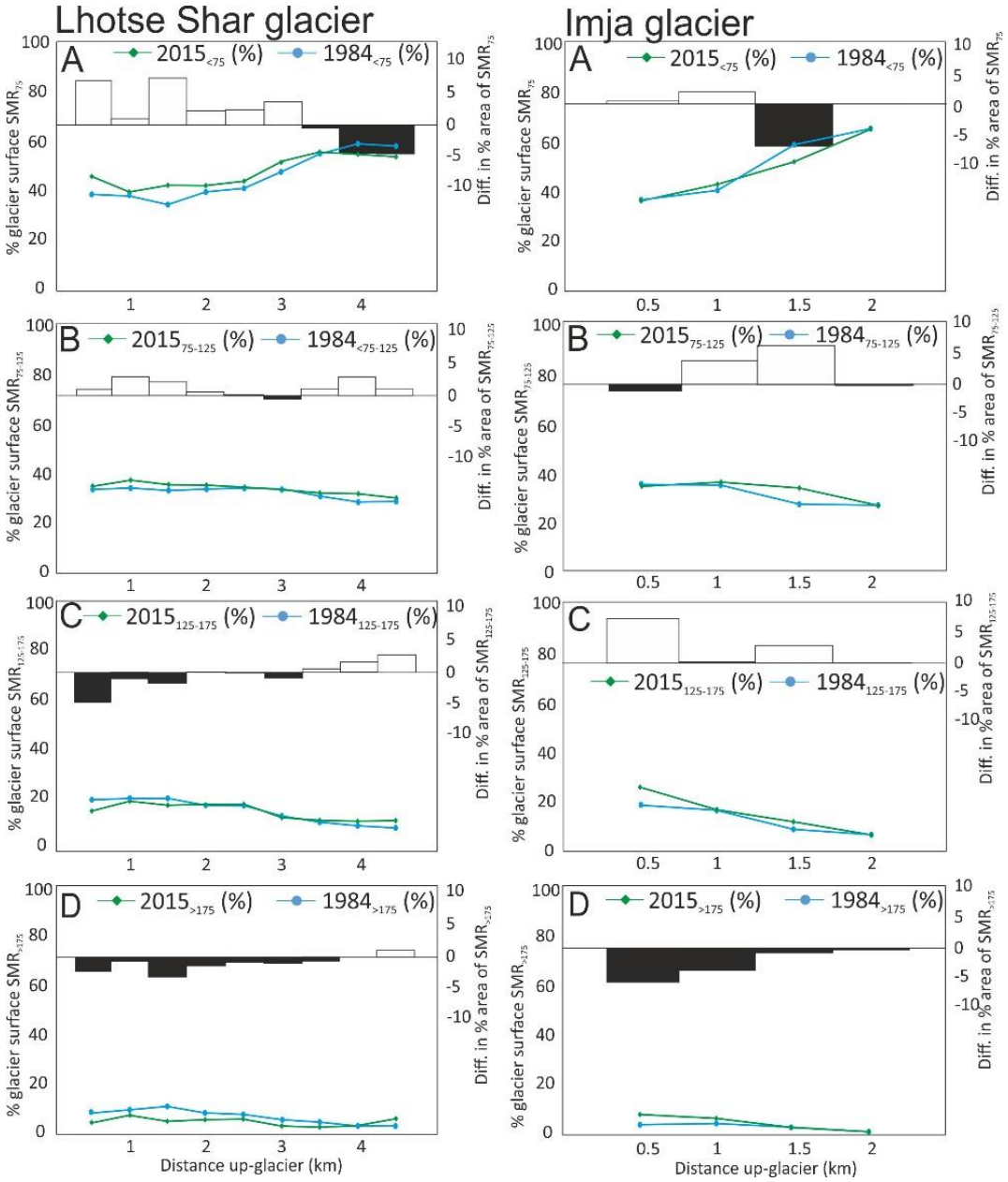

Figure 5.8. The percentage of glacier surface area made up of different classes of topography distinguished by the sum of negative elevation differences in a local (8 pixel) area for Lhotse Shar and Imja glaciers. Also shown is the change in the area covered by different topographic classes over the period 1984-2015/16. SMR_{75} (A) represents gently undulating, debris covered glacier surfaces, $SMR_{75\text{-}125}$ (B) represents debris covered areas of sufficient slope to allow debris slumping, $SMR_{125\text{-}175}$ (c) represents ice cliff flanks & SMR_{175} (D) represents ice cliff faces.

Off-glacier, changes in the spatial extent of different metric classes were not substantial, lending confidence to the changes in spatial extent of metric classes on-glacier (Supplementary Figure 8). We limited our comparison of off-glacier metric areas to slopes of less than 15° to avoid the comparison of erroneous data caused by topographic shading. There was a 1.26% difference in the total area of the SMR_{75} between the AP- & WV-DEMs; a -2.05% difference in the total area of $SMR_{75\text{-}125}$; a 0.50% difference in the total area of $SMR_{125\text{-}175}$, and a 0.29% difference in the total area of SMR_{175}.

5.5.5 Supraglacial pond evolution

Total supraglacial pond area increased on four of the six glaciers we assessed over the study period (Table 3.2). The greatest increases in supraglacial pond area occurred over the lowermost 3-4 km of Khumbu and Lhotse Nup Glaciers, and in the middle reaches of Lhotse Glacier (Figure 5.8). Total ponded area decreased on Ama Dablam and Imja Glaciers, but pond area also decreased within the lowermost 2.5 km of Lhotse and Lhotse Shar Glaciers termini (Figure 5.9). The increases in ponded area on Khumbu and Lhotse Nup Glaciers primarily occurred where glacier surface velocity was low (< ~10 m a^{-1}). There were also increases in the ponded area on parts of these glaciers where surface velocities were > 10 m a^{-1}, and the increases in pond area on Lhotse Glacier also occurred where glacier surface velocity was elevated. Similarly, pond area decreases occurred over areas of Lhotse and Ama Dablam Glaciers that were flowing very slowly (< 10 m a^{-1}), and over parts of Lhotse Shar Glacier that were flowing more actively (~15 m a^{-1}).

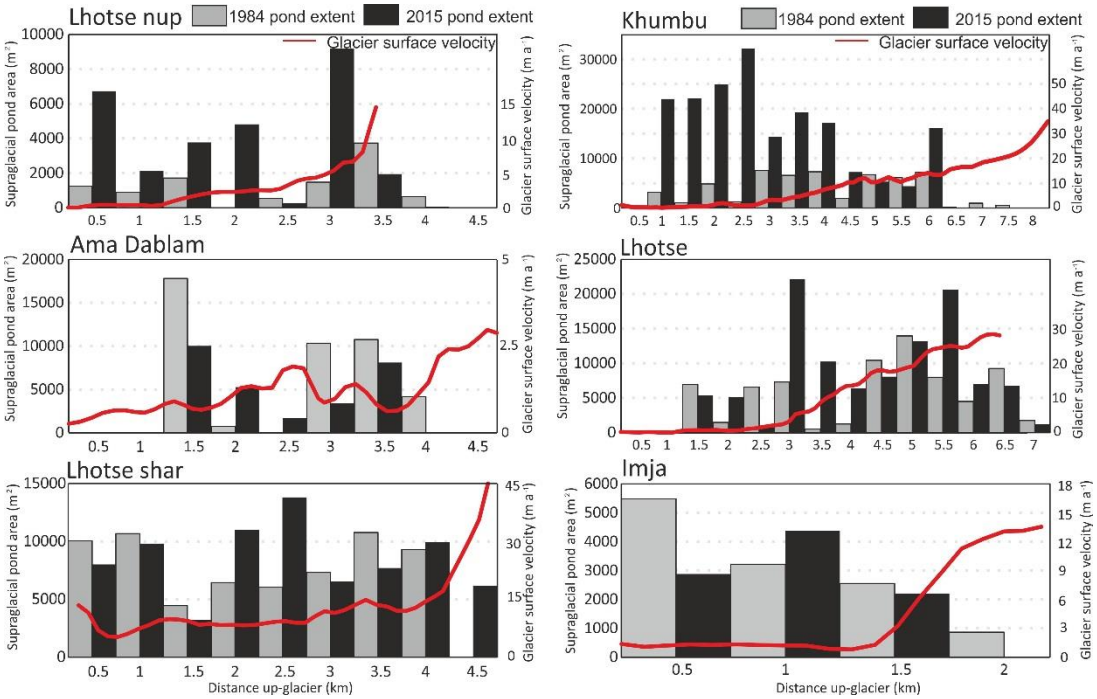

Figure 5.9. Supraglacial pond area mapped using the AP-DEM and data from Watson et al. (2016, in revision), and glacier surface velocity data from Dehecq et al. (2015).

5.5.6 Contemporary evolution of glacier surfaces

The predominance of ice cliff expansion and retreat as the primary source of ice melt in the lower region of Khumbu Glacier (Figure 5.5) is evident in the topographic metric data generated from the WV-DEM (Jan 2015) and 2017 SfM-DEM. Figure 5.10 shows the SMR metrics generated for these two time periods, and the difference in SMR values between the two datasets. Heavily negative values in the difference between the two SMR metric datasets represent areas where local relief diminished between Jan 2015 and May 2017 over the lower part of Khumbu Glacier. These large negative differences are restricted to the former locations of ice cliffs that backwasted over the study period, and to parts of the unstable lateral moraines that slumped or collapsed over the study period. Large positive differences between the two SMR metric datasets indicate areas that developed much more vertical relief over the study period. Such positive differences are again focused where cliff backwasting occurred, or where substantial slumping occurred on lateral moraines, to increase local topographic relief. Isolated, positive differences between the two SMR metric sets are also evident in many areas of the lower Khumbu Glacier (Figure 5.10), which represent newly developed areas of localised relief (primarily new ice cliffs). The area of positive differences (values >100) was greater (58810 m^2 Vs 56434 m^2) than the area of negative differences (values <100) by 4% in this subset of the Khumbu Glacier between Jan

2015 and May 2017, indicating the development of a slightly rougher glacier surface in this subset area overall.

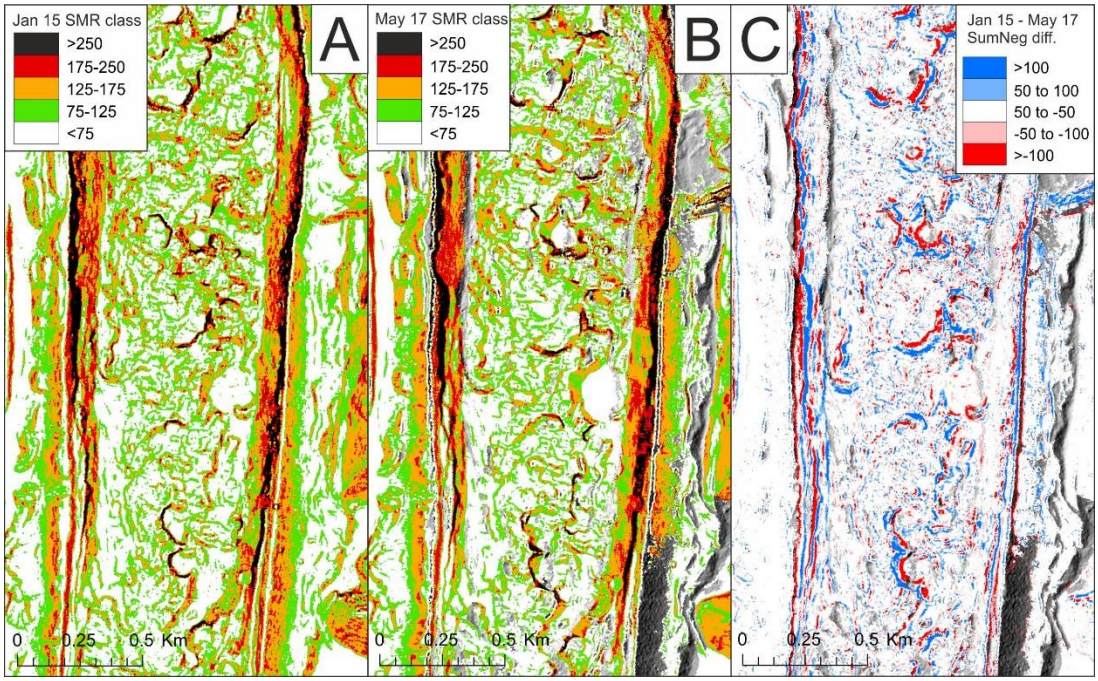

Figure 5.10. SMR metric scores generated using the WV-DEM over the lower reaches of Khumbu Glacier in January 2015 (A) and May 2017 (B). Panel C shows the difference in metric scores between these two time periods.

5.6 Discussion

5.6.1 Processes driving topographic evolution

Our assessment of the evolution of ice surface topography on six debris-covered glaciers in the Everest region of the central Himalaya has shown spatially heterogenous patterns. The inconsistent nature of topographic change suggests either that a single process of spatially variable intensity, or a combination of different processes have been in operation across different parts of each glacier surface during the study period.

Across the majority of the debris covered area of Khumbu and Lhotse Nup Glaciers, and towards the debris-clean ice transition zones of Ama Dablam and Lhotse Glaciers, surface lowering has been accompanied by substantial reductions in low-relief topography, and an associated increase in the area covered by topography of high-relief (Figures 5.6 and 5.7). The results of SfM-MVS DEM differencing over the lower reaches of Khumbu Glacier (Figure 5.5) and multi-temporal surface metric comparisons (Figure 5.10) pinpoint ice cliff and pond network expansion as the main driver of topographic change here. The SMR class

changes between the AP- and WV-DEMs (Figures 5.6-5.8) were similar for Khumbu Glacier, Lhotse Nup Glacier and the higher reaches of Ama Dablam and Lhotse Glaciers, suggesting their surface topography has evolved in a similar manner over the last three decades. There have also been considerable increases in supraglacial ponded area on four of the six glaciers we studied, over the period 1984-2015, and Watson et al. (2016 a, b) documented increased ice cliff density over the same glaciers over a more recent time period (2003-2015). Thus we suggest that the expansion of both their extent and total area has been responsible for the development of a more pitted surface topography on these glaciers.

Supraglacial ponds and associated ice cliffs are prevalent over the lower reaches of debris covered glaciers in the Everest region because those glaciers typically flow very slowly or are completely stagnant (Quincey et al., 2009; Figure 5.9). Thus little crevassing occurs to aid rerouting or drainage of ponded supraglacial meltwater (Quincey et al., 2009). The multi-decadal surface lowering and ice loss that these glaciers have experienced (Figure 5.3; Bolch et al., 2011) has also reduced their longitudinal surface gradient (King et al., 2018) to a point where supraglacial meltwater flow is inhibited, thus meltwater ponds readily form. Quincey et al. (2009) show how many glaciers in the region are already effectively stationary, and King et al. (2018) measured further slowdown of a number of additional land-terminating glaciers in the Everest region in recent years (2000-2015). Watson et al. (2016, 2017a) show how ice cliff and supraglacial pond network development has occurred on many of these glaciers, and we would therefore suggest that the increasingly pitted surface topography we have documented has been replicated across many glaciers in the region, not just those we have studied. Similarly, the backwasting rates of ice cliffs (Figure 5.4) in the subset region of Khumbu glacier (mean of 13.51 m a^{-1}, ranging from 6.43-18.55 m a^{1}) are comparable to those measured on other Himalayan glaciers (see Thompson et al., 2016 and references within). The contribution of ice cliffs and ponds to the overall mass loss budget on the subset of Khumbu glacier (13.2% area covered, 35% ice loss) is also similar to estimates made for other debris covered glaciers (e.g. Immerzeel et al., 2014; Juen et al., 2014; Thompson et al., 2016). We would therefore expect that the topographic characteristics of the stagnant areas of other debris-covered glaciers (outside our study area) hosting expanding pond and cliff networks to have evolved in a similar way to those we have assessed.

A different process may be responsible for topographic change in debris covered areas where surface velocities are too high to allow the development of supraglacial pond networks. Towards the debris-covered clean-ice transition zone on four of the six glaciers we studied, glacier flow was >10 m a^{-1} (Figure 5.9), thus supraglacial ponding was minimal

and the contribution of pond-contact ice cliff backwasting presumably negligible. In this transitional zone, debris thicknesses are typically low (Rounce and McKinney, 2014; Rowan et al., 2015), thus sub-debris melt rates are much higher (Østrem, 1959; Nicholson and Benn, 2006) than in the lower reaches of debris covered glaciers, where debris layers can be several metres thick (Nakawo et al., 1999). In the absence of substantial supraglacial ponding, it may be that enhanced, spatially variable melt under a thin debris mantle has driven the development of a topography of greater relief that we have documented. Indeed, Watson et al. (2017a) documented peak ice cliff densities around the clean-ice-debris covered transition zone of many of the glaciers we studied, and we documented slight increases in the area covered by the topographic class SMR_{175} in these areas, although many smaller cliffs were likely too small to be resolved in the 2 m DEMs used in this study.

On two of the land-terminating glaciers we assessed (Ama Dablam and Lhotse Glaciers), a less pitted surface developed over the study period (Figure 5.7). On both of these glaciers, decreases in supraglacial pond extent occurred over the same part of the glacier (lowermost 2.5 km) as the less pitted surface developed, thus the contribution of ice cliff backwasting and pond expansion to topographic change must have diminished over the study period (Figure 5.7). Slight surface lowering did still occur in the terminal regions of these glaciers (–11.03 and –10.62 m mean within 1 km of glacier termini for Lhotse and Ama Dablam glaciers), thus some degree of debris redistribution must have occurred alongside the sub-debris melt to produce the less pitted topography we have observed. The exhumation of englacial debris (Gulley and Benn, 2007; McCarthy et al., 2017) following sub-debris melt and the loading of supraglacial debris through lateral moraine instability (which can be seen in Figure 5.10 on Khumbu Glacier) could have caused the infilling of hollows on the glacier surface, thus reducing the local relief over the lower parts of Lhotse and Ama Dablam Glaciers (Figure 5.7). Alternatively, the transport of debris away from glacier surfaces, rather than debris redistribution could have produced the less pitted topography on Ama Dablam and Lhotse Glaciers. The lack of distinct terminal moraines on Lhotse Glacier (Figure 5.10) has allowed a linked supraglacial-proglacial hydrological network to develop (Rounce et al., 2017), so the active removal of melted out debris by the glacio-hydrological network may have produced the less pitted surface evident in our glacier surface metrics (Figure 5.7) and shown in Figure 5.11. Without much more detailed, field-based observations from these two glaciers, further assessment of the debris transport processes in operation in their lower reaches can only be speculative.

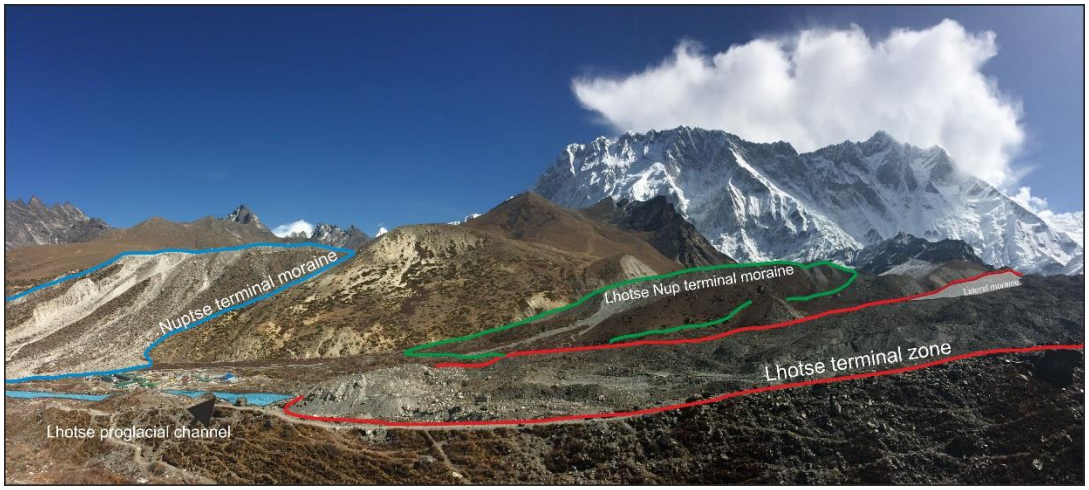

Figure 5.11. The terminal areas of Lhotse (foreground), Lhotse Nup (middle) and Nuptse (farthest) Glaciers. Nuptse Glacier (not included in morphometric analyses) and Lhotse Nup glaciers have prominent terminal moraines and decoupled supraglacial-proglacial hydrological systems. Lhotse glacier is lacking a distinct terminal moraine and therefore has a linked supraglacial-proglacial hydrological system.

We also documented the development of a less pitted surface topography on Lhotse Shar glacier over the study period. This glacier also has a linked supraglacial-proglacial hydrological system (due to its contact with Imja Tsho) and large lateral moraines that have disintegrated as the glacier surface has lowered (Figure 5.3). To assess whether debris deposition alone could have been sufficient to produce the smoother glacier surface topography on Lhotse Shar glacier, we calculated the volume of debris released by moraine slope instability by clipping the AP DEM-WV DEM surface lowering data to the former lateral moraine extent within 3 km of the glacier terminus. The volume of released moraine debris would have been sufficient to cover the entirety of the lowest 3 km of the glacier in 3.11 m of additional debris. Given the active flow of Lhotse Shar Glacier (Thakuri et al., 2016; King et al., 2018), the non-instantaneous nature of the delivery of this debris and the fact that ice cliff and supraglacial pond environments can often have a height of >20 metres (Watson et al., 2017), it seems unlikely that increased debris delivery alone could have altered the characteristics of the surface topography of such a large area of Lhotse Shar Glacier.

The surface velocity regime of Lhotse Shar Glacier has evolved in a contrasting way to nearby, land-terminating glaciers in recent years (King et al., 2018), with the lower reaches of the glacier accelerating in response to proglacial lake development, rather than decelerating, as many land-terminating glaciers in the Himalaya have (Heid and Kääb, 2012; King et al., 2018; Robson et al., 2018). The positive strain associated with

accelerating flow of the last 15 years may have had a hand in altering the overall surface topography of this glacier. The extensional flow associated with surface velocity increases would cause more crevassing (Herzfeld et al., 2004), creating a surface of greater relief on a debris-free glacier. On a debris covered glacier, crevasses are readily infilled by debris (Gulley and Benn, 2007; McCarthy et al., 2017), such as that from unstable lateral moraines, thus a smoother glacier surface of less local relief could develop. Similarly, the crevassing caused by extensional flow would promote the rerouting and drainage of supraglacial water (Quincey et al., 2007), such as that we measured on Imja Glacier and over the lower 1.5 km of Lhotse Shar Glacier (Figure 5.9), and the diminished contribution of supraglacial pond expansion to surface melt and topographic change.

5.6.2 Implications of topographic evolution

Our assessment of fine resolution DEMs of the surface of several debris covered glaciers has shown how a number of different melt and debris transport processes have caused the spatially variable evolution of glacier surface topography over the last three decades in the Everest region of the Central Himalaya. The three most spatially extensive changes that are evident in our data are, 1) the up- and down-glacier expansion of surface topography of high relief in association with ice cliff and supraglacial pond network expansion, 2) the up-glacier expansion of glacier surface topography of high local relief that may be associated with differential melt beneath thin surface debris and, 3) the terminus-proximal reduction of topographic relief over glaciers with a linked supraglacial-proglacial hydrological system.

The degree of spatial variability in local relief of a glacier surface can impact heavily on both the energy balance at the surface, and therefore the energy budget available for ice melt, and also on the supraglacial hydrology. A more pitted glacier surface may be more susceptible to melt because of the modification of the radiative and turbulent heat fluxes (Hock, 2005). Energy that has been reflected from a different part of a glaciers surface is more likely to be re-absorbed by features of greater relief, thus less energy is lost back to the atmosphere when compared to a smooth glacier surface (Cathles et al., 2011; Rippin et al., 2015) and the net radiative fluxes make a greater contribution to the glacier energy balance. Similarly, the turbulent fluxes of sensible and latent flux, which are driven by vertical air exchange close to the glaciers surface (Hock, 2005), may be substantially different over complex topography (King and Anderson, 1994; Martin and Lejeune, 1998) when compared to smoother, clean ice, particularly where local maxima in air flow exist (Denby and Geuell, 2000). Sakai et al. (2009) showed how wind speeds, and therefore near surface turbulence, peak at ice cliff crests, thus the expanding network of ice cliffs documented by Watson et al. (2017a), and generally more pitted topography we have documented may have driven a

greater contribution of the turbulent heat fluxes to the energy balance at the glacier surface, and therefore greater ice melt.

An additional implication of the development of a more pitted glacier surface developing on debris covered glaciers is the impact of a much increased accommodation space for supraglacial meltwater ponding (Benn et al., 2017; Miles et al., 2017). An increased prevalence of hollows, along with decreased slope and glacier surface velocities (King et al., 2018) have clearly preconditioned glacier surfaces in the Everest region for water storage. Watson et al. (2016) showed how supraglacial pond extent increased over the same glaciers in our sample over the period 2000-2015, and Figure 5.9 confirms that such increases in ponded area have been occurring for the past three decades. Irvine-Fynn et al. (2017) showed the importance of the now extensive pond and cliff network on Khumbu Glacier, with >23% of the daily discharge now being stored in the supraglacial pond network, thus the runoff regime is buffered when compared with a clean ice glacier devoid of ponds, cliffs and supraglacial debris. Substantial increases in supraglacial pond area and debris cover have been documented elsewhere in the Everest region, as well as in other regions of the Himalaya (Thakuri et al., 2016; Watson et al., 2016; Miles et al., 2017), thus they may play an important role in modulating freshwater runoff and quality in the Himalaya (Irvine-Fynn et al., 2017). Miles et al. (2016) also emphasise the significance of extensive supraglacial pond networks because of their ability to transmit incident solar radiation to the interior of their host glacier. The energy absorbed by supraglacial ponds is capable of causing englacial melt both in-situ and further down the linked portions of the supraglacial-englacial network (Miles et al., 2017; Benn et al., 2017). As glacier surfaces have become more pitted over the last three decades and therefore primed for more water storage, and because glacier velocities have generally reduced in the area (King et al., 2018), we might expect more spatially extensive water ponding to occur in coming decades.

5.7 Conclusions

In this study we have used a variety of fine resolution DEMs to examine the long-term and contemporary evolution of the debris covered surfaces of six glaciers in the Everest region of the central Himalaya. We developed a metric of glacier surface relief to examine how sustained ice loss has impacted on the characteristics of glacier ablation zones, and used a time series of contemporary SfM-MVS derived DEMs to identify the melt processes responsible for driving topographic change. The predominant change in glacier surface topography has been the development of a more pitted surface of greater, local relief, in response to an increase in the extent and density of supraglacial pond and ice cliff networks. Pond and ice cliff networks expanded in both up- and down-glacier directions on different

glaciers. We also documented the development of a less pitted, terminus environment where debris covered glaciers have a linked supraglacial-proglacial hydrological network. Debris removal by the hydrological network, or debris redistribution following englacial melt out may be responsible for the development of a less pitted topography here. Substantial reductions in both supraglacial ponded area and the extent of pitted topography on the lake-terminating Lhotse Shar glacier occurred. We have attributed these changes to an extensional ice flow regime caused by glacier-lake interactions leading to debris redistribution and meltwater drainage through crevasses. Continued expansion of debris cover, reduction of surface gradients in response to glacier surface lowering, and velocity reductions will all serve to precondition glacier surfaces for more ice cliff and supraglacial pond development. Thus the areal coverage of pitted topography associated with pond expansion can reasonably be expected to expand on debris covered glaciers.

Overall, the changes in surface topography quantified in this study have important implications for both the hydrology and surfrace energy balance of those glaciers. Development of a glacier surface that is of greater relief is likely to lead to an increased contribution of the net radiative and turbulent heat fluxes to the overall energy balance at that glaciers surface. Development of a more pitted glacier surface will also increase accommodation space available for meltwater ponding, likely creating a positive feedback between ponding, ice cliff backwasting, and topographic change. Continued expansion of the pond and cliff networks on debris covered glaciers may enhance the buffering of meltwater discharge that has been observed in the region, and indeed elsewhere in the Himalaya.

Acknowledgements

OK is a recipient of a NERC SPHERES DTP PhD studentship (grant award NE/L002574/1). The Natural Environment Research Council Geophysical Equipment Facility (NERC GEF) is thanked for loaning Global Navigation Satellite Systems receivers and technical assistance under loan numbers 1050, 1058 and 1065. Dhananjay Regmi and Himalayan Research Expeditions are thanked for their support in fieldwork logistics.

References

Anderson, L.S. & Anderson, R. 2016. Modeling debris-covered glaciers: response to steady debris deposition. The Cryosphere, 10, 1105-1124, doi:10.5194/tc-10-1105-2016.

Benn, D.I. & Lehmkuhl, F. 2000. Mass balance and equilibrium-line altitudes of glaciers in high-mountain environments. Quaternary International, 65-66, 15-29, doi.org/10.1016/S1040-6182(99)00034-8.

Bhutiyana, M.R. Kale, V.S. & Pawar, N.J. 2010. Climate change and the precipitation variations in the northwestern Himalaya: 1866-2006. International Journal of Climatology, 30, 535-548.

Bolch, T., Pieczonka, T. & Benn, D. I. 2011. Multi-decadal mass loss of glaciers in the Everest area (Nepal Himalaya) derived from stereo imagery. The Cryosphere, 5, 349-358.

Bollasina, M. A., Ming, Y. & Ramaswamy, V. 2011. Anthropogenic Aerosols and the Weakening of the South Asian Summer Monsoon. Science, 334, 502-505.

Brasington, J., Vericat, D. & Rychkov, I. 2012. Modeling river bed morphology, roughness, and surface sedimentology using high resolution terrestrial laser scanning, Water Resource Research, 48, W11519, doi:10.1029/2012WR012223.

Brock, B.W., Willias, I. C. & Sharp, M.J. 2006. Measurement and parameterization of aerodynamic roughness length variations at Haut Glacier d'Arolla, Switzerland. Journal of Glaciology, 52, 177, 281-297.

Carrivick, J.L., & Tweed, F.S. 2016. A global assessment of the societal impacts of glacier outburst floods. Global and Planetary Change (144), 1-16, doi:10.1016/j.gloplacha.2016.07.001.

Cathles LM, Abbot DS, Bassis JN, MacAyeal DR. 2011. Modeling surface-roughness/solar ablation feedback: application to small-scale surface channels and crevasses of the Greenland ice sheet. Annals of Glaciology 52(59): 99–108.

Dehecq, A., Gourmelen, N. & Trouve, E. 2015. Deriving large-scale glacier velocities from a complete satellite archive: Application to the Pamir-Karakoram-Himalaya. Remote Sensing of Environment (162), 55-66, doi: 10.1016/j.rse.2015.01.031.

Denby, B. and Greuell, W. 2000. The use of bulk and profile methods for determining surface heat fluxes in the presence of glacier winds. Journal of Glaciology, 46, 445-452.

Frey, H., Machguth, H., Huss, M., Huggel, C., Bajracharya, S., Bolch, T., Kulkarni, A., Linsbauer, A., Salzmann, N. & Stoffel, M. 2014. Estimating the volume of glaciers in the Himalayan-Karakoram region using different methods. The Cryosphere, 8, 2313-2333.

Gulley, J., & Benn, D. 2007. Structural control of englacial drainage systems in Himalayan debris-covered glaciers. *Journal of Glaciology, 53*(182), 399-412. doi:10.3189/002214307783258378.

Herried, S., Pellicciotti, F., Ayala, A., Chesnokova, A., Kienholz, C., Shea, J. & Shrestha, A. 2015. Satellite observations show no net change in the percentage of supraglacial debris-covered area in northern Pakistan from 1977 to 2014. Journal of glaciology, 61, 227, 524-536, doi:10.3189/2015JoG14J227.

Herzfeld, U.C., Clarke, G.K.C., Mayer, H. & Greve, R. 2004. Derivation of deformation characteristics in fast-moving glaciers. Computers and Geosciences, 30, 3, 291-302, doi.org/10/1016/j.cageo.2003.10.012.

Hock, R. 2005. Glacier melt: a review on processes and their modelling. Progress in Physical Geography. 29 (3), 362–391.

Irvine-Fynn, T. D. L., Porter, P. R., Rowan, A. V., Quincey, D. J., Gibson, M. J., Bridge, J. W., Glasser, N. F. 2017. Supraglacial ponds regulate runoff from Himalayan debris-covered glaciers. Geophysical Research Letters, 44, 11,894–11,904. https://doi.org/10.1002/2017GL075398.

Kääb, A., Berthier, E., Nuth, C., Gardelle, J. & Arnaud, Y. 2012. Contrasting patterns of early twenty-first-century glacier mass change in the Himalayas. Nature, 488, 495-498.

King, J. C. & Anderson, P. S. 1994. Heat and water vapour fluxes and scalar roughness lengths over an Antarctic ice shelf. Boundary-Layer Meteorology 69, 101-121.

Martin, E. and Lejeune, Y. 1998: Turbulent fluxes above the snow surface. Annals of Glaciology 26, 179-183.

Noh, M. J. & Howat, I. M. 2015. Automated stereo-photogrammetric DEM generation at high latitudes: Surface Extraction with TIN-based Search-space Minimization (SETSM) validation and demonstration over glaciated regions. Remote Sensing (52), 198–217.

Nicholson, L. & Benn, D.I. 2006. Calculating ice melt beneath a debris layer using meteorological data. Journal of Glaciology, 52, 178, 463-470.

Nie, Y., Sheng, Y., Liu, Q., Liu, L., Liu, S., Zhang, Y. & Song, C. 2017. A regional-scale assessment of Himalayan glacial lake changes using satellite observations from 1990-2015. Remote sensing of Environment (189), 1-13, doi:10.1016/j.rse.2016.11.008.

Nuth, C. & Kääb, A. 2011. Co-registration and bias corrections of satellite elevation data sets for quantifying glacier thickness change. The Cryosphere, 5, 271-290.

Miles, E.S., Willis, I, C., Arnold, N.S., Steiner, J. & Pellicciotti, F. 2016. Spatial, seasonal and interannual variability of supraglacial ponds in the Langtang Valley, 1999-2013. Journal of Glaciology, 63 (237), 88-105, doi:10.1017/jog.2016.120.

Østrem, G. 1959. Ice Melting under a Thin Layer of Moraine, and the Existence of Ice Cores in Moraine Ridges. Geografiska Annaler, 41, 228–230.

Pellicciotti, F., Stephan, C., Miles, E., Herreid, S., Immerzeel, W. W. & Bolch, T. 2015. Mass-balance changes of the debris-covered glaciers in the Langtang Himal, Nepal, from 1974 to 1999. Journal of Glaciology, 61, 373-386.

Quincey, D., Richardson, S., Luckman, A., Lucas, R., Reynolds, J., Hambrey, M., and Glasser, N. 2007. Early recognition of glacial lake hazards in the Himalaya using remote sensing datasets, Global Planet. Change, 56, 137–152, doi:10.1016/j.gloplacha.2006.07.013.

Quincey, D., Smith, M., Rounce, D., Ross, A., King, O., and Watson, C. 2017. Evaluating morphological estimates of the aerodynamic roughness of debris covered glacier ice. Earth Surface Process and Landforms, 42, 2541–2553. doi: 10.1002/esp.4198.

Rippin, D. M., Pomfret, A. & King, N. 2015. High resolution mapping of supra-glacial drainage pathways reveals link between micro-channel drainage density, surface roughness and surface reflectance. Earth Surface Process and Landforms, 40, 1279–1290. doi: 10.1002/esp.3719.

Robson, B.A., Nuth, C., Nirlsen, P.R., Girod, L., Hendrickx, M. & Dahl, S.O. 2018. Spatial variability in patterns of glacier change across the Manasalu range, Central Himalaya. Frontiers in Earth Science, 6:12, doi: 10.3389/feart.2018.00012.

Rounce, D. R. and McKinney, D. C. 2014. Debris thickness of glaciers in the Everest area (Nepal Himalaya) derived from satellite imagery using a nonlinear energy balance model, The Cryosphere, 8, 1317-1329, https://doi.org/10.5194/tc-8-1317-2014.

Rounce, D. R., Byers, A. C., Byers, E. A., and McKinney, D. C. 2017. Brief communication: Observations of a glacier outburst flood from Lhotse Glacier, Everest area, Nepal, The Cryosphere, 11, 443-449, https://doi.org/10.5194/tc-11-443-2017.

Rowan, A. V., Egholm, D. L., Quincey, D. J. & Glasser, N. F. 2015. Modelling the feedbacks between mass balance, ice flow and debris transport to predict the response to

climate change of debris-covered glaciers in the Himalaya. Earth and Planetary Science Letters, 430, 427-438.

Sakai A, Nishimura K, Kadota T,. & Takeuchi N. 2009. Onset of calving at supraglacial lakes on debris covered glaciers of the Nepal Himalayas. Journal of Glaciology, 55(193), 909-917, doi:10.3189/002214309790152555.

Smith, M.W., Carrivick, J.L. & Quincey, D.J. 2016. Structure from motion photogrammetry in physical geography. Progress in Physical Geography: Earth and Environment, 40 (2), 247-275, doi.org/10.1177/0309133315615805.

Shrestha, A. B., Wake, C. P., Mayewski, P. A. & Dibb, J. E. 1999. Maximum temperature trends in the Himalaya and its vicinity: An analysis based on temperature records from Nepal for the period 1971-94. Journal of Climate, 12, 2775-2786.

Somos-Valenzuela, M. A., Mckinney, D. C., Rounce, D. R. & Byers, A. C. 2014. Changes in Imja Tsho in the Mount Everest region of Nepal. The Cryosphere (8), 1661-1671.

Thakuri, S., Salerno, F., Smiraglia, C., Bolch, T., D'Agata, C., Viviano, G. & Tartari, G. 2014. Tracing glacier changes since the 1960s on the south slope of Mt. Everest (central Southern Himalaya) using optical satellite imagery. The Cryosphere, 8, 1297-1315.

Thakuri, A., Salerno, F., Bolch, T., Guyennon, N. & Tartari, G. 2016. Factors controlling the accelerated expansion of Imja Lake, Mount Everest region, Nepal. Annals of Glaciology, 57(71), doi: 10.3189/2016AoG71A063.

Thompson, S., Benn, D.I., Mertes, J. & Luckman, A. 2016. Stagnation and mass loss on a Himalayan debris-covered glacier: processes, patterns and rates, Journal of Glaciology, 62, 233, 467-485, doi:10.1017/jog.2016.37.

Washburn, B. 1989. Mapping Mount Everest. Bulletin of the American Academy of Arts and Sciences, 42(7), 29-44. doi:10.2307/3824352.

Watson, C.S. Quincey, D.J, Carrivick, J.L. & Smith, M.W. 2016. The dynamics of supraglacial ponds in the Everest region, central Himalaya. Global and Planetary Change, 142, 14-27.

Watson, C.S., Quincey, D.J., Carrivick, J.L. & Smith, M.W. 2017a. Ice cliff dynamics in the Everest region of the central Himalaya, Geomorphology, 278, 238-251, doi.org/10/106/j.geomorph.2016.11.017.

Watson, C.S., Quincey, D.J., Smith, M.W., Carrivick, J.L., Rowan, A.V. & James, M.R. 2017b. Quantifying ice cliff evolution with multi-temporal point clouds on the debris-covered Khumbu Glacier, Nepal, Journal of Glaciology, doi:10.1017/jog.2017.47.

Watson, Cameron Scott. 2017c. *The evolution of supraglacial ponds and ice cliffs on Himalayan debris-covered glaciers.* PhD thesis, University of Leeds.

Watson, C. S., Quincey, D. J., Carrivick, J. L., Smith, M. W., Rowan, A. V., and Richardson, R. 2018. Heterogeneous water storage and thermal regime of supraglacial ponds on debris-covered glaciers. Earth Surface Process and Landforms, 43: 229–241. doi: 10.1002/esp.4236.

Watson, C.S., King, O., Miles, E.S. & Quincey, D.J. Optimising NDWI supraglacial pond classification on Himalayan debris-covered glaciers. *In review in Remote Sensing of Environment.*

6. Discussion

6.1 Factors influencing contemporary ice loss

This thesis has presented an analysis of a number of factors that may impact on the future evolution of debris covered glaciers in the Himalaya. The impact of sustained ice loss on glacier geometry (chapters 3 & 5), glacier velocity (chapter 4), glacier surface morphometry and supraglacial hydrology (chapter 5) has been assessed, and these observations have been used to predict the likely evolution of both lake- and land-terminating glaciers in the central Himalaya. The possibility of decadal scale glacier response to glacial lake development has become apparent, although it is also evident that glaciers can host lakes over much longer timescales without experiencing dynamic ice loss (chapter 4). The datasets generated and analysed in this work represent the first extensive comparisons of lake vs land-terminating glacier change in the Himalaya, thus they inform on a previously poorly quantified interaction. The examination of glacier surface topography at each end of a period of sustained ice loss also shows marked changed in the relief of debris covered glacier surfaces. The following sections discuss the key findings presented in chapters 3, 4 and 5, along with their potential impact on future glacier evolution.

The work presented in chapter 3 compared ice loss rates from glaciers depending on their terminus type, ice loss rates on either side of the main Himalayan orographic divide, and the distribution of glacierised area through the elevation range of different catchments in the Everest region. Very few other studies have made explicit comparisons between mass loss rates of different terminus type in the Himalaya. Maurer et al. (2016) estimated that 5 debris-covered, land-terminating glaciers in Bhutan had a mass balance of –0.19 ± 0.11 m w.e.a^{-1} between 1974-2006, whereas 6 neighbouring lake-terminating glaciers had a mass balance of –0.28 ± 0.11 m w.e.a^{-1} over the same period; a 38% difference in mass loss. Bolch et al. (2011) estimated that the Lhotse Shar/ Imja glacier complex had a mass balance of –0.50 ± 0.09 m w.e.a^{-1} over the period 1970-2007, with the 9 land-terminating glaciers in their sample displaying a mass balance of –0.26 ± 0.08 m w.e.a^{-1}; a 63% difference in mass loss rates. The results of these two studies show that divergent ice loss from lake Vs land-terminating glaciers has occurred for several decades in the central Himalaya. The 32% difference in more contemporary (2000-2015) mass loss rates from lake Vs land-terminating glaciers as presented in chapter 3 shows that this trend has continued to the present day, at least in the central Himalaya.

Aside from these two studies and the work presented in chapter 3, little other work is available to assess whether the divergent mass balance estimates for glaciers of different

terminus type is a phenomenon that is prevalent across the Himalaya. A larger number of studies have examined glacial lake expansion rates, which may indicate where associated, enhanced lake-terminating glacier mass loss is most likely. Nie et al. (2017) showed a wide range of lake expansion rates (5-23%) for different sub-regions of the Himalaya over the period 1990-2015. The Everest region is located in the sub region of Nie et al. (2017) which showed the most substantial lake expansion (23% from 1990-2015), so the strongest link may exist between glacial lake growth and glacier behaviour here than elsewhere across the range. Veettill et al. (2016) assessed glacial lake expansion over the same area of Bhutan as the mass loss study by Maurer et al. (2016), and showed similarly elevated lake expansion (19% from 1990-2010) in the Bhutan region. Elsewhere in High Mountain Asia, high levels of lake expansion have been documented in the Tien Shan (16.7 ± 2.9% from 1990-2010; Wang et al., 2013), the West Kunlun (27.8% from 1990-2010; Wang et al., 2016), the Altun Shan (55.2% from 1990-2010; Wang et al., 2016) and parts of the Hengduan Shan (up to 18% from 1990-2014; Wang et al., 2017). Brun et al. (2017) measured amplified (regionally averaged) mass loss in many of these areas over the period 2000-2016, thus glacial lake expansion could well have been a large contributing factor in glacier evolution in those regions. Conversely, glacial lake expansion has been less substantial in the Pamir (10.3% from 1990-2013; Wang et al., 2016), and the Karakoram (5% from 1990-2015; Nie et al., 2017), as has glacier mass loss (Bolch et al., 2017; Brun et al., 2017). Direct comparisons of glacier mass loss depending on terminus type are still required in some regions to confirm the link between lake expansion and glacier mass loss outside of the central Himalaya.

A number of other mass balance studies have been undertaken in the Everest region that have covered different study periods to that of chapter 3 (Table 6.1). This allows an assessment of whether mass loss rates might have accelerated or decelerated in recent decades. To the north of the orographic divide, the mass balance of 9 glaciers over the period 2000-2015 was –0.59 ± 0.26 m w.e.a^{-1} (chapter 3). This figure agrees well with that of Neckel et al. (2014), who estimated mass loss of –0.66 ± 0.32 m w.e.a^{-1} over a broad area (north of the divide) stretching from the Langtang to Kangchenjunga over the period 2003-2009. Both of these estimates are above those of Ye et al. (2015) who calculated ice loss of –0.40 ± 0.27 m w.e.a^{-1} from 1974-2006 for glaciers of the Rongbuk catchment. Whilst the ice loss estimates of chapter 3 and Neckel et al. (2014) are not elevated outside the uncertainty bounds of Ye et al. (2015), the greater mean mass loss rates from a large population of glaciers suggests an acceleration in glacier thinning to the north of the orographic divide in recent decades. To the South of the orographic divide, the mass balance of 18 glaciers was –0.54 ± 0.20 m w.e.a^{-1} over the period 2000-2015 (chapter 3). This figure is slightly above that of Nuimura et al. (2011), who estimated mass loss of –0.45 ± 0.25

w.e.a^{-1} for 42 glaciers in the Dudh Koshi catchment over the period 1992-2008, and it is markedly higher than the estimate of Bolch et al. (2015); –0.32 ± 0.08 w.e.a^{-1} from 9 glaciers over the period 1970-2007. Again, these data suggest accelerated ice loss from glaciers to the south of the orographic divide in the Everest region over the last few decades.

Table 6.1. Geodetic mass balance estimates from different studies focused on the Everest region.

		Mass balance estimate (m w.e.a^{-1})			
Study	**Study period**	North of orographic divide	South of orographic divide	Entire Everest region	**Data used**
Chapter 3	2000-2015	–0.59 ± 0.26			SRTM-WV
Li et al (2018)	2000-2012	–0.35 ± 0.04			SRTM-TerraSAR
Neckel et al (2014)	2003-2009	–0.66 ± 0.32			Icesat
Ye et al. (2015)	1974-2006	–0.40 ± 0.27			Hexagon-ALOS PRISM
Chapter 3	2000-2015		–0.54 ± 0.20		SRTM-WV
Li et al (2018)	2000-2012		–0.41 ± 0.05		SRTM-TerraSAR
Nuimura et al (2011)	1992-2008		–0.45 ± 0.25		Map-ASTER
Bolch et al (2011)	1970-2007		–0.32 ± 0.08		Corona-ASTER
Bolch et al (2008)	1962-2002		–0.28 ± 0.20		Corona-ASTER
Chapter 3	2000-2015			–0.52 ± 0.22	SRTM-WV
Li et al (2018)	2000-2012			–0.38 ± 0.04	SRTM-TerraSAR
Kääb et al (2012)	2003-2008			–0.39 ± 0.11	Icesat
Gardelle et al (2013)	1999-2011			–0.26 ± 0.13	SRTM-SPOT

Zhou et al. (2018) provide a similar comparison of pre- and post-millennium mass loss rates from a wide variety of geodetic mass balance studies across High Mountain Asia. Zhou et al. (2018) (and references within) show evidence for accelerating mass loss rates over the past few decades (since the 1970s) in the Spiti Lahaul, the Langtang and eastern Nyainqêntanglha regions, alongside the Everest region. Mass balance seems to have been sustained for glaciers of the Karakoram since at least the 1970s (Bolch et al., 2017; Zhou et al., 2018), and mass loss rates seem to have been steady in the Hindu Raj, the Kunlun and the Pamir (Zhou et al., 2018) both pre- and post-millennium. Comparisons of mass loss rates for broad regions of the Tibetan Plateau are difficult because of the large degree of spatial heterogeneity of mass loss (Neckel et al., 2014; Brun et al., 2017).

The occurrence of much higher surface lowering rates (Figure 3.5), and the surface lowering through a much broader altitudinal range (Figure 3.5), of glaciers flowing north (into the Pumqu catchment) when compared to glaciers flowing south (into the Tama Koshi and Dudh Koshi catchments) is an interesting observation (chapter 3). Glaciers in the Pumqu catchment lowered at a maximum rate of –1.62 ± 0.14 m a^{-1} between 5300 and 5400 m a.s.l. In the Tama Koshi catchment, maximum surface lowering (–1.08 ± 0.12 m a^{-1}) occurred around 5400 m a.s.l., and in the Dudh Koshi catchment, maximum surface lowering (–1.06 ± 0.10 m a^{-1}) also occurred at 5400 m a.s.l. Surface lowering rates in the Pumqu catchment were higher than the maximum rates measured in the Tama Koshi and Dudh Koshi catchments to an altitude of 5700 m a.s.l (Figure 3.5). This difference may be expected given the apparently large difference in the total annual precipitation that falls, and presumably accumulation input for glaciers, either side of the divide. Approximately 449 mm a^{-1} of rainfall has been measured at the Pyramid research station (5000 m a.s.l.) alongside Khumbu glacier (Salerno et al., 2015) on the south side of the orographic divide, whereas Dingri (4300 m a.s.l.) receives just 263 ± 84.3 mm a^{-1} on the northern side of the divide. The bottom heavy hypsometry (Supplementary Table 3) of glaciers in the Pumqu catchment, and therefore the situation of a large proportion of glacier area at an altitude of high surface melt, may also have contributed to such widespread surface lowering.

However, despite this gradient in precipitation, the mass balance of glaciers flowing in opposing directions either side of the orographic divide were not markedly different (–0.54 ± 0.20 m w.e.a^{-1} for glaciers in the Tama Koshi and Dudh Koshi catchments, versus –0.61 ± 0.24 m w.e.a^{-1} for glaciers in the Pumqu catchment). The slight but long-term (1959-2007) increase in total annual precipitation measured at Dingri by Yang et al. (2011), and the decadal scale increases in accumulation measured by Kaspari et al. (2008) in the East Rongbuk Col may have occurred elsewhere in the Everest region. Such accumulation increases could have offset the ice mass loss measured over the broad elevation ranges shown in chapter 3, thus the mass balance estimates for glaciers in catchments either side of the orographic divide are not markedly different.

6.2 Factors influencing future ice loss

To examine the influence of glacier hypsometry on ice loss from the Everest region, contemporary and potential future glacier AARs were calculated, and the hypsometric index of Jiskoot et al. (2009) employed (chapter 3). The Pumqu and Dudh Koshi catchments contain numerous long, heavily debris covered glaciers that drain from some of the tallest mountains on the planet (Everest, Makalu, Cho Oyu, all >8000 m a.s.l.), and were accordingly classified as very bottom heavy (HI >1.5) according to the scheme of Jiskoot et

al. (2009). The presence of debris cover across many other glacierised catchments in the central Himalaya would suggest a similar hypsometric character might apply for other glaciers in the area. However, glaciers in the Tama Koshi catchment were classified as equidimensional (HI -1.2 to 1.2) under the scheme of Jiskoot et al. (2009), and a greater portion of glacier area is currently stored above the ELA in this catchment. This may be responsible for the Tama Koshi displaying the least negative contemporary mass balance estimate ($–0.54 \pm 0.20$ m w.e.a^{-1}) of the three catchments. The five clean ice glaciers also displayed an equidimensional HI score, perhaps as a result of the absence of debris, which can lead to the persistence of glacier tongues out of balance with contemporary climate (Rowan et al., 2015).

The adjustment of glacier AARs, and therefore long-term glacier mass balance (Dyugerov et al., 2009; König et al., 2014) response to continued warming and ELA rise will be spatially variable as a result of the differing hypsometry within and between different catchments. The glaciers in the Tama Koshi catchment and the five clean ice glaciers currently have the highest AARs (mean of 0.43 and 0.47, respectively) of all the glaciers assessed in chapter 3. Using previously published lapse rates (Immerzeel et al., 2014; Kattel et al., 2015) to simulate ELA rise in response to RCP 4.5 scenario warming (+0.9 to +2.3 °C by 2100), chapter 3 shows how AARs may respond to 165-425 m of ELA rise. Because of the concentration of glacierised area close to the current ELA of glaciers in the Tama Koshi catchment, a large area (24-61% increase) of these glaciers will fall below the ELA under the RCP 4.5 warming scenario. AAR adjustments and associated increases in glacier area below the ELA will be less substantial in the Dudh Koshi (23-40%) or Pumqu catchments (12-30%), primarily because of the extreme maximum altitudes these glaciers reach (<7500 m a.s.l.in a number of cases- Supplementary Table S1). More pessimistic warming scenarios (RCP 6.0 and RCP 8.5) may lead to ELAs rising above the maximum elevation of some glaciers in the Tama Koshi catchment. Should temperature increases (e.g. Shrestha et al., 1999; Salerno et al., 2015) continue, it is likely that mass loss from the Tama Koshi will increase in the near future, and indeed from other catchments hosting equidimensional or top-heavy glaciers in the central Himalaya.

In summary, the work of chapter 3 provides evidence for substantial inter and intra catchment variability in glacier mass loss depending on glacier terminus type, glacier situation in relation to the orographic divide, and glacier hypsometry. The identification of lake-terminating glaciers as ‘hot-spots’ of glacier mass loss has implications across the Himalaya due to the presence of more than 5000 glacial lakes across the range (Nie et al., 2017). Although simplistic, the prediction of future AARs in response to temperature warming emphasises the potential of glacier hypsometry to both inhibit and exacerbate

glacier mass loss given further temperature increases. Disentangling the impact of precipitation trends, temperature increases on mass loss rates across the orographic divide requires more detailed assessment.

6.3 Lake versus land-terminating glacier evolution

The evolution of the geometry and dynamics of glaciers of contrasting terminus type was assessed in chapter 4. In this study, a time series of DEMs, glacier velocity fields and Landsat imagery were analysed to quantify changes in glacier flow, glacier surface slope and lake-terminating glacier retreat rates, and the observations were combined to suggest a set of processes that may be in operation to drive the enhanced mass loss from lake-terminating glaciers shown in chapter 3.

The contrasting locations of maximum surface lowering on lake and land-terminating glaciers (Figures 3.5 and 3.6) caused divergent changes in glacier geometry in the last 15 years. Land-terminating glaciers displayed a consistent trend in gradient change, with their lower reaches (0-6 km from respective termini) becoming markedly shallower in response to surface lowering. Across the debris-clean ice transition zone, slight increases in surface slope were documented, presumably because of the enhanced ablation caused by thin (<1-3 cm) debris when compared to the clean ice immediately up-glacier. The evolving geometry of lake-terminating glaciers can be divided into two groups. Five of the nine glaciers assessed in chapter 4 developed a steeper longitudinal surface gradient, whereas the remaining four glaciers showed no distinct trend in surface gradient change, or a trend more akin to land-terminating glaciers (in the case of Trakarding and Drogpa Nagtsang glaciers-Figure 4.5). Changes in glacier velocity were examined alongside glacier geometry changes, and similar changes in glacier flow were identified. Without exception, land-terminating glaciers assessed showed areas of decreased flow. Glacier surface velocities reduced by up to 15 m a^{-1} over the study period (1999-2003 to 2013-2015) on some glaciers, and the areas of maximum slowdown coincided with areas of most substantial thinning and surface slope reductions (Figures 4.2 and 4.3). Lake-terminating glaciers could again be split into two categories. The five glaciers that developed a steeper surface gradient displayed terminus proximal ice velocity increases of 10 m a^{-1} or more. The four glaciers which showed no distinct trend in surface gradient change, or gradient change more akin to land-terminating glaciers, either decelerated either over the majority of their ablation zones, or decelerated several kilometres from their terminus. Observations of glacier geometry and velocity change were combined with measurements of lake-terminating glacier ice front retreat rates, strain rate measurements and the findings of previous work on glacial lakes of the Everest

region to examine the processes that might be driving terminus type dependant glacier change in the region.

A number of similarities in the behaviour of the five lake-terminating glaciers shown in Figure 4.4 and dynamically retreating marine or lake-terminating glaciers in other glacierised regions were evident, thus a similar set of processes were attributed to be driving glacier retreat in these five cases. Benn et al. (2007) incorporated such processes into models of water terminating glacier behaviour, and showed that dynamic retreat can occur where terminus proximal thinning, for example through increased surface melt, can set up a positive feedback where reduced effective pressure triggers flow acceleration, increased longitudinal strain and calving retreat. The same processes are obviously not attributable to all lake-terminating glaciers in light of the contrasting behaviour of four lake-terminating glaciers in the Everest region (Figure 4.5). In three of these four cases (Trakarding Hunku and Longmojian glaciers- Figure 4.5), it is implied that the longevity of ice thinning that has occurred through lake expansion has served to reduce glacier driving stresses, and that the narrowing of glacier termini during the late stages of retreat or maybe even disconnection from the glacial lake they host, has increased resistive stresses and therefore caused glacier flow deceleration. On Drogpa Nagtang glacier, which has developed a large proglacial lake only recently (since the early 1990s), it is likely that lake has not yet reached a sufficient depth to impact upon ice dynamics in the way proposed by Benn et al. (2007), thus its evolution, and indeed the observations made in chapter 4, are more like those of a land-terminating glacier.

The magnitude of the changes in lake-terminating glacier dynamics documented in chapter 4 are relatively small compared to other, larger lake-terminating glaciers found in other glacierised regions around the world. Terminus proximal ice flow rates peak at ~40 m a^{-1} on land-terminating glaciers in the Everest region, and flow acceleration was generally between 10-15 m a^{-1} over the period 1999-2015. Terminus proximal glacier velocities may be several hundred metres per year on Alaskan lake-terminating glaciers (Trussel et al. 2013; Burgess et al., 2013), or several thousand metres per year on Patagonia lake-terminating glaciers (Sakakibara et al., 2014). Flow acceleration on the order of 10s to 100s m a^{-1} has been documented on lake-terminating glaciers in these regions. Ice front retreat rates of lake-terminating glaciers in the Everest region (–14 to –64 m a^{-1}) also fall below Alaskan (Trussel et al., 2013) and Patagonian (Sakakibara et al., 2014) examples.

Ultimately, the magnitude of retreat and ice loss on Himalayan land-terminating glaciers will be limited by the maximum attainable lake depth and the size of the host glacier; both major controls on the intensity of the feedback proposed by Benn et al. (2007) and therefore

calving retreat. The current maximum depth of Imja Tsho, one of the lakes hosted by a glacier (Lhotse Shar) that displayed more dynamic mass loss than most others, is ~110 m (Fujita et al., 2009; Somos-Valenzuela et al., 2014). In comparison, Yakutat glacier, a lake-terminating glacier in south Alaska, has a maximum depth of 325 m (Trussel et al., 2013) at the glacier's terminus, and Sugiyama et al. (2016) measured lake depths of ~200-580 m at glacier calving fronts in Patagonia. Similarly, the mean calving front width of the nine lake-terminating glaciers assessed in chapter 4 is 442 m (ranging from 222-790 m), whereas the width of the calving front on Yakutat glacier was 4200 m in 2007 (Trussel et al., 2013), and of a similar scale in south Patagonia. Despite these limiting factors, the results of chapters 3 and 4 both show that calving retreat of Himalayan lake-terminating glaciers can result in greater ice loss compared to that of land-terminating glaciers, and their role in the evolution of glacier dynamics remains substantial.

The evolution of the land-terminating glaciers was assessed in chapter 4, and was found to be more consistent than lake-terminating glaciers, with all nine glaciers assessed showing reductions in ice flow over their ablation zones and towards their median altitude (used as a proxy for their ELA). The slowdown of land-terminating glaciers has been noted before in different glacierised regions (Heid and Kääb, 2012) and in the Everest region (Nuimura et al., 2011), and has been attributed to reductions in ice flux from accumulation zones (Nuimura et al., 2011; Heid and Kääb, 2012) in response total annual precipitation reductions (Salerno et al., 2015) and changing precipitation phase (Bhutiyana et al., 2010). The examination of glacier surface gradients and their long-term changes in surface elevation (Bolch et al., 2015; chapter 3) also emphasises the importance of reduced driving stresses in glacier slowdown, although disentangling the contribution of each factor to glacier velocity change is obviously difficult.

The glacier geometry and velocity data generated in chapter 4 were also used to identify areas suitable for meltwater ponding on land-terminating glaciers either yet to host a supraglacial lake, or to identify areas of glaciers that do host glacial lakes that are primed for expansion. Previous studies (Reynolds, 1999; Quincey et al., 2009; Sakai and Fujita, 2010) have shown a set of glacier surface conditions that must exist for suprglacial meltwater to pond, namely a surface slope of less than 2° and negligible glacier flow. These conditions were applied to nine land-terminating glaciers, and the high resolution imagery archive available in GoogleEarth was used to confirm the presence of coalescing ponds at glacier surfaces. These results show that these conditions are appropriate to identify parts of glaciers primed for supraglacial ponding and, later, lake development. This technique could easily applied to a wide area, given the availability of global DEM products (SRTM, ALOS PRISM DEM) and archival glacier surface velocity datasets (Dehecq et al.,2015), and the

NDWI (e.g. Miles et al., 2017; Nie et al., 2017) could be used to confirm the presence of coalescing ponds above a certain size threshold (commonly 3600-8100 m^2). This would serve as a first pass assessment of the likely trajectory of future lake development in the Himalaya.

6.4 Glacier morphometrics

The work presented in Chapter 5 examined the changes in surface morphometry of a smaller subset of glaciers in the Everest region, using fine spatial and high temporal resolution DEMs of debris covered areas between 1984 and 2015/16. The predominant change in the surface topography of these glaciers was the development of a glacier surface of greater relief in response to substantial ice loss over the study period. This high relief topography expanded up-glacier in 4 cases, but also down-glacier (towards glacier termini) in two cases. A time series of SfM-MVS DEMs of the surface of the Khumbu glacier showed that the expansion of supraglacial ponds and ice cliffs is the dominant ice loss mechanism in the slowly flowing, debris covered portions of the studied glaciers. Watson et al. (2016) showed an increase in the number of ice cliffs present at the surface of the same glaciers over the period 2010-2015, and the mapping of supraglacial ponds in the aerial photographs acquired in 1984 showed much expanded supraglacial pond networks over this extended time period. The expansion of the supraglacial pond network and the increased density of ice cliffs are attributed as the drivers of topographic change on the four glaciers where the prevalence of pitted topography increased.

The development of a more pitted glacier surface topography (Figures 5.6-5.8) may impact on the energy balance of a glaciers surface through the modification of the net radiation and turbulent heat fluxes, therefore it is capable of directly impacting on glacier surface melt rates. A more pitted topography is likely to re-absorb energy that has already been reflected from another part of the glacier surface (Cathles et al., 2011; Rippin et al., 2015), thus less energy is lost back to the atmosphere when compared to a smoother glacier surface. As a result, the net radiative flux is more positive (Hock, 2005) and more energy is available to drive sub-debris melt. Such a scenario can be envisaged over areas of debris covered glaciers where local relief is high, for example where supraglacial pond and ice cliff networks are dense. The expansion of ice cliff and pond networks up- and down-glacier that was documented in chapter 5 may therefore have increased the likelihood of energy re-absorption and the contribution of the net radiative fluxes in such areas.

The development of a more pitted glacier topography could also impact on the turbulent heat flux component of the energy balance equation. The turbulent fluxes of sensible and

latent heat are driven by gradients of temperature and moisture between the air and glacier surface, and by turbulence in the lower atmosphere, which drives vertical air exchange (Hock, 2005). The turbulent fluxes are difficult to quantify directly without the use of specialised field equipment (Hock, 2005; Fitzpatrick et al., 2017), so they are often approximated using gradient-flux relations. Such approximations are based on assumptions of constant fluxes in homogenous conditions and over a homogenous surface (Sverdrup, 1936; Hock, 2005), which is an approach that is too simplistic to apply to the highly variable surface of a debris covered glacier (Evatt et al., 2015). King and Anderson (1994) and Martin and Lejeune (1998) showed the sensitivity of the magnitude of the turbulent heat fluxes to surface topography, and Denby and Greuell (2000) showed how turbulent fluxes could be severely underestimated by simpler methods of flux approximation where a locally focussed wind speed maxima exist, for example at the top of an ice cliff (Sakai et al., 2009). The spread of ice cliff networks (Watson et al., 2016) and the development of a generally more complex topography (chapter 5) may therefore have resulted in a greater contribution from the turbulent heat fluxes towards surface melt on glaciers of the Everest region in recent decades. Conversely, on areas of glaciers that developed topography of less vertical relief (terminal zones of Lhotse, Lhotse Shar and Ama Dablam glaciers), the contribution of the turbulent heat fluxes to melt may well have decreased over the past few decades.

Lastly, the development of a more pitted glacier surface topography (chapter 5) may heavily modify the supraglacial hydrological network present at the surface of a debris covered glacier. A glacier surface of greater relief will host a greater number of basins in which supraglacial meltwater can collect. Such basins may become linked in a cascade or persist as hydrologically isolated features. Benn et al. (2017) identified 70 individual basins on Ngozumpa Glacier (Everest region), 56 of which (80%) now contain supraglacial ponds. Benn et al. (2017) examined the evolution of the supraglacial hydrology of Ngozumpa glacier since the 1960s, showing a substantial reordering of its drainage system over the extended period of surface lowering and suspected velocity reductions. The main change Benn et al. (2017) documented was a reduction in the extent of the more efficiently draining, channelized supraglacial system from the 1960s to present day, with isolated hydrological basins forming instead. A similar situation can be envisaged on the land-terminating glaciers studied in chapter 5, all of which showed substantial surface lowering, surface gradients decreases (chapter 4), velocity reductions (chapter 4) pond and ice cliff network (Watson et al., 2016) expansion over the last few decades. Irvine-Fynn et al. (2017) estimated that the cascade of supraglacial ponds that has developed on Khumbu glacier now stores as much as 23% of the glacier's daily discharge, thus the glacier's meltwater contribution to downstream flow is becoming progressively buffered, and will continue to

do so should ponds grow further. The widespread replication of supraglacial hydrology reorganisation that has occurred on Ngozumpa, Khumbu and other glaciers in the Everest region may therefore have a substantial impact on water availability on a regional scale.

In summary, the work presented in chapter 5 examined the morphometric evolution of surface of six debris covered glaciers in the Everest region since the 1980s, along with a contemporary time series of fine resolution DEMs to identify the processes driving topographic change through the period of sustained ice loss. Two main scenarios of glacier surface evolution have been identified. First, where land-terminating glaciers have experienced substantial surface lowering, surface gradient decreases and velocity reductions, widespread supraglacial pond and ice cliff network expansion has occurred and has driven the development of a highly irregular glacier surface topography. This surface topography is of locally high relief and has facilitated further supraglacial water storage, and may impact on the energy balance of the debris covered glacier surface. Alternatively, where a glacier's supraglacial and proglacial hydrological networks are linked, supraglacial pond expansion and associated ice cliff backwasting were limited, and a less pitted glacier surface developed. This situation occurred on glaciers where a large terminal moraine was not present to decouple the hydrological systems, or where flow acceleration and likely crevasse formation facilitated supraglacial meltwater drainage. These divergent scenarios of glacier surface evolution complicate the approach to glacier surface melt or glacier surface hydrological modelling, but are important considerations given the reliance of downstream communities on the meltwater yield of such glaciers.

6.5 Integration of results

The completion of the objectives outlined in section 1.6 has allowed the examination of the importance of different processes operating on glaciers of the central Himalaya to contemporary ice loss rates, and therefore inferences about their role in future ice loss in the region to be made. The role of glacial lake expansion in exacerbating ice loss from a lake's host glacier has been examined in detail in many other glacierised regions (e.g. Patagonia- Sakakibara et al., 2014; Alaska- Trüssel et al., 2016) and was identified as a topic requiring more detailed study in the Himalaya, given the increasing population of glacial lakes across the region (Nie et al., 2017). The influence of the extreme topography of the Himalaya on glacier area-altitude distribution is a topic that has received limited attention previously, but is an important one given the unique relief of Himalayan mountain massifs. The variability of glacier hypsometry and prospective future glacier AARs were assessed to inform on the influence of catchment topography on long-term glacier mass balance (Dyugerov et al., 2009; König et al., 2014). Finally, the impact of the increased prevalence of supraglacial

features such as ice cliffs and ponds (Watson et al., 2016, 2017 a) on the topographic characteristics of debris covered glacier surfaces was examined. The importance of expansive pond and cliff networks as dominant ablative features is now well-documented (e.g. Immerzeel et al., 2015; Thompson et al., 2016; Watson et al., 2017b), but the impact of their persistence on glacier surface characteristics requires more detailed study to improve our understanding of atmosphere/glacier energy transfer (Miles et al., 2016) and supraglacial hydrological reorganisation (Benn et al., 2017).

The work presented in chapter 3 is only the second (Maurer et al., 2015) specific comparison of terminus-type dependant glacier mass balance in the Himalaya. Although the heightened lake-terminating glacier mass loss rates measured in this study were detected from a spatially concentrated sample of glaciers, the replication of the same retreat processes at other lake terminating glaciers across the Himalaya would undoubtedly amplify the mass loss rates from a region hosting numerous glacial lakes. Spatially heterogenous mass loss rates have been detected across populations of glaciers with similar climatic settings (e.g. Figure 2b in Brun et al., 2017) in the western, central and eastern Himalaya; areas where spatially variable lake expansion rates were also detected recently (Wang et al., 2016; Nie et al., 2017). At this sub-regional scale, glacial lake presence and expansion may therefore be a substantial contributing factor to glacier mass loss variability.

The divergent scenarios of evolving glacier velocity and geometry depending on glacier terminus type shown in chapter 4 provides contrast to the general trend of land-terminating glacier slowdown detected by previous studies of Himalayan glacier velocity (Heid and Kääb, 2012 ; Quincey et al., 2009; Robson et al., 2018). Recent modelling studies (e.g. Rowan et al., 2015; Anderson and Anderson, 2016) have replicated such changes in land-terminating glacier dynamics, but the contrasting behaviour of actively retreating lake-terminating glaciers suggests the dominance of an alternative set of processes that must be incorporated into models used to predict glacier behaviour in the region in the future.

Finally, the results of the work presented in chapter 5 emphasise the complicated influence of a debris layer on glacier mass loss. Traditionally, debris covered glaciers were thought to respond less dramatically to climatic change than clean ice glaciers because of the insulating effect of thick debris mantles (Kirkbride and Deline, 2013; Vincent et al., 2016). However, some studies have shown similar ice loss rates from debris covered and clean ice glaciers within the same altitudinal range in the Himalaya (Nuimura et al., 2012; Ragettli et al., 2016), and the impact of supraglacial pond and ice cliff network expansion has been cited as an important factor that might counter the insulating effect of debris (Buri et al., 2015; Miles et al., 2016). The results of chapter 5 reinforce the view that supraglacial pond and ice cliff

network expansion could exacerbate melt, both as ‘hot-spots’ of melt and as the main drivers of topographic change at the glacier surface which could impact on the glacier surface energy balance and feed back to alter supraglacial hydrology further.

6.6 Future work

A number of the main findings of this thesis represent initial observations of glacier behaviour that had previously not been documented in the Himalaya, thus they can only provide a snapshot of what is likely to be a wide spectrum of future glacier behaviour in the region. A number of obvious further research questions have therefore arisen as a result of this work.

The timeline associated with the impact of lake development on glacier dynamics is perhaps the most important topic that remains unanswered from this thesis. Dynamic lake-terminating glacier behaviour has been shown to occur over two to three decades in the central Himalaya, but this time slice only represents part of the dynamic phase of retreat that some glaciers have experienced. Incorporation of ice front retreat rates and surface lowering data gathered from pre-Landsat era satellite imagery (Hexagon, Corona) would yield a better understanding of both the duration of amplified ice loss on land-terminating glaciers, and the time taken for a lake to switch from supraglacial to full-depth proglacial, and therefore influence glacier dynamics. Should attempts be made to model the evolution of Himalayan land-terminating glaciers, boundary conditions such as lake depth and ice thickness would obviously be required. Imja Tsho is the obvious candidate for such a study, with repeat lake bathymetry data available here. Ice thickness data is still required, however, but studies such as Mertes et al. (2017) emphasise the feasibility of GPR studies in the region, and automated ice thickness estimate models (e.g. Frey et al., 2014; James and Carrivick, 2016) could be used to approximate ice thicknesses over large areas.

The variability of glacial lake expansion rates across the Himalaya raises the question of whether the impact of glacial lake growth on glacier behaviour has been as dramatic elsewhere as it has in the Everest region. The extensive archives of stereo satellite imagery (ASTER, ALOS PRISM, WorldView 1-3) that provide coverage of the wider region certainly provide the opportunity to examine the surface lowering and mass loss rate of glaciers of different terminus type anywhere in the Himalaya. The availability of improved global DEM datasets, principally the ALOS PRISM (30 m) DEM, and the wide range of techniques (feature tracking, interferometry) and datasets (Landsat and Sentinel archives) with which glacier velocity datasets could be generated, raises the possibility of wide scale assessments of the suitability of glacier surfaces for supraglacial water storage. The

classification of glacier surfaces using the conditions of Quincey et al. (2007) and Reynolds (1999) may serve as a first pass assessment of potential future glacial lake number and area, alongside recent assessments of glacier overdeepening volumes (Linsbauer et al., 2016), which constitute estimates of potential, maximum lake volume in response to complete glacier melt.

The assessment of glacier surface morphometry (chapter 5) revealed spatial variability in glacier surface relief and contrasting changes in glacier surface characteristics over the last few decades in the Everest region. The development of a less efficient, lagged supraglacial hydrological system in response to such topographic change has now been observed on several debris covered glaciers (e.g. Benn et al., 2017; Miles et al., 2017), thus similar changes in supraglacial hydrology could be expected on other stagnant glaciers hosting cliff and pond networks. GIS based flow modelling (e.g. Miles et al., 2017) could be employed to quantify the supraglacial water storage capacity of stagnant, debris covered glacier surfaces, which may better constrain the yield of meltwater to downstream communities local to debris covered glaciers.

7. Conclusions

The work presented in this thesis has sought to identify variability in contemporary mass loss from glaciers in the Everest region of the central Himalaya, to attribute the role of specific glaciological processes as drivers of such variability, and to discuss to role of those processes in future glacier mass loss. The examination of ice loss on a catchment and regional scale builds on the findings of previous studies, which typically averaged ice mass loss over a wide area, masking variability in glacier behaviour.

The impact of glacial lake development on glacier behaviour in the central Himalaya has been quantified in more detail than in previous studies focussing on the region. The analyses of glacier mass loss, glacier velocity, and glacier area change data have shown that a continuum of potential lake-terminating glacier behaviour may exist. At some point along this continuum, a phase of dynamic ice mass loss may occur, although stages of lake development may exist where only a weak link between lake growth and glacier dynamics exists. The timeline associated with land-terminating glacier behaviour remains uncertain, and may be glacier specific, but the observation of dynamic retreat is an important one given the populous nature of glacial lakes across the region.

Ice mass loss may also be exacerbated or inhibited by glacier hypsometry, which is arguably at its most extreme amongst the 8000 m mountain massifs of the Everest region. Ice loss rates are currently at their highest over the same altitudinal range as the peak glacier area

distribution in two catchments draining either flank of Mt Everest, but the extreme altitudinal range of glaciers here may limit ice loss slightly in the future. In catchments where maximum mountain elevation is slightly lower (the Tama Koshi), glacier area is concentrated at a lower altitude, thus the impact of continued warming in the region may be greater.

The evolution of debris covered glacier surfaces during times of negative glacier mass balance has been shown to be complex, with various ablative and distributive processes governing glacier morphometric change. Ice cliff backwasting and supraglacial pond expansion are by far the most dominant processes driving glacier surface topography change, and the development of a more rugged surface in response to their expansion may have important implications for supraglacial hydrology and energy balance. A greater number of hydrological basins will increase the water storage capacity of the glacier's surface, and a surface of greater relief will amplify the contribution of the turbulent and radiative heat fluxes to the energy budget available to force ice melt.

Overall, the work presented in this thesis highlights processes that must be considered and ideally incorporated into any attempted simulation of future glacier behaviour or extent in the Himalaya, and indeed any other region with debris covered glaciers. The influence of glacial lake development, glacier hypsometry and glacier surface morphometric change along Himalayan range may be of variable strength, and assessments of such factors in areas outside of the central Himalaya is an obvious avenue of additional research. Only by incorporating such processes into numerical simulations will close the gap between predictions of future glacier volume in the region (c.f. Rowan et al., 2015 vs Shea et al., 2015) be closed.

In summary, this thesis has:

1. Quantified the contrasting mass balance of glaciers terminating on land or into a glacial lake in the Everest region.
2. Examined the hypsometry of glaciers across the Everest region, highlighting inter- and intra-catchment variability in area-altitude distribution of ice masses.
3. Explored the adjustment of glacier accumulation area ratios depending on glacier hypsometry and future warming scenarios.
4. Compared lake versus land-terminating glacier geometry change over a period of negative mass balance.
5. Compared lake versus land-terminating glacier velocity change over a period of negative mass balance.

6. Compiled observations of glacier behavior to propose a set of processes driving divergent glacier evolution depending on glacier terminus type.
7. Examined the impact of multi-decadal glacier mass loss on glacier surface morphometry, and explored the likely impacts of the development of a more heterogeneous glacier surface topography.
8. Outlined future research directions that would more tightly constrain scenarios of ice loss from the Himalaya in the near future.

8. References (chapters 1, 2 and 6)

Allen, S., Owens, I. & Sirguey, P. 2008. Satellite remote sensing procedures for glacial terrain analyses and hazard assessment in the Aoraki Mount Cook region, New Zealand. New Zealand Journal of Geology and Geophysics, 51, 1, 73-87, doi:10.1080/00288300809508851.

Arendt, A., Echelmeyer, K., Harrison, W., Lingle, C., Zirnheld, S., Valentine, V., Ritchie, B. and Druckenmiller, M. 2006. Updated estimates of glacier volume changes in the western Chugach Mountains, Alaska, and a comparison of regional extrapolation methods, Journal of Geophysical Research-Earth Surface, 111 (F3).

Basnet, S., Kulkarni, A.V. & Bolch, T. 2013. The influence of debris cover and glacial lakes on the recession of glaciers in Sikkim Himalaya, India. Journal of Glaciology. 59 (218), doi.org/10.3189/2013JoG12J184.

Benn, D. I., C. R. Warren, and R. H. Mottram. 2007. Calving processes and the dynamics of calving glaciers, Earth Science Reviews, 82, 143 – 179.

Benn, D. I., Thompson, S., Gulley, J., Mertes, J., Luckman, A., & Nicholson, L. 2017. Structure and evolution of the drainage system of a Himalayan debris-covered glacier, and its relationship with patterns of mass loss, The Cryosphere, 11, 2247-2264, https://doi.org/10.5194/tc-11-2247-2017.

Berthier E, Cabot V, Vincent C & Six, D. 2016. Decadal Region-Wide and Glacier-Wide Mass Balances Derived from Multi-Temporal ASTER Satellite Digital Elevation Models. Validation over the Mont-Blanc Area. Frontiers in Earth Science. 4:63. doi: 10.3389/feart.2016.00063.

Bhutiyana, M.R. Kale, V.S. & Pawar, N.J. 2010. Climate change and the precipitation variations in the northwestern Himalaya: 1866-2006. International Journal of Climatology, 30, 535-548.

Bolch, T., Pieczonka, T. & Benn, D. I. 2011. Multi-decadal mass loss of glaciers in the Everest area (Nepal Himalaya) derived from stereo imagery. The Cryosphere, 5, 349-358.

Bolch, T., Kulkarni, A., Kääb, A., Huggel, C., Paul, F., Cogley, J. G., Frey, H., Kargel, J. S., Fujita, K., Scheel, M., Bajracharya, S. & Stoffel, M. 2012. The State and Fate of Himalayan Glaciers. Science, 336, 310-314.

Bolch, T., Pieczonka, T., Mukherjee, K., and Shea, J. 2017. Brief communication: Glaciers in the Hunza catchment (Karakoram) have been nearly in balance since the 1970s, The Cryosphere, 11, 531-539, https://doi.org/10.5194/tc-11-531-2017.

Bollasina, M. A., Ming, Y. & Ramaswamy, V. 2011. Anthropogenic Aerosols and the Weakening of the South Asian Summer Monsoon. Science, 334, 502-505.

Boyce, E., Motyka, R., & Truffer, M. 2007. Flotation and retreat of a lake-calving terminus, Mendenhall Glacier, southeast Alaska, USA. Journal of Glaciology, 53(181), 211-224. doi:10.3189/172756507782202928.

Brasington, J., D.Vericat, & I.Rychkov. 2012. Modelling river bed morphology, roughness, and surface sedimentology using high resolution terrestrial laser scanning, Water Resource. Research, 48, W11519, doi:10.1029/2012WR012223.

Brun F, Berthier E, Wagnon P, Kääb A. & Treichler D. 2017. A spatially resolved estimate of High Mountain Asia glacier mass balances from 2000 to 2016. Nature Geoscience, https://doi.org/10.1038/ngeo2999.

Buchroithner, M. F., Jentsch, G. & Wanivenhaus, B. 1982. Monitoring of recent geological events in the Khumbu area (Himalaya, Nepal) by digital processing of landsat MSS data. Rock mechanics, 15, 181-197.

Buri, P., E. S. Miles, J. F. Steiner, W. W. Immerzeel, P. Wagnon. & F. Pellicciotti. 2016. A physically based 3-D model of ice cliff evolution over debris-covered glaciers, Journal of Geophysical Research- Earth Surface, 121, 2471–2493, doi:10.1002/2016JF004039.

Buri, P., F. Pellicciotti, J. F. Steiner, E. S. Miles. & Immerzeel, W.W. 2016. A grid-based model of backwasting of supraglacial ice cliffs on debris-covered glaciers, Annals of Glaciology, 57(71), 199–211, doi:10.3189/2016AoG71A059.

Burgess E.W, Forster R.R. & Larsen C.F. 2013. Flow velocities of Alaskan glaciers. Nature Commun,4, 2146, doi: 10.1038/ncomms3146.

Carrivick, J.L., & Tweed, F.S. 2016. A global assessment of the societal impacts of glacier outburst floods. Global and Planetary Change (144), 1-16, doi.org/10.1016/j.gloplacha.2016.07.001.

Cathles LM, Abbot DS, Bassis JN, MacAyeal DR. 2011. Modeling surface-roughness/solar ablation feedback: application to small-scale surface channels and crevasses of the Greenland ice sheet. Annals of Glaciology, 52(59), 99–108.

Chernos, M., Koppes, M. & Moore, R.D. 2016. Ablation from calving and surface melt at lake-terminating Bridge Glacier, British Columbia, 1984-2013. The Cryosphere (10), 87-102, doi.org/10.5194/tc-10-87-2016.

Chikita, K.A. 2007. Topographic effects on the thermal structure of Himalayan glacial lakes: Observations and numerical simulation of wind. Journal of Asian Earth Sciences, (30), 344-352, doi.org/10.1016/jseas.2006.10.005.

Chinn, T.J. 1996. New Zealand glacier responses to climate change of the past century. New Zealand Journal of Geology and Geophysics, 39 (3), 415-428, doi.org/10.1080/00288306.1996.9514723.

Chinn, T., Fitzharris, B.B., Willsman, A., Salinger, M.J. 2012. Annual ice volume changes 1976-2008 for the New Zealand Southern Alps. Global and Planetary Change, 92-93, 105-118.

Cox, L. H. & March, R. S. 2004. Comparison of geodetic and glaciological mass-balance techniques, Gulkana Glacier, Alaska, U.S.A. Journal of Glaciology, 50, 363-370.

Davies, B. & Glasser, N. 2012. Accelerating shrinkage of Patagonian glaciers from the Little Ice Age (~AD 1870) to 2011. Journal of Glaciology, 58 (212), 1063-1084. doi:10.3189/2012JoG12J026.

Dehecq, A., Gourmelen, N. & Trouve, E. 2015. Deriving large-scale glacier velocities from a complete satellite archive: Application to the Pamir-Karakoram-Himalaya. Remote Sensing of Environment (162), 55-66, doi: 10.1016/j.rse.2015.01.031.

Denby, B. and Greuell, W. 2000. The use of bulk and profile methods for determining surface heat fluxes in the presence of glacier winds. Journal of Glaciology 46, 445-452.

Dyurgerov, M., Meier, M. F. & Bahr, D. B. 2009. A new index of glacier area change: a tool for glacier monitoring. Journal of Glaciology, 55, 710-716.

Evatt, G., Abrahams, I., Heil, M., Mayer, C., Kingslake, J., Mitchell, S., Fowler, A.C. & Clark, C. 2015. Glacial melt under a porous debris layer. Journal of Glaciology, 61 (229), 825-836, doi:10.3189/2015JoG14J235.

Fitch, A.J., Kadyrov, A., Christmas, W.J. & Kitller, J. 2002. Orientation correlation. Proceedings of the British Machine Conference (pp.11.1-11.10). BMVA Press, doi.org/10.5244/C.16.11.

Fitzpatrick, N., Radic, V. & Menounos B. 2017. Surface Energy Balance Closure and Turbulent Flux Parameterization on a Mid-Latitude Mountain Glacier, Purcell Mountains, Canada. Frontiers in Earth Science, 5 (67), doi:10.3389/feart.2017.00067.

Frey, H., Machguth, H., Huss, M., Huggel, C., Bajracharya, S., Bolch, T., Kulkarni, A., Linsbauer, A., Salzmann, N. & Stoffel, M. 2014. Estimating the volume of glaciers in the Himalayan-Karakoram region using different methods. The Cryosphere, 8, 2313-2333.

Fujita, K., Sakai, A., Nuimura, T., Yamaguchi, S. & Sharma, R.R. 2009. Recent changes in Imja Glacial Lake and its damming moraine in the Nepal Himalaya revealed by in-situ surveys and multi-temporal ASTER imagery. Environmental Research Letters, 4(4), 045205, doi:10.1088/1748-9326/4/4/045205.

Gardelle, J., Arnaud, Y. & Berthier, E. 2011. Contrasted evolution of glacial lakes along the Hindu Kush Himalaya mountain range between 1990 and 2009. Global and Planetary Change, 75, 47-55.

Gardelle, J., Berthier, E., Arnaud, Y. & Kääb, A. 2013. Region-wide glacier mass balances over the Pamir-Karakoram-Himalaya during 1999-2011. The Cryosphere, 7, 1263-1286.

Gardner, A. S., Moholdt, G., Cogley, J. G., Wouters, B., Arendt, A. A., Wahr, J., Berthier, E., Hock, R., Pfeffer, W. T., Kaser, G., Ligtenberg, S. R. M., Bolch, T., Sharp, M. J., Hagen, J. O., van den Broeke, M. R., & Paul, F. 2013. A Reconciled Estimate of Glacier Contributions to Sea Level Rise: 2003 to 2009, Science, 340, 852–857, doi:10.1126/science.1234532.

Glasser, N., Holt, T., Evans, Z., Davies, B., Pelto, M. & Harrison S. 2016. Recent spatial and temporal variations in debris cover on Patagonian glaciers. Geomorphology, 273, 202–216.

Hambrey, M. J., Quincey, D. J., Glasser, N. F., Reynolds, J. M., Richardson, S. J. & Clemmens, S. 2008. Sedimentological, geomorphological and dynamic context of debris-mantled glaciers, Mount Everest (Sagarmatha) region, Nepal. Quaternary Science Reviews, 27, 2361-2389.

Heid, T. & Kääb, A. 2012. Repeat optical satellite images reveal widespread and long term decrease in land-terminating glacier speeds, The Cryosphere, 6, 467–478, doi:10.5194/tc-6-467-2012.

Hock, R. 2005. Glacier melt: a review on processes and their modelling. Progress in Physical Geography, 29(3), 362–391.

Huss, M. 2013. Density assumptions for converting geodetic glacier volume change to mass change, The Cryosphere, 7, 877-887, doi:10.5194/tc-7-877-2013.

Immerzeel, W.W., van Beek, L.P.H. & Bierkens, M.F.P. 2010. Climate change will affect the Asian water towers. Science, 328, 1382–1385.

Immerzeel, W.W., Kraaijenbrink, M. Shea, J.M., Shrestha, A.B., Pellicciotti, F., Bierkens, M.F.P. & de Jong, S.M. 2014. High-resolution monitoring of Himalayan glacier dynamics using unmanned aerial vehicles. Remote Sensing of Environment, 150, 93-103.

International Centre for Integrated Mountain Development (ICIMOD). 2011. Glacial Lakes and Glacial Lake Outburst Floods in Nepal; ICIMOD: Kathmandu, Nepal.

Irvine-Fynn, T. D. L., Porter, P. R., Rowan, A. V., Quincey, D. J., Gibson, M. J., Bridge, J. W. & Glasser, N. F. 2017. Supraglacial ponds regulate runoff from Himalayan debris-covered glaciers. Geophysical Research Letters, 44, 11,894–11,904. https://doi.org/10.1002/2017GL075398.

James, W. & Carrivick, J.L. 2016. Automated modelling of spatially-distributed glacier ice thickness and volume. Computers and Geosciences, 92, 90-103, doi.org/10/1016/j.cageo.2016.04.007.

Jiskoot, H., Curran, C. J., Tessler, D. L. & Shenton, L. R. 2009. Changes in Clemenceau Icefield and Chaba Group glaciers, Canada, related to hypsometry, tributary detachment, length, slope and area & aspect relations. Annals of Glaciology, 50, 133-143.

Kääb, A., Berthier, E., Nuth, C., Gardelle, J., & Arnaud, Y. 2012. Contrasting patterns of early 21st century glacier mass change in the Himalayas, Nature, 488, 495–498, doi:10.1038/nature11324.

Kattel, D. B., Yao, T., Yang, W., Gao, Y. & Tian, L. 2015. Comparison of temperature lapse rates from the northern to the southern slopes of the Himalayas. International Journal of Climatology, 35, 4431-4443.

Kienholz, C., S. Herreid, J. L. Rich, A. A. Arendt, R. Hock. & Burgess, E. 2015. Derivation and analysis of a complete modern-date glacier inventory for Alaska and northwest Canada. Journal of Glaciology,61 (227), 403–420.

King, J. C. & Anderson, P. S. 1994. Heat and water vapour fluxes and scalar roughness lengths over an Antarctic ice shelf. Boundary-Layer Meteorology 69, 101-121.

Kirkbride, M.P., Deline, P. 2013. The formation of supraglacial debris covers by primary dispersal from transverse englacial debris bands. Earth Surface Processes and Landforms, 38, 1779–1792, doi.org/10.1002/esp.3416.

Koch, J., Menounos, B. & Clague, J.J. 2009. Glacier change in Garibaldi Provincial Park, southern Coast Mountains, British Columbia, since the Little Ice Age. Global Planet Change 66, 161-178.

König, M., Nuth, C., Kohler, J., Moholdt, G. & Pettersen, R. 2014. A digital glacier database for svalbard. In: Kargel, S. J., Leonard, J. G., Bishop, P. M., Kääb, A. & Raup, H. B. (eds.) Global Land Ice Measurements from Space. Berlin, Heidelberg: Springer Berlin Heidelberg.

Larsen, C. F., Motyka, R. J., Arendt, A. A., Echelmeyer, K. A. & Geissler, P. E. 2007. Glacier changes in southeast Alaska and northwest British Columbia and contribution to sea level rise. Journal of Geophysical Research: Earth Surface, 112, F01007.

Larsen, C. F., E. Burgess, A. A. Arendt, S. O'Neel, A. J. Johnson. & C. Kienholz. 2015. Surface melt dominates Alaska glacier mass balance, Geophysical Research Letters, 42, 5902–5908, doi:10.1002/2015GL064349.

Li, G., Lin, H. & Ye, Qinghua. 2018. Heterogeneous decadal glacier downwasting at Mt Everest (Qomolangma) from 2000-~2012 based on multi-baseline bistatic SAR interferometry. Remote Sensing of Environment, 206, 336-349, doi.org/10/1016/j.rse.2017.12.032.

Maurer, J. M., Rupper, S. B. & Schaefer, J. M. 2016. Quantifying ice loss in the eastern Himalayas since 1974 using declassified spy satellite imagery, The Cryosphere, 10, 2203-2215, https://doi.org/10.5194/tc-10-2203-2016.

Melkonian, A., Willis, M.K. & Pritchard, M.E. 2016. Stikine icefield mass loss between 2000 and 2013/2014. Frontiers in Earth Science, 4 (89), doi.org/10.3389/feart.2016.0089.

Martin, E. and Lejeune, Y. 1998. Turbulent fluxes above the snow surface. Annals of Glaciology 26, 179-183.

Mattson, L. E. 2000. The influence of a debris cover on the mid-summer discharge of Dome Glacier, Canadian Rocky Mountains. In Nakawa, M., Raymond, C. F., and Fountain, A., editors, Debris Covered Glaciers, number 264 in Proceedings and Reports, pages 25–33. IAHS Press.

Mertes, J. R., Thompson, S. S., Booth, A. D., Gulley, J. D., & Benn, D. I. A conceptual model of supraglacial lake formation on debris-covered glaciers based on GPR facies analysis, Earth Surf. Proc. Land., 42, 903–914, https://doi.org/10.1002/esp.4068, 2016.

McCarthy, M., Pritchard, H., Willis, I. & King, G., 2017.Ground-penetrating radar measurements of debris thickness on Lirung Glacier, Nepal. Journal of Glaciology, 543-555. doi:10.1017/jog.2017.18.

McNabb, R.W., & Hock, R. 2014. Alaska tidewater glacier terminus positions, 1948-2012. Journal of Geophysical Research: Earth Surface (119), 153-167, doi.org/10.1002/2013JF002915.

Miles, E., Pellicciotti, F., Willis, I., Steiner, J., Buri, P., & Arnold, N. 2016. Refined energy-balance modelling of a supraglacial pond, Langtang Khola, Nepal. Annals of Glaciology, *57*(71), 29-40. doi:10.3189/2016AoG71A421.

Miles, E.S., Willis, I, C., Arnold, N.S., Steiner, J. & Pellicciotti, F. 2017. Spatial, seasonal and interannual variability of supraglacial ponds in the Langtang Valley, 1999-2013. Journal of Glaciology, 63 (237), 88-105, doi.org/10.1017/jog.2016.120.

Miles, E. S., Steiner, J.F. & Brun, F. 2017. Highly variable aerodynamic roughness length (z0) for a hummocky debris-covered glacier, Journal of Geophysical Research: Atmosphere, 122, 8447–8466, doi:10.1002/2017JD026510.

Miles, E.S, Steiner, J., Willis, I., Buri, P., Immerzeel, W.W., Chesnokova A. & Pellicciotti, F. 2017. Pond Dynamics and Supraglacial-Englacial Connectivity on Debris-Covered Lirung Glacier, Nepal. Frontiers in Earth Science, 5(69), doi: 10.3389/feart.2017.00069.

Moon, T. & Joughin, I. 2008. Changes in ice front position on Greenland's outlet glaciers from 1992 to 2007. Journal of Geophysical Research (113), F02022, doi.org/10.1029/2007JF000927.

Mouginot, J. & Rignot, E. 2015. Ice motion of the Patagonian Icefields of South America: 1984–2014, Geophysical Research Letters, 42, 1441–1449, doi:10.1002/2014GL062661.

Nakawo M, Iwata S, Watanabe O. & Yoshida M. 1986. Processes which distribute supraglacial debris on the Khumbu Glacier, Nepal Himalaya. Annals of Glaciology, 8, 129-131.

Nakawo M, Yabuki H. & Sakai A. 1999. Characteristics of Khumbu Glacier, Nepal Himalaya: recent change in the debris-covered area. Annals of Glaciology, 28, 118-122, doi:10.3189/172756499781821788.

Neckel, N., Kropacek, J., Bolch, T. & Hochschild, V. 2014. Glacier mass changes on the Tibetan Plateau 2003–2009 derived from ICESat laser altimetry measurements. Environmental Research Letters, 9, 014009, doi:10.1088/1748-9326/9/1/014009.

Nicholson, L., & Benn, D. 2006. Calculating ice melt beneath a debris layer using meteorological data. Journal of Glaciology, 52 (178), 463-470, doi:10.3189/172756506781828584.

Nie, Y., Sheng, Y., Liu, Q., Liu, L., Liu, S., Zhang, Y. & Song, C. 2017. A regional-scale assessment of Himalayan glacial lake changes using satellite observations from 1990-2015. Remote sensing of Environment (189), 1-13, doi:10.1016/j.rse.2016.11.008.

Nuimura T, Fujita K, Fukui K, Asahi K, Aryal R. & Ageta Y. 2011. Temporal changes in elevation of the debris-covered ablation area of Khumbu Glacier in the Nepal Himalaya since 1978. Arctic, Antarctic, and Alpine Research, 43(2), 246-255, doi:10.1657/1938-4246-43.2.246.

Nuimura. T., Fujita, K., Yamaguchi, S. & Sharma, R.R. 2012. Elevation changes of glaciers revealed by multitemporal digital elevation models calibrated by GPS survey in the Khumbu region, Nepal Himalaya, 1992–2008. Journal of Glaciology, 58(210), 648-656, doi:10.3189/2012JoG11J061.

Nuth, C. & Kääb, A. 2011. Co-registration and bias corrections of satellite elevation data sets for quantifying glacier thickness change. The Cryosphere (5), 271-290.

Osti, R., Bhattari, T.N., Miyake, K., 2011. Causes of catastrophic failure of Tam Pokhari moraine dam in the Mt. Everest region. Natural Hazards 58, 1209–1223.

Østrem, G. 1959. Ice Melting under a Thin Layer of Moraine, and the Existence of Ice Cores in Moraine Ridges. Geografiska Annaler (41), 228–230, doi.org/10.1080/20014422.1959.11907953.

Paul, F., Kääb, A. & Haeberli, W. 2007. Recent glacier changes in the Alps observed by satellite: Consequences for future monitoring strategies, Global and Planetary Change, doi:10.1016/j.gloplacha.2006.07.007.

Pellicciotti, F., Stephan, C., Miles, E., Herreid, S., Immerzeel, W. W. & Bolch, T. 2015. Mass-balance changes of the debris-covered glaciers in the Langtang Himal, Nepal, from 1974 to 1999. Journal of Glaciology, 61, 373-386.

Quincey, D. J. & Glasser, N. F. 2009. Morphological and ice-dynamical changes on the Tasman Glacier, New Zealand, 1990–2007, Global and Planetary Change, 68, 185–197, doi:10.1016/j.gloplacha.2009.05.003.

Quincey, D., Richardson, S., Luckman, A., Lucas, R., Reynolds, J., Hambrey, M., and Glasser, N. 2007. Early recognition of glacial lake hazards in the Himalaya using remote sensing datasets, Global and Planetary Change, 56, 137–152, doi:10.1016/j.gloplacha.2006.07.013.

Quincey, D. J., Luckman, A. & Benn, D. 2009. Quantification of Everest region glacier velocities between 1992 and 2002, using satellite radar interferometry and feature tracking. Journal of Glaciology, 55, 596-606.

Quincey, D., Smith, M., Rounce, D., Ross, A., King, O. & Watson, C. 2017. Evaluating morphological estimates of the aerodynamic roughness of debris covered glacier ice. Earth surface processes and landforms, 42: 2541–2553. doi: 10.1002/esp.4198.

Radic, V. & Hock, R.2011. Regionally differentiated contribution of mountain glaciers and ice caps to future sea-level rise, Nat.Geosci., 4, 91–94.

Ragettli, S., Bolch, T. & Pellicciotti, F. 2016. Heterogeneous glacier thinning patterns over the last 40 years in Langtang Himal. The Cryosphere, 10, 2075–2097, doi: 10.5194/tc-2016-25.

Reynolds, J.M. 1999. Glacial hazard assessment at Tsho Rolpa, Rolwaling, Central Nepal. Quaterly Journal of Engineering Geology and Hydrogeology, 32, 209-214.

Reznichenko, N., Davies, T., Shulmeister, J., & McSaveney, M. 2010. Effects of debris on ice-surface melting rates: an experimental study. Journal of Glaciology, 56, 384–394.

Rippin, D. M., Pomfret, A. & King, N. 2015. High resolution mapping of supra-glacial drainage pathways reveals link between micro-channel drainage density, surface roughness and surface reflectance. Earth Surface Processes and Landforms, 40, 1279–1290. doi: 10.1002/esp.3719.

Robson, B.A., Nuth, C., Nielsen, P.R., Girod, L., Hendrickx, M. & Dahl S.O. 2018. Spatial Variability in Patterns of Glacier Change across the Manaslu Range, Central Himalaya. Frontiers in Earth Science, 6:12. doi: 10.3389/feart.2018.00012

Rounce, D. R., Quincey, D. J. & McKinney, D. C. 2015. Debris-covered glacier energy balance model for Imja–Lhotse Shar Glacier in the Everest region of Nepal. The Cryosphere, 9, 2295-2310, doi.org/10.5194/tc-9-2295-2015.

Rounce, D.R., Watson, C.S. & McKinney, D.C. 2017. Identification of hazard and risk for glacial lakes in Nepal Himalaya using satellite imagery from 2000-2015. Remote Sensing 9 (654), doi.org/10.3390/rs9070654.

Rowan, A. V., Egholm, D. L., Quincey, D. J. & Glasser, N. F. 2016. Modelling the feedbacks between mass balance, ice flow and debris transport to predict the response to climate change of debris-covered glaciers in the Himalaya. Earth and Planetary Science Letters, 430, 427-438.

Sakai, A. Nakawo, M. and Fujita, K. 1998. Melt rate of ice cliffs on the Lirung Glacier, Nepal Himalayas. *Bulletin of Glaciological Research.* **16**, 57-66.

Sakai A, Nishimura K, Kadota T,. & Takeuchi N. 2009. Onset of calving at supraglacial lakes on debris covered glaciers of the Nepal Himalayas. Journal of Glaciology, 55(193), 909-917, doi:10.3189/002214309790152555.

Sakai, A. & Fujita, K., 2010. Formation conditions of supraglacial lakes on debris-covered glaciers in the Himalaya (Letter). Journal of Glaciology 56 (195), 177–181, doi:10.3189/002214310791190785.

Sakai, A., Chikita, K. & Yamada, T. 2000. Expansion of a moraine-dammed glacial lake, Tsho Rolpa, in Rolwaling Himal, Nepal Himalaya. Limnology and Oceanography, 45, 1401-1408.

Sakai A, Nishimura K, Kadota T,. & Takeuchi N. 2009. Onset of calving at supraglacial lakes on debris covered glaciers of the Nepal Himalayas. Journal of Glaciology, 55(193), 909-917, doi:10.3189/002214309790152555.

Sakakibara, D. & Sugiyama, S. 2014. Ice-front variations and speed changes of calving glaciers in the Southern Patagonia Icefield from 1984 to 2011. Journal of Geophysical Research: Earth Surface (119), 2541-2554, doi.org/ 10.1002/2014JF003148.

Salerno, F., Guyennon, N., Thakuri, S., Viviano, G., Romano, E., Vuillermoz, E., Cristofanelli, P., Stocchi, P., Agrillo, G., Ma, Y. & Tartari, G. 2015. Weak precipitation, warm winters and springs impact glaciers of south slopes of Mt. Everest (central Himalaya) in the last 2 decades (1994–2013). The Cryosphere, 9, 1229-1247.

Salerno, F., Thakuri, S., Tartari, G., Nuimura, T., Sunako, S., Sakai, A., and Fujita, K. 2017. Debris-covered glacier anomaly? Morphological factors controlling changes in the mass balance, surface area, terminus position, and snow line altitude of Himalayan glaciers. Earth and Planetary Science Letters, 471, 19–31, https://doi.org/10.1016/j.epsl.2017.04.039.

Shea, J.M., Immerzeel, W.W., Wagnon, P., Vincent, C. & Bajracharya, S. 2015. Modelling glacier change in the Everest region, Nepal Himalaya. The Cryosphere, 9(3), pp.1105-1128.

Scherler, D., Bookhagen, B., and Strecker, M. R. 2011. Spatially variable response of Himalayan glaciers to climate change affected by debris cover, Nat. Geosci., 4,156–159.

Shrestha, A. B., Wake, C. P., Mayewski, P. A. & Dibb, J. E. 1999. Maximum temperature trends in the Himalaya and its vicinity: An analysis based on temperature records from Nepal for the period 1971-94. Journal of Climate, 12, 2775-2786.

Smith, M. W., Carrivick, J. L., and Quincey, D. J. 2015. Structure from motion photogrammetry in physical geography, Progress in Physical Geography, 1–29, doi:10.1177/0309133315615805.

Smith, M. W., D. J. Quincey, T. Dixon, R. G. Bingham, J. L. Carrivick, T. D. L. Irvine-Fynn. & Rippin, D.M. 2016. Aerodynamic roughness of glacial ice surfaces derived from high-resolution topographic data, Journal of Geophysical Research: Earth Surface, 121, 748–766, doi:10.1002/2015JF003759.

Somos-Valenzuela, M. A., Mckinney, D. C., Rounce, D. R. & Byers, A. C. 2014. Changes in Imja Tsho in the Mount Everest region of Nepal. The Cryosphere (8), 1661-1671, doi.org/10.5194/tc-8-1661-2014.

Song, C., Sheng, Y., Wang, J., Ke, L., Madson, A. & Nie, Y. 2017. Heterogeneous glacial lake changes and links of lake expansions to the rapid thinning of adjacent glacier termini in the Himalayas. Geomorphology 280. 30-28.

Spedding, N. 2000. Hydrological controls on sediment transport pathways: implications for debris-covered glaciers. In: Nakawo, M., Raymond, C.F., Fountain, A. (Eds.), Debris-Covered Glaciers, Proceedings of the Seattle Workshop, USA, September 2000. IAHS Publication 264, pp. 133–141.

Sugiyama, S., M. Minowa, D. Sakakibara, P. Skvarca, T. Sawagaki, Y. Ohashi, N. Naito. & Chikita, K. 2016. Thermal structure of proglacial lakes in Patagonia. Journal of Geophysical Research: Earth Surface, 121, 2270–2286, doi:10.1002/2016JF004084.

Thakuri, S., Salerno, F., Smiraglia, C., Bolch, T., D'Agata, C., Viviano, G. & Tartari, G. 2014. Tracing glacier changes since the 1960s on the south slope of Mt. Everest (central Southern Himalaya) using optical satellite imagery. The Cryosphere, 8, 1297-1315.
Thakuri, A., Salerno, F., Bolch, T., Guyennon, N. & Tartari, G. 2016. Factors controlling the accelerated expansion of Imja Lake, Mount Everest region, Nepal. Annals of Glaciology, 57(71), doi: 10.3189/2016AoG71A063.

Thompson, S., Benn, D.I., Mertes, J. & Luckman, A. 2016. Stagnation and mass loss on a Himalayan debris-covered glacier: processes, patterns and rates, Journal of Glaciology, 62, 233, 467-485, doi:10.1017/jog.2016.37.

Truffer, M. & Motyka, R.J. 2016. Where glaciers meet water: Subaqueous melt and its relevance to glaciers in various settings. Reviews of Geophysics (54), 220-239, doi.org/10.1002/2015RG000494.

Trüssel, B., Motyka, R.J., Truffer, M. & Larsen, C.F. 2013. Rapid thinning of lake-calving Yakutat Glacier and the collapse of the Yakutat Icefield, southeast Alaska, USA. Journal of Glaciology, 59 (213), doi.org/10.3189/2013J0G12J081.

Tsutaki. S., Sugiyama, S., Sakakibara, D. & Sawagaki, T. 2016. Surface elevation changes during 2007-13 on Bowdoin and Tugto Glaciers, northwestern Greenland. Journal of Glaciology, 62 (236), 1083-1092, doi.org/10.1017/jog.2016.106.

Van der Veen, C.J. 2002. Calving glaciers. Progress in Physical Geography, 26 (1), 96-122, doi.org/10.1191/0309133302pp327ra.

Veettil, B., Bianchini, N., de Andrade, A., Bremer, U., Simões, J. & de Souza Junior, E. 2015. Glacier changes and related glacial lake expansion in the Bhutan Himalaya, 1990–2010. Regional Environmental Change, 16 (5), 1267-1278.

Vincent, C., Wagnon, P., Shea, J. M., Immerzeel, W. W., Kraaijenbrink, P., Shrestha, D., Soruco, A., Arnaud, Y., Brun, F., Berthier, E. & Sherpa, S. F. 2016. Reduced melt on debris-covered glaciers: investigations from Changri Nup Glacier, Nepal, The Cryosphere, 10, 1845-1858, doi.org/10.5194/tc-10-1845-2016.

Vuichard, D. & Zimmerman, M. 1987. The 1985 Catastrophic Drainage of a Moraine-Dammed Lake, Khumbu Himal, Nepal: Cause and Consequences. Mountain Research and Development, 7, 91-110.

Wang, X., Ding, Y., Liu, S., Jiang, L., Wu, K., Jiang, Z. & Guo, W. 2013. Changes of glacial lakes and implications in Tian Shan, central Asia, based on remote sensing data from 1990 to 2010. Environmental Research Letters, 8 (4), 044052.

Wang, X., Liu, Q., Liu, S., Wei, J. & Jiang, Z. 2016. Heterogeneity of glacial lake expansion and its contrasting signals with climate change in Tarim Basin, Central Asia. Environmental Earth Sciences, 75:696, doi.org/10.1007/s12665-016-5498-4.

Wang, X., Chai, K.G., Liu, S.Y., Wei, J., Jiang, Z. & Liu, Q. 2017. Changes of glaciers and glacial lakes implying corridor-barrier effects and climate change in the Hengduan Shan, southeastern Tibetan Plateau. Journal of Glaciology 63(239):1-8. https://doi.org/10.1017/jog.2017.14.

Warren, C.R & Kirkbride, M.P. 2003. Calving speed and climatic sensitivity of New Zealand lake-calving glaciers. Annals of Glaciology (36), 173-178, doi.org/10.3189/172756403781816446.

Watson, C.S. Quincey, D.J, Carrivick, J.L. & Smith, M.W. 2016. The dynamics of supraglacial ponds in the Everest region, central Himalaya. Global and Planetary Change, 142, 14-27.

Watson, C.S., Quincey, D.J., Carrivick, J.L. & Smith, M.W. 2017a. Ice cliff dynamics in the Everest region of the central Himalaya, Geomorphology, 278, 238-251, doi.org/10/106/j.geomorph.2016.11.017.

Watson, C.S., Quincey, D.J., Smith, M.W., Carrivick, J.L., Rowan, A.V. & James, M.R.2017b. Quantifying ice cliff evolution with multi-temporal point clouds on the debris-covered Khumbu Glacier, Nepal, Journal of Glaciology, doi:10.1017/jog.2017.47.

Watson, Cameron Scott. 2017c.*The evolution of supraglacial ponds and ice cliffs on Himalayan debris-covered glaciers.* PhD thesis, University of Leeds.

Watson, C. S., Quincey, D. J., Carrivick, J. L., Smith, M. W., Rowan, A. V. & Richardson, R. 2018. Heterogeneous water storage and thermal regime of supraglacial ponds on debris-covered glaciers. Earth Surface Processes and Landforms, 43: 229–241. doi: 10.1002/esp.4236.

Watson, C.S., King, O., Miles, E.S. & Quincey, D.J. Optimising NDWI supraglacial pond classification on Himalayan debris-covered glaciers. *In review in Remote Sensing of Environment.*

Westoby, M.J., Glasser, N.F., Hambrey, M.J., Brasington, J., Reynolds, J.M. & Hassan, M.A.A.M. 2014. Reconstructing historic Glacial Lake Outburst Floods through numerical modelling and geomorphological assessment: Extreme events in the Himalaya. Earth Surface Processes and Landforms (39), 1675-1692, doi.org/10.1002/esp.3617.

WGMS (2017): Global Glacier Change Bulletin No. 2 (2014-2015). Zemp, M., Nussbaumer, S.U., Gärtner-Roer, I., Huber, J., Machguth, H., Paul, F., and Hoelzle, M. (eds.), ICSU(WDS)/IUGG(IACS)/UNEP/UNESCO/WMO, World Glacier Monitoring Service, Zurich, Switzerland, 244 pp. Based on database version: doi: 10.5904/wgms-fog-2017-10.

Willis, M.J., Melkonian, A.K., Pritchard, M.E. & Ramage, J.M. 2012. Ice loss rates at the Northern Patagonian Icefield derived using a decade of satellite remote sensing. Remote Sensing of Environment, 117, doi.org/10.1016/j.rse.2011.09.017.

Wilson, R., Glasser, N. F., Reynolds, J. M., Harrison, S., Iribarren Anacona, P., Schaefer, M. & Shannon, S. 2018. Glacial lakes of the Central and Patagonian Andes, Global and Planetary Change, doi.org/10.1016/j.gloplacha.2018.01.004.

Yang, X., Zhang, T., Qin, D., Kang, S. & Qin, X. 2011. Characteristics and Changes in Air Temperature and Glacier's Response on the North Slope of Mt. Qomolangma (Mt. Everest). Arctic, Antarctic, and Alpine Research (43), 147-160, doi.org/stable/41240408.

Ye, Q., Bolch, T., Naruse, R., Wang, Y., Zong, J., Wang, Z., Zhao, R., Yang, D. & Kang, S. 2015. Glacier mass changes in Rongbuk catchment on Mt. Qomolangma from 1974 to 2006 based on topographic maps and ALOS PRISM data. Journal of Hydrology, 530, 273-280.

Zhou, Y., Li, Z., Li, J., Zhao, R. & Ding, X. 2018. Glacier mass balance in the Qinghai-Tibetan Plateau and its surroundings from the mid-1970s to 2000 based on Hexagon KH-9 and SRTM DEMs. Remote Sensing of Environment, 210, 96-112, doi.org/10/1016/j.rse.2018.03.020.

9. Appendices

Appendix 1

Supplementary information for ‘Spatial variability in mass loss of glaciers in the Everest region, central Himalaya, between 2000 and 2015’ shown in chapter 3.

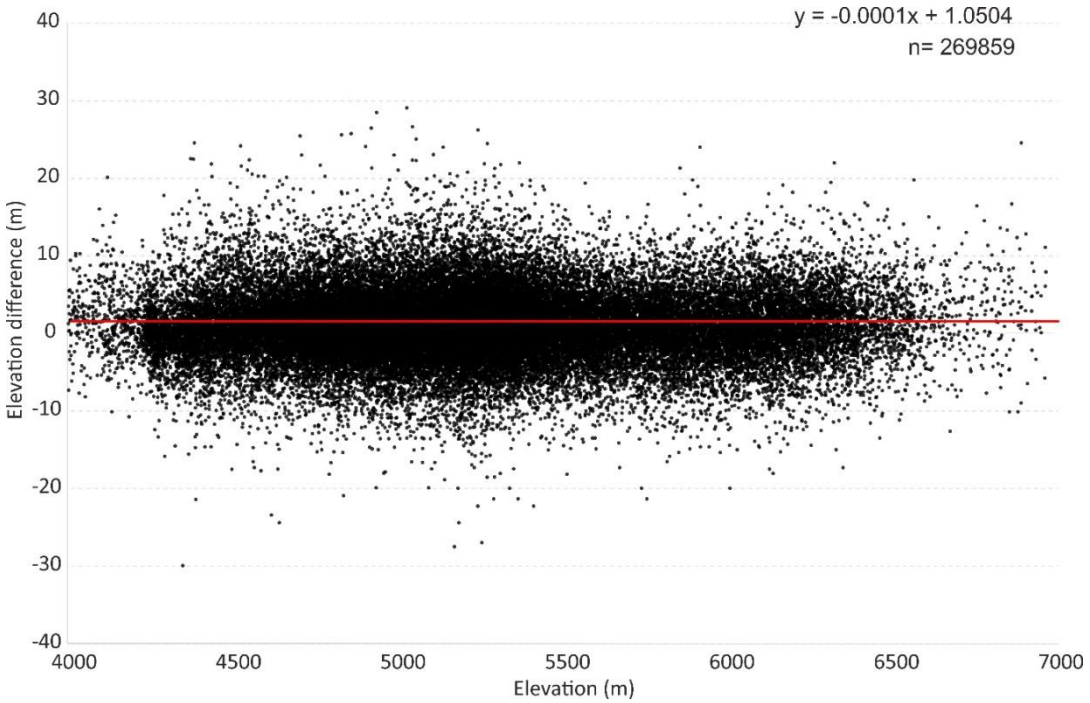

Supplementary Figure 1. Elevation differences for stable ground (off-glacier) between SETSM and SRTM DEMs, plotted against elevation. There is no clear relationship between DEM differences and increasing/ decreasing elevation (often labelled an elevation dependent bias).

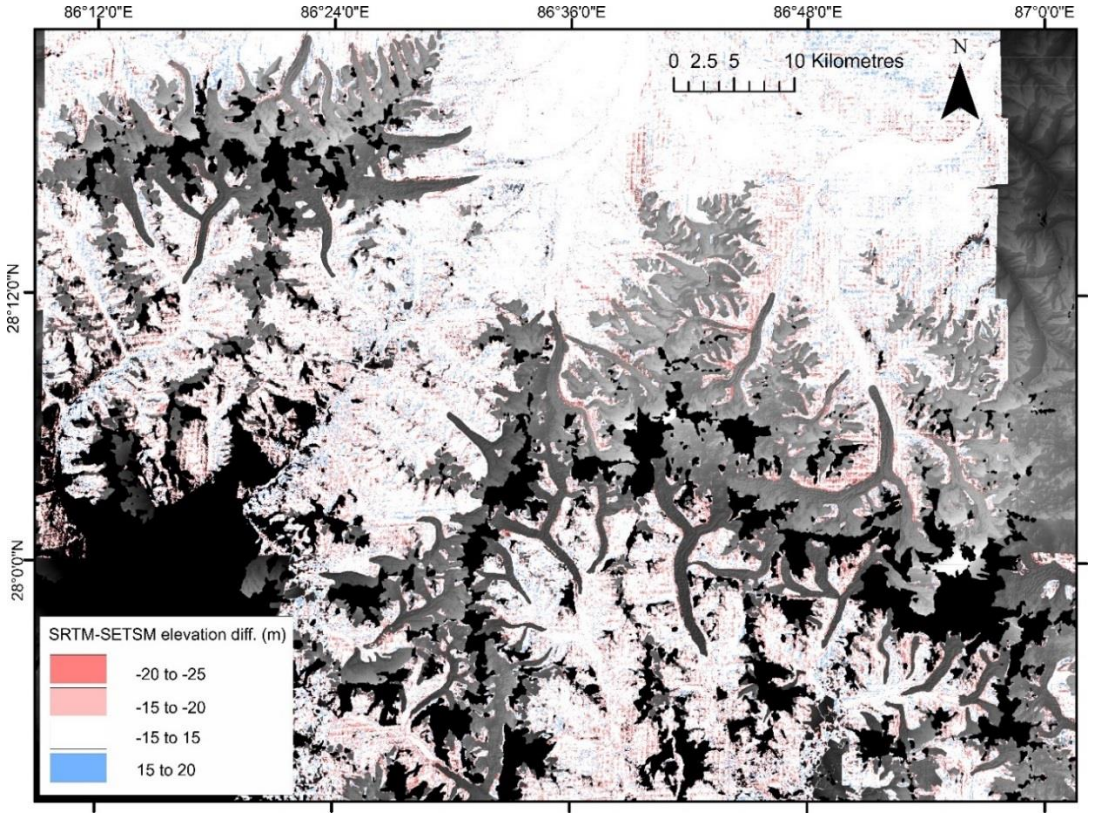

Supplementary Figure 2. Elevation differences between the SRTM and SETSM DEMs over stable ground away from glacier surfaces.

Supplementary Table 1. Glaciers highlighted in the study. Data on glacier area and altitudinal range are taken from the GLIMS database. Glacier length is measured along centrelines from the bergschrund. Catchment notation: TK- Tama Koshi; DK- Dudh Koshi; P- Pumqu; P clean (surface debris-free) glaciers in the Pumqu catchment.

				Altitude (m)				
GLIMS ID	Name	Length (km)	Area (km^2)	Min	Max	Range	Lake status	Catchment
G086218E28282N	Bamolelingja	7.4	15.4	5013	6745	1732	No lake	TK
G086280E28276N	G1	12.3	42.7	4778	7045	2467	No lake	TK
G086550E28133N	Yanong	3.4	4.4	4984	6377	1393	Proglacial lake	TK
G086548E28174N	Yanong North	3.2	4.1	5025	6524	1499	Proglacial lake	TK
G086384E28259N	Erbu	10.9	25.8	5020	7130	2310	No lake	TK
G086471E27959N	Drogpa Nagtsang	8.2	25.3	5018	7031	2013	Supraglacial lake	TK
G086537E27874N	Trakarding	17.7	35.4	4561	6659	2098	Proglacial lake	TK
G086519E27919N	Ripimo Shar	10.3	19.7	4600	6683	2083	No lake	TK
G086533E28088N	Shalong	7.9	18.4	5301	6835	1534	No lake	TK
G086771E28015N	Ngozumpa	22.2	80.7	4686	8176	3490	Supraglacial lake	DK
G086949E27913N	Imja	6.5	15.3	5021	7998	2977	Supraglacial lake	DK
G086820E27978N	Khumbu	15.7	39.5	4915	8062	3147	Coalescing ponds	DK
G086625E28029N	Lumbsamba	9.1	12.5	4936	7258	2322	No lake	DK
G086917E27925N	Lhotse	7.1	6.9	4821	6082	1261	No lake	DK
G086541E27988N	Melung	6.5	7.6	5271	6028	757	No lake	DK
G086587E28039N	Bhote Kosi	14.4	28.4	4793	6679	1886	No lake	DK
G086900E27843N	Hungu	4.7	13.9	5207	6942	1735	Proglacial lake	DK
G086900E27843N	Marala	2.9	13.9	5366	5920	554	Proglacial lake	DK
G086798E28111N	Jiuda	10.1	15.9	5405	7801	2396	No lake	P
G086719E28132N	Gyachung	13.6	47.1	5309	7853	2544	No lake	P
G086939E28060N	Rongbuk East	10.9	26.7	5640	8361	2721	No lake	P
G086866E28050N	Rongbuk	19.5	73.2	5153	8758	3605	Supraglacial lake	P
G086466E28321N	Ayi	8.6	7.27	5313	6863	1550	Coalescing ponds	P
G086456E28291N	Tibet 1	12.9	26.8	5138	7085	1947	Coalescing ponds	P
G086633E28122N	Gyabrag	11.5	33.2	5095	8182	3087	No lake	P
G086235E28330N	Longmojian	4.5	9.3	5348	6788	1440	Proglacial lake	P
G086382E28331N	Duiya	9.3	22.5	5480	7201	1721	Proglacial lake	P
G086395E28347N	Duosangpuxi	5.5	7.7	5561	6992	1431	No lake	P clean
G086657E28179N	Siguang	5.2	5.8	5652	6866	1214	No lake	P clean
G086423E28367N	Duosangpudong	6.3	8.8	5502	6925	1423	No lake	P clean
G086709E28242N	G08	3.8	6.4	5726	6475	749	No lake	P clean
G086275E28322N	G06	6.0	6.0	5545	6926	1381	No lake	P clean

Supplementary Table 2. Mean and maximum surface lowering rates measured in glacier ablation zones, and geodetic mass balance estimates for each glacier included in the study. Bold text indicates lake-terminating glaciers; means are italicised. The uncertainty of mass balance estimates contains an additional 7% error compared to the surface lowering estimates due to potential errors in the density conversion.

Glacier	Mean SL rate (m a^{-1})	Maximum SL rate (m a^{-1})	Mass balance (m w.e. a^{-1})	Catchment
Bamolelingja	–0.58 ± 0.19	–1.50 ± 0.19	–0.63 ± 0.20	TK
G1	–0.47 ± 0.19	–1.25 ± 0.19	–0.42 ± 0.20	TK
Erbu	–0.50 ± 0.13	–0.73 ± 0.13	–0.32 ± 0.14	TK
Ripimo Shar	–0.72 ± 0.24	–0.97 ± 0.24	–0.30 ± 0.25	TK
Shalong	–0.52 ± 0.10	–0.96 ± 0.10	–0.32 ± 0.11	TK
Mean	*–0.55 ± 0.17*	*–1.08 ± 0.17*	*–0.40 ± 0.18*	
Ngozumpa	–0.64 ± 0.18	–1.17 ± 0.18	–0.53 ± 0.19	DK
Khumbu	–0.84 ± 0.14	–1.34 ± 0.14	–0.35 ± 0.15	DK
Lumbsamba	–0.31 ± 0.15	–0.89 ± 0.15	–0.17 ± 0.16	DK
Lhotse	–0.66 ± 0.13	–0.99 ± 0.13	–0.65 ± 0.14	DK
Melung	–0.40 ± 0.11	–1.12 ± 0.11	–0.74 ± 0.12	DK
Bhote Kosi	–0.72 ± 0.14	–1.33 ± 0.14	–0.58 ± 0.15	DK
Mean	*–0.59 ± 0.14*	*–1.14 ± 0.14*	*–0.50 ± 0.15*	
Jiuda	–0.64 ± 0.23	–1.33 ± 0.23	–0.55 ± 0.24	P
Gyachung	–0.66 ± 0.29	–1.07 ± 0.29	–0.44 ± 0.31	P
Rongbuk East	–1.04 ± 0.18	–2.45 ± 0.18	–0.44 ± 0.19	P
Rongbuk	–1.31 ± 0.32	–2.02 ± 0.32	–0.57 ± 0.34	P
Ayi	–0.68 ± 0.24	–1.45 ± 0.24	–0.58 ± 0.26	P
Tibet 1	–1.17 ± 0.20	–2.14 ± 0.20	–0.83 ± 0.21	P
Gyabrag	–1.22 ± 0.22	–3.40 ± 0.22	–0.74 ± 0.23	P
Mean	*–0.96 ± 0.24*	*–1.98 ± 0.24*	*–0.59 ± 0.26*	
Duosangpuxi	–0.53 ± 0.20	–1.30 ± 0.20	–0.24 ± 0.26	P-clean
Siguang	–0.61 ± 0.23	–1.06 ± 0.23	–0.29 ± 0.36	P-clean
Duosangudong	–0.31 ± 0.24	–0.91 ± 0.24	–0.29 ± 0.16	P-clean
G08	–0.49 ± 0.21	–0.96 ± 0.21	–0.21 ± 0.36	P-clean
G06	–0.51 ± 0.22	–0.98 ± 0.22	–0.24 ± 0.16	P-clean
Mean	*–0.49 ± 0.22*	*–1.04 ± 0.22*	*–0.25 ± 0.24*	
Longmojian	**–1.12 ± 0.21**	**–2.53 ± 0.21**	**–0.91 ± 0.22**	**P**
Duiya	**–0.65 ± 0.12**	**–1.45 ± 0.12**	**–0.45 ± 0.13**	**P**
Hungu	**–0.54 ± 0.25**	**–1.10 ± 0.25**	**–0.56 ± 0.27**	**DK**
Marala	**–0.61 ± 0.30**	**–2.24 ± 0.30**	**–0.88 ± 0.32**	**DK**
Imja	**–0.84 ± 0.22**	**–1.62 ± 0.22**	**–0.79 ± 0.24**	**DK**
Drogpa Nagtsang	**–0.78 ± 0.33**	**–1.91 ± 0.33**	**–0.75 ± 0.35**	**TK**
Trakarding	**–0.94 ± 0.39**	**–2.19 ± 0.39**	**–0.48 ± 0.41**	**TK**
Yanong	**–1.55 ± 0.17**	**–3.78 ± 0.17**	**–0.76 ± 0.18**	**TK**
Yanong North	**–1.13 ± 0.24**	**–3.06 ± 0.24**	**–0.62 ± 0.25**	**TK**
Mean	***–0.90 ± 0.25***	***–2.20 ± 0.25***	***–0.70 ± 0.27***	

Supplementary Table 3. Hypsometric Index (HI) scores and classification, accumulation area ratio (AAR) and total area loss for each glacier included in the study. EQ = Equidimensional; BH = Bottom Heavy; VBH = Very Bottom Heavy; TH = Top Heavy. The ELA of the Lhotse and Melung glaciers are now above their altitudinal ranges, thus AARs cannot be calculated. Catchments: TK- Tama Koshi; DK- Dudh Koshi; TP- Tibetan Plateau. Lake- terminating glaciers are in bold; mean values are italicised.

Glacier	HI score	HI classification	AAR	Area change (km^2) & % of total area.	Approximate ELA (m)	Catchment
Bamolelingja	0.91	EQ	0.37	–0.07 ± 0.08 (0.44%)	5593	TK
G1	1.45	BH	0.46	–0.49 ± 0.22 (1.15%)	5659	TK
Yanong	**0.94**	**EQ**	**0.50**	**–0.31** ± 0.02 **(6.33%)**	**5557**	TK
Yanong North	**1.22**	**EQ**	**0.43**	**–0.16** ± 0.02 **(4.07%)**	**5622**	TK
Erbu	1.15	EQ	0.45	–0.05 ± 0.13 (0.24%)	5654	TK
Drogpa	**1.18**	**EQ**	**0.38**	**–2.37** ± 0.13 **(9.12%)**	**5623**	TK
Nagtsang						
Trakarding	**0.69**	**EQ**	**0.33**	**–0.35** ± 0.18 **(0.98%)**	**5708**	TK
Ripimo Shar	0.98	EQ	0.57	–0.04 ± 0.10 (0.20%)	5408	TK
Shalong	1.21	BH	0.41	–0.09 ± 0.09 (0.45%)	5288	TK
Mean	*1.14*	*EQ*	*0.43*	*–0.43 ± 0.11 (2.55%)*	*5568*	
Ngozumpa	2.62	VBH	0.39	–0.13 ± 0.16 (0.16%)	5815	DK
Imja	**5.93**	VBH	**0.50**	**–0.5** ± 0.06 **(3.21%)**	**5366**	DK
Khumbu	3.95	VBH	0.51	–0.06 ± 0.18 (0.22%)	5568	DK
Lumbsamba	3.11	VBH	0.40	–0.02 ± 0.05 (0.15%)	5527	DK
Lhotse	1.93	VBH	0.27	0 ± 0.03 (0%)	5149	DK
Melung	1.52	VBH	0.50	–0.20 ± 0.03 (2.55%)	5270	DK
Bhote Kosi	2.36	VBH	0.38	–0.13 ± 0.12 (0.51%)	5310	DK
Hungu	**1.69**	**VBH**	**0.54**	**–0.13** ± **0.06 (1.53%)**	**5687**	DK
Marala	**0.56**	**EQ**	**0.20**	**–0.11** ± 0.06 **(2.2%)**	**5607**	DK
Mean	*2.63*	*VBH*	*0.41*	*–0.14 ± 0.11 (1.17%)*	*5477*	
Jiuda	1.45	BH	0.35	–0.10 ± 0.06 (0.62%)	6223	P
Gyachung	1.85	VBH	0.36	–0.06 ± 0.17 (0.21%)	6290	P
Rongbuk East	2.58	VBH	0.44	–0.80 ± 0.10 (2.85%)	6419	P
Rongbuk	3.25	VBH	0.48	–0.14 ± 0.27 (0.16%)	5923	P
Ayi	3.00	VBH	0.30	–0.31 ± 0.03 (3.90%)	5722	P
Tibet 1	2.80	VBH	0.54	–0.35 ± 0.10 (1.38%)	5653	P
Gyabrag	2.83	VBH	0.33	–1.17 ± 0.12 (3.32%)	6059	P
Longmojian	**3.09**	**VBH**	**0.41**	**–0.44** ± 0.03 **(4.28%)**	**5795**	P
Duiya	**1.39**	**BH**	**0.17**	**–0.50** ± 0.08 **(2.07%)**	**6256**	P
Mean	*2.47*	*VBH*	*0.37*	*–0.39* ± 0.11 *(1.91%)*	*6037*	
Duosangpuxi	1.23	BH	0.40	–0.16 ± 0.22 (2.07%)	6276	P clean
Siguang	1.03	EQ	0.50	–0.06 ± 0.16 (1.03%)	6259	P clean
Duosangpudong	1.19	EQ	0.42	–0.10 ± 0.15 (1.13%)	6213	P clean
G08	0.76	EQ	0.68	–0.07 ± 0.18 (1.09%)	6100	P clean
G06	1.73	VBH	0.36	–0.08 ± 0.07 (1.25%)	6235	P clean
Mean	*1.18*	*EQ*	*0.47*	*–0.09* ± 0.15 *(1.31%)*	*6216*	

Appendix 2

Supplementary information for ‘Contrasting geometric and dynamic evolution of lake and land-terminating glaciers in the central Himalaya’ shown in chapter 4.

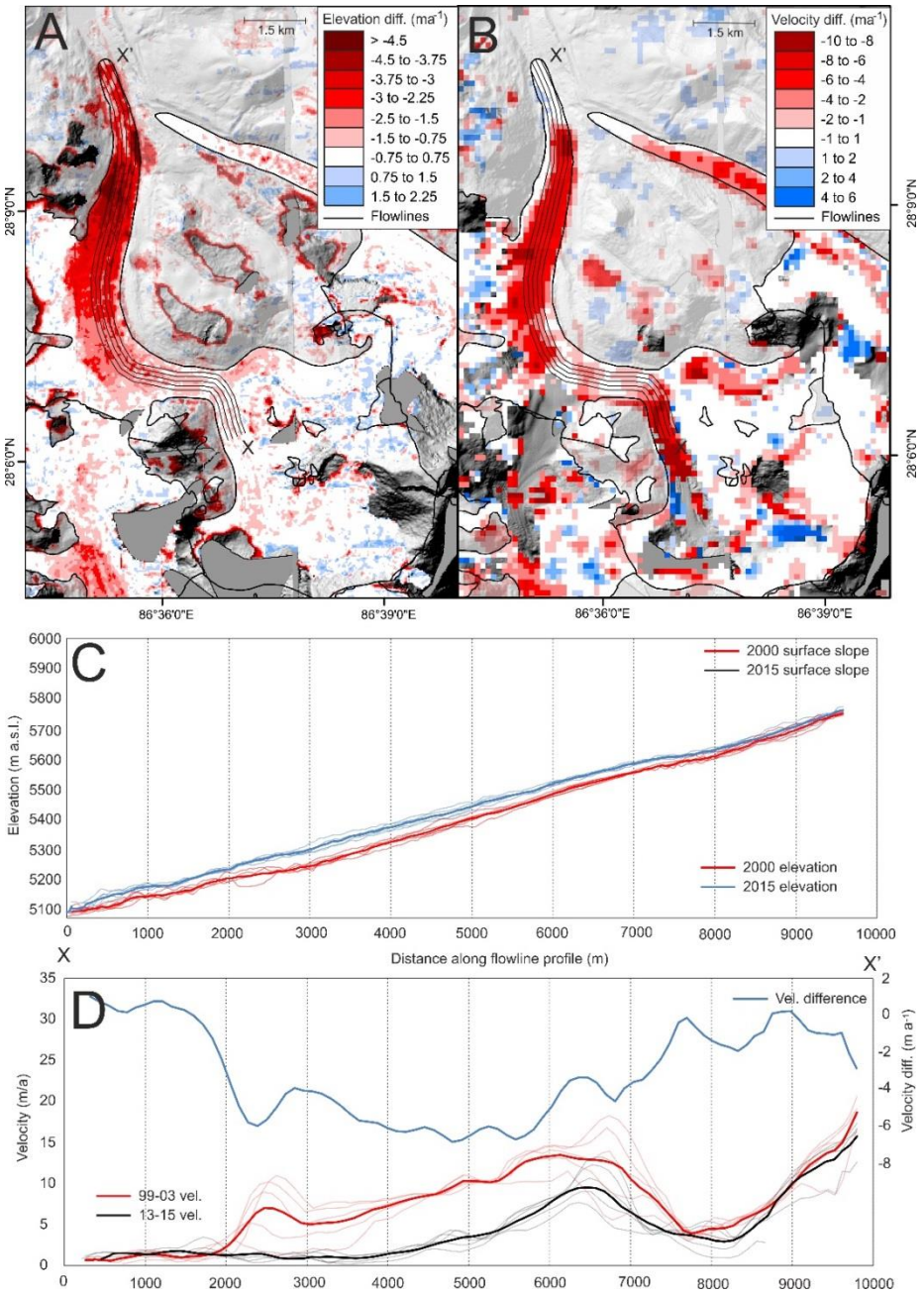

Supplementary Figure 3. An example of flowline data extracted from DEM (A) and glacier velocity difference (B) datasets. Semi-transparent elevation and velocity profiles in panels C and D represent different flow parallel profiles taken across the glacier surface (spaced apart by 100 m), with the bold profile representing the mean surface elevation or surface velocity profile from each time period.

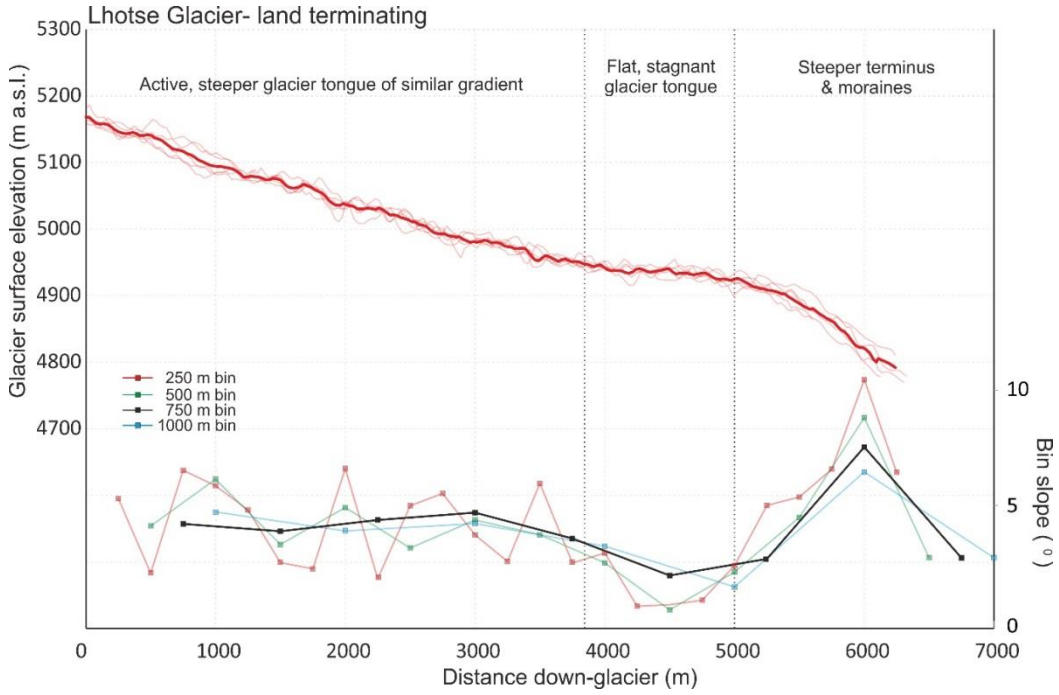

Supplementary Figure 4. The variability of estimates of glacier surface slope depending on different bin lengths for Lhotse glacier. Semi-transparent elevation profiles represent different flow parallel profiles taken across the glacier surface, with the bold red profile representing the mean surface elevation profile.

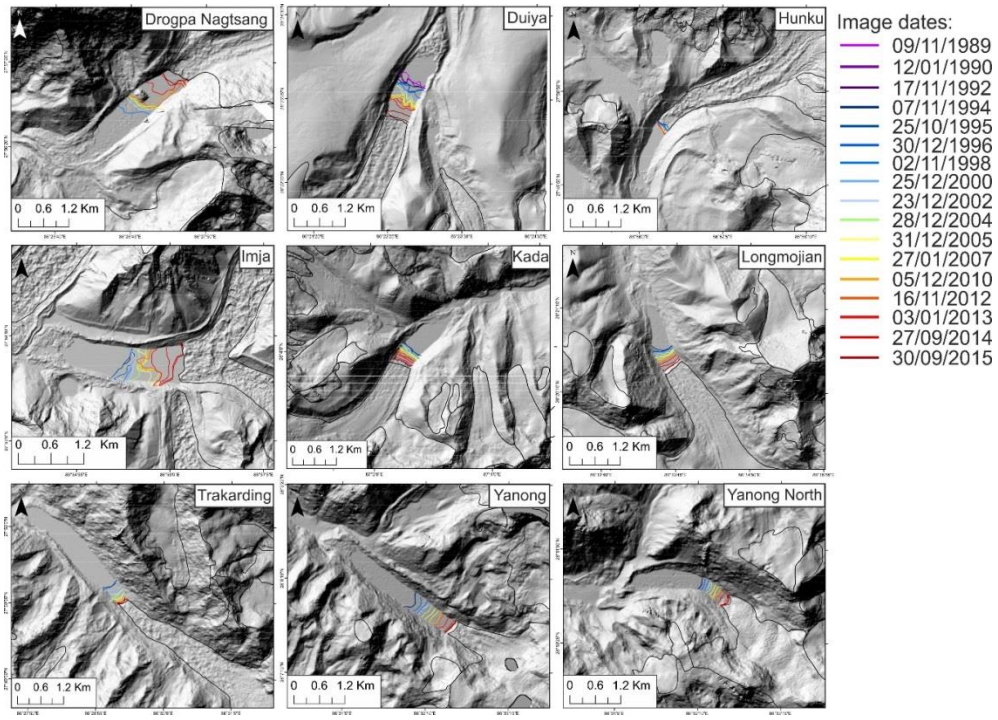

Supplementary Figure 5. DEM hillshades generated from SETSM (2014/2015) data and ice front positions of the nine lake-terminating glaciers between 1989 and 2015.

Supplementary Table 4 Glaciers highlighted in the study. Data on glacier area and altitudinal range are taken from the GLIMS database. Glacier length is measured along centrelines from the bergschrund.

GLIMS ID	Name	Length (km)	Area (km^2)	Lat	Lon	Altitude Min (m a.s.l)	Max (m a.s.l)	Range (m a.s.l)	Lake status
G086280E28276N	G1	12.3	42.7	28°13’04.30” N	86°15’34.47” E	4778	7045	2467	No lake
G086550E28133N	Yanong	3.4	4.4	28°07’42.80” N	86°32’29.55” E	4984	6377	1393	Proglacial lake
G086548E28174N	Yanong North	3.2	4.1	28°11’06.94” N	86°32’31.66” E	5025	6524	1499	Proglacial lake
G086384E28259N	Erbu	10.9	25.8	28°12’17.15” N	86°24’07.99” E	5020	7130	2310	No lake
G086471E27959N	Drogpa Nagtsang	8.2	25.3	27°56’18.60” N	86°26’09.83” E	5018	7031	2013	Supraglacial lake
G086537E27874N	Trakarding	17.7	35.4	27°50’54.30” N	86°29’20.89” E	4561	6659	2098	Proglacial lake
G086949E27913N	Lhotse Shar	6.5	15.3	27°54’00.71” N	86°54’43.21” E	5021	7998	2977	Proglacial lake
G086820E27978N	Khumbu	15.7	39.5	27°55’57.90” N	86°48’30.56” E	4915	8062	3147	Coalescing ponds
G086917E27925N	Lhotse	7.1	6.9	27°54’11.44” N	86°52’31.86” E	4821	6082	1261	No lake
G086900E27843N	Hunku	4.7	13.9	27°50’30.70” N	86°56’18.50” E	5207	6942	1735	Proglacial lake
G086939E28060N	Rongbuk East	10.9	26.7	28°05’36.62” N	86°54’26.74” E	5640	8361	2721	No lake
G086866E28050N	Rongbuk	19.5	73.2	28°07’59.43” N	86°51’17.56” E	5153	8758	3605	Supraglacial lake
G086466E28321N	Ayi	8.6	7.27	28°19’55.20” N	86°31’15.18” E	5313	6863	1550	Coalescing ponds
G086456E28291N	Tibet 1	12.9	26.8	28°17’17.12” N	86°31’31.17” E	5138	7085	1947	Coalescing ponds
G086633E28122N	Gyabrag	11.5	33.2	28°10’25.17” N	86°35’12.63” E	5095	8182	3087	No lake
G086235E28330N	Longmojian	4.5	9.3	28°20’29.49” N	86°13’39.71” E	5348	6788	1440	Proglacial lake
G086382E28331N	Duiya	9.3	22.5	28°24’20.34” N	86°23’02.44” E	5480	7201	1721	Proglacial lake
G087011E28048N	Kada	8.6	19.1	28°04’23.09” N	87°03’22.70” E	5624	7183	1559	Proglacial lake

Supplementary Table 5. Landsat archive scenes used in lake-terminating glacier ice front positions delineation and glacial lake area mapping.

Scene ID	Date (dd/mm/year)	Used for
LT51400411989313BKT00	09/11/1989	Ice front/lake area mapping
LT51400411990012BKT00	12/01/1990	Ice front/lake area mapping
LT51400411992322ISP00	17/11/1992	Ice front/lake area mapping
LT51400411994311ISP00	07/11/1994	Ice front/lake area mapping
LT51400411995298ISP00	25/10/1995	Ice front/lake area mapping
LT51400411996365BKT00	30/12/1996	Ice front/lake area mapping
LT51400411998306BKT00	02/11/1998	Ice front/lake area mapping
LT51400412000360BKT00	25/12/2000	Ice front/lake area mapping
LE71400412002357SGS00	23/12/2002	Ice front/lake area mapping
LE71400412004363EDC00	28/12/2004	Ice front/lake area mapping
LE71400412005365PFS00	31/12/2005	Ice front/lake area mapping
LE71400412007323PFS00	27/01/2007	Ice front/lake area mapping
LE71400412010347PFS00	05/12/2010	Ice front/lake area mapping
LE71400412012321PFS00	16/11/2012	Ice front/lake area mapping
LE71400412013003PFS00	03/01/2013	Ice front/lake area mapping
LC81400412014142LGN00	19/09/2014	Ice front/lake area mapping
LE71400412015281NPA00	30/09/2015	Ice front/lake area mapping
WV03_20150121_10400100076C0700	21/01/2015	SETSM DEM
WV01_20150504_102001003C5FB900	04/05/2015	SETSM DEM
WV01_20140115_102001002A289F00	15/01/2014	SETSM DEM
WV01_20140324_102001002D263400	24/04/2014	SETSM DEM
WV01_20150204_102001003A5B7900	04/02/2015	SETSM DEM
WV02_20150202_103001003D4C7900	02/04/2015	SETSM DEM
WV01_20140218_102001002C5FA100	18/02/2014	SETSM DEM
WV01_20141022_102001003525D400	22/10/2014	SETSM DEM
WV02_20141110_1030010039013C00	10/11/2014	SETSM DEM
WV01_20141129_102001002776B500	28/11/2014	SETSM DEM
WV01_20140514_102001003001E400	14/05/2014	SETSM DEM

Appendix 3

Supplementary information and figures for ‘Quantifying the morphometric evolution of Himalayan debris covered glaciers using fine resolution digital elevation models’ shown in chapter 5.

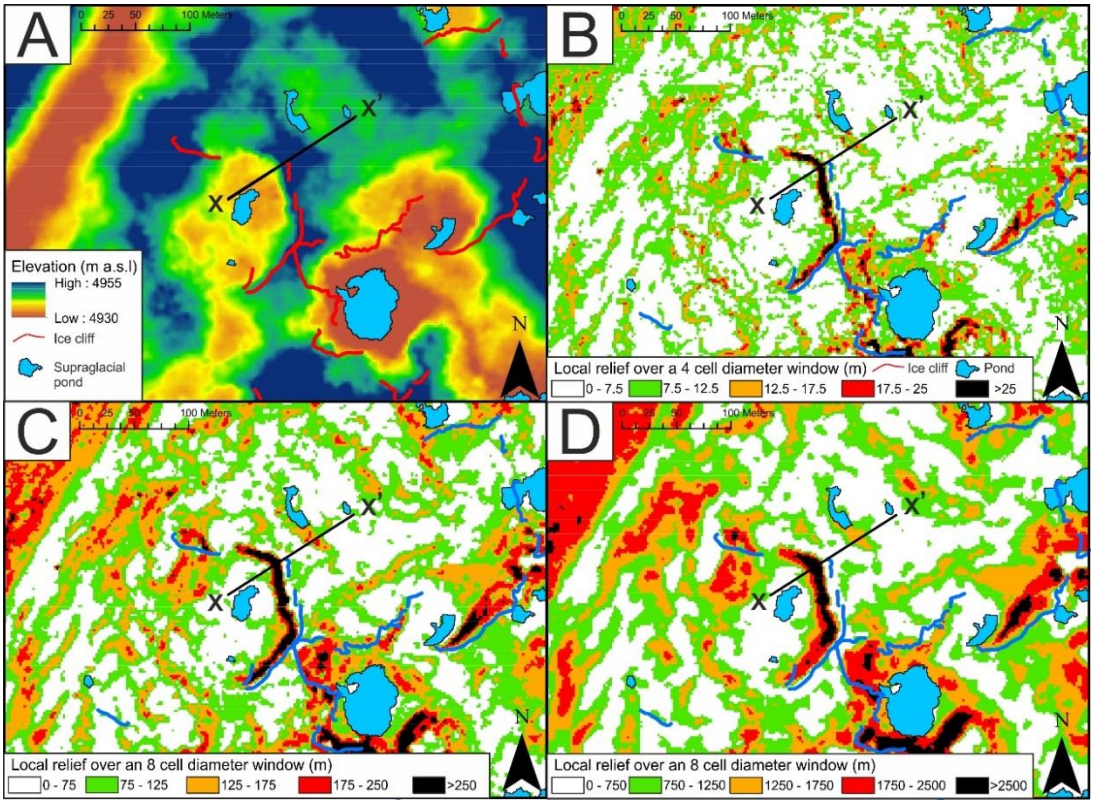

Supplementary Figure 6. Comparison of SumNeg metrics generated using different window sizes over an area of the Khumbu glacier hosting numerous ice cliffs (A). B) an 4 cell diameter window, C) an 8 cell diameter and, D) a 16 cell diameter moving window. The surface topography and SMR profiles shown in Supplementary Figure 7 were taken from X to X’.

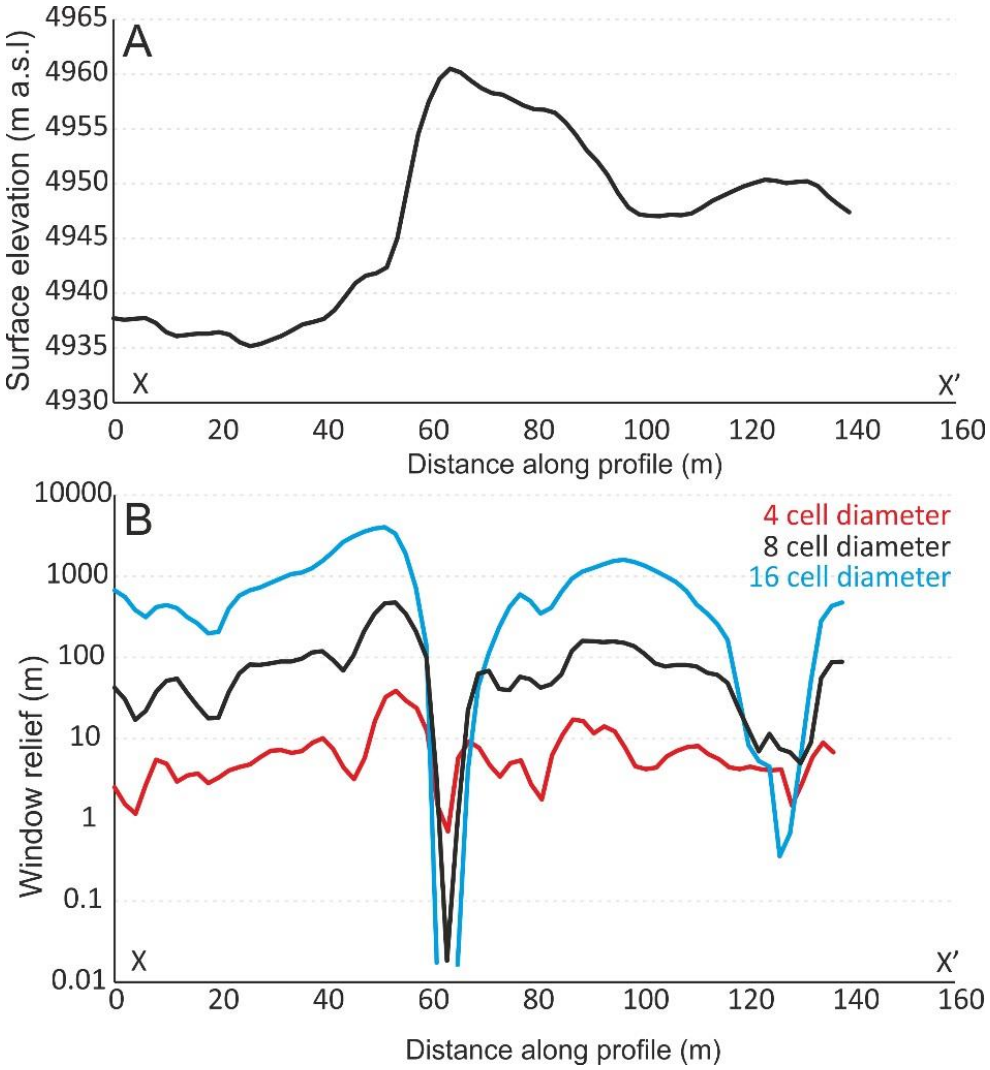

Supplementary Figure 7. A) Surface elevation profile taken along the X – X' profile shown in Figure S1. B) The variability in SumNeg values taken along the X – X' profile depending on window diameter.

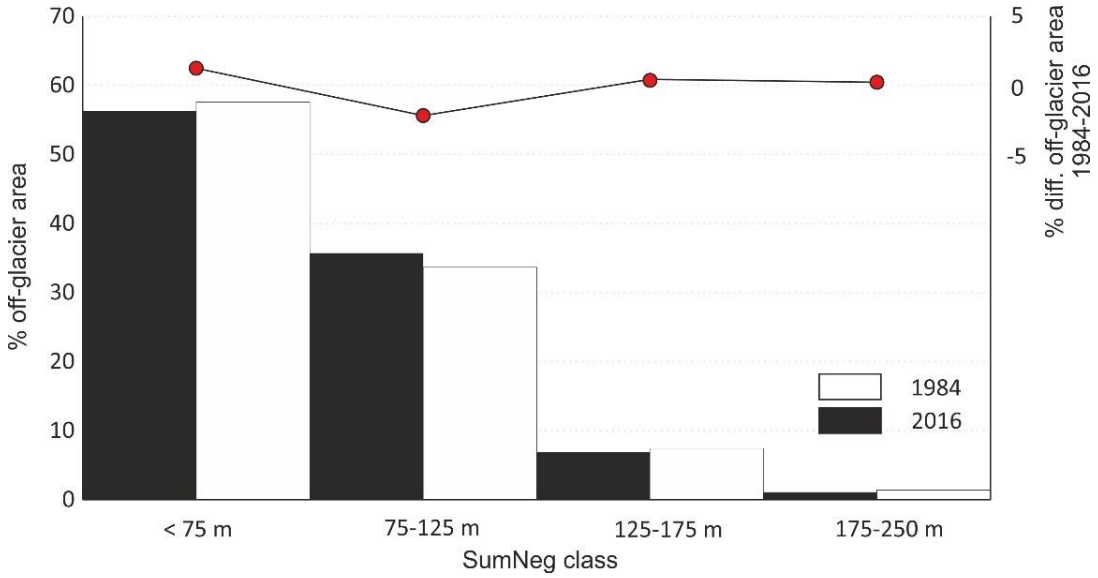

Supplementary Figure 8. Comparison of metric class prevalence off-glacier. Analyses has been limited to areas of surface slope of less than 15° to limit the impact of spurious data caused by topographic shading or poor image quality.